SYNTHESIS AND CHARACTERISATION OF PILLARED CLAY CATALYSTS FOR HYDRO-CRACKING OF HEAVY LIQUID FUELS

MARIA ELENI GYFTOPOULOU

Doctor of Philosophy

ASTON UNIVERSITY

December 2005

Aston University

SYNTHESIS AND CHARACTERISATION OF PILLARED CLAY CATALYSTS FOR HYDRO-CRACKING OF HEAVY LIQUID FUELS

Maria Eleni Gyftopoulou

A thesis submitted for the degree of Doctor of Philosophy 2005

Thesis summary

A range of chromia pillared montmorillonite and tin oxide pillared laponite clay catalysts, as well as new pillared clay materials such as cerium and europium oxide pillared montmorillonites were synthesised. Methods included both conventional ion exchange techniques and microwave enhanced methods to improve performance and/or reduce preparation time. These catalytic materials were characterised in detail both before and after use in order to study the effect of the preparation parameters (starting material, preparation method, pillaring species, hydroxyl to metal ratio etc.) and the hydrocracking procedure on their properties. This led to a better understanding of the nature of their structure and catalytic operation. These catalysts were evaluated with regards to their performance in hydrocracking coal derived liquids in a conventional microbomb reactor (carried out at Imperial College). Nearly all catalysts displayed better conversions when reused.

The chromia pillared montmorillonite CM3 and the tin oxide pillared laponite SL2a showed the best "conversions". The intercalation of chromium in the form of chromia (Cr_2O_3) in the interlayer clearly increased conversion. This was attributed to the redox activity of the chromia pillar. However, this increase was not proportional to the increase in chromium content or basal spacing. In the case of tin oxide pillared laponite, the catalytic activity might have been a result of better access to the acid sites due to the delaminated nature of laponite, whose activity was promoted by the presence of tin oxide. The manipulation of the structural properties of the catalysts via pillaring did not seem to have any effect on the catalysts' activity. This was probably due to the collapse of the pillars under hydrocracking conditions as indicated by the similar basal spacing of the catalysts after use. However, the type of the pillaring species had a significant effect on conversion. Whereas pillaring with chromium and tin oxides increased the conversion exhibited by the parent clays, pillaring with cerium and europium oxides appeared to have a detrimental effect. The relatively good performance of the parent clays was attributed to their acid sites, coupled with their macropores which are able to accommodate the very high molecular mass of coal derived liquids.

A microwave reactor operating at moderate conditions was modified for hydrocracking coal derived liquids and tested with the conventional catalyst NiMo on alumina. It was thought that microwave irradiation could enable conversion to occur at milder conditions than those conventionally used, coupled with a more effective use of hydrogen. The latter could lead to lower operating costs making the process cost effective. However, in practice excessive coke deposition took place leading to negative total conversion. This was probably due to a very low hydrogen pressure, unable to have any hydrocracking effect even under microwave irradiation.

The decomposition of bio-oil under microwave irradiation was studied, aiming to identify the extent to which the properties of bio-oil change as a function of time, temperature, mode of heating, presence of char and catalyst. This information would be helpful not only for upgrading bio-oil to transport fuels, but also for any potential fuel application. During this study the rate constants of bio-oil's decomposition were calculated assuming first order kinetics.

Keywords: Pillared clays; characterisation; conversion; coal derived liquids; bio-oil.

To my family

Acknowledgements

Firstly I would like to thank my supervisor Professor Tony Bridgwater for his encouragement, guidance and advice during the course of this research. I would also like to thank Dr. David Miller for the long and useful chemistry discussions, as well as his guidance.

I gratefully acknowledge the financial support from EPSRC (Engineering and Physical Sciences Research Council) for this joint project with Imperial College. In this respect, I would like to thank Marcos Millan, Professor Rafael Kandiyoti and Professor Denis Dugwell from Imperial College for the successful collaboration during the course of the project.

Many thanks are also due to the technical staff within Chemical Engineering and Applied Chemistry (CEAC) for their assistance on so many occasions and especially Steve Ludlow for putting up with my nagging! I am also grateful to Dr. M.C. Perry for providing the solid state MAS NMR spectra and assisting me in their interpretation.

I want to express my gratitude to Dr. S.O. Saied, Electronics Engineering, Aston University, for providing the XPS spectra and Dr. J.A. Hriljac, Chemistry Department, Birmingham University, for his help in obtaining the x-ray diffractograms and interpreting them.

I would also like to thank all the members of our research group and my other friends in CEAC, who have provided help and encouragement along the way and made my time at Aston an enjoyable one.

Finally I would like to thank my family for their support and understanding during the course of this research.

List of Contents

List of Tables

CHAPTER 8

CHAPTER 9

CHAPTER 10

List of Figures

CHAPTER 2

CHAPTER 3

CHAPTER 4

CHAPTER 5

CHAPTER 6

CHAPTER 7

CHAPTER 8

CHAPTER 9

CHAPTER 10

1 INTRODUCTION

Interest in direct coal liquefaction has been historically dependent on oil prices, and therefore it decreased with the return of low oil prices in the 1980s and 1990s. However, if the current situation of oil prices in the region of 60 US$ per bbl continues, coal liquefaction could become a strategic alternative in many countries with significant coal reserves. As coal reserves are overall much larger than those of oil and gas, coal liquefaction may still be an option when oil and gas become unavailable or their production difficult or expensive. It could supplement renewable energy sources to cover energy demand for liquid fuels, particularly transport fuels.

At the same time the use of catalytic hydrocracking to upgrade heavy oil fractions is becoming more attractive, due to a decline in light oil reserves and production together with an increase in the reserves of heavy oil discovered. The market for heavy oils such as fuel oil is decreasing due to substitution by natural gas and tightening of environmental regulations. In addition, the dramatic recent increase of crude oil prices has increased the importance of maximising of the value of the crude through upgrading of the heavier fractions. This price increase has narrowed the cost margin between petroleum derived and coal derived liquid transport fuels, rendering coal liquefaction technology more attractive economically [1].

Catalysts currently available for hydrocracking petroleum feedstocks, such as NiMo and CoMo supported on alumina, were developed for hydrotreating, mainly hydrodesulfurisation, and they present severe problems of deactivation when dealing with heavier feedstocks. This has led to the search for better catalysts, which would enhance the conversion of the high molecular mass fractions into lighter materials. A chromia pillared montmorillonite and a tin oxide pillared laponite exhibited particularly good results in hydrocracking of coal derived liquids and petroleum residues in terms of conversions, molecular mass reduction, polynuclear aromatic ring system reduction, heteroatom removal and resistance to rapid deactivation, proving to be significantly more efficient than a presulfided supported NiMo catalyst and a dispersed Mo-based catalyst precursor [2, 3, 4].

Pillared clays (PILCs) have been employed in the field of acid-catalysed reactions, such as cracking and hydrogenation [5 and cited references]. They have high permanent porosity obtained by separating the clay sheets by a molecular prop or pillaring agent. They are prepared by exchanging the native cations of the parent clay with partially hydrated polymeric or oligomeric metal cation complexes which, upon heating, undergo dehydration /dehydroxylation resulting in thermally stable pillars composed of metal oxide clusters. An even distribution of pillars leads to a two-dimensional channel system comparable to that of zeolites and increases the accessibility of reactant molecules to the interlamellar catalytic sites. Furthermore, particular large pillaring agents can establish channels in the range of 5 to 20 Å, which make pillared clays suitable catalysts for cracking of large molecules, such as heavy hydrocarbons [5]. Moreover, the pillar can exert a shape-selective effect, which controls diffusion rates of reactants and products or formation of reaction intermediates [6], and can incorporate a second functionality in the catalyst apart from its mild acidic properties [7].

This research aimed to further develop the work performed on novel catalysts based on pillared clays for hydrocracking heavy hydrocarbon liquids [2, 3, 4]. These catalysts could also find a potential application in the catalytic upgrading of biomass fast pyrolysis liquids (bio-oil). Like coal derived liquids and petroleum residues, bio-oil requires high temperatures and pressures in order to be upgraded by hydro-processing to transport fuel [8] and the conventional catalysts (NiMo or CoMo on alumina) employed until now are rapidly deactivated and unable to handle high water contents.

1.1 Objectives

The following objectives were addressed in this thesis:

- Synthesis and optimisation of a range of chromia pillared montmorillonite and tin oxide pillared laponite clay catalysts, as well as new pillared clay materials such as cerium and europium oxide pillared montmorillonites. Methods included both conventional ion exchange techniques and microwave enhanced methods to improve performance and/or reduce preparation time (Section 3.3).

- Characterisation of these materials both before and after use via:
  - X-ray powder diffraction to measure their basal spacing (Chapter 4).

- Thermogravimetric analysis to assess their thermal stability (Chapter 5).
- X-ray photoelectron spectroscopy to identify their composition (Chapter 6).
- Nitrogen sorption to measure their textural properties (Chapter 7).
- Magic angle spinning nuclear magnetic resonance to study their aluminosilicate framework (Chapter 8).

These methods study the effect of the preparation parameters (starting material, preparation method, pillaring species, hydroxyl to metal ratio etc.) and the hydrocracking procedure on the properties of the pillared materials in order to develop a more fundamental understanding of the nature of their structure and catalytic operation.

- Evaluation of these catalytic materials with regards to their performance in hydrocracking coal derived liquids in a conventional microbomb reactor (carried out at Imperial College). This includes correlation of the catalysts' performance with their properties, which were identified via the characterisation route (Section 9.1).

- Modification of a microwave reactor for hydrocracking coal derived liquids and testing with the conventional catalyst NiMo on alumina. Microwave irradiation would be expected to preferentially excite the catalytic surface and enhance reactions at lower bulk material temperatures and pressures and with more effective use of hydrogen. This could lead to lower operating costs (Section 9.2).

- Investigation of bio-oil's decomposition under microwave irradiation in order to provide information on the effect of parameters such as temperature, time, char content etc. in bio-oil's properties, which is not only important for upgrading but also would be useful for any potential fuel application (Chapter 10).

In Chapter 2 the literature and theory providing the background to this research is presented. In Chapter 3 the experimental work (catalyst preparation and hydrocracking of coal derived liquids) is described, including references to raw materials and analytical methods.

2 LITERATURE & THEORY

2.1 Smectite clay minerals

Clays are earthy, extremely fine-grained sediments composed of micron-size or colloidal particles, having high plasticity and clay mineral content. Clays may be classified by use, origin, mineral composition or colour [9].

Clay minerals are hydrous layer silicates of the so-called phyllosilicate family, in which a tetrahedral sheet of polymerised SiO_4 units and an octahedral sheet formed from oxygen and metal ions are the basic building blocks. Most often the metal ions in the octahedral sheet are aluminium, and that is why clay minerals are loosely described as aluminosilicates, or magnesium [10].

The layer lattice structure of smectite clays consists of two tetrahedral sheets sandwiching one octahedral sheet and, in this basis, are classified as 2:1 phyllosilicates. This structural characteristic differentiates smectite clays from kaolinite clay structures containing one tetrahedral and one octahedral sheet and from chlorite clay structures that contain two tetrahedral and two octahedral sheets. Illite clay structures (mica group) are similar to smectite clay structures, but in illite adjacent tetrahedral sheets are bounded by K^+ ions which are not exchangeable [11].

In a half unit cell containing ten oxygen and two hydroxyl ions, there are four tetrahedral cation sites and three octahedral cation sites. When two-thirds of the octahedral sites are occupied by trivalent cations, the structures are classified as dioctahedral, and when all three octahedral sites are occupied by divalent cations the structures are classified as trioctahedral. Pyrophyllite $[Al_4Si_8O_{20}(OH)_4]$ and talc $[Mg_6Si_8O_{20}(OH)_4]$ are considered as the respective idealised structural types with electronically neutral layers [7]. However, deviation from these ideal structures occurs by isomorphous substitution of cations from the tetrahedral and/or octahedral sheet by alternative cations of similar size and lower valency leading to charge deficiency. In dioctahedral montmorillonite Al^{3+} is substituted by Mg^{2+} in the octahedral sheets, whereas in dioctahedral beidellite and trioctahedral saponite Si^{4+} is substituted by Al^{3+} in the tetrahedral sheet. In trioctahedral hectorite substitution of Li^+ for Mg^{2+} occurs in the octahedral sheet. Nontronite is an analogue of beidellite that is iron rich. The

chemical composition of the most common smectite clay minerals as given by Brindley and Brown is presented in Table 2.1.

Table 2.1 Chemical composition of most common smectite clay minerals [12]

Dioctahedral smectites	
Montmorillonite	$M_y^+ nH_2O\ (Al_{2y}Mg_y)Si_4O_{10}(OH)_2$
Beidellite	$M_x^+ nH_2O\ Al_2(Si_{4-x}Al_x)O_{10}(OH)_2$
Nontronite	$M_x^+ nH_2O\ Fe_2^{3+}(Si_{4-x}Al_x)O_{10}(OH)_2$
Trioctahedral smectites	
Saponite	$(M_{x-y}^+ nH_2O)(Mg_{3-y}(AlFe)_y)(Si_{4-x}Al_x)O_{10}OH_2$
Hectorite	$(M_y^+ nH_2O)\ (Mg_{3-y}Li_y)Si_4O_{10}(OH)_2$

The layer charge of an octahedrally substituted smectite (e.g. montmorillonite) is distributed over the complete oxygen framework, whereas tetrahedral substitution (as e.g. in beidellite) leads to a more localised charge distribution and the latter smectites tend to have a higher three-dimensional order [13].

The idealised structural formula for montmorillonite is $Na_{0.35}(Al_{1.65}Mg_{0.35})Si_4O_{10}(OH)_2.nH_2O$ [14] (Figure 2.1). However, deviations occur from this formula because montmorillonite is a naturally occurring material, which leads to slight variations from one deposit to another. Isomorphous substitution of small amounts of Al^{3+} and/or Fe^{3+} in the tetrahedral layer and of Fe^{2+} in the octahedral layer is commonly encountered. Carbonaceous deposits and particulate impurities such as quartz are also present in the unrefined bulk material.

In addition to the naturally occurring clay minerals, there is also a range of synthetic equivalents in the market place. Laponite is described as a synthetic virtually iron-free trioctahedral smectite clay, similar to hectorite. All its octahedral sites are occupied by Mg^{2+} and Li^+ ions, whereas the tetrahedral layers are composed in the same way as montmorillonite. Its idealised structural formula is $Na_{0.67}(Mg_{5.33}Li_{0.67})(Si_8O_{20}(OH)_4)$ [15].

Figure 2.1 Montmorillonite Clay [16]

2.1.1 Physicochemical properties of smectite clay minerals

The vast range of uses and the scientific interest in the smectite clay minerals derive from their physicochemical properties, many of which are not displayed by any other known natural minerals. They are the result of extremely small crystal size (average size 0.5 μm), variations in internal chemical composition, large cation exchange capacity, large surface area that is chemically active, variations in types of exchangeable ions and surface charge and interactions with inorganic and organic liquids.

2.1.1.1 Cation exchange

Perhaps the most unique property of smectite clays, known as cation exchange capacity (C.E.C), is the presence of cations adsorbed on interlamellar surfaces that can be exchanged. The most common exchangeable ions are Ca^{2+}, Mg^{2+}, Na^{+} and H^{+}, although small amounts of exchangeable K^{+} and Li^{+} occur in some smectites. Significantly more major commercial smectite clay deposits contain Ca^{2+} and Mg^{2+} than Na^{+} or H^{+} as exchangeable ions [11].

The C.E.C. of a clay is generally understood to be equal to the layer charge, hence it is considered to be a material constant for each clay mineral [17]. It is made up of two components. The predominant portion (~80%) is derived from lattice substitution in both the octahedral and to a lesser extent the tetrahedral layers. The remaining 20% is caused by broken bonds around the edges of the clay platelet which cause charge deficiencies. The cation exchange capacity of relatively pure smectite clays ranges between 70 and 130 meq/100g.

However, the measured cation exchange capacity is only equivalent with the layer charge if all charge compensating cations are accessible for exchange. This does not occur for illites in which the interlayer cations are not exchangeable, or partially collapsed smectites, such as potassium montmorillonite after heating or several drying and wetting cycles resulting in potassium fixation [17].

The exchangeable ions associated with smectite clays are easily and reversibly replaceable, usually by treatment with ions in aqueous solution. This exchange reaction is stoichiometric. Many factors influence the rate and degree of cationic exchange in smectite clays. Divalent ions will readily replace monovalent ions, while the reverse reaction is not as easily achieved. If ions are of the same valency the size of the unhydrated ion plays the decisive role. The larger ion will readily replace the smaller ion. Consequently the following series of increasing replacing power can be derived: $Li^+ < Na^+ < K^+ < Mg^{2+} < Ca^{2+}$ [17].

2.1.1.2 Hydration and swelling

The hydration of interlamellar surfaces is another unique property of smectite clays. Although it occurs regardless of the type of exchangeable cation present, the degree of hydration is dependent on the species of exchangeable ion, on the size and charge of the cations, and on the magnitude and location of the layer charge of the adjacent silicate sheets [11]. Presently, it is generally accepted that the hydration of the interlamellar surfaces of smectite clays occurs in a series of steps when these clays are subjected to increasing relative humidity levels. At high humidity levels between one and four layers of water molecules may be formed, depending on the cation adsorbed. When only a few water layers are adsorbed, the water molecules are arranged in a highly ordered manner.

Smectites containing exchangeable Ca^{2+} and Mg^{2+} even when fully hydrated show only a small degree of swelling, whereas some smectites containing Na^+ and Li^+ are particularly susceptible to swelling by water adsorption. In the latter case the clay layers may be separated by water layers many Angstroms thick, even to the point that dissociation of the layers may occur [11].

Hydration is principally driven by the electrostatic attraction between the polar water

molecule and the charge of the exchangeable cation. It is affected more by the nature of the interlayer cation than by the silicate surface. Despite this, in smectite clays some water is associated with the silicate surface. This is called crystalline water and is relatively constant. Nevertheless, there is another type of interlayer water found in highly hydrated smectite clays, free water. Free water is not associated with either the interlayer cation or the silicate surface, thus it is very labile [12].

2.1.1.3 Colloidal properties

When certain smectite clays are added in very small amounts to water, their chemical and hydration properties cause the crystals to separate and disperse. In addition, their electric potential cause the particles to repel each other, and because the crystals are so small they may remain suspended in the liquid indefinitely resulting in a colloid state [11].

The same smectite clays when added to water in larger concentrations (5-6%) may cause the liquid to become highly resistant to flow or viscous, and when the shear stress on the liquid is removed the smectite particles usually develop a rigid gel structure. Naturally occurring montmorillonite, hectorite and some saponite clays with high amounts of exchangeable Na^+ have the unique ability to impart high viscosity and develop thixotropy. On the contrary Ca^{2+}-Mg^{2+} smectites do not give high viscosity values or display thixotropic behaviour even when the percentage solid is very high. The viscosity developed by Na^+-smectites is believed to be due primarily to small particle size, large surface area, and high dispersibility, and secondarily to the electrical forces between the particles. The negatively charged basal surfaces and the positive charges present on crystal edges attract each other, and so an internal "card house" structure is formed, which results in thixotropy. A thixotropic smectite clay system can be returned to a viscous system through shear or agitation [11].

2.1.1.4 Dehydration and rehydration

In smectite clays the loss of the adsorbed water, most of which is interlayer water, occurs at low temperatures (100-200°C). The amount of adsorbed water loss depends on the nature of the adsorbed ions, if pre-treatment of the samples is the same, and to a lesser degree on the structure of the smectite. In Na^+-smectites the adsorbed water is

usually lost in a single stage, but when Ca^{2+} and Mg^{2+} are the predominant cations the adsorbed water is sometimes lost in two stages.

There are wide variations of the temperature at which loss of OH groups or lattice water occurs among smectites. These variations in dehydroxylation are primarily related to crystalline structure, strength of metal hydroxide bonds and chemical composition, as dehydroxylation involves the breakdown of the silicate structure [12]. Among dioctahedral smectites, Na-montmorillonites with low substitution of Fe^{2+} and Mg^{2+} for Al^{3+} show loss of OH groups at the highest temperature, beginning gradually at 550°C and ending at about 750°C, with a peak at about 680-700°C. Large replacement of Al^{3+} by Fe^{2+} or Mg^{2+} causes a reduction in the temperature of the reaction, and for nontronite the peak temperature of OH loss is 500-600°C [11]. In Mg rich trioctahedral hectorite, however, the rapid loss of OH groups may not begin until 700°C, possibly because the F atoms that replace some of them are more tightly held within the lattice structure than the OH groups themselves [12].

The rehydration characteristics of smectite clays after heating to various temperatures are not as well understood as the dehydration characteristics. If all of the adsorbed water is removed from smectite clays under heating up to 200°C, rehydration will occur. However, the amount will depend on the relative humidity level and the properties of the clay. Ca^{2+} and Mg^{2+} smectites usually rehydrate more rapidly, and at a lower humidity level, than do Na^{+}-smectite clays, due to the hydration properties of Ca^{2+} and Mg^{2+} ions [11]. Furthermore, there will be some effects on certain properties such as swelling and/or dispersion. In most industrial processes adsorbed water content is rarely reduced below 8% in order to retain primary properties. Smectite clays will generally rehydrate to some degree, even after heating to temperatures as high as 500-700°C, in the presence of liquid water. The degree of rehydration depends mainly on the degree of structural change owing to loss of OH lattice water [11].

2.1.1.5 Organic reactions

There is an almost endless number of organic compounds that interact in a variety of ways with smectite clays because of the many types of bonding that are possible between the oxygen surfaces and the organic molecules [11].

Organic anions are adsorbed at the edges of the clay particles. Organic cations (amine or quaternary ammonium salts), on the contrary, are adsorbed initially by exchange on the negative face surfaces of the clay. This fact is evident from the much larger adsorption capacity of the clay for these cations and also from the increase of the basal spacing of montmorillonite clays after treatment with organic cations [18].

Many organic compounds containing polar groups, such as alcohols, amines and ketones are strongly adsorbed on the layer surfaces of a clay displacing the adsorbed water. Such organo-clay complexes may be prepared either by mixing the water-clay suspension with the organic liquid or by contacting the dry clay directly with the organic liquid [18].

There is a growing use of smectite clays for adsorbing various organic and inorganic contaminants from industrial waste water. In these processes a small amount of clay is added to the water to adsorb the contaminants. Then other chemicals are added to flocculate the clay for easy removal from the system [11].

2.2 Pillared clays (PILCs)

2.2.1 Synthesis of PILCs

Pillared clays (PILCs) are prepared by exchanging the native cations of the parent clay with partially hydrated polymeric or oligomeric metal cation complexes. Upon heating, these cations undergo dehydration/dehydroxylation, resulting in thermally stable pillars composed of metal oxide clusters that are "grafted" on the clay layers separating them permanently (Figure 2.2).

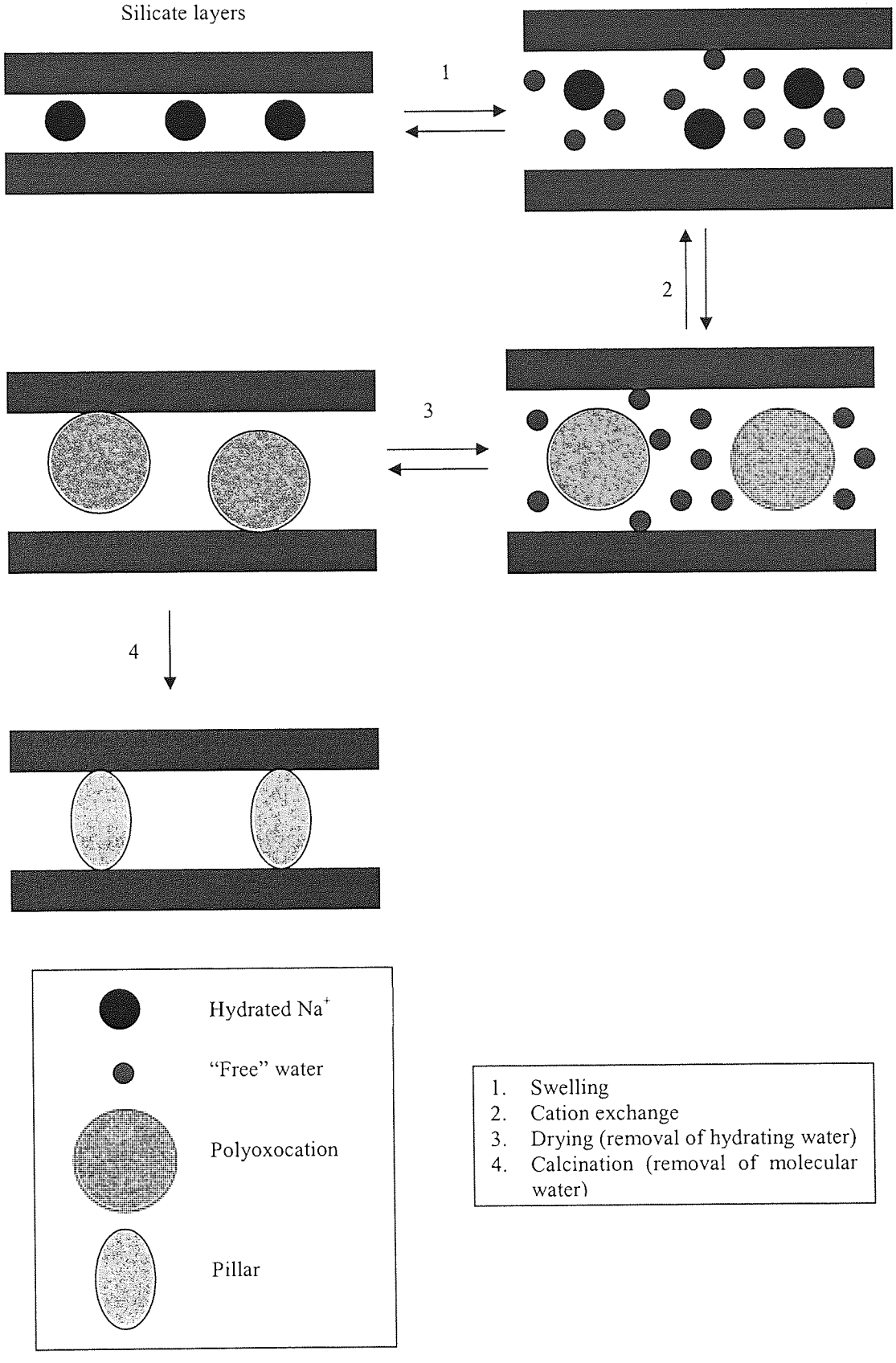

Figure 2.2 Schematic representation of the preparation of a PILC

Many different pillaring species have been reported in the literature such as organic compounds (alkyl ammonium, bicyclic amine cations) and organometallic complexes. However, organic and organometallic pillaring agents decompose at relatively modest temperatures causing the pillared clay structure to collapse. On the contrary the use of inorganic hydrated polyoxocations as pillaring agents provides thermally stable pillared clays with high specific surface areas (200 to 500 m^2/g)[13]. Many different polyoxocations (Al, Ni, Zr, Fe, Cr, Mg, Si, Bi, Be, B, Nb, Ta, Mo, Ti and more recently Cu and Ga), as well as multimetallic pillars have been reported so far in the open and patent literature. However, the chemical composition, structure and charge are well defined only for the Al-polyoxocation, in which the Keggin ion $[Al_{13}O_4(OH)_{24}(H_2O)_{12}]^{7+}$ is identified [19]. A detailed review on the synthesis of pillared clay catalysts has been recently published by Kloprogge [13].

The synthesis of chromia pillared clays, as reported by Tzou & Pinnavaia, is presented herein as an example [20]. According to these authors, pillaring reagent solutions containing substantial concentrations of large polyoxochromium polymers are prerequisites for the preparation of chromia pillared clays with high basal spacings.

The preparation of polyoxometal complexes for the pillaring of smectite clays normally is carried out by hydrolysing metal ion solutions with NaOH as base. High local concentrations of base can develop depending in part on the concentration of NaOH and the mode of addition of the solutions, which can lead to premature precipitation of the metal hydroxide. Tzou and Pinnavaia have used Na_2CO_3 as the source of base to minimise such problems in the hydrolysis of chromium. Analogous hydrolysis chemistry can be expected for NaOH and other non-complexing bases, provided that high local concentrations of the base can be avoided.

When Na_2CO_3 was added to a solution of $Cr(NO_3)_3.9H_2O$ at 25°C the pH of the solution increased, as expected. However, upon ageing particularly at elevated temperatures, the pH of the solution decreased. Tzou and Pinnavaia attributed the changes in pH and spectral properties of the solution, which occur upon ageing, in the relatively slow process of hydrolysis of chromium to higher polymers. Solutions with carbonate to chromium ratios of 2.5 or higher were unsuitable for pillaring due to the formation of extensive amounts of precipitate. For solutions with ratios of 2, hydrolysis was

essentially complete after a reaction time of 36h at 95°C, compared to the respective time of months at 25°C.

The Na-montmorillonite suspension and the hydrolysed chromium solution were mixed while the latter solution was still warm, because the polymers formed at 95°C could undergo rearrangements or perhaps dissociation to smaller aggregates upon additional ageing at room temperature. The mixture was then stirred for 1.5 h and repeatedly centrifuged and washed with de-ionised water until the wash water was colourless. The resulting material was filtered and air dried, followed by calcination in order to be converted to Cr-PILC. The conversion had to be accomplished in the absence of air to avoid chromium oxidation and subsequent loss of chromium in the form of volatile oxides. Cr-PILCs decompose when heated in air above 300°C.

The basal spacings of Cr-PILCs depend on the extent of metal ion hydrolysis, which, in turn, depends on the ratio of carbonate to chromium, hydrolysis time, and hydrolysis temperature, and the overall metal/clay ratio used in the pillaring reaction (reaction stoichiometry). The optimum carbonate to chromium and chromium to clay ratios were found to be 2 and 50 respectively.

The synthesis of PILCs may be affected by various other factors apart from those described above in the synthesis of chromia pillared montmorillonites, such as the nature of the clay. For instance, when highly charged vermiculites are used ($(Mg,Ca,K,Fe^{2+})_3$ $(Si,Al,Fe^{3+})_4O_{10}(OH)_2O$ $4H_2O$), the polyoxocations are not stable and may hydrolyse almost completely in the interlayer region, while a regular pillar spacing has been observed for clays in which the charge varies markedly from interlayer to interlayer, due to the capacity of the oxocations to adopt variable charge through hydrolysis.

PILCs are not yet available in large quantities, hindering this way their potential commercial use. The main reason is that the synthesis and the properties of PILCs are very much dependent on the preparation method as proven from the significant differences in basal spacings arising among different authors for the same clays and which are attributed to the formation of different types of pillaring agents. Furthermore it is common practice to use highly diluted clay slurries during pillaring because of the

diffusional limitations that control the exchange of the initial cations of the smectites by the polymeric cation species, which is unsuitable for large scale production [21]. However, Tichit and Figueras have reported that a competitive ion exchange of the polyhydroxy cations with NH_4^+ indices a homogeneous distribution of the pillars and a well ordered structure independently of the clay particle size and slurry concentration reducing the diffusional limitations [22]. Sanchez et al. have successfully used intermediate aluminium and clay concentrations in the conventional preparation of Al-PILCs [23]. Furthermore Fetter et al. have prepared Al-PILCs from concentrated clay suspensions up to 50 wt % under microwave irradiation (see also section 2.3.4) [24]. This is of great interest for the preparation of commercial PILC catalysts.

2.2.2 Properties of PILCs

2.2.2.1 Porous structure

The final properties of PILCs can be modulated by control of experimental variables in the pillaring solution prior to addition of the clay, during clay addition, and in the manipulations of the post pillaring reactions. Thus PILCs offer a very powerful and flexible way to design new catalysts with a desirable predominant pore size in the approximate range of 5 to 20Å. Zeolites have a more restricted range of pore sizes, varying between 3 to 11 Å. It is therefore possible to use PILC catalysts in the reactions of bulky organic molecules such as coal derived liquids or heavy hydrocarbons whose dimensions are larger than the pore size of zeolites.

The micropore is defined by the interlayer distance, which is the space between the clay layers, and the lateral distance, which is the space between the metal oxide pillars (Figure 2.3). Certain factors have a significant influence on the size of micropores of the pillared clay such as the dimensions and the charge of the pillaring polyoxocation which are dependent on the degree of hydrolysis, the orientation of the pillaring cation between the clay layers, the charge density and distribution of the clay layers [25].

Significant differences in basal spacings, which arise among different authors for the same types of PILCs, are attributed to the formation of different types of pillaring agents due to slight variations in the experimental conditions. Several experimental variables influence the degree of hydrolysis of the metal cation leading to partially

hydrated polymeric or oligomeric metal cation complexes: i.e. pH, concentration of reagents (i.e. metal cation and NaOH or Na_2CO_3 as base), temperature and ageing. Increasing the pH, lowering the concentration, heating or increasing the ageing time of the solution at any specific temperature, all favour the hydrolysis reaction and therefore increase the degree of polymerisation of the metal cation [26]. Hydrothermally treated pillaring solutions (reflux conditions) consist of polymeric metal cation complexes that yield more thermally stable pillared clays and in most cases with larger interlayer spacings. Both could be explained partly by the lower charge per metal ion in the treated solutions as more material is exchanged into the interlayer region of the smectite [27].

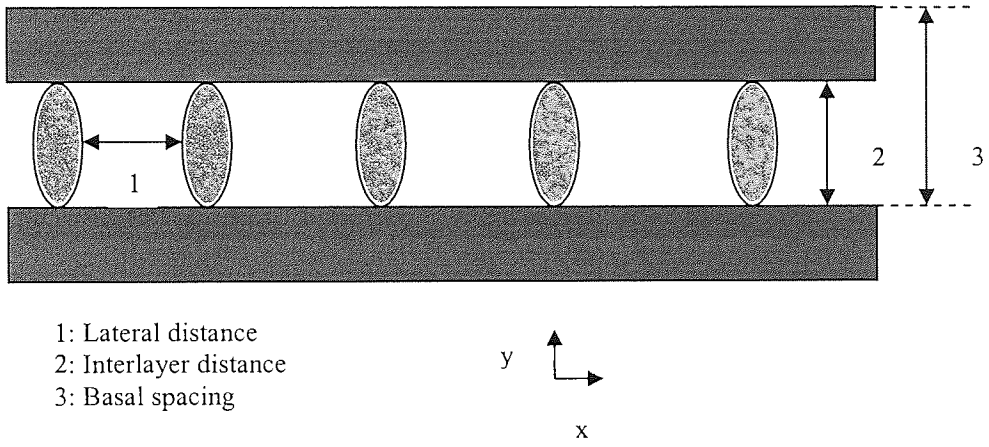

Figure 2.3 Schematic structure of a PILC

The porosity of PILCs also depends on the manner of aggregation of the clay layers. Long-range face-to-face stacking of the silicate layers, which are held apart by regularly spaced pillars results in microporosity comparable to that of zeolites. Short-range (typically 3 to 8) face-to-face stacking of the silicate layers and extensive edge-to-edge and edge-to-face interactions, i.e. a house-of-card structure, lead to the formation of mesopores (20Å <diameter<500Å) and macropores (diameter>500Å) which are characteristic of mixed oxides, aluminas and silicas [28] (Figure 2.4). Those PILCs with a 'house-of-card' structure are known as delaminated clays.

Aston University

Illustration removed for copyright restrictions

Figure 2.4 Schematic representation of a lamellar (face-to-face) and a house-of-cards like aggregation [13]

The manner of aggregation is basically dependent on the nature of the clay. Hectorite and its synthetic analogue laponite which consist of particles less than ca. 100 nm in size have been found to facilitate the preparation of delaminated clay catalysts, while montmorillonites, which comprise relatively large particles, give rise to well-organised pillared clays with the typical 18 Å spacing [28]. However, the type of pores formed

may be manipulated by the drying method used. A freeze-drying procedure promotes edge-to-edge or edge-to-face aggregation and consequently macropores are formed, whereas air-drying promotes only face to face aggregation resulting in formation of zeolite-like structures [21].

2.2.2.2 Thermal stability

The porous structure of PILCs is, in general, stable up to 400-500°C. Further increase in the temperature leads to the collapse of the clay layers because of the dehydroxylation of the pillars followed by dehydroxylation of the clay sheets. Both the nature of the clay materials and the type of metal oxide pillars affect the thermal stability of the resulting PILCs. The most stable clay mineral for pillaring is rectorite, the structure of which is consisted of one montmorillonite like layer and one mica like layer. Its improved thermal stability has been attributed to these mica-like layers [5].

With regards to the metal oxide pillars, two factors appear to control thermal stability: the density of the pillars and their distribution within the layers. A homogeneous distribution of pillars improves thermal stability. In addition, intercalating clay layers by mixed oxide pillars, such as Ga/Al, Ce/Al, Ce/Zr and Nd-Zr also has a beneficial effect [22, 5].

2.2.2.3 Surface acidity

PILCs possess both Bronsted acid (proton donor) sites and Lewis acid (electron pair acceptor) sites. It is believed that Bronsted acidity mainly derives from the clay structural hydroxyl groups, while Lewis acidity is attributed to the metal oxide pillars. The amount and strength of Bronsted and Lewis acid sites are closely related to the types of clays and metal oxide pillars, as well as to the calcination process. For instance, incorporation of aluminium into a chromia pillar increases the surface acidity of the clay [29]. Bronsted acidity decreases markedly with increasing calcination temperature, by either dehydroxylation of the surface or by migration of protons from the interlayer space into the octahedral sheet. Although Lewis acidity is more thermally stable than Bronsted acidity, upon high calcination temperature both Bronsted and Lewis sites decrease [13, 5].

The most common methods to investigate surface acidity in PILCs are by infrared (IR) spectroscopy of adsorbed ammonia or pyridine and temperature programmed desorption (TDP) of adsorbed ammonia [5]. The number and strength of the acid sites can be determined by choosing adsorbed substrates with different basicity. For example 2,6-dimethylpyridine (DMPY) is selectively adsorbed on Bronsted acid sites and hence it can be used for the determination of Bronsted acidity in clays and PILCs.

2.2.3 Applications of PILCs

PILCs are employed in the field of acid-catalysed reactions, i.e. cracking, hydroisomerisation, dehydration, dehydrogenation, hydrogenation, aromatisation, disproportionation, esterification, alkylation and selective catalytic reduction. Other applications related to porosity include membranes for gas separation, ion-exchange, adsorption and control release. Detailed reviews of the catalytic applications of PILCs have been conducted by Figueras [21] and, more recently, Ding et al. [5]. The scope of this section is limited to those applications of PILCs that are relevant to the objectives of the research, i.e. cracking, hydrocracking and hydroprocessing.

Sulfided chromia pillared montmorillonites have exhibited high activity and selectivity in the hydrodesulfurisation of thiophene and the consecutive hydrogenation of butane, whilst the respective activity of the non-sulfided form was considerably lower. In addition the sulfided form of the parent clay sodium montmorillonite, did not exhibit any thiophene conversion. These findings suggest that the finely dispersed and well distributed chromium sulfide phase in the chromia pillared clay is of primary importance for a high thiophene conversion. With respect to the selectivity of these catalysts it was shown that hydrodesulfurisation of thiophene results exclusively in the formation of butane and butenes. No comparison with conventional catalysts has been reported [30].

Many researchers have selected cumene as a model compound for their studies of Cr-PILCs, since the reactions that occur depend on the acid sites of the catalyst. Cumene cracking mainly occurs on Bronsted acid sites, whereas dehydrogenation takes place on Lewis acid sites. However, the reported results with regards to chromia pillared montmorillonite are contradictory. According to Bradley and Kydd, the chromia

pillared montmorillonite exhibited dehydrogenation activity almost exclusively, as the sodium montmorillonite did, with very little benzene being formed (very little cracking) [31]. The increase observed in overall conversion resulted from an increased yield of α-methylstyrene, with no appreciable increase in benzene production.

On the contrary Mishra and Parida [32] have reported that cumene conversion on both sodium montmorillonite and chromia pillared montmorillonite resulted in cracking as well as in dehydrogenation products. The total conversion was higher for the PILC in comparison to that of the parent clay. Mishra and Parida have suggested that the low cumene conversion on the parent clay may be attributed to the low number of acid sites and the unavailability of interlayer pores.

Carrado et al. [33] have reported that adding chromium to a bentonite clay, whether pillared or not, improved the overall behaviour of the catalysts for decane conversion. They used, among others, a chromium-exchanged (not PILC) and a mixed Al/Cr-PILC, but not a Cr-PILC. However, it was not clear how chromium influenced the cracking/dehydrogenation ratio. The PILCs exhibited markedly higher yields of coke. The authors attributed this to the open two-dimensional structure of PILCs, which allows easier access for heavier hydrocarbons, and the abundance of Lewis acid sites, where polycondensation reactions and coke formation typically occur. They suggested the reduction of coke formation in the presence of chromium might be related to the acidity.

Gonzalez et al. investigated the effect of the incorporation of cerium in an Al-PILC with regards to the conversion of n-heptane [34, 35]. It was shown that cerium increases the total conversion and yields high selectivity for cracking of n-heptane, approaching results obtained for the reference zeolite. Gonzalez et al. suggested that the reverse of selectivity towards cracking as opposed to isomerisation in the presence of cerium might indicate the increase in the number of the Bronsted acid centers or in the strength of the acid centers, or both of these factors, since hydroisomerisation requires milder conditions of temperature and acid strength than hydrocracking,

PILCs have been tested as catalysts in cracking of different gas-oils in comparison to commercial zeolites. Three examples are presented below [21]:

- Heavy gas oil (23.9° API, unspecified sulfur content)

Al-PILC, Zr-PILC, amorphous silica-alumina and commercial zeolites (REY) have been compared. Catalytic activities were similar for the PILCs (conversion 71 vol %) and REY (73.5 vol %) and substantially higher than for the amorphous aluminosilicate (55.5 vol %). Gasoline yields were also analogous for the PILC (51.5 vol %) and REY (58.0 %). The octane yield of the gasoline produced by the PILCs (90.5%) was higher than that yielded by the zeolitic catalyst (89%), but the coke formation was higher on the clay (7.1 wt % compared to 4.3 wt %).

- Light gas oil (27.9° API, 0.59 wt% sulfur)

Al-PILCs have been compared to a commercial zeolite catalyst. The gasoline yield was lower on the PILCs (52.5%) than on zeolite (56.6%) at the same conversion of 70%. The coke yield was also higher on the clays (7% on clays versus 3% on zeolites).

- Heavier gas oil (21° API, 2.46 wt% sulfur)

A series of Al-PILCs after steaming at increasing temperatures has been compared to REY zeolites. The PILC activity observed after steaming at 650°C for 17h (81.7 wt %) is higher than that obtained on zeolites steamed at 775°C (72.5 wt %), but the selectivity for gasoline is lower (43.3 compared to 51.3 wt %) and coke formation is higher (15.2 compared to 3.3 wt %). Although steaming caused loss of a large fraction of the surface area of the PILCs, their activity remained high. This was attributed to the presence of diffusional limitations in the kinetics. Furthermore, the high activity observed for the PILCs was probably due to acidity shifting from strong Lewis to strong Bronsted during steaming. Coking formation was influenced by the gravity of the fuel and the sulfur content.

Therefore, PILCs exhibit higher activities than zeolites in cracking of heavy gas oils and slightly lower activities for lighter charges. However, in any case they show slightly lower selectivity for gasoline, although it has an increased octane number, and much higher coke formation compared to zeolites.

Some preliminary results for bitumen conversion on a range of large-pore zeotype catalysts and pillared smectite clays have also been reported [36]. Overall conversions in bitumen were low (< 0.5%). The highest overall conversions were obtained on the acidic MCM-41 and its (more highly acidic) Fe-framework analogue. Montmorillonite-based Al-PILCs and acid-treated clays had little effect on bitumen. However, the

saponite-based Al-PILC was more active compared to the other clays but less than acidic MCM-41, although it had a higher selectivity of aromatics versus aliphatics than MCM-41. Mordenite appeared to hinder bitumen cracking, despite easy accessibility (6.5 x 7.0Å channels).

PILCs with high surface area can also be used as support for hydrogenation metal catalysts to achieve homogeneous dispersion, increased adsorption area of reactants and shape selectivity yielding hydrotreating catalysts. However, the results obtained so far in the field of hydrotreating with metal catalysts supported on PILCs are contradictory. Occelli and Rennard have reported that pillared clays are ineffective when used as the cracking component in composite hydrocracking catalysts because of rapid deactivation due to excessive coke formation [37]. The same authors have obtained an excellent catalyst for hydrocracking of vacuum gas oil by using PILCs as support for Ni-Mo in a composite catalyst promoted with 30% zeolite. No excessive coke formation was found, as the catalytic activity increased with the reaction temperature. This is probably due to the moderation of the PILC acidity resulting from the addition of hydrogenation metals like Mo and Ni (moderate acidity favours desorption of high molecular weight hydrocarbons which otherwise would be retained as coke) and to the open microstructure resulting from pillaring (which appears to control the cleavage of high molecular weight hydrocarbons and retards further hydrocracking to lighter fractions). The coke formation may be suppressed by the interaction of Lewis sites and the hydrogen carrier gas.

On the contrary Ramos-Galvan et al. have reported that in hydrotreating of residual atmospheric gas oil (3.7 wt% sulfur, 11 wt% asphaltenes, 21.5 wt% aromatics, 16%wt polars, 3.5°API) NiMo supported on Ti-PILCs has exhibited superior results compared to a $NiMo/Al_2O_3$ catalyst [38]. At 400°C NiMo/Ti-PILC lowers the asphaltene fraction by 77.2 wt%, while aromatics decrease by 53.5 wt% and polar fractions diminishes by 43.8 wt%. This is about 4.5, 9.3 and 22.5 wt% higher than $NiMo/Al_2O_3$ reference catalysts. The relative hydrodesulfurisation (HDS) rates for NiMo/Ti-PILC are 40.4, 22.8 and 18% HDS/m^2 for sulfur removal in the asphaltene, polar and aromatic fractions, respectively. In the same sequence $NiMo/Al_2O_3$ catalysts give 11.4, 1.6 and 19.6% HDS/m^2. Moreover, the NiMo on Al- and Ti-PILC catalysts caught vanadium impurities which remained on the clay flakes even after regeneration by means of

tetrahydrofuran solvents, refluxing and calcination in air at 380°C, confirming the remarkable property of clays to trap vanadium. This is potentially interesting for many catalytic applications, where vanadium is generally a poison and it must be retained before reaching the other catalytic processes downstream.

Other examples where PILCs are being used as supports for metal catalysts and exhibit better activities than the respective metal catalysts supported on alumina, are presented in the following:

- Hydrogenation of benzene and bigger molecules, such as xylene and mesitylene has been studied on Pt- or Pd-loaded Al-PILC and γ-Al_2O_3. For the benzene hydrogenation the activities were similar for the Pt/Al-PILC and Pt/ γ-Al_2O_3 catalysts. However for xylene and mesitylene hydrogenation, much higher activities were observed for the Pt (Pd)/Al-PILC than for the Pt (Pd)/ γ-Al_2O_3 catalysts due to larger pore size in the Al-PILC than on γ-Al_2O_3. Furthermore, anti-poisoning against sulfur was dramatically improved when using bimetallic loading (Pt-Pd/Al-PILC) [39].
- Hydrogenation of benzene as a probe reaction has been used to investigate the activity of Ni on Al-pillared montmorillonites compared to the respective of a common Ni catalyst on γ-Al_2O_3. The most active catalyst resulted from Al^{3+} ion-exchange of the pillared montmorillonite and subsequent introduction of 12% (w/w) Ni [40].
- Hydroisomerisation of hexanes has been studied with palladium supported on Al-pillared montmorillonite, Al-pillared acid-activated montmorillonite and sulfated Zr-pillared montmorillonite. These catalysts were compared to a conventional 1wt% Pd on γ-Al_2O_3. The Pd on Al-pillared acid-activated montmorillonite and sulphated Zr-pillared sodium montmorillonite were the most active catalysts [41].

Occelli [28] has suggested that delaminated clays in particular could be useful in the preparation of hydrotreating catalysts for the upgrading of heavy oil for two reasons:

- Relatively large size organic molecules, such as aromatic compounds, which are normally too large to enter the micropores formed by the pillars can penetrate the macropores of the delaminated clays where the acidity introduced by the metal oxide clusters causes the conversion to occur.

- Delaminated clays exhibit higher resistance to coke formation compared to pillared clays, probably due to the weaker acidity and the macroporosity of the catalyst which facilitate desorption of aromatics which otherwise would be retained (occluded) as coke.

Pillared and delaminated clays have been used successfully as hydrocracking catalysts for coal derived liquids and a petroleum residue (for conversion data see section 2.4.2). In particular, a tin oxide pillared laponite (delaminated) clay and a chromia pillared montmorillonite have exhibited superior results compared to a presulfided supported $NiMo/Al_2O_3$ catalyst and a dispersed Mo-based catalyst precursor. The pillaring of the clay substrates was considered to better accommodate the larger molecules of the feedstocks in the galleries of the catalyst structures, leading to more efficient catalyst action than interaction with the surface of the alumina catalyst [2, 3]. The activity of chromia pillared montmorillonite was attributed to the redox activity of the chromia pillar which promotes reduction of the organic material in the presence of pressurised hydrogen, coupled with the further increased basal spacing which allows improved access to the active sites. In the case of the tin oxide pillared laponite the catalytic activity was credited to better access to active sites due to the macropores formed, further enhanced by the presence of tin oxide, promoting the activity of these sites, rather than being caused by any intrinsic activity of tin oxide [4].

2.3 Microwave assisted chemistry

2.3.1 Microwave heating

A microwave is a form of electromagnetic energy that falls in the 300 to about 300,000 MHz frequency range of the electromagnetic spectrum. With microwaves the energy transfer is not primarily by conduction or convection as in conventional heating, but by dielectric loss. Thus the tendency of a sample to undergo microwave heating is highly dependent on its dielectric properties, i.e. dielectric loss, dielectric constant and tangent delta.

Dielectric loss (ϵ'') is the amount of input microwave energy that is lost to the sample by being dissipated as heat. This value best provides the coupling efficiency of a particular substance. The dielectric constant (ϵ'), also known as the relative permittivity

measures the ability of a substance to store electric charges and is dependent on both temperature and frequency. Mathematically it is the ratio of the electrical capacity of a capacitor filled with the substance to the electrical capacity of the evacuated capacitor. Tangent delta (tan δ) or loss tangent is the dissipation factor of the sample, high values of which indicate ready susceptibility to microwave energy. It is defined as the ratio of the dielectric loss to the dielectric constant [42, 43].

Most commercial microwave systems are set to a frequency of 2450 MHz. At this frequency the dielectric properties are temperature dependent. In general, as the temperature of a substance increases, its dielectric parameters and consequently its coupling efficiency decrease [43].

High absorbers like small chain alcohols, dimethyl sulfoxide and nitrobenzene all have high dielectric losses. As a result they heat very quickly within the microwave chamber (Table 2.2). Medium absorbers, such as dimethylformamide, acetonitrile, butanols, ketones and water, require more time to reach desired temperatures. Finally chloroform, dichloromethane, ethyl acetate, ethers and hydrocarbons, which are very low absorbing solvents, take much longer to heat up (as liquids) to temperatures above their boiling points [43].

Materials dissipate microwave energy by two fundamental mechanisms: dipole rotation and ionic conduction. Dipole rotation refers to the alignment with the electric field component of the radiation of molecules that have permanent or induced dipoles such as water. At 2450 MHz, the oscillating field causes agitation of the molecules generating heat. The second dissipation mechanism, ionic conduction, is the migration of dissolved ions with the oscillating electric field. Heat generation is due to frictional losses which depend on the size, charge, and conductivity of the ions, and their interactions with the solvent. Ionic conduction increases with temperature allowing ionic solutions to become stronger absorbers as they heat up [43, 44].

Table 2.2 Boiling point, dielectric constant (ϵ'), tan δ and dielectric loss (ϵ'') for common solvents, measured at room temperature and 2450 MHz [43]

Solvent	Normal boiling point (°C)	Dielectric loss (ϵ'')	Dielectric constant (ϵ')	Tan δ
High absorbers				
Ethylene glycol	197	49.95	37.0	1.350
Formic acid	100	42.24	58.5	0.722
Dimethyl sulfoxide	189	37.12	45.0	0.825
Ethanol	78	22.87	24.3	0.941
Methanol	65	21.48	32.6	0.659
Nitrobenzene	202	20.50	34.8	0.589
1-Propanol	97	15.22	20.1	0.757
2-Propanol	82	14.62	18.3	0.799
Medium absorbers				
Water	100	9.89	80.4	0.123
1-Butanol	118	9.76	17.1	0.571
NMP	215	8.85	32.2	0.275
Isobutanol	108	8.25	15.8	0.522
Dimethylformamide	153	6.07	37.7	0.161
Acetonitrile	82	2.32	37.5	0.062
Acetone	56	1.12	20.7	0.054
Acetic acid	113	1.08	6.2	0.174
Low absorbers				
Chloroform	61	0.44	4.8	0.091
Dichloromethane	40	0.38	9.1	0.042
Ethyl acetate	77	0.35	6.0	0.059
Tetrahydrofuran	66	0.35	7.4	0.047
Chlorobenzene	132	0.26	2.6	0.101
Toluene	111	0.1	2.4	0.040
o-Xylene	144	0.05	2.6	0.018
Hexane	69	0.04	1.9	0.020

2.3.2 Microwave assisted chemistry-Accelerated reaction rates

The initial use of the microwave oven in the early 1980s was limited to rapid sample preparation in certain sectors of analytical chemistry. Since then interest has grown in the application of microwave irradiation to reaction chemistry. Several detailed reviews of microwave assisted chemistry have been published, displaying the huge potential of microwaves for chemical synthesis [43, 44]. Virtually all types of thermally driven chemical reactions (additions, cycloadditions, substitutions, eliminations, fragmentations etc.) either in the presence or absence of solvent can be accelerated by microwaves.

Organic synthesis in aqueous media can be conducted under microwave irradiation [43]. Under normal conditions water maintains a very high dielectric constant and persistent hydrogen bonding. In a contained environment (sealed vessel) as the temperature of water increases above its boiling point more and more pressure builds up and water begins to act more like an organic solvent. It changes from a very polar liquid to an almost non polar one and organic compounds become more soluble. With these enhanced conditions water has increased acidity, reduced density and a lower dielectric constant.

Microwave technology can be very useful for chemical processing, because reactants are heated directly. This means that energy is absorbed solely by the reagents and catalysts, and is not wasted on heating the reaction vessel, leading to a reduction of the total processing time, no overheating and degradation of the product, reduced equipment size, faster response to process heat control and faster start-up, increased production and elimination of process steps [45]. These benefits of microwave heating in many cases overcome the higher cost of microwave energy. In addition flow-through microwave heating will allow continuous chemical processing.

Enhancements in rates of homogeneous reactions through superheating of solvents under microwave irradiation were first reported by Mingos and Baghurst [46]. They attributed this to elevated boiling points, 13 to 26°C above the conventional atmospheric boiling points, exhibited by the majority of organic solvents under microwave irradiation (Table 2.3). According to Mingos and Baghurst microwave power is dissipated over the whole volume of the solvent, where nucleation points necessary for boiling are absent. The loss of the excess of thermal energy by boiling can therefore only occur at the side of the reactor or at the solvent/air interface. This results in a reversed temperature profile with a steady average reflux temperature above the classical boiling point, which is called superheating or superboiling. If superheating is avoided such that the reaction is conducted at conventional reflux temperatures, then the rate of the reaction is independent of heating method [46, 45].

Table 2.3 Boiling points (atmospheric) for common solvents relevant to microwave applications [46]

Solvent	Normal boiling point (°C)	Elevated boiling point (°C)	Δ T
Water	100	104	4
Acetone	56	81	25
Acetonitrile	82	107	25
Ethanol	78	103	25
Methanol	65	84	19
p-xylene	140	170	30

When a heterogeneous reaction is conducted using a dissipative and/or catalytic solid phase under microwave heating, the reaction rate increases compared to classical heating under the same conditions (pressure, temperature and reagents concentration). The increase in reaction rate corresponds to a virtual difference in reaction temperature [45, 47]. Since the bulk temperature is equal for both the conventional and microwave heated systems, there must be an elevated temperature at the local reaction site: the catalytic surface. This is possible since the heat transfer by microwaves depends on the specific loss factor of the different materials: the catalyst and the solvent. Many metallic catalysts are semiconductors and will readily absorb microwave energy especially at higher temperatures. This selective increase of reaction rates cannot be achieved by conventional heating since the catalysts and reagents will be both at the same temperature.

Chemat and Esveld used a continuous flow microwave reactor in two different set ups to prove the essential combination of microwave and catalyst [45]. In the first experimental set-up the solid catalyst was submitted to microwave irradiation and the liquid was heated when it passed through the catalyst, whereas in the second experiment, only the liquid was heated by microwaves when it circulated in the cavity vessel and the catalyst was placed outside the microwave cavity. The temperature was maintained and checked to be constant throughout the circuit. They also conducted a third experiment in a conventional continuous reactor operating under the same conditions (temperature, concentration and pressure) as the microwave continuous reactor. Only direct heating of the catalyst by microwaves gave an increase of initial esterification reaction rate of 150%. Conventional heating of the catalyst vessel and microwave heating with the catalyst outside the cavity gave identical results because

the temperature at the catalytic surface was equal to the bulk temperature.

Leskovsek et al. [48] have reported an up to eight times greater reaction rate with microwave irradiation compared with conventional heating at the same temperature on the catalytic transfer hydrogenation of soybean oil from an aqueous sodium formate solution in the presence of Pd/C. They assumed that rapid mixing of the contents assured the uniformity of the bulk temperature in the laboratory reactor and excluded hot spots. They suggested instead that microwave heating may have assisted transport phenomena at the catalysts and oil-water interfaces.

A pressurised environment can be very advantageous to many different kinds of chemistries. The group of Gedye was one of the first to report that the increased reaction rates found in the microwave oven syntheses were the result of superheating of the reaction mixture which led to pressure increase in the reaction vessel. They demonstrated that organic compounds can be synthesised up to 1240 times faster in sealed Teflon vessels in a microwave oven than by conventional (reflux) techniques [49]. Solvents under microwave irradiation can be heated in a contained environment up to temperatures that are two to four times their respective boiling points. This characteristic of microwave synthesis provides the large rate enhancements (up to 1000x) that are observed [43]. Pressurised environments can also provide inert atmospheres for use of air-and moisture-sensitive reagents [43].

Although microwave irradiation is becoming a common source of energy in accelerating chemical reactions, it is difficult to include reactions requiring both high temperatures (>200°C) and pressures (>250 psig), basically because of the limitations of microwave-transparent materials. Microwave vessels are usually made from polymers or quartz and can therefore sustain only limited temperatures and pressures, whereas metal is not appropriate for vessels, since it is not a microwave-transparent material. These temperature and pressure limitations have hindered the application of microwave heating in the field of hydrocracking coal derived liquids and hydrotreating biomass derived liquids and heavy petroleum residues.

2.3.3 *The nature of the microwave effect*

Since the first publications on accelerated microwave-assisted synthesis reactions, there has been discussion about the source of the rate enhancements observed. Speculations about non-thermal "microwave effects" have been made. However, within the microwave region of electromagnetic energy (i.e. 300 to 300,000 MHz), only molecular rotation is affected, not molecular structure. The energy in microwave photons (0.037 kcal/mole) is very low relatively to the typical energy required to cleave molecular bonds (80-120 kcal/mole). Therefore, microwaves would not be expected to affect the structure of a molecule. In the excitation of molecules the effect of microwave absorption is purely kinetic [43].

Based on the Arrhenius reaction rate equation ($k=Ae^{-Ea/RT}$), the reaction rate constant is dependent on two factors: the frequency of collisions between molecules that have the correct geometry for a reaction to occur (A) and the fraction of those molecules that have the minimum energy required to overcome the activation energy barrier ($e^{-Ea/RT}$). There has been some speculation that microwaves affect the orientation of the molecular collisions and the activation energy, but there is no evidence that supports either of these ideas. Microwave energy will affect the temperature parameter in the Arrhenius equation. An increase in temperature causes molecules to move about more rapidly, which leads to a greater number of more energetic collisions. This occurs much faster with microwave energy, due to the high instantaneous heating of the substances and is the primary factor for the observed rate enhancements [43].

The level of instantaneous heating will be dependent on the amount of microwave energy that is used to irradiate the reactants. The higher the level of microwave energy the higher the instantaneous temperature will be with regards to the bulk temperature. Recent experimentation has shown that simultaneous cooling of the reaction vessel during a reaction will ensure a constant, high power level for direct molecular heating. This has dramatically improved reaction rates and nearly doubled the percentage yields of some lower yielding reactions [43].

Reactions with temperature sensitive reagents can also be accelerated under microwave irradiation by using a non polar solvent as a heat sink. As microwaves are being added

to a reaction, the non polar solvent, which is not interacting with the irradiation, will help to draw away the thermal heat being produced from the polar reagents. The reaction is still receiving activation energy, but its internal temperature will remain low. Simultaneous cooling of the microwave cavity can benefit this reaction condition and ensure a constant high power level.

2.3.4 Microwave assisted catalyst preparation

Microwave irradiation has been applied in the production of supported catalysts resulting in changes in their catalytic activity.

- Crystalline alumina and silica supported palladium hydrotreating catalysts prepared under microwave conditions exhibited improved catalytic activity over their conventionally prepared counterparts, despite a reduction in surface area. This indicates that microwave irradiation modifies crystal morphology leading to enhanced activity of each site to such a degree that the loss of surface area is negated [50].
- A 0.3wt% Pt/Al_2O_3 catalyst containing 0.95% chlorine prepared under microwave irradiation showed a permanent increase by a factor of 2 in the isomer selectivity of 2-methylpentane compared to that of the conventionally prepared catalyst [51]. This has been attributed to a permanent surface modification of the metal or a permanent metal-support interface modification (between the metallic crystallites and the support) probably caused by localised heating due to microwave irradiation. A 0.3 wt% Pt- 0.3 wt% Re/Al_2O_3 exhibited different distributions of hexane products according to the heating mode during preparation and reaction. It has been suggested that the enhancement of the amount of extensive cracking (methane) under microwave conditions could be due to the formation of a Pt-Re alloy, whereas the small demethylation fraction (methane plus pentane) decrease could be related to the presence of chlorine, which is known to affect the geometrical distribution of the initial 2-methylpentane molecules over the metal and support during the reaction [51].

Microwave irradiation has also been applied in the synthesis of PILC catalysts, which in general are prepared by exchanging the native cations of the clay with partially hydrated polyoxometal cation complexes.

- Microwave assisted Al-PILCs were prepared faster and showed better reproducibility and 20-30% higher surface area than those prepared conventionally [52]. This result indicated that the pillaring distribution was homogeneous. However, it was not possible to determine if more pillars really were introduced into the clay particle with microwave irradiation. In addition, Al-PILCs from highly concentrated clay suspensions (up to 50 wt%) and highly concentrated aluminium solutions were successfully synthesised under microwave irradiation [24].
- Microwave assisted Zr-PILCs exhibited the same surface areas and acidity features compared to the conventional ones with the advantageous reduction of synthesis time from 18h to 10-30 min [53].
- Microwave assisted Ti-PILCs showed higher stability of the layer stacking and more homogeneous pillar distribution with respect to their conventional counterparts [54]. CoMo catalysts supported on the microwave assisted Ti- and Al-PILCs displayed higher activity in the hydrodesulfurisation of heavy vacuum gas oil compared to that of CoMo catalysts supported on conventionally prepared PILCs. This could be attributed to the particular structure and textural features of the solids prepared by microwave methods (more homogeneous distribution of pores) [54].

Tin oxide pillared laponite belongs to another type of PILCs that is prepared by intercalation of organotin compounds within the interlayer region of the clay and subsequent removal of the organic fragments to form tin(IV) oxide pillars. The application of microwave irradiation in this case has reduced preparation time from one week under ambient conditions to 5 min [55].

2.3.5 Catalytic transfer hydrogenation and catalytic cracking

Microwave heating has been applied in the performance of catalytic transfer hydrogenation reactions. β-lactams, sterols and bile alcohols have been reduced to their corresponding saturated derivatives by hydrogen abstraction from a donor molecule (ammonium formate) assisted by catalysis (Pd/C or Raney nickel) at elevated temperatures without the need for high pressure hydrogen and decreasing reaction times to minutes [56, 57]. Similarly benzaldehyde has been reduced to benzyl alcohol in the presence of formic acid as hydrogen donor and a ruthenium(II) complex as catalyst

[58]. However, these reactions are limited to relatively small molecules with few double bonds.

The following cracking reactions have been successfully performed under microwave irradiation:

- Catalytic cracking of hydrocarbons, e.g. conversion of methane to ethylene and hydrogen [59]. The conversion is highly endothermic. The process involves the utilisation of an appropriate catalyst providing catalytic sites for the hydrocracking reaction, which is capable of absorbing microwave irradiation. A preferred group of such catalysts is particulate metal powders such as Fe, Ni, Co and their mixtures. The methane gas is introduced into the reaction zone under pressure, typically between 0.3 and 1.0 atmospheres. It is brought into contact with the metal powder catalyst and subjected to a pulse train of microwave irradiation for a sufficient period of time to effect conversion. It is important to note that hydrocarbons, such as methane, do not usually have the capability of absorbing microwave radiation. Thus irradiation of methane in the absence of a catalyst does not selectively yield ethylene and hydrogen.
- Decomposition of methane over carbon at atmospheric pressure yielding acetylene [60]. Methane is known to chemisorb well on carbon at high temperatures. It has also been observed that carbon is an excellent absorber of incident microwave energy and can efficiently convert it into thermal energy. Sensible use of incident time, irradiation time, initial methane and hydrogen pressure can result in high acetylene production and selectivity.
- Retorting of Australian shales [61]. Australian shales is a family of hydrocarbon bearing minerals closely related to coals but containing a higher ash and hydrogen content. It was shown that a higher quality product than that achieved by conventional heating could be obtained with microwave heating, shifted towards light hydrocarbons and containing lower heteroatom content (sulfur and nitrogen), while maintaining high yields. The production of higher percentages of the lighter fractions from microwave retorted shale could be associated with cracking of the heavier fractions in regions of the retort where micro-arcing between shale particles occurred, or at other regions of plasma formation where the local temperatures would be considerably higher than the measured bulk temperature, and would be expected to be higher than 1000°C.

Recently, radio frequency heating has been applied successfully in the catalytic cracking of gas oils in a three-phase spouted-bed catalytic reactor with zeolitic catalysts producing lower alkenes and aromatics. In this technique, similarly to microwave heating, heat is generated in the catalyst held in the electromagnetic field and thermal energy is dissipated to the surroundings of the catalyst volume preventing carbon formation by eliminating secondary reactions. Energy transfer from the radio frequency field to the reaction was solely dependent on the dielectric properties of solids in the reactor, effectively the catalyst or transient carbon [62].

2.3.6 Summary

Microwave energy is absorbed solely by the reagents and catalysts, and is not wasted on heating the reaction vessel, leading to a reduction of the total processing time, no overheating and degradation of the product, reduced equipment size, faster response to process heat control and faster start-up, increased production and elimination of process steps [45]. The energy transfer occurs by dielecetric loss and not by conduction or convection as in conventional heating. Thus the tendency of a reagent to undergo microwave heating is highly dependent on its dielectric properties, i.e. dielectric loss, dielectric constant and tangent delta.

Enhancements in rates of homogeneous reactions at atmospheric pressure have been attributed to superheating of solvents (elevated boiling points, 13 to 26°C above the conventional atmospheric boiling points) under microwave irradiation. In addition, the large rate enhancements (up to 1000x) observed for chemical reactions occurring in a contained environment under microwave heating [43] have been credited to the solvents' ability to be heated up to temperatures that are two to four times their respective boiling points. If superheating is avoided such that the reaction is conducted at conventional reflux temperatures, then the rate of the reaction is independent of heating method [46, 45].

Enhancements in rates of heterogeneous reactions conducted using a dissipative and/or catalytic solid phase under microwave heating, compared to classical heating under the same conditions (pressure, temperature and reagents concentration), have been attributed to a virtual difference in reaction temperature [45, 47]. Since many metallic

catalysts are semiconductors, they will readily absorb microwave energy resulting in localised heating above the normal bulk temperature. This selective increase of reaction rates cannot be achieved by conventional heating since the catalysts and reagents will be both at the same temperature. Leskovsek et al. [48] have attributed an eight times increase in the reaction rate of the catalytic transfer hydrogenation of soybean oil in the presence of Pd/C under microwave irradiation compared to conventional heating at the same temperature to microwave assisted transport phenomena at the catalysts and oil-water interfaces. They assumed that rapid mixing of the contents assured the uniformity of the bulk temperature in the laboratory reactor and excluded hot spots.

These significant rate enhancements have raised discussions about their source and speculations about non-thermal "microwave effects". However, the energy in microwave photons (0.037 kcal/mole) is very low relatively to the typical energy required to cleave molecular bonds (80-120 kcal/mole). Thus, microwaves would not be expected to affect the structure of a molecule. In the excitation of molecules the effect of microwave absorption is purely kinetic [43]. Microwave irradiation does not affect the activation energy but provides the momentum to overcome this barrier and complete the reaction faster than conventional heating methods. Microwave energy will affect the temperature parameter in the Arrhenius equation ($k=Ae^{-Ea/RT}$). An increase in temperature causes molecules to move about more rapidly, which leads to a greater number of more energetic collisions. This occurs faster with microwave energy, due to the high instantaneous heating of the substances and is the primary factor for the observed rate enhancements [43].

Microwave irradiation has been applied to the production of supported catalysts and has reportedly resulted in changes in their catalytic activity. For instance it seems that microwave irradiation has modified crystal morphology in crystalline alumina and silica supported palladium hydrotreating catalysts leading to enhanced activity of each site to such a degree that the loss of surface area is negated. Nevertheless, these changes in morphology, which lead to changes in catalytic activity, may well be a result of localised heating.

Microwave heating has been also applied to catalytic transfer hydrogenation and cracking reactions. However, these reactions are limited to relatively small molecules.

Although microwave irradiation is becoming a common source of energy in accelerating chemical reactions, it is difficult to include reactions requiring both high temperatures (>200°C) and pressures (>250 psig), basically because of the limitations of microwave-transparent materials. Microwave vessels are usually made from polymers or quartz and can therefore sustain only limited temperatures and pressures, whereas metal is not appropriate for vessels, since it is not a microwave-transparent material. These temperature and pressure limitations have hindered the application of microwave heating in the field of hydrocracking coal derived liquids and hydrotreating biomass derived liquids and heavy petroleum residues.

2.4 Catalytic hydrocracking of coal derived liquids

2.4.1 Introduction

Coal is a combustible, sedimentary, organic rock, composed mainly of carbon, hydrogen and oxygen. It is formed from vegetation, which has been consolidated between other rock strata and altered by the combined effects of pressure and heat over millions of years to form coal seams [63].

The degree of change undergone by a coal as it matures from peat to anthracite is known as coalification and influences significantly its physical and chemical properties (Figure 2.5). It is referred to as the 'rank' of the coal. Low rank coals, such as lignite and sub-bituminous coals are typically softer, friable materials with a dull, earthy appearance. They are characterised by high moisture levels and low carbon content, and therefore low energy content. Higher rank coals are generally harder and stronger and often have a black vitreous lustre. They contain more carbon, have lower moisture content, and hence higher energy content [63].

Coal and microwave heating

There are various receptive functionalities within as-mined coal, both organic and mineral in nature. For example, on heating the pyrite present within coal it decomposes to a non-stoichiometric FeS_x, which under irradiation experiences dielectric loss and as a result heats the surrounding matrix by thermal conduction. Monsef-Mirzai et al. have showed that mixtures of middle rank British coals with transition metal oxides (e.g. CuO, Fe_3O_4) or coke heat rapidly in the microwave oven and induce coal pyrolysis on a

time scale of 1-3 min [64]. This microwave-driven pyrolysis is not directly comparable with conventional pyrolysis methods (e.g. wire mesh, fluidised bed). Chars, the solid products of coal pyrolysis, will heat rapidly in a microwave field and induce the pyrolysis of sub-bituminous coals [65]. Sorption of SO_x and NO_x (emitted from coal combustion) in a char bed which is then subjected to microwave treatment has been reported to reduce the oxides to elemental sulfur and dinitrogen, resulting up to 98% removal of these pollutants from the flue gas stream [65].

Figure 2.5 Types of coal [66]

Coal liquefaction

The investigation of methods to produce liquid fuels from coal, i.e. coal liquefaction, has a long history. In most processes, a heavy hydrocarbon liquid is produced and subsequently refined. There are two key liquefaction methods:

- direct coal liquefaction, where coal is converted to liquid fuel in a single process
- indirect coal liquefaction, where coal is first gasified and then converted to liquid products by a process of synthesis.

The only commercial scale coal liquefaction process currently in operation worldwide is the indirect Sasol (Fischer-Tropsch) process. South Africa leads the world in coal liquefaction technologies and currently supplies about a third of its domestic liquid fuel

requirements from coal. China is experiencing growth in coal liquefaction aiming to utilise its enormous coal reserves and reduce dependence on imported oil [63].

A two-step direct liquefaction process was developed by British Coal at the Point of Ayr Coal Liquefaction Pilot Plant. During this process an extract is produced in the first step and hydrogenated in the second. During production extracts may undergo some thermal degradation due to the occurrence of secondary reactions, such as cracking, hydrogenation and repolymerisation [67]. These secondary reactions are responsible for the observed differences in hydrocracking reactivities of extracts from the same coal prepared under different reaction conditions such as residence time.

2.4.2 Catalytic hydrocracking of coal liquids

The concept of polynuclear aromatic ring systems embedded in molecules held together by various types of bridging systems, including etheric, aliphatic, hydroaromatic and alkyl-aromatic structures is generally used to describe coal derived liquids. They contain complex, large molecular weight materials, incorporating heteroatoms and other polar groups. Usually, these materials are catalytically upgraded under intense reaction conditions, at high temperatures and hydrogen pressures and in the presence of a catalyst. The overall performance of a hydrocracking catalyst is assessed in terms of conversion, molecular mass reduction (e.g. by size exclusion chromatography, UV-Fluorescence spectroscopy, Maldi MS), polynuclear aromatic ring system reduction, heteroatom removal (by elemental analysis) and resistance to deactivation [2, 3].

Catalysts commonly used in the hydrocracking of coal derived materials (e.g. $NiMo/Al_2O_3$,) have mostly been designed for use with light petroleum fractions. However, due to the higher concentrations of polynuclear aromatic structures and heteroatoms (N, S, O) and the lower hydrogen-to-carbon ratios and higher asphaltene contents of coal derived liquids compared to light petroleum derived fractions the catalysts experience a loss of activity and selectivity with time. Carbonaceous material builds up rapidly on the catalyst particles from the start of the run and typically over about the first 10-100 h of operation, resulting in deactivation [67, 68, 69, 70 and cited references]. After that the mass of carbonaceous deposit on catalyst particles appears to stabilise and the proportion of elemental carbon in the deposit slowly increases [71]. It

is thought that bridging structures between polynuclear aromatic ring systems break down during hydrocracking and the larger polynuclear aromatic groups liberated by the hydrocracking process deposit on the catalyst surface [2].

The continued decline in activity after the carbon content has reached a relatively constant value is attributed to the accumulation of contaminant metals, which is a slower process than the build up of carbonaceous material. There are several reasons causing loss of activity such as coverage of active sites by coke and by trace metals, increased diffusional restrictions due to pore filling or blocking by the deposition of coke and trace metals, and poisoning of active sites by the adsorption of heterocyclic compounds, thus reducing the number of active catalytic sites [72, 73].

Some of the trace metals that are present in the coal liquids before the hydrocracking stage deposit on the catalyst, causing irreversible deactivation. Therefore, the mineral matter in the coal should be minimized and this is achieved by the deashing process. It has been suggested that the decline in activity due to carbon deposition can be reduced by removing the more intractable material from the feed. Feeds with high concentrations of nitrogen-containing species, toluene insolubles, or preasphaltenes induce rapid deactivation in addition to higher levels of carbon deposition [74, 75, 76]. Furthermore, asphaltenes and preasphaltenes not converted to lower molecular mass material become increasingly more intractable with successive hydrocracking [77, 78, 79]. Non-deashed coal liquids have also been found to cause faster and more severe catalyst deactivation during hydrocracking than their deashed counterparts [75, 76]. It is clear that the nature of the feed strongly influences the activity, rate and level of carbon deposition during the early life of hydrocracking catalysts.

Martin and Snape have demonstrated the feasibility of removing the more intractable material from a typical coal extract solution prepared with hydrogenated anthracene oil by precipitation with toluene both prior to and after filtration [70]. As a result a 50% removal of THF insolubles and a 10-fold reduction in trace metal content concentration occurred, leading to improved conversions in both batchwise and continuous hydroprocessing tests through lower levels of carbon deposition and consequently smaller losses of surface area.

Changes in catalyst design leading to larger pore sizes that would be able to accommodate large coal derived molecules may also result in improvements in the process. Previous work by Song et al. has shown the importance of increasing pore size in catalysts [80, 81]. Asphaltene and preasphaltene conversion and heteroatom removal were dependent on the pore size distribution of NiMo catalyst. At 425°C under 4.9 MPa hydrogen pressure, conversions increased with catalyst pore diameter up to 290Å for the asphaltenes and up to 730Å for the preasphaltenes. These observations were interpreted in terms of resistance to the diffusion of large molecular mass materials in relatively small pores.

A comprehensive review on hydroprocessing catalysts has been conducted by Furimsky and Masoth [82]. Briefly, two approaches have been employed in research to develop new hydroprocessing catalysts with improved performance:

- Modification of γ-Al_2O_3 supports or use of other oxides as the support, while using the same active metals (Co/Ni and Mo/W).
- Modification of the active phase by adding other metals, such as the platinum group metals.

Highly efficient Co/Mo and Ni/Mo hydroprocessing catalysts with extremely high surface area can be prepared using alumina hydrogel or phosphated alumina hydrogel. The addition of boron to $CoMo/Al_2O_3$ and $NiMo/Al_2O_3$ catalysts significantly improved hydrodesulfurisation (HDS) as well as hydrogenation activity. The addition of fluoride to a NiW/Al_2O_3 catalyst resulted in a marked improvement in hydrodenitrogenation (HDN) activity, whereas the addition of 0.6 wt.% P_2O_5 increased its hydrogenation activity [82 and cited references].

RuS_2 and RhS_2 were more active than MoS_2 during simultaneous HDS, HDN and hydrodeoxygenation (HDO) of a coal-derived naphtha. However, in order to be cost competitive with the commercial Co(Ni)/Mo(W) catalysts, the content of the noble metal in the catalyst would have to be less than 1%. Furthermore, supports with higher acidity than γ-Al_2O_3 are required to achieve a desirable sulfur tolerance. A Ru/zeolite catalyst containing 0.77% Ru has been compared with a commercial $CoMo/Al_2O_3$ catalyst during hydroprocessing of a coal-derived naphtha between 275 and 400°C. The former was much more active for HDN, whereas the commercial catalyst exhibited

better HDS activity. Some progress is being made in developing sulfur tolerant noble metal-based catalysts enabling processing the feeds containing up to 1000 ppm of sulfur [82 and cited references].

Metal-containing carbides, nitrides, oxynitrides and oxycarbonitrides have attracted attention. Nevertheless, commercial catalysts based on metal nitrides and carbides still need to be developed and their long term performance under commercial operating conditions has to be demonstrated [82 and cited references].

Bodman et al. [2] recently described a screening study for testing the effectiveness of a set of Al-, Cr- and Sn-pillared clays, as well as polyoxo-vanadate and molybdate layered double hydroxides as catalysts in hydrocracking coal liquefaction extracts. The hydrocracking activities of these catalysts were compared with that of a commercial supported pre-sulfided $NiMo/Al_2O_3$ catalyst for short contact (10 min) runs.

All the pillared clays exhibited higher conversion than the conventional supported $NiMo/Al_2O_3$ catalyst, which does not become active until after 10 min reaction time according to the study by Begon et al. [69]. The results were particularly impressive for the Sn laponite with 70% conversion without inclusion of deposits (i.e. material with b.p.>450°C), but only 28% with inclusion of deposits. The Cr-montmorillonite calcined at 500°C showed surprisingly lower conversions than expected (34.6 and 17.7% without and with inclusion of catalyst deposits respectively), but gave the greatest overall shift to smaller molecular masses. Nevertheless, based on the overall performance, the Sn-laponite and the Cr-montmorillonite calcined at 500°C were seen to be the most efficient in terms of molecular mass reduction and general improvement of hydrocracking product quality [2]. These two catalysts, as well as the conventional NiMo on alumina and the dispersed molybdenum catalyst were selected by Bodman et al. for longer time trials (120 min) with several different coal extracts and a petroleum vacuum residue [3].

Point of Ayr coal extract

The two pillared clays produced greater shifts of the size exclusion chromatography (SEC) profiles to longer times, i.e. smaller molecules, than did either $NiMo/Al_2O_3$ or the dispersed molybdenum catalyst. The conversion data for $Mo(CO)_6$ and $NiMo/Al_2O_3$

support this conclusion but only marginally. The 3 x 120 min conversions with deposit (49.6 and 59.0 for the pillared clays vs 36.9 and 47.2 for the supported and dispersed catalysts) do not indicate the more pronounced shifts to longer elution times (smaller molecules) observed for the pillared clays [3].

Pittsburgh No. 8 (high rank coal, 83.2% C) extract

67.6% of materials with boiling point above 450°C were converted into lower boiling fractions after only 10 min, and up to 83.6% was converted after 2 h.

Illinois No. 6 (middle rank coal, 77.7% C) extract

Only 24.6% of the high boiling materials (>450°C) were converted into lighter fractions after 10 min, and 73.4% after 2 h.

These results agree with Zhang's previous study [68] suggesting that polynuclear aromatic ring systems and large molecular weight materials in high rank coal extract are more stable to break-down than those in lower rank coal extract.

Petroleum vacuum (Petrox) residue

Both products from NiMo and the Sn laponite catalysts had significantly smaller molecular weights (MW) than the original Petrox residue. The smallest MW distribution was obtained with the Sn-laponite. The overall extent of reaction was enhanced with increasing reaction time from 10 to 120 min. The supported catalyst exhibited satisfactory results, but it was surpassed by both pillared clays. These data confirmed the high efficiency of the Sn-laponite already detected after 10 minutes and indicated that the Cr-pillared clay performs much better at longer reaction times [3].

All catalysts appeared to be coated by a heavy, insoluble material, which did not appear to change in concentration with reaction time. The novel pillared clay catalysts performed at least as well as either the commercial NiMo on alumina or the dispersed $Mo(CO)_6$ catalysts in hydrocracking of coal liquids from a pilot or laboratory scale plant and in the hydrocracking of a petroleum residue. The high efficiency of these pillared clays was attributed to their high basal spacings which allow the adsorption of large molecules, their strong acid sites suitable for the cracking of hydrocarbons and their thermal stability. Furthermore, the redox efficiency of transition metal oxides

intercalated between the layers could potentially create catalytic hydrogenation. Nevertheless, further investigations are needed before confirming their potential commercial application, to allow conversion of the intractable portions of coal liquids and vacuum residues from petroleum processing, into useful products.

2.5 Catalytic hydrotreating of bio-oil

2.5.1 Introduction

When biomass is heated in the absence of air, it decomposes to a gas, a liquid and a solid. The proportions of the main products can be influenced by controlling the temperature, rate of heating, and vapour residence time. Biomass fast pyrolysis is conducted at temperatures of typically 500°C, very high heating rates and short hot vapour residence times of typically less than 1 s. It maximises liquid yields at up to 75 wt.-% on a dry feed basis [83].

The liquid product, often referred to as bio-oil, is similar to biomass in elemental composition and is composed of a very complex mixture of oxygenated hydrocarbons [83]. It has higher energy density compared to raw biomass, is easily transportable and offers the possibility of de-coupling conversion and utilisation processes. However, during storage for extended periods at ambient or elevated temperature bio-oil exhibits a significant increase in its viscosity. This is attributed to polymerisation, esterification and etherification reactions, induced by the high oxygen content [84] and apparently catalysed by the char particles present in the bio-oil [85].

The extent to which the properties of bio-oil change over a certain period of time is very important for fuel applications [86]. For example, polymerisation reactions result in high viscosity and slower combustion [87]. On the other hand preheating of bio-oil in order to reduce its viscosity could lead to possible physical or chemical transformations due to water and volatiles components' loss. The addition of methanol to the bio-oil has proven to hinder these polymerisation reactions and has an even more significant effect when added before storage at high temperature [84].

Combustion tests indicate that bio-oil burns effectively in standard or slightly modified boilers and engines with rates similar to those for commercial fuels, although it has

heating values of only 40–50% of that for hydrocarbon fuels [88]. However, combustion of bio-oil without upgrading faces a range of problems. Bio-oil's high water content is detrimental for ignition. The organic acids present are highly corrosive to common construction materials, whereas high concentrations of submicron char particles can block injectors or erode turbine blades [83, 88]. In order to address these concerns and problems, research is conducted on upgrading bio-oil to products that more closely resemble conventional fuels.

2.5.2 Full catalytic hydrotreating

Catalytic hydrotreating of bio-oil has been developed based on the conventional hydrotreating process of the petroleum refinery industry and proposes the deoxygenation of the liquid under high hydrogen partial pressure (70 to 200 bars) using traditional hydrodesulfurisation catalysts (NiMo or CoMo supported on alumina). Under these reaction conditions oxygen is eliminated as water with simultaneous hydrocracking of large molecules and hydrogenation of double bonds [89]. The produced hydrocarbons can, in principle, either be used directly for firing a turbine or engine, or produce orthodox transport fuels via a conventional refining process consisting of established catalytic operations such as reforming, alkylation and hydrotreating [90].

Hydrotreating of bio-oil can be conceptually characterized as:

$$C_6H_8O_4 + 6\ H_2 \rightarrow 6CH_2 + 4H_2O$$

This is a carbon limited system and gives a maximum stoichiometric yield of 58 wt % on liquid bio-oil or a maximum energetic yield of about 50 wt % ignoring the significant hydrogen generation requirement [90, 83].

One of the advantages of full hydrotreating, i.e. less than 2 wt % oxygen in the final product, is that the product water readily separates from the hydrocarbon product, tending to strip out the alkali metals present, for example in ash and resolve one of the problems in using biomass derived fuels in turbines and, moreover, is relatively clean at high levels of de-oxygenation [83].

Catalytic hydrotreating of bio-oil, in particular, is a two stage process consisting of a stabilisation stage at lower temperatures (*ca.* 250-280°C) aiming to the elimination of

more reactive molecules such as aldehydes, ketones and alkenes, followed by full refining (350-400°C) with elimination of stable oxygenated molecules such as phenols and furans [91]. Without initial stabilisation bio-oil rapidly polymerises and cokes the catalyst. The process can be also performed in a single step by means of a non-isothermal continuous catalytic bed reactor [92].

Most petroleum hydrotreating is performed in continuous feed, downflow, fixed-bed (trickle-bed) reactors. In contrast catalytic hydrotreating of bio-oil was originally investigated in a continuous feed, fixed bed catalyst system with an upflow configuration [91]. Baldauf and Balfanz have reported that during catalytic hydrotreating tests in a continuous bench scale unit and a process development unit severe deactivation of the catalyst was observed after 100 h of operation leading to coking and plugging short time after [93]. Variation of catalyst and flow direction did not improve the performance. This has been contradicted by Elliott and Neuenschwander [94] who managed to overcome non-steady operations plaguing the experiments by redesigning the continuous feed reactor system from upflow to downflow configuration. Hence, the best reactor configuration (upflow or downflow) and the optimum process parameters are yet to be established.

Cobalt/molybdenum and nickel/molybdenum hydrotreating catalysts in sulfide forms on alumina supports have given good results in work at PNL, University of Louvain and the Institute of Wood Chemistry. They are multifunctional catalysts presenting hydrogenating, hydrogenolysing and acidic properties. In cases requiring a stronger hydrocracking activity, silica-alumina, zeolites and aluminophosphates have shown promise in place of the alumina as a support for the CoMo and the NiMo catalysts, as has addition of phosphate to the alumina support [95]. Soltes et al. [96, 97] have reported superior results in hydrocarbon conversion and water yield from noble metal catalysts (5 % wt. Pt or Pd on support) after performing preliminary screening studies with twenty catalysts in a batch reactor. Four of the catalysts (Pt/Al_2O_3, CoMo, NiMo, NiW) were selected for tests in a trickle bed reactor. The Pt/Al_2O_3 catalyst again exhibited the best activity for oxygen removal for pine pyrolysis oil. Platinum and palladium metals have the ability to adsorb hydrogen and lead to its dissociation, which makes them good hydrogenating catalysts for pyrolysis oil. However, they could not be

employed in hydrocracking coal liquids due to their low resistance in sulfur. Pyrolysis oil has very low sulfur content.

Churin et al. [98, 99] have reported that the presence of a hydrogen donor solvent leads to higher percentages of hydrodeoxygenation and hydrodenitrogenation, as well as higher product yield. They have suggested that the hydrogen donor saturates the free radicals preventing their recombination which can lead to high molecular weight compounds. These compounds could adsorb irreversibly on the catalyst surface and produce coke, thus blocking active sites and pores.

Although tetralin and decalin work well as hydrogen donor solvents, they exhibit boiling points in the diesel fuel range. Hence their use prevents both their recovery and the evaluation of the hydrotreated product. However, the light ends of the hydrotreated product contain the alkyl cyclohexanes, especially methyl cyclohexane, which has similar hydrogen donor activity in the system as decalin [96]. Soltes et al. [96, 97] hydrotreated biomass tars in methyl-cyclohexane hydrogen donor solvent. Moreover, Churin et al. [98] replaced tetralin by a bio-oil fraction with similar results to those obtained with pure tetralin.

For a given catalyst, the severity of the treatment is fixed by the pressure and temperature of the reaction and the residence time. As hydrogen is involved in all reactions, the higher the pressure, the higher the rate of transformation and the lower the deactivation by coke [98]. Increasing the temperature improves deoxygenation, but also accelerates the competing polymerisation reactions which lead to high molecular weight compounds blocking the access to the catalyst and leading to catalyst deactivation. In order to avoid this, the coke precursors must be destroyed by hydrocracking to smaller molecules. This process could be the kinetically limiting step responsible for the very long residence time required rather than the hydrodeoxygenation reactions themselves [100].

Grange et al. [100] have studied the role of water in the deactivation of the catalysts using model compounds in a batch reactor. The presence of water hydrated the γ-alumina support into a boehmite phase causing the catalyst to lose its texture with time and the dispersion of the active elements to decrease. In addition, fine modification of

the chemical nature of some of the active nickel species occurred, but this modification only causes an activity decrease during initial reaction times. It is thus difficult to ascertain the influence of this process on the long term deactivation.

The alumina support plays key role in formation of coke [101]. It has been suggested that coke arises from the interaction of phenol-type molecules containing two or more oxygenated substitutes, like guaiacol and catechol with the γ-Al_2O_3 support rather than with the active metals. Grange et al. [100] have investigated two ways to avoid coke formation: either to use neutral supports as activated carbon or to modify the γ-alumina with alkaline metals. In the former case the alumina supported catalyst was five times more active than the carbon supported one, which was even less active than alumina alone. In the latter case the catalyst supported on alumina modified with lithium showed similar activity to the non modified catalyst and selectivity towards the elimination of the methoxy group by hydrogenolysis of the aromatic carbon-oxygen bond leading to the production of phenol with a low coke deposition.

Further research is required for the development of more active and selective catalysts. In particular the long term stability of the catalytic system needs to be investigated, since it will be a determining aspect for the implementation of the bio-oil hydrotreating process at a larger scale.

2.5.3 Mild hydrotreating

Mild or low severity hydrotreating of bio-oils employs less severe processing conditions (lower temperature, shorter residence time) than those required for naphtha production (naphtha is subsequently refined to yield gasoline or diesel). It involves partial hydrodeoxygenation, minimal hydrocracking and effective hydrogenation to stabilise the bio-oil and improve its energy density. Such treatment would produce an oil that would show better properties for storage or transport and could be used as a low grade fuel or for phenols recovery with better economic possibilities compared to full hydrotreating due to the lower hydrogen consumption [102].

In the literature mild hydrotreating usually coincides with the stabilisation step in the overall hydrotreating process leading to oxygen contents in the range of 15 to 20 % wt similar to those of high pressure liquefaction oils. Laurent et al. [103] have performed a

series of mild hydrotreating experiments in a continuous reactor system at low temperature (180-220°C) using different catalysts. With the CoMo and NiMo catalysts a limited but sensible deoxygenation was obtained, while the ruthenium catalyst was almost immediately deactivated when bio-oil was fed. Conti et al. [104, 105, 106] has conducted mild hydrotreating experiments in a continuous reactor at 280°C and 14 MPa total pressure producing stabilised oil with a 23.2 % oxygen content. Meier et al. [107] have performed a series of tests with different bio-oils at different reaction severities (hydrogen pressures from 100 bar to a few mbar, temperatures from 200°C to 20°C). The best results were obtained with dry Raney nickel at 2-3 bar hydrogen pressure and 80°C. Most of the aldehydes and ketones were completely reduced to corresponding alcohols, but it was not possible to reduce acetic acid under the conditions applied.

However, the term mild hydrotreating has also been applied in cases of hydrotreating resulting in a higher than 2% wt oxygen content. Elliott and Neuenschwander [94] have conducted a series of experiments in a down-flow (trickle bed) reactor system in which the top catalyst bed served as the low temperature stabilisation reaction vessel at approximately 150°C and the bottom catalyst bed served as the main hydrotreater at higher temperature varying between 350 and 400°C at 21 MPa, whereas the space velocity varied from 0.52 to 0.78 g/g/h. The accomplished deoxygenation was in the range of 98.6 to 94.5% with respect to the increasing space velocity.

Hydrotreating severity should be defined by the end use (chemicals, turbine fuels, transport fuels), since there is a correlation between the severity (temperature, pressure, resident time) and the respective quality of the product. Therefore, the product quality requirements for the specific application will dictate the appropriate extent of upgrading.

2.5.4 Hydrogen consumption

The hydrogen consumed by the elimination of the various chemical groups shows an evolution parallel to the severity required. As the unsaturated bonds (olefins, aldehydes, ketones) are easily hydrogenated, the hydrogen addition is relatively specific. On the contrary, the reactions taking place at higher temperature are less specific and a high quantity of hydrogen is consumed by the hydrogenation of adjacent aromatic rings [102].

Full hydrotreating requires significant hydrogen consumption of around 0.0557 tones per ton of bio-oil according to a PNL study conducted in 1992 [108]. This is approximately the stoichiometric requirement, although an excess of 100%- 200% is required for processing to maintain a high hydrogen partial pressure. This hydrogen can be generated in a number of ways including recovery and regeneration from the spent gases and supply from refinery hydrogen. A 1000 ton/day biomass processing plant will require about 50 ton/day hydrogen for complete hydrotreating which, if generated from biomass by gasification and CO shifting, would require up to 700 to 800 ton/day additional biomass at a significant cost [83]. However, there is an alternative route for the production of liquid hydrocarbon fuels from biomass without hydrogen addition via biomass gasification followed by Fischer-Tropsh synthesis.

2.5.5 Thermal hydrotreating

Veba Oel (Germany) stopped all activities in catalytic hydrotreating during 1996. They found that the process was restricted by several operational problems such as rapid catalyst deactivation, coking and plugging. Furthermore, due to high feedstock and hydrogen addition costs, upgrading of bio-oil by catalytic hydrotreating was significantly more expensive than petroleum derived oil at those oil prices. They developed instead a slurry phase reactor operating under high hydrogen pressure (up to 200 bar), which was a modification of the Veba Combi Cracking Process. Liquid feedstock was mixed with a small amount of fine ground solids (lignite, spent catalyst) and hydrogen and fed to the bottom of the reactor. A total runtime of a week at deoxygenation rates of 75-85% has been reported without any operational problems. Organic liquid yields varied between 30 and 55 wt %, depending on severity and on water content of the feedstock [109, 93]. However, it should be mentioned that the presence of spent catalyst is expected to have some catalytic effect and therefore the process should not be considered as non-catalytic.

2.5.6 Summary

Although bio-oil burns effectively in standard or slightly modified boilers and engines with rates similar to those for commercial fuels, its combustion without upgrading faces a range of problems such as bio-oil's high water content which is detrimental for ignition and the presence of organic acids which are highly corrosive to common

construction materials [83, 88]. Research is conducted on upgrading bio-oil to products that more closely resemble conventional fuels in an attempt to address these problems.

Catalytic hydrotreating of bio-oil has been developed based on the conventional hydrotreating process of the petroleum refinery industry. It consists of deoxygenation of bio-oil under high hydrogen partial pressure (70 to 200 bars) using traditional hydrodesulfurisation catalysts (NiMo or CoMo supported on alumina) eliminating oxygen as water with simultaneous hydrocracking of large molecules and hydrogenation of double bonds [89]. The produced hydrocarbons can, in principle, either be used directly for firing a turbine or engine, or produce transport fuels via a conventional refining process [90].

The best hydrotreating reactor configuration (upflow or downflow) and the optimum process parameters are yet to be established. Cobalt / molybdenum and nickel / molybdenum hydrotreating catalysts in sulfide forms on alumina supports or silica-alumina, zeolites and aluminophosphates supports for stronger hydrocracking activity have given good results [95]. In addition noble metal catalysts (5 % wt. Pt or Pd on support) have also exhibited good performance in hydrocarbon conversion [96, 97]. However, during continuous operation severe catalyst deactivation has been observed leading to coking and plugging [93].

Bio-oil's high water content plays a significant role in catalyst's deactivation. It hydrates the γ-alumina support into a boehmite phase causing the catalyst to lose its texture with time and the dispersion of the active elements to decrease. Furthermore coke is blocking the access to the active sites and leading to catalyst deactivation. It has been suggested that the alumina support plays key role in formation of coke [101]. The use of neutral supports such as activated carbon and the modification of the γ-alumina support with alkaline metals have been proposed as alternatives [100].

Mild or low severity hydrotreating of bio-oils employs less severe processing conditions (lower temperature, shorter residence time) than those required for naphtha production. It involves partial hydrodeoxygenation, minimal hydrocracking and effective hydrogenation to stabilise the bio-oil yielding a product that would show better properties for storage or transport and could be used as a low grade fuel or for

phenols recovery. In addition the economic possibilities for mild hydrotreating compared to full hydrotreating are better due to the lower hydrogen consumption [102].

Most activities in catalytic hydrotreating were stopped in the mid '90s due to several operational problems, in particular rapid catalyst deactivation, coking and plugging. Furthermore, due to high feedstock and hydrogen costs, upgrading of bio-oil by catalytic hydrotreating was significantly more expensive than petroleum derived oil at those oil prices. Today the high crude oil prices have improved the potential of bio-oil upgrading. Further research is required for the development of more active and selective catalysts. In particular the long term stability of the catalytic system needs to be investigated, since it will be a determining aspect for the implementation of the bio-oil hydrotreating process at a larger scale. Pillared clays may be suitable hydrotreating catalysts, since they would not be affected by bio-oil's high water content. However, high coke formation could remain a cause of catalyst deactivation. Nevertheless, the Veba oil thermal hydrotreating process with spent catalyst indicates that partially deactivated catalysts may still show good results. The potential of pillared clays as hydrotreating catalysts deserves investigation.

The development of a microwave reactor for mild hydrotreating of bio-oil is also worth pursuing. It is difficult to conduct reactions requiring both high temperatures (>200°C) and pressures (>250 psig) under microwave irradiation, basically because of the limitations of microwave-transparent materials. Microwave vessels are usually made from polymers or quartz and can therefore sustain only limited temperatures and pressures, whereas metal is not appropriate for vessels, since it is not a microwave-transparent material. These temperature and pressure limitations would limit the application of microwave irradiation to mild, and not full, hydrotreating.

3 EXPERIMENTAL

This chapter is divided into five sections. In Section 3.1 the raw materials employed in the preparation of the pillared clay catalysts, the hydrocracking runs and the bio-oil decomposition runs are described. In Section 3.2 the analytical methods applied to the characterisation of the parent clays and their pillared derivatives (3.2.1 to 3.2.5), as well as the characterisation of the products of the bio-oil decomposition runs (3.2.6 to 3.2.9) are presented. In Section 3.3 the experimental procedure followed for the preparation of the pillared clay catalysts is explained. In Section 3.4 the respective procedure followed during the hydrocracking runs in either a conventional microbomb reactor or a microwave reactor is depicted. Finally, in Section 3.5 the experiments undertaken for the investigation of bio-oil's decomposition under microwave irradiation and conventional heating are described.

3.1 Raw materials

Chemicals were obtained from Sigma-Aldrich and used as received, unless otherwise stated. Pressurised gases were obtained from BOC.

3.1.1 Preparation of pillared clays

Wyoming Bentonite, a naturally occurring dioctahedral smectite, and Laponite RD, a synthetic virtually iron-free trioctahedral smectite were used as starting materials in the preparation of the pillared clay catalysts.

Wyoming Bentonite, consisting of about 85% montmorillonite and 15% non-clay minerals such as quartz, was supplied by WYO-BEN, Inc, USA. A typical chemical analysis (wt %) was: SiO_2 60.34, Al_2O_3 19.28, Fe_2O_3 3.48, Na_2O 2.34, TiO_2 0.22, CaO 0.38, MgO 1.67, K_2O 0.1, other 0.07, H_2O 7.75, loss on ignition 4.37 %.

Wyoming Bentonite was either used with some refining or a combination of some refining with pre-exchange with sodium to yield monoionic sodium montmorillonite. A simple sedimentation / decantation technique was undertaken for refining [110]. Wyoming Bentonite was dispersed in de-ionized water. After stirring for 48 h the suspension was allowed to settle and the quartz impurities to sediment. The upper half of the suspension was then used for the preparation of the pillared clays.

Monoionic sodium montmorillonite was prepared as follows: Wyoming Bentonite (20 g) was suspended in a 1M aqueous solution of sodium chloride (2l) and stirred for at least 12 h [2]. Silica was removed by sedimentation and decantation and the resulting suspension was acidified to pH 3 with 1M hydrochloric acid. After stirring for a short time, the suspension was allowed to settle and the supernatant sodium chloride solution decanted. The residue was made up to 2l with 1M sodium chloride solution and again acidified. This process was repeated two more times, followed by a 24 h stirring after the final addition. The suspension was centrifuged and the slurry was either transferred to a semi-permeable membrane and dialyzed with de-ionized water or repeatedly washed with de-ionized water and subsequently centrifuged until the wash water was free of chloride (silver nitrate test). The slurry was finally dried overnight at 80°C and the resulting clay was ground for subsequent use in pillaring experiments.

Laponite RD was obtained from Southern Clay Products - Rockwood Additives Limited, USA. (Typical composition on a w/w basis: SiO_2 59.5, MgO 27.5, Li_2O 0.8, Na_2O 2.8, loss on ignition 8.2%, moisture content 10%). Since it was a synthetic material, without impurities, it was used as received.

3.1.2 Coal liquids

A coal extract (not filtered) with 5% wt. ash content and 45.6% wt. fraction with boiling points over 450°C was used as feed for the hydrocracking runs. It had been generated by heating coal mixed with a recycled solvent for 1h at 410-430°C and 15 bar (vapour pressure) in the Point of Ayr Liquefaction Facility. Its typical analysis after filtration in a dry and ash free basis was: C: 90.2%, H: 7.6%, N:0.6%, S:0.2% and O (by difference):1.4%.

3.1.3 Bio-oil

A batch of bio-oil produced via fast pyrolysis of mixed softwood in a rotating cone reactor at 500°C (yield 70%) by BTG (Netherlands) was used in the bio-oil decomposition investigation.

3.2 Analytical methods

3.2.1 X-ray powder diffraction (XRD)

X-ray diffraction is a phenomenon in which the atoms of a crystal, by virtue of their uniform spacing, cause an interference pattern of the waves present in an incident beam of X rays. The atomic planes of the crystal act on the X rays in exactly the same manner as does a uniformly ruled grating on a beam of light.

For the two adjacent rows shown in Figure 3.1, the path difference between beams is $2h=2d\sin\theta$. For constructive interference this must be an integer number of wavelengths, $n\lambda$, where the integer n is called the order of interference. The result is Bragg's law of diffraction:

$$n\lambda = 2d\sin\theta$$

where:

n = number of wavelengths in the path length (integer)

λ = the wavelength

d = interplanar spacing between the atoms in the crystal

θ = the reflected (and incident) angle

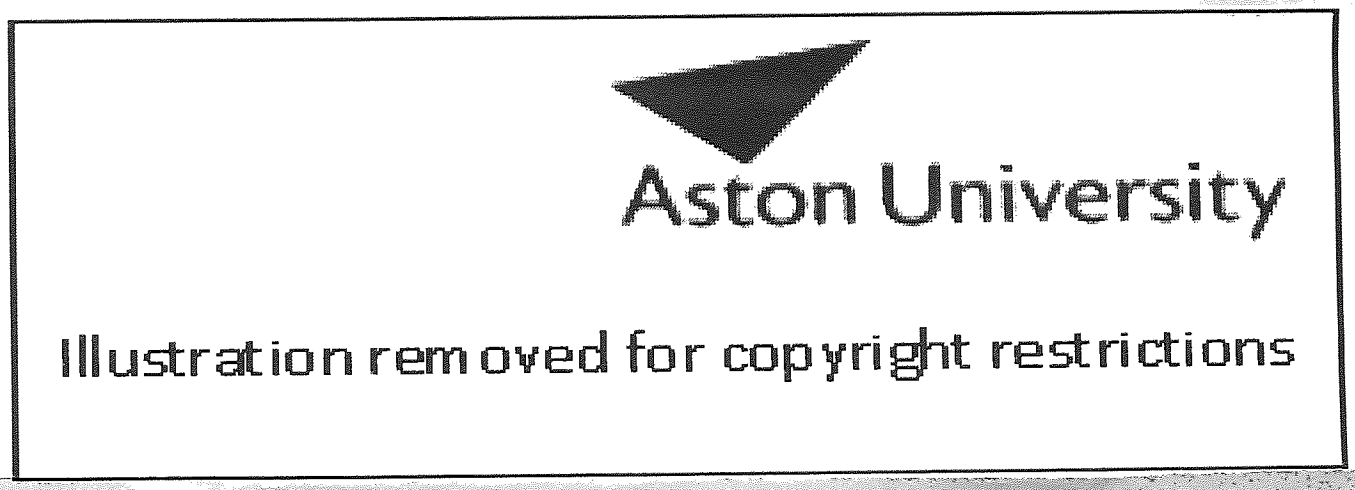

Figure 3.1 Schematic representation of Bragg's law [111]

A diffraction pattern records the X-ray intensity as a function of 2θ angle. When the incident beam strikes a powder sample (i.e. hundreds of crystals), diffraction occurs in every possible orientation of 2θ. The diffracted beam may be detected by using a

moveable detector, which is connected to a chart recorder. In normal use, the counter is set to scan over a range of 2θ values at a constant angular velocity.

X-ray powder diffraction patterns were obtained using Cu K_α radiation and a Bruker AXS D5005 diffractometer, at Birmingham University, equipped with a multilayer Goebbel mirror, long Soller slits and a scintillation counter detector by scanning powder specimens between 2° to 10° 2θ with a step size of 0.04° 2θ and step time of 25 sec.

XRD was used as the principal characterisation method to study changes in the clays during pillaring reactions and subsequent calcination steps. The d_{001} reflection, known as the basal spacing, or d spacing, corresponds to the variable c crystallographic dimension, i.e. it is a measure of the distance between the silicate layers. Hence, any addition or changes of pillaring agents in the interlayer will directly affect these values.

The basal reflections occur in conjunction with the series hk reflections. The relative intensities of the two series depend on the particular technique used, including in this term the method of preparation of the specimen. The randomly oriented powder samples used herein show the two systems (general hk band system and basal 00l system) superposed.

3.2.2 Thermogravimetric and differential thermogravimetric analysis (TGA and DTG)

Thermogravimetry was performed on Model Pyris 1 TGA from Perkin Elmer to study the thermal behaviour of the catalysts and indicate structural changes occurring during heating. A powder sample of approximately 10 mg was heated in an inert atmosphere (nitrogen) up to $1000^\circ C$ with a heating rate of $20^\circ C$/min. The derivative thermogravimetric (DTG) curves were calculated using software provided by the manufacturer to elucidate the weight loss steps.

Thermogravimetric and derivative thermogravimetric analysis was conducted in all three starting materials, i.e. Wyoming Bentonite, sodium montmorillonite and laponite, and their pillared derivatives before and after calcination. The aim was to investigate

how pillaring with different metal oxides and subsequent calcination influence the thermal stability of the starting materials and identify the structural changes that take place during heating.

3.2.3 X-ray photoelectron spectroscopy (XPS)

In X-ray photoelectron spectroscopy (XPS) the sample is irradiated with X-rays, which produce photoelectrons from core levels in atoms near to the surface. The XPS technique is highly surface specific due to the short range of the photoelectrons that are excited from the solid.

The binding energy of the peaks is characteristic of each element. The peak areas can be used (with appropriate sensitivity factors) to determine the composition of the materials surface. The shape of each peak and the binding energy can be slightly altered by the chemical state of the emitting atom, and, therefore, XPS can also provide chemical bonding information. Although XPS is not sensitive to hydrogen or helium, it can detect all other elements given the fact that their content exceeds 0.1% of the analysed layer. Nevertheless, it is rather difficult to draw any conclusions on the chemical environment of species with a content lower than 0.3 to 0.5% in the analysed layer.

XPS was conducted in a VG Escalab 200D electron spectrometer equipped with HAS energy analyser at Aston Surface Analysis Laboratories. Mg K_{α} non-chromatised radiation (1253.6 eV) was employed at a source excitation energy of 15 keV, emission current of 20 mA and an energy step size of 0.1 eV. Correction of the charge shift for all the studies of wafers were accomplished by taking the C1S peak at 284.6 eV.

XPS was applied to all the starting materials and a selection of the derivative pillared clays as a complementary method to XRD. It was used primarily to identify the composition of the pillars.

3.2.4 Nitrogen sorption

According to IUPAC [112] pores are classified (based on their diameter) into three categories:

- micropores (diameter below 20 Å)

- mesopores (diameter in the range of 20 to 500 Å)
- macropores (diameter above 500 Å).

The classification of adsorption isotherms by Brunauer, Deming, Deming and Teller (B.D.D.T. system) correlates the type of isotherm with the porosity of the material leading to six types of isotherm characteristic of adsorbents that are microporous (type I), nonporous or macroporous (types II, III, and VI) or mesoporous (types IV and V) (Figure 3.2).

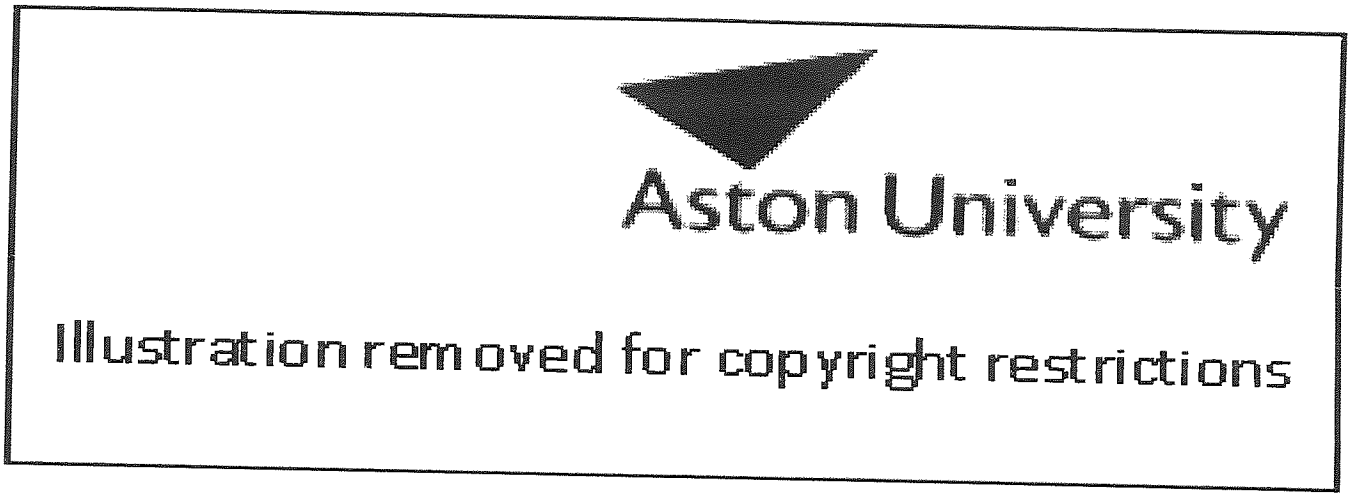

Figure 3.2 Types of adsorption isotherms (B.D.D.T. system) [113]

For the specific surface area determination the BET method, which extends the Langmuir model of gas sorption to multi-layer, was applied, although the assumptions do not take into account micropore filling. The BET equation is:

$$\frac{1}{W((P_o/P)-1)} = \frac{1}{W_mC} + \frac{C-1}{W_mC}\left[\frac{P}{P_o}\right]$$

W is the weight of gas adsorbed at a relative pressure P/P_o and W_m is the weight of adsorbate constituting a monolayer of surface coverage. The term C, the BET C

constant, is related to the energy of adsorption in the first adsorbed layer and consequently its value is an indication of the magnitude of the adsorbent / adsorbate interactions. The BET equation requires a linear plot of $1/[W(P_o/P)-1]$ versus P/P_o, which for most solids, using nitrogen as the adsorbate, is restricted to a limited region of the adsorption isotherm, usually in the P/P_o range of 0.05 to 0.35. However, for micropore samples the linear BET range is shifted to relative pressures lower than 0.1 [114].

The standard multi point BET method requires at least three points in the appropriate reltive pressure range. The weight of a monolayer of adsorbate W_m can be obtained from the slope S and the intercept I of the BET plot.

$S= (C-1)/W_mC$ and $I= 1/W_mC$

Therefore $W_m= 1/(S+I)$.

The total surface area of the sample can be expressed as:

$S_t= W_m N A_{cs} /M$

where N is Avogadro's number (6.023×10^{23} molecules/mol), M is the molecular weight of the adsorbate and A_{cs} the molecular cross sectional area of the adsorbate. For nitrogen the cross sectional area is 16.2 $Å^2$.

The specific surface area S of the solid can be calculated from the total surface area S_t and the sample weight w:

$S= S_t/w$

Specific total pore volumes were evaluated from nitrogen uptake at a relative pressure of 0.99 from the following equation:

$V_{liq}= (P_a\ V_{ads}\ V_m)/RT$,

where P_a, T: ambient pressure and temperature, V_m: molar volume of liquid adsorbate, 34.7 cc/mol for nitrogen [114].

Since pores which would not be filled below a relative pressure of 1 have a negligible contribution to the total pore volume and the surface area of the sample, the average pore size can be estimated from the pore volume assuming cylindrical pore geometry:

$R = 2\ V_{liq}/S$,

where S is the BET surface area [114].

Multi-layer formation is modelled mathematically to calculate a layer thickness, t as a function of increasing relative pressure (P/Po). The resulting t-curve is compared with the experimental isotherm in the form of a t-plot (de Boer). The linear range lies between monolayer and capillary condensation. The slope of the t-plot (V/t) is equal to the "external area", i.e. the area of those pores which are not micropores, whereas the intercept gives the micropore volume. Mesopores, macropores and the outside surface is able to form a multilayer, whereas micropores which have already been filled cannot contribute further to the adsorption process. The micropore surface area is the difference between the BET surface area and the external surface area from the t-plot [114].

Mesopore size distribution was calculated using the Barrett, Joyner and Halenda (BJH) method which is based on the modified Kelvin equation. The Kelvin equation predicts pressure at which adsorptive will spontaneously condense (and evaporate) in a cylindrical pore of a given size. Since condensation occurs in pores that already have some multilayers on the walls, the pore size is calculated from the Kelvin equation and the selected statistical thickness (t-curve) equation. The desorption branch of the isotherm was taken into account for the calculations [114].

Surface areas, pore volumes and average pore diameters were calculated from nitrogen adsorption-desorption isotherms using NOVA 1000 from Quantachrome. Prior to the adsorption-desorption measurements, all the samples were degassed under vacuum at 200°C for 16 h.

Adsorption - desorption isotherms were obtained for the starting materials and their derivatives with single oxide or mixed oxide pillars in order to compare their textural properties (specific surface area, pore size distribution) and investigate the effect of the raw material and the pillaring species.

3.2.5 Magic angle spinning nuclear magnetic resonance (MAS NMR)

Nuclear magnetic resonance (NMR) is a phenomenon, which occurs when the nuclei of certain atoms are subjected to a static magnetic field and exposed to a second oscillating magnetic field. Some nuclei experience this phenomenon, and others do not,

dependent upon whether they possess a property called spin, which can be thought of as a small magnetic field, and will cause the nucleus to produce an NMR signal [115].

Solid state NMR spectroscopy uses the NMR phenomenon to determine the molecular structure of solids. The chemical shift interaction is due to the shielding effect on the nucleus of the fields produced by the surrounding electrons. In a spherically symmetric molecule, the chemical shift is independent of molecular orientation, whereas in an asymmetric molecule it is not. The magnetic field experienced by the nucleus varies as a function of the orientation of the molecule in the magnetic field [115].

A group of dipoles with a random distribution of orientations, as in a solid, gives the spectrum shown in Figure 3.3.

Figure 3.3 NMR spectrum of a group of dipoles with random orientations [115]

The higher signal at mid-field strength is due to the larger presence of orientations perpendicular to the direction of the B_0 field. This signal is made up of components from the nuclei in the dipole. In a non viscous liquid, the interaction averages out due to the presence of rapid tumbling of the molecule (Figure 3.4).

The NMR spectra of solid samples display broad spectral lines due to anisotropic chemical shift and dipolar broadening. A dipolar interaction is one between two spin 1/2 nuclei. The magnitude of the interaction varies with angle and distance r. As a function of θ, the magnetic field B_0 experienced by one of the nuclei is $(3\cos^2\theta - 1)$ (Figure 3.5).

Figure 3.4 Typical NMR spectrum of a non viscous liquid sample [115]

Figure 3.5 Variation of $B_o=3\cos^2\theta - 1$ as function of θ [115]

When the angle θ in the above equation is 54.7°, 125.3°, 234.7°, or 305.3°, the dipole interaction vanishes. The angle 54.7° is called the magic angle, m_θ. If all the molecules could be positioned at m_θ, the spectrum would narrow to the fast tumbling limit. Since this is not usually possible, the best alternative is to cause the average orientation of the molecules to be m_θ by rapidly spinning the entire sample at an angle m_θ relative to B_o. In solid state MAS NMR, samples are placed in a special sample tube and the tube is placed inside a rotor. The rotor, and hence the sample, are oriented at an angle m_θ with respect to the B_o magnetic field. The sample is then spun at a rate of thousands of revolutions per second. The spinning rate must be comparable to the solid state line width called Chemical Shift Anisotropy (CSA) [115].

MAS NMR ^{29}Si and ^{27}Al spectra were recorded with a Bruker Avance-300 instrument at a carrier frequency of 59.62 MHz in order to collect information about their aluminosilicate framework. The same relaxation time was used for all samples although the number of scans varied. Tetra-methyl silane and aluminium sulfate were used as the reference materials.

3.2.6 Water content determination

Volumetric Karl Fisher titration was performed by means of a Metrohm 758 KFD Titrino, 703 Ti stand and Hydranal Composite 5 titrant. A chemical reaction takes place between iodine and water with the reactants being in a 1 to 1 ratio in the presence of a

base and a solvent (a typical solvent could be methanol, and a base imidazole). Volumetric KF determinations are preferentially carried out between pH 4-7.

The components of Metrohm Volumetric Titration are:

1. The exchange unit (burette) that dispenses the KF reagent, which contains iodine, for reaction with the water present in the reaction cell.
2. The platinum measuring indicator electrode that determines whether or not iodine needs to be added to react with any water present.
3. The onboard microprocessor that records the volume of KF reagent dispensed, then based on the concentration of iodine in the KF reagent, it calculates how much water was present in the sample (one ml of titrant is analogous to 5mg of water).

Karl Fisher titration was used for the water content determination of the bio-oil samples. Triplicate analyses were performed for each sample. Since most bio-oil samples were diluted with tetrahydrofuran (THF), these dilutions were taken into account for the calculation of the final water content.

3.2.7 Char content determination

The char content of the bio-oil used in the study (raw material) was determined as the methanol insoluble materials in the bio-oil. Two grams (2 g) of bio-oil were dissolved in 200 ml of methanol and the resulting solution was vacuum filtered via Whatman filter paper #1 (particle retention of 11μm). The filter paper was washed with methanol until the filtrate was clear, dried in the oven at 105°C for 1 h and placed in a desiccator prior to being weighed. The char content percentage was calculated as the weight of material collected on the filter paper, divided by the weight of the bio-oil sample.

3.2.8 Gel permeation chromatography (GPC)

Bio-oil consists of a distribution of molecular species. The average molecular mass, M, results from several possible methods of averaging the different species present:

$M = \Sigma(N_i M_i^{n+1}) / \Sigma(N_i M_i^{n})$

where N_i is the number of molecules of molecular weight M_i and the averages can be expressed as:

Number average molecular weight M_n, n=0

Weight average molecular weight, M_w, n=1

Z average molecular weight M_z, n=2

Z+1 average molecular weight M_{z+1}, n=3

The peak molecular weight, M_p, is defined as the molecular weight of the species with maximum N_i. It is therefore the most probable molecular weight in the distribution. The polydispersity index PD is expressed as the ratio of M_w to M_n.

Gel permeation chromatography (GPC) is used for the determination of molecular weight distribution. A PL-GPC-50 Integrated GPC/SEC System (Polymer Laboratories Ltd.) designed for operation from ambient to 40°C was used for the analysis of the bio-oil samples. The system comprises a precision solvent delivery system, a sample injection system, a high performance differential refractive index detector and a column oven, with fully integrated software control. A packed column from polystyrene / polydivinylbenzene (PL-gel, 3μm mixed-E, 7.5 mm (ID) x 300 mm) was used for the separation. Tetrahydrofuran (THF) was used as the eluent at a flow rate of 1ml/min.

The bio-oil samples were dissolved in THF at a concentration of 7mg/ml and filtered before injection (particle retention 0.2μm). A pre-filter (particle retention 0.5μm) installed before the column in order to protect it from any undissolved materials was used as an additional precaution. Elution times were converted to apparent molecular weight by calibration with polystyrene standards (Polymer Lab. Ltd.). The mixed-E column exhibits a linear range up to polystyrene of molecular mass of 20,000 daltons.

Data were collected via the PL Data stream and Cirrus software was used for their processing based on the calibration curve.

3.2.9 Fourier transform infra red spectroscopy (FTIR)

Fourier transform infrared (FTIR) spectra were measured for selected bio-oil samples to identify their functional group composition. A mathematical function called a Fourier transform allows an intensity-versus-time spectrum to be converted into an intensity-versus-frequency spectrum. A different measure, the wavenumber, is given the unit cm^{-1}. The relationship can be derived by the relationship:

ν (cm $^{-1}$) = 10,000/λ(μm)

Spectra of organic compounds have two general areas:

- The Functional Group Region: 4000-1500 cm^{-1}

Peaks in this region are characteristic of specific kinds of bonds, and therefore can be used to identify whether a specific functional group is present.

- The Fingerprint Region: 1500-400 cm^{-1}

Peaks in this region arise from complex deformations of the molecule. They may be characteristic of molecular symmetry, or combination bands arising from multiple bonds deforming simultaneously.

A Perkin Elmer FTIR spectrometer Model Spectrum RXI was used to record the FTIR spectra. A few sample drops were placed between two sodium chloride discs by a pipette in order to form a thin film. For each sample thirty-two spectra were accumulated between 4000 and 400 cm^{-1} and averaged and the background spectrum was deducted. Since most bio-oil samples were diluted in THF, a separate spectrum of THF was also recorded for comparison purposes.

3.3 Catalysts preparation

3.3.1 Preparation of chromia pillared clays

(i) Conventional method

Montmorillonites and laponites pillared with polyoxochromium oligomers were prepared conventionally following slightly modified literature methods [116, 117, 118].

In all cases the pillaring solution was prepared by slow addition of either solid or aqueous sodium carbonate to an aqueous solution of chromium nitrate until the desired hydroxyl to chromium ratio was reached. The resulting solution was refluxed and, once cool, was added dropwise to a vigorously stirred clay suspension following specific pillaring stoichiometries (mmol of chromium per gram of clay). The mixture was stirred for 1.5 h and then repeatedly centrifuged and washed with water until the wash water was colourless. The water used throughout the experiments was de-ionized. The resulting material was filtered under vacuum and air dried, followed by calcination under argon for 1 h at 500°C. Calcination was performed in the absence of air in order

to avoid chromium oxidation and subsequent loss of chromium in the form of volatile oxides leading to the decomposition of the pillared clay. In particular the formation of Cr(VI) had to be avoided, since it is considered a carcinogen [4].

The experimental conditions for the preparation of chromia pillared clays are presented in detail in Table 3.1.

(ii) Microwave heating method

No literature references could be found for the synthesis of chromia pillared clays under microwave irradiation.

The CEM Focused Microwave™ Synthesis System, Model Discover, which was used in this work, consists of:

- A continuous microwave power delivery system with operator selectable power output from 0 – 300 watts (+/- 30 watts) programmable in 3-watt increments.
- A self-adjusting, single mode microwave cavity that is manually accessed via one of two attenuator ports.
- A 4-line x 20-character vacuum fluorescent display with alphanumeric keypad and on-board computer for programming and operational control of the system.
- Safety interlocks and an interlock monitoring system to prevent microwave emission when the attenuator port is not properly installed.
- Two serial ports for computer interface and optional feature connections.

The Discover system can accommodate an 80 ml sealed vessel with a working volume of 50 ml for reactions performed at elevated temperatures and pressures (Figure 3.7). It has a maximum operating temperature of 220°C and a maximum operating pressure of 200 psig (~20 bar). The fibre optic temperature control system consists of a fibre optic temperature probe that monitors and controls the temperature conditions of the reaction vessel. The pressure control system consists of a load cell to enable pressure measurement and control of the reaction environment (Figure 3.6).

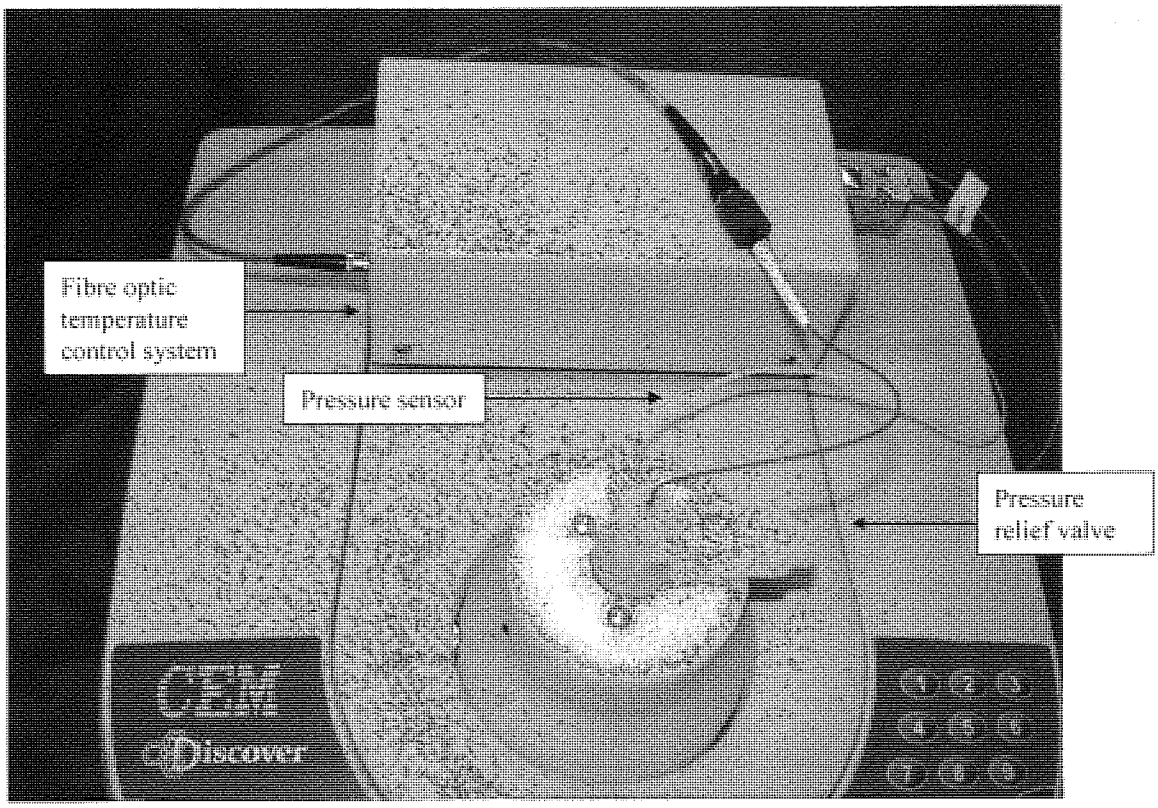

Figure 3.6 CEM Focused Microwave™ Synthesis System, Model Discover

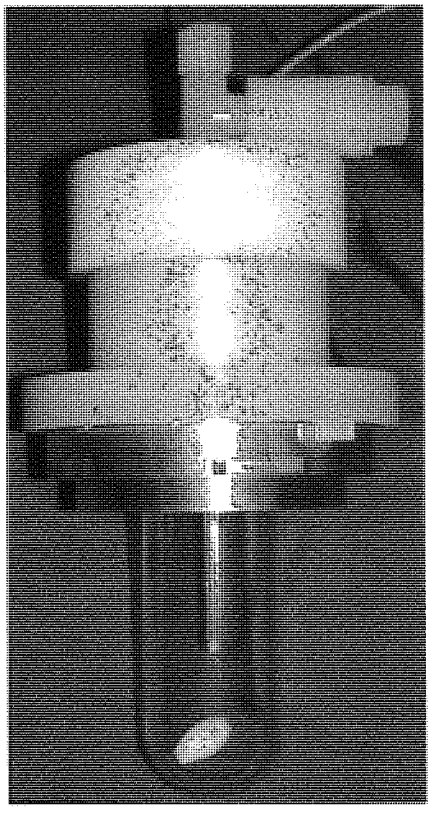

Figure 3.7 50 ml pressure reaction vessel

Stirring Option: The stirring option consists of a rotating magnetic plate located below the floor of the microwave cavity. "Stirring" occurs when the rotating magnetic field couples with a stir bar in the vessel. The method setup enables the stirring feature.

Cooling Option: The cooling option consists of necessary valves and ports to direct a cooling gas (either nitrogen or "clean" air) onto the vessel in the system cavity. Method setup enables the cooling feature. The gas is user supplied at a minimum pressure level of 20 psi (~1.5 bar) and a flow rate of 25 liters/min.

Two approaches were investigated in attempts to synthesize chromia pillared montmorillonite from refined Wyoming Bentonite. At first the intermixed solution of chromium nitrate and sodium carbonate was added slowly to the clay suspension without any thermal treatment and the resulting suspension was microwave irradiated at different power, time and temperature settings, either with or without simultaneous cooling and under continuous stirring. Secondly the mixed chromium nitrate and sodium carbonate solution was microwave irradiated at 150W and 105°C for 15 min as an alternative to the refluxing step of the conventional method. It was then added dropwise to the stirred clay suspension under vigorous stirring. The resulting suspension was stirred for 1.5 h. In both cases the final suspension was repeatedly centrifuged and washed with de-ionized water until the wash water was colourless. The resulting material was filtered under vacuum and air-dried.

The precise experimental conditions for the microwave synthesis of chromia pillared montmorillonites are presented in Table 3.2.

Table 3.1Pillared clays prepared via conventional methods

Sample	Starting material	Refluxing time (h)	Metal salt	OH/Me	Metal salt moles	Metal salt conc/tion (M)	Na_2CO_3 moles	Na_2CO_3 conc/tion (M)	Me/Clay (moles/gr)	Clay conc. (% w/v)
Chromia pillared clays										
CM1	WB	16	$Cr(NO_3)_3.9H_2O$	1	0.03	0.1	0.015	N/A	0.015	2
CM2	WB	36	$Cr(NO_3)_3.9H_2O$	1	0.03	0.1	0.015	N/A	0.015	2
CM3	Na-mont	36	$Cr(NO_3)_3.9H_2O$	1	0.03	0.1	0.015	N/A	0.015	2
CM4	WB	36	$Cr(NO_3)_3.9H_2O$	2	0.05	0.1	0.05	N/A	0.05	1
CM5	WB	36	$Cr(NO_3)_3.9H_2O$	2	0.05	0.1	0.05	0.25	0.05	1
CM6	WB	36	$Cr(NO_3)_3.9H_2O$	2	0.15	0.5	0.15	0.75	0.05	1
CM8	WB	36	$Cr(NO_3)_3.9H_2O$	2	0.15	0.5	0.15	0.75	0.05	100
CM13	WB	36*	$Cr(NO_3)_3.9H_2O$	2	0.1125	0.5	0.1125	0.75	0.05	1
CM16	Na-mont	36	$Cr(NO_3)_3.9H_2O$	2	0.175	0.5	0.175	0.75	0.05	1
CL	Laponite	36	$Cr(NO_3)_3.9H_2O$	2	0.069	0.23	0.069	0.18	0.0345	1
Montmorillonite with mixed chromium and cerium oxide pillars										
Cr/Ce mont	Na-mont	36	$Cr(NO_3)_3.9H_2O$ / $Ce(NO_3)_3.6H_2O$	2	0.1 / 0.02	0.5 / 0.1	0.12	0.75	0.05 / 0.01	1
Montmorillonite with single cerium or europium oxide pillars										
Ce-mont	Na-mont	0.17	$Ce(NO_3)_3.6H_2O$	2	0.03	0.1	0.03	0.2	0.015	1
Eu-mont	Na-mont	0.17	$Eu(NO_3)_3.5H_2O$	2	0.03	0.1	0.03	0.2	0.015	1
Tin oxide pillared montmorillonite										
Sn-mont	WB	20	$(NH_4)_2SnCl_6$	N/A	0.01	0.1	N/A	N/A	0.00125	2.67
Tin oxide pillared laponites										
SL1	Laponite	N/A	$(C_6H_5)_3SnCl$	N/A	0.0039	N/A	N/A	N/A	0.0008	5 **
SL9	Laponite	N/A	$(C_6H_5)_3SnCl$	N/A	0.0015	N/A	N/A	N/A	0.0008	2 **

* The pillaring solution was mixed with the clay suspension before refluxing

** Laponite was suspended in ethanol. No refluxing, instead 168h mechanical agitation at room temperature

Table 3.2 Pillared clays prepared via microwave methods

Sample	Starting material	P (W)	T(°C)	Hold time (min)	Cooling	OH/ Me	Metal salt	Metal salt moles	Salt conc. (M)	Na_2CO_3 moles	Na_2CO_3 conc. (M)	Me/Clay (moles/g)	Clay conc. (% w/v)
Chromia pillared montmorillonites													
CM7	WB	100	95	2	Yes	2	$Cr(NO_3)_3.9H_2O$	0.015	0.6	0.015	1	0.05	2
CM9	WB	165	105	10	No	2	$Cr(NO_3)_3.9H_2O$	0.015	0.6	0.015	1	0.05	2
CM10	WB	165	105	20	No	2	$Cr(NO_3)_3.9H_2O$	0.015	0.6	0.015	1	0.05	2
CM11	WB	165	105	2	No	2	$Cr(NO_3)_3.9H_2O$	0.015	0.6	0.015	1	0.05	2
CM12	WB	165	105	5	No	2	$Cr(NO_3)_3.9H_2O$	0.015	0.6	0.015	1	0.05	2
CM14	WB	150	105	15	Yes	2	$Cr(NO_3)_3.9H_2O$	0.019	0.6	0.019	1	0.05	2*
CM15	WB	150	105	15	Yes	2	$Cr(NO_3)_3.9H_2O$	0.015	0.6	0.015	1	0.05	2
CM17	WB	200	150	15	Yes	2	$Cr(NO_3)_3.9H_2O$	0.015	0.5	0.015	0.75	0.05	2
Tin oxide montmorillonites													
SM2	WB	100	100	6	Yes	N/A	$(NH_4)_2SnCl_6$	0.0012	0.1	N/A	N/A	0.00125	2.67
SM3	WB	150	110	10	No	N/A	$(NH_4)_2SnCl_6$	0.0012	0.1	N/A	N/A	0.00125	2.67
SM4	WB	150	110	15	Yes	N/A	$(NH_4)_2SnCl_6$	0.0012	0.1	N/A	N/A	0.00125	3.33
SM5	WB	200	150	15	Yes	N/A	$(NH_4)_2SnCl_6$	0.0012	0.1	N/A	N/A	0.00125	2.67
Tin oxide pillared laponites **													
SL2	Laponite	150	N/A	1 (x5)	Yes	N/A	$(C_6H_5)_3SnCl$	0.0015	N/A	N/A	N/A	0.0006	10
SL3	Laponite	150	N/A	3	Yes	N/A	$(C_6H_5)_3SnCl$	0.0016	N/A	N/A	N/A	0.0006	10
SL4	Laponite	100	N/A	5	Yes	N/A	$(C_6H_5)_3SnCl$	0.0013	N/A	N/A	N/A	0.0005	10
SL5	Laponite	100	N/A	5	Yes	N/A	$(C_6H_5)_3SnCl$	0.0039	N/A	N/A	N/A	0.0008	10
SL6	Laponite	150	N/A	1 (x5)	Yes	N/A	$(C_6H_5)_3SnCl$	0.0015	N/A	N/A	N/A	0.0005	20
SL7	Laponite	150	N/A	3	Yes	N/A	$(C_6H_5)_3SnCl$	0.0015	N/A	N/A	N/A	0.0005	20
SL8	Laponite	100	N/A	5	Yes	N/A	$(C_6H_5)_3SnCl$	0.0015	N/A	N/A	N/A	0.0005	20
* Only the pillaring solution was irradiated, ** Laponite was suspended in ethanol													

3.3.2 Preparation of tin oxide pillared clays

3.3.2.1 Preparation of tin oxide pillared montmorillonite

(i) Conventional method

The intercalation of tin oxide between the layers of refined Wyoming Bentonite was attempted through the hydrolysis of ammonium hexachlorostannate in an aqueous clay suspension under reflux following a slightly modified literature method [116].

Ammonium hexachlorostannate (3.67 g) was dissolved in de-ionized water (100 ml) and added dropwise to a suspension of aqueous Wyoming Bentonite (8 g in 300 ml) under vigorous stirring. After 3 h stirring at ambient temperature the suspension was refluxed for 20 h at 100°C. The clay was separated by centrifugation and then it was repeatedly washed with de-ionized water and centrifuged until it was free of chloride (silver nitrate test). The product was separated by vacuum filtration and air-dried. A sample of the prepared material was heated at 500°C for 1 h.

(ii) Microwave method

An aliquot of the above suspension (0.46 g ammonium hexachlorostannate in 12.5 ml water and 1 g Wyoming Bentonite in 37.5 ml water) was irradiated at different power, time and temperature settings, either with or without simultaneous cooling and under continuous stirring (Table 3.2). Again the solid was separated by vacuum filtration and air-dried before a small quantity was heated at 500°C for 1 h.

3.3.2.2 Preparation of tin oxide pillared laponite

(i) Conventional method

Tin oxide pillared laponite was prepared following a literature method involving mechanical agitation [4, 15]. Sodium exchanged laponite RD (5.0g or 2.0g) and triphenyltin chloride (1.5g or 0.6g respectively) were mixed with dry ethanol (100 ml) in a stoppered conical flask and mechanically shaken for one week (Table 3.1).

(ii) Microwave method

Microwave treatment involved use of similar proportions of reactants being irradiated with simultaneous cooling for a total of 5 min, delivered as 1 min bursts at a power of 150 W, 3 min applied continuously at 150 W or 5 min applied continuously at 100 W

(Table 3.2). Every time the ethanolic suspension was filtered, washed with portions of ethanol and air-dried.

3.3.3 Preparation of montmorillonite with mixed chromium and cerium oxide pillars

Montmorillonite pillared with mixed chromium and cerium oxides was prepared conventionally based on the preparation method of aluminium-cerium oxide pillared montmorillonite (Table 3.1) [35]. The pillaring solution had a cerium to chromium molar ratio of 1 / 5 and was prepared by slow addition of aqueous sodium carbonate (0.75 M) to a mixture of aqueous solutions of chromium nitrate (0.5 M) and cerium nitrate (0.1 M) until a hydroxyl to metal (chromium + cerium) ratio of 2 was reached. Metal salt concentrations as close as possible to saturation were employed in the preparation in order to minimise the manipulated water volume and were defined based on the water solubility of the respective metal salts. The resulting solution was refluxed for 36 h and, once cool, was added dropwise to a vigorously stirred clay suspension (1% w/v). The pillaring stoichiometry employed was 0.05 mol of chromium per gram of clay. The mixture was stirred for 1.5 h and then repeatedly centrifuged and washed with water until the wash water was colourless. The water used throughout the experiments was de-ionized. The resulting material was filtered under vacuum and air dried, followed by calcination under argon for 1 h at 500°C. Calcination was performed in the absence of air in order to avoid chromium oxidation and subsequent loss of chromium in the form of volatile oxides leading to the decomposition of the pillared clay. In particular the formation of Cr(VI) had to be avoided, since it is considered a carcinogen [4].

3.3.4 Preparation of montmorillonite with single cerium and europium oxide pillars

Montmorillonite pillared with either cerium or europium oxide was prepared in a similar way as the typical recipe for the preparation of chromia pillared clays (Table 3.1): The pillaring solution was prepared by slow addition of aqueous sodium carbonate to a dilute (0.1 M) aqueous solution of cerium or europium nitrate until a hydroxyl to metal ratio of 2 was reached. The resulting solution was heated at 100°C for 10 min while air was blown into the solution to aid oxidation. Cerium and europium cations reach hydrolysis equilibrium faster than chromium cations and that is why they do not

require a lengthy refluxing period. Once cool, the resulting solution was added dropwise to a vigorously stirred clay suspension (1% w/v) following specific pillaring stoichiometry (0.015 mol of metal per gram of clay). The mixture was stirred for 1.5 h and then repeatedly centrifuged and washed with water six times. The water used throughout the experiments was de-ionized. The resulting material was filtered under vacuum and air dried, followed by calcination in a muffle oven for 1 h at 500°C.

3.4 Catalytic hydrocracking of coal liquids

3.4.1 Catalytic hydrocracking of coal liquids in a conventional microbomb reactor

A selection of pillared clay catalysts, as well as the original clays, were employed in two series of hydrocracking runs in a conventional microbomb reactor at Imperial College. The first series of runs was conducted with fresh catalysts and fresh feed, whereas the second series was performed using fresh feed and a selection of the coated catalysts recovered from the first series. NiMo supported on alumina, a conventional catalyst usually employed in hydrocracking, was used as reference catalyst in both series of runs. In addition, a run was conducted without any catalyst in order to distinguish the thermal effect of the hydrocracking process from the catalytic effect. Finally, two runs were repeated in order to check the reproducibility of the process, whereas three runs were conducted using pillared clay catalysts prepared previously by Bodman for comparison purposes [4].

The micro-bomb reactor consisted of a ½" bored-through Swagelok union tee connected to a control-head via a pressurisation line. Coal extract (1 g) was introduced, together with 250 mg catalyst. The assembly was first pressurised with helium in order to check for leaks and purge air from the system. Afterwards it was depressurised and pressurised again with hydrogen. The reactor was then immersed into a preheated fluidized sand bath heater and connected to a stepper-motor driven shaker. It was kept for 2 h at the reaction temperature and pressure, 440°C and 190 bar respectively [2]. A (4:1 v/v) mixture of chloroform and methanol was used to wash the reactor and to recover the products after each run. Product mixtures were first vacuum filtered, in order to separate undissolved substances and catalyst particles from the soluble products. The filter cake was washed with fresh 4:1 chloroform/methanol mixture to recover residual soluble product. Then it was dried in a vacuum oven at 50°C for 3 h

and the dry solids were weighed. The proportion of carbonaceous deposit on the catalyst cake was determined using a Perkin-Elmer Corporation TGA-7 thermogravimetric balance. Samples were heated in air from ambient to 600°C at 10°C/min to remove the carbonaceous layer [2, 3].

The filtrate was transferred to a pre-weighed round-bottom flask and the wash-solvent was evaporated in a rotating evaporator until the chloroform/methanol content was less than 1 wt. %. The solvent removal was monitored by gas chromatography. Once weighed the sample was homogenized by addition of chloroform/methanol and analysed by thermogravimetric analysis (TGA) to determine boiling point ranges [2, 3].

3.4.2 Catalytic hydrocracking of coal liquids in a microwave reactor

Although microwave radiation is becoming a common source of energy in accelerating chemical reactions, it is impossible to carry out reactions at high temperatures and pressures in commercial laboratory microwave ovens, because metal may not be used for vessels, since it is not a microwave-transparent material. The microwave vessels are made from polymers or quartz and, therefore, their pressure and temperature tolerance is limited to around 15 bars and 250°C.

Apart from the limited operational conditions, the introduction and flammability of hydrogen had to be addressed to modify a microwave reactor (CEM Focused Microwave™ Synthesis System, Model Discover) for hydrocracking, since it is a completely new application. The resulting reactor configuration with nominal capacity 10 ml is presented in Figures 3.9 to 3.13. Temperature, pressure and microwave power can be monitored on-line and stirring can be applied. The temperature control system consists of a non-contact infrared sensor which monitors and controls the temperature conditions of the reaction vessel located in the instrument cavity. The temperature sensor is centrally located beneath the cavity floor and "looks" up at the bottom of the vessel measuring the temperature there (Figure 3.8). Therefore the temperature measured in every case is the bulk temperature. A lens is positioned between the sensor and the cavity floor to protect the sensor. The sensor is used in a feedback loop with the on-board computed to control the temperature rise rate and control point of the vessel contents. The pressure control system consists of a load cell to enable pressure

measurement and control.

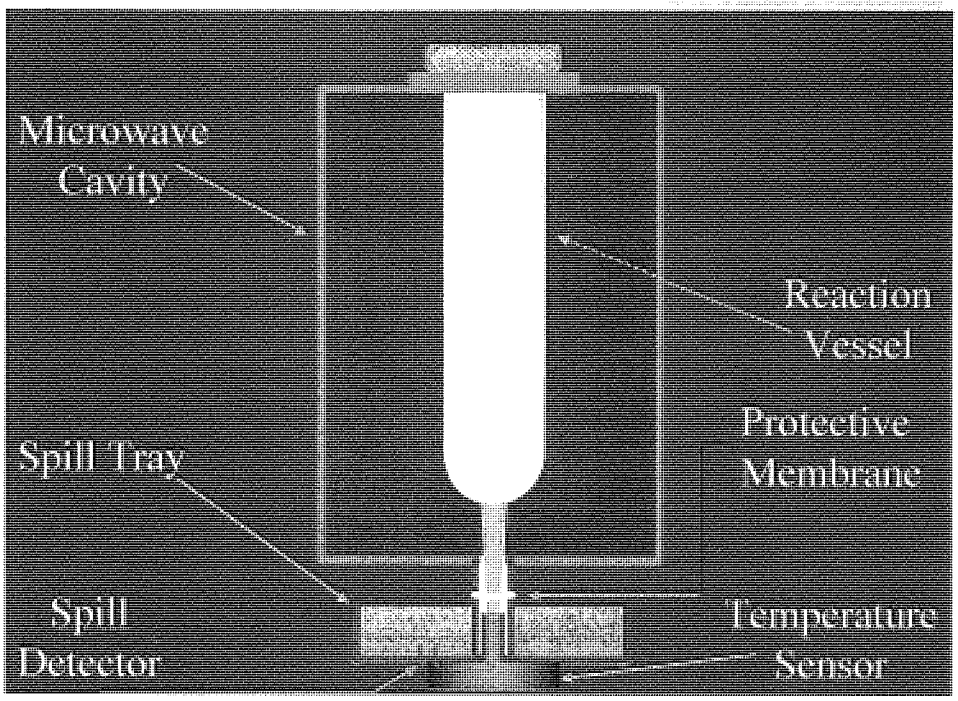

Figure 3.8 Infrared thermometry

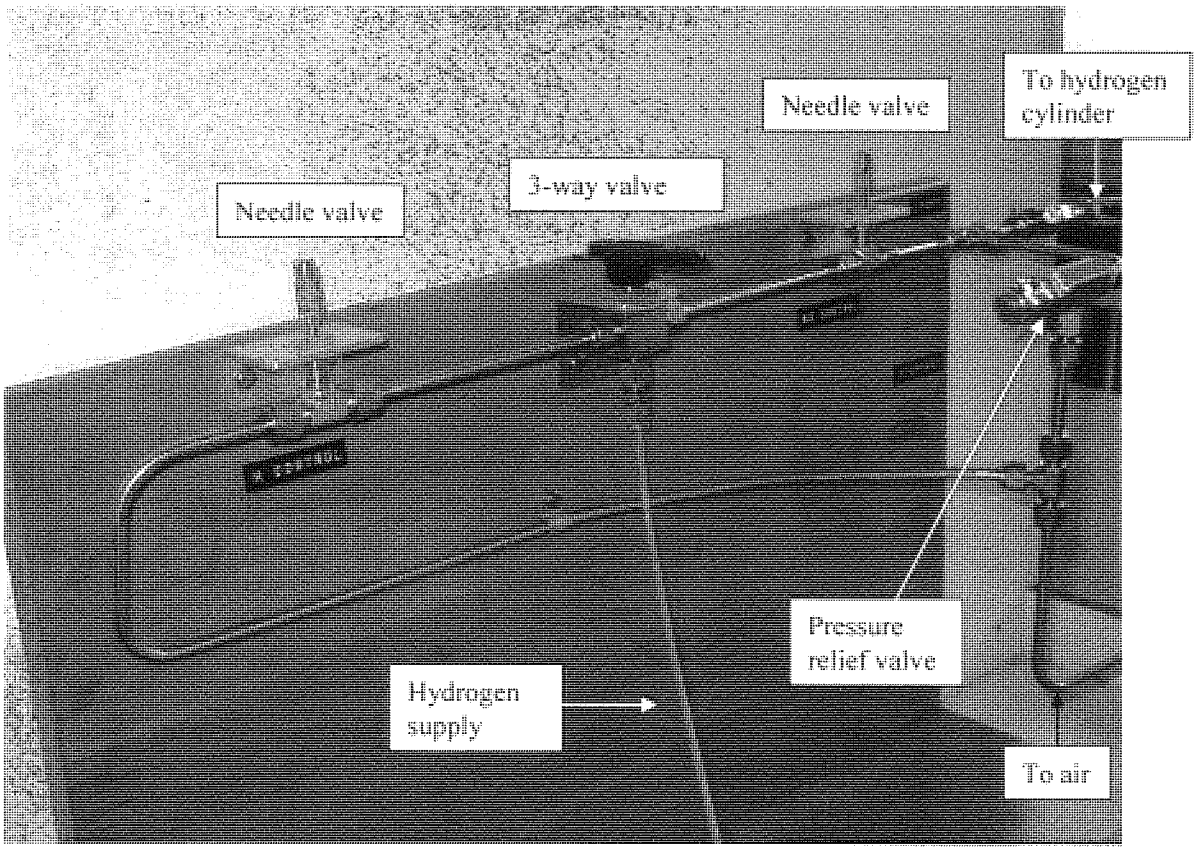

Figure 3.9 Hydrogen supply for the microwave reactor

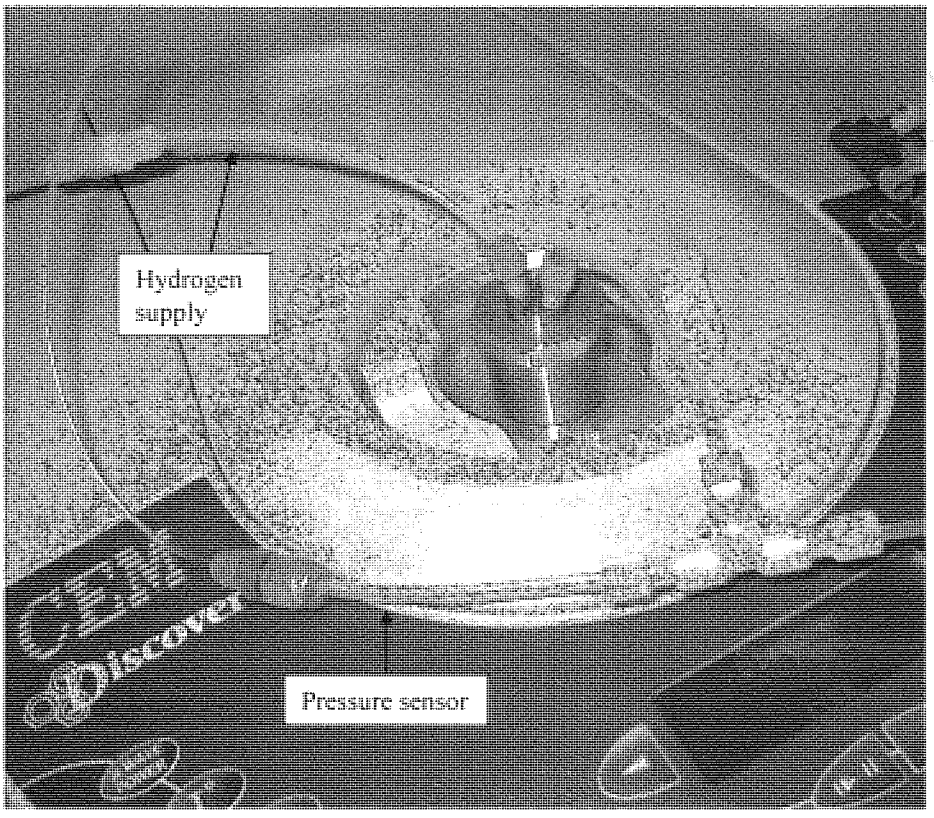

Figure 3.10 Microwave hydrocracking reactor

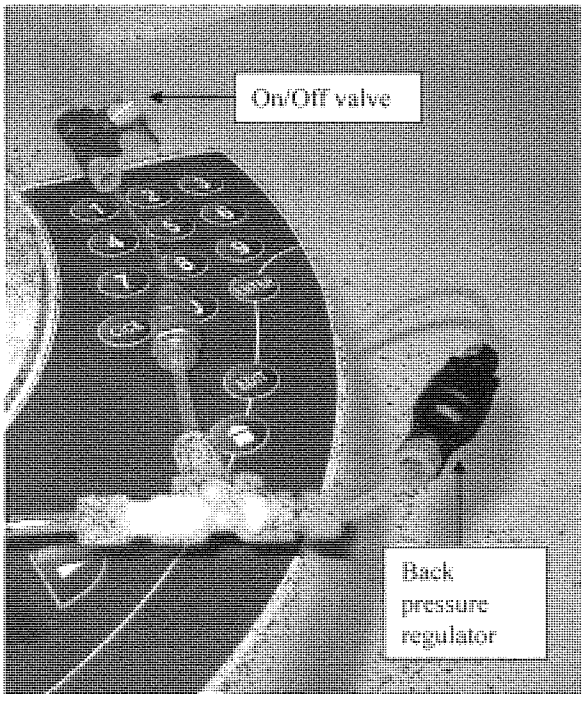

Figure 3.11 On/Off valve, back pressure regulator details

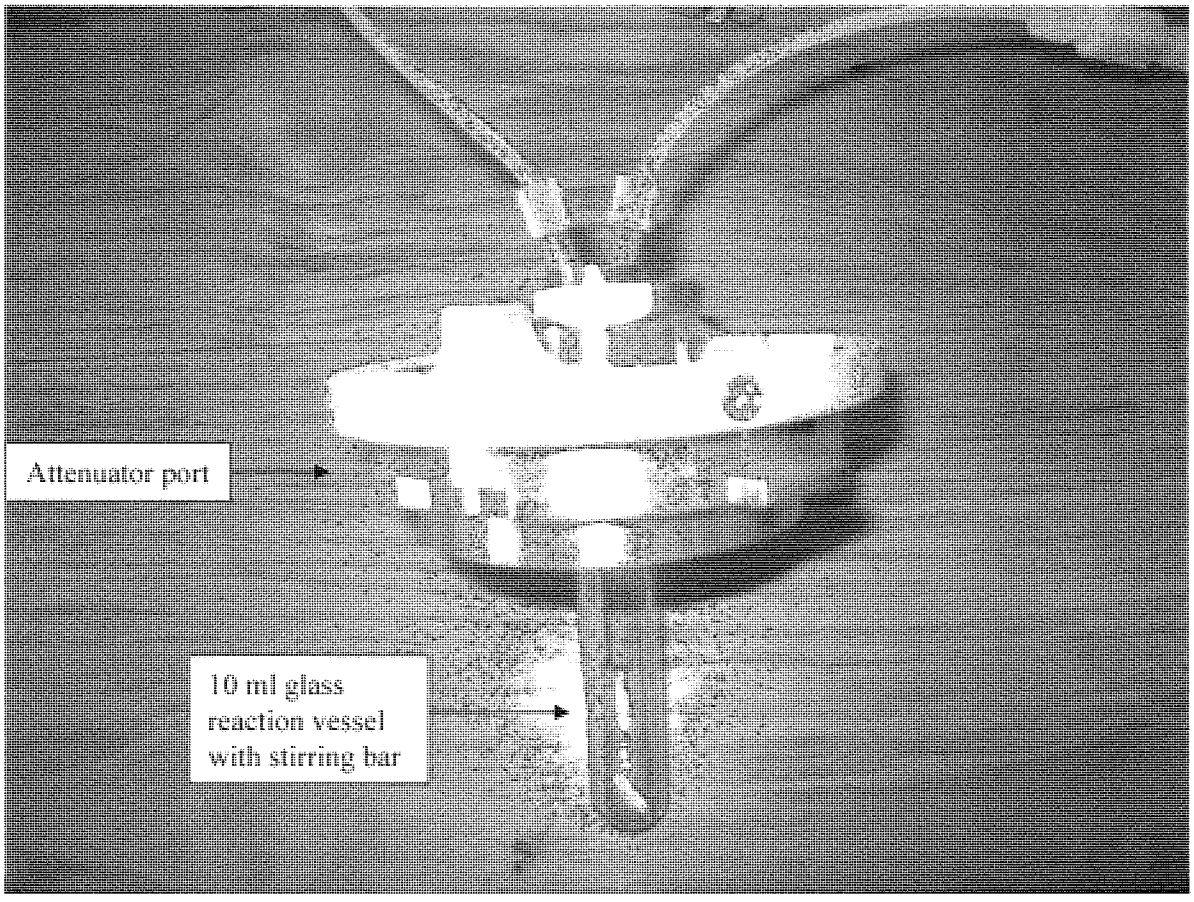

Figure 3.12 Reaction vessel topped with attenuator

The presence of hydrogen, which is a very flammable gas, made safety a critical issue. Therefore, two safety features were installed in the system, a pressure relief valve set up at 20 bar (Figure 3.9) in order to deal with potential failure of the hydrogen cylinder and a back pressure regulator set at 17.2 bar (250 psig)(Figure 3.11) in order to keep the pressure in the microwave reactor below 17 bar and prevent any vial, tubing or fitting failure.

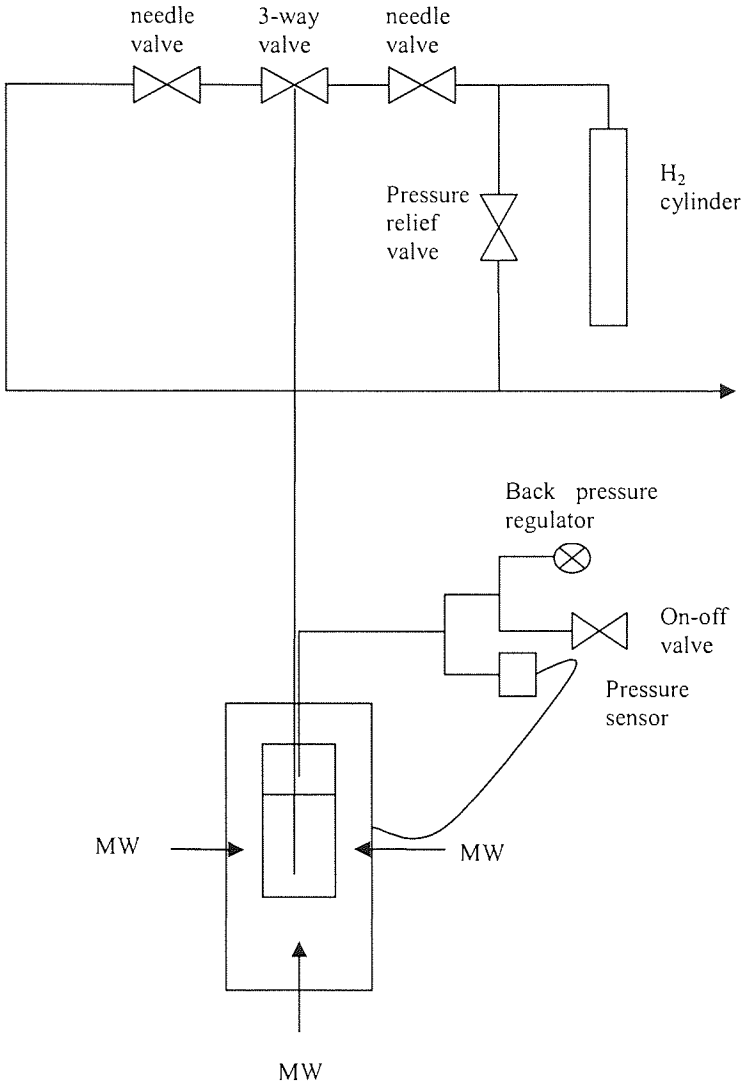

Figure 3.13 Schematic diagram of the microwave hydrocracking reactor

The reactor charged with the feed, the solvent, the catalyst and a stirring bar had to be purged before heating in order to exclude any air present that could cause an explosion. The 3-way valve and the on-off valve were turned on, while the right needle valve was set up at minimum flow. The hydrogen regulator was set up at a minimum pressure (1 bar), the needle valve was set up to maximum flow and the system was purged for 15 min. After that the on-off valve was turned off and the needle valve was set to minimum flow again. The hydrogen regulator was set up to the desired pressure and the system was pressurised. The operational parameters (temperature, pressure, power and time) were programmed and microwave irradiation was applied. The 3-way valve was turned off.

Experimental runs involving different solvents alone or with coal liquids and/or NiMo supported on alumina as catalyst were conducted under argon in order to assure the safety of the system before the introduction of hydrogen, because of its high flammability. Chloroform, methanol or a mixture of those two were tested as solvents, since the products would be sent to Imperial College for analysis and they collect their products in chloroform/methanol. The chloroform used in the experiments at Aston had been stabilised with amylene by the supplier.

The hydrocracking run was performed with coal extract (1 g), NiMo on alumina (250 mg) as a catalyst and chloroform as a solvent. The system was initially purged with hydrogen for 15 min to remove any air and then pressurised at 165 psig (ca. 11 bar). Power was set at 300W, temperature initially at 200°C and run time at 30 min. Again it should be noted that the measured temperature was that of the bulk liquid (coal liquid and chloroform) and not of the catalyst, which should have been considerably higher. After the run the system was depressurised by opening the on-off valve and the products were recovered and sent to Imperial College for analysis.

3.5 Decomposition of bio-oil under heating

3.5.1 Microwave irradiation of bio-oil

A series of runs was performed with bio-oil under microwave irradiation aiming to investigate the effect of temperature, hold time and char content in bio-oil's decomposition. Simultaneous cooling and stirring was applied in all the runs, whereas temperature, pressure and power were monitored throughout and during the cooling down period.

More specifically: Bio-oil (ca. 8g) was introduced via a pipette in a pre-weighed glass vial containing a stirring bar and the vial was sealed and placed in the microwave. The pressure sensor was placed on top of the vial, the nitrogen cylinder (required for cooling) was opened and the regulator set to 1.5 bar. Temperature, power and time were programmed in the microwave and irradiation started. After each run a cooling period occurred until the bio-oil reached ambient temperature. The seal was removed, the vial reweighed and the bio-oil transferred in another vial for analysis.

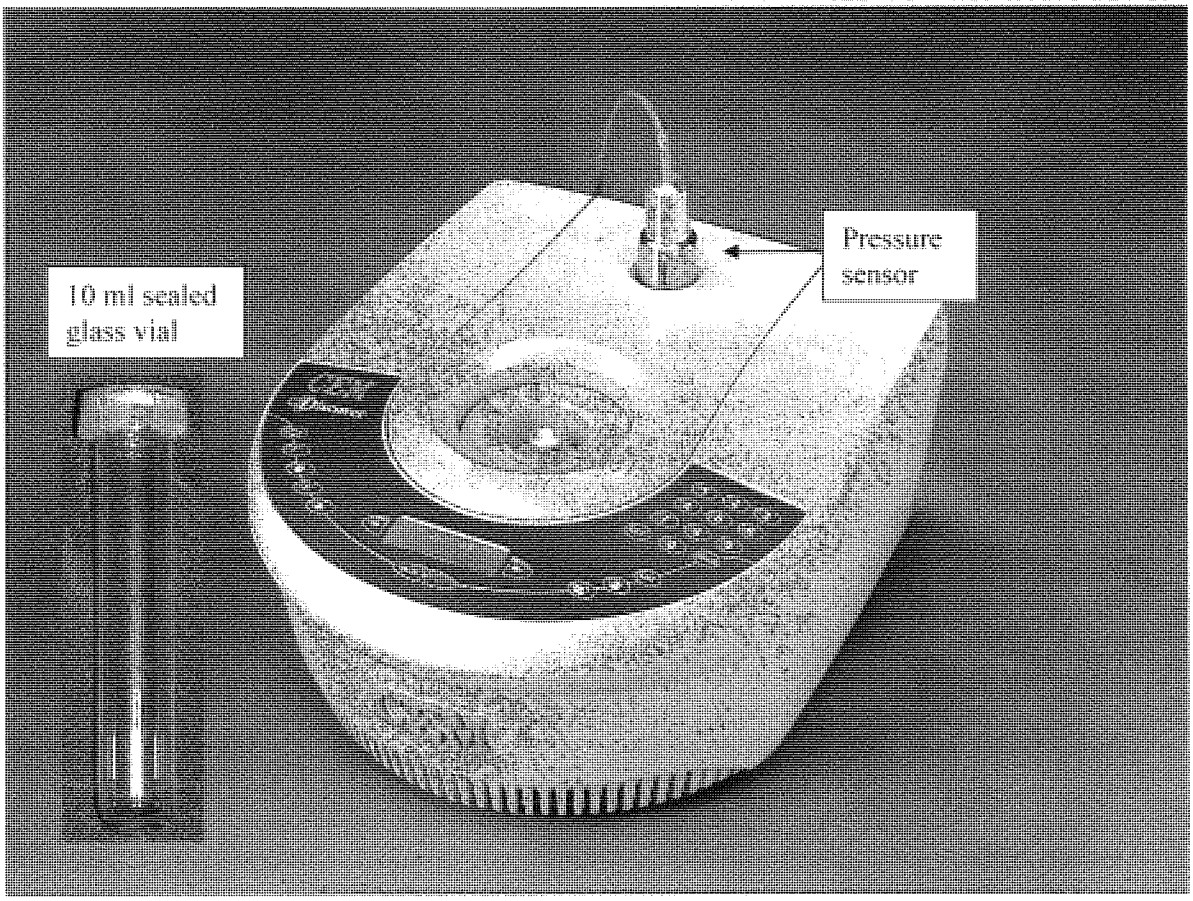

Figure 3.14 CEM Focused Microwave™ Synthesis System, Model Discover

The following experimental conditions were employed during the runs:

- 50, 75, 100, 125, 150 and 175°C and hold times 0 and 30 min respectively
- 150°C, 250 W and 0, 10, 20, 30 and 40 min hold time respectively
- 125°C, 200 W and 30 min hold time with four different bio-oils, the original bio-oil (char content 0.14%), filtered bio-oil and bio-oil with 2% either wood or grass char content.

Another series of runs was conducted with bio-oil under microwave irradiation in the presence of a range of clays and their pillared derivatives to investigate if they have any catalytic effect in bio-oil's decomposition.

Initially a series of tests was carried out with bio-oil and laponite aiming to determine the conditions under which 30 min reproducible runs could be performed. Those runs, which were conducted at 175 or 150°C under simultaneous cooling and stirring, were stopped before the end of the 30 min hold time due to excessive pressure increase and

in two occasions the vials ruptured. Due to the temperature and pressure variations at these conditions, in addition to the lower hold time because of the pressure increase, another set of runs was conducted without cooling at 160°C in an attempt to achieve the 30 min hold time. In this case the temperature increase was more controlled, the final pressure was below 200 psig and the 30 min hold time achieved.

A set of runs was then conducted under these conditions (160°C, 150 W, 30 min hold time, no cooling, stirring) with bio-oil and a range of catalysts: sodium montmorillonite, europium, cerium and chromium oxide pillared montmorillonites, laponite, tin oxide pillared laponite and NiMo on alumina. A blank run was also performed under the same conditions (bio-oil only) to act as a reference for the analysis.

The same procedure with that described for the runs conducted with bio-oil was followed with the only difference that catalyst (10% wt of the feed) was also introduced in the vial before irradiation. After each run the products were recovered and the catalyst particles separated via vacuum filtration. The filter cake was washed with THF until the washings were clear. Samples of the filtrates (dilute product solutions in THF) were stored for analysis.

3.5.2 Conventional heating of bio-oil

A series of runs was performed with bio-oil treated at 50, 100, 125, 150 and 175°C for 30 min in a conventional mineral oil bath in order to compare the effect of microwave irradiation in bio-oil's decomposition with that of conventional heating under the same conditions. Before each run bio-oil (ca. 8g) was introduced in a pre-weighed glass vial (10 ml) via a pipette and the vial was sealed and placed in the bath which was equipped with a heating resistance and a thermostat. After each run the vial was immersed in an ice bath in order to cool down the bio-oil and stop it from degrading further, the seal was removed and the vial reweighed. The bio-oil was transferred in another vial and kept for analysis.

Since it was not possible to monitor the actual temperature of the bio-oil, a series of tests was performed in advance correlating the temperature in the vial (filled with mineral oil) with that in the bulk of the bath.

4 X-RAY POWDER DIFFRACTION; RESULTS AND DISCUSSION

X-ray powder diffraction (XRD) is used for the determination of basal spacing and was employed as the principal method for the characterisation of the starting clay materials and their pillared derivatives. Since basal spacings are a measure of the distance between the clay layers, addition of pillaring agents and subsequent changes via calcination steps directly affect these values. It should be noted that the intensity of the peaks depends on how well the sample is packed on the sample holder and the specific X-ray beam applied. It is not an absolute measure for comparing scans.

XRD results (Table 4.1) are presented in this chapter and used to assess the effectiveness of the different preparation methods (either conventional or microwave) with regards to pillaring and investigate the influence of the preparation parameters (starting material, pillaring species, hydroxyl to metal ratio etc.) in the end products. XRD results from a starting material and a small selection of its pillared derivatives after being used as hydrocracking catalysts are also exhibited herein (Table 4.2), aiming to elucidate the effect of the hydrocracking procedure on their structure.

4.1 Wyoming Bentonite, sodium montmorillonite and pillared montmorillonites

4.1.1 Wyoming Bentonite and sodium montmorillonite

The XRD pattern of Wyoming Bentonite exhibited a broad and asymmetric peak indicating the presence of two unresolved peaks (Figure 4.1) representing two basal spacings, one at 15.2Å and a second corresponding to 13Å. These were attributed to sodium cations with different hydration spheres between the sheets of montmorillonite. After calcination at 500°C the asymmetric peak almost disappeared and another peak appeared corresponding to 9.7Å which is the average thickness of the silicate layer of montmorillonite [119, 120].

However, the XRD pattern of refined Wyoming Bentonite (Figure 4.2) showed a less intense peak compared to the clay as received, indicating that the stirring undertaken during the refining process leads to degradation of crystallinity. The slightly higher basal spacing (16Å) was attributed to the higher degree of hydration of the sodium cations in the interlayer.

The XRD pattern of the homoionic sodium montmorillonite exhibited two separate peaks, one weak corresponding to a basal spacing of 16Å and a second one sharp and intense corresponding to 9.7Å (Figure 4.3). The former was attributed to the hydrated sodium cations and its low intensity indicated low extent of order in the clay layers caused by the continuous stirring and centrifugation employed during the preparation of sodium montmorillonite leading to degradation of crystallinity. The latter resembled the average thickness of the montmorillonite layer and was attributed to the introduction of protons in the interlayer during preparation (addition of HCl). After calcination at 500°C the first peak became even weaker and the second one sharper and more intense indicating the complete collapse of the clay.

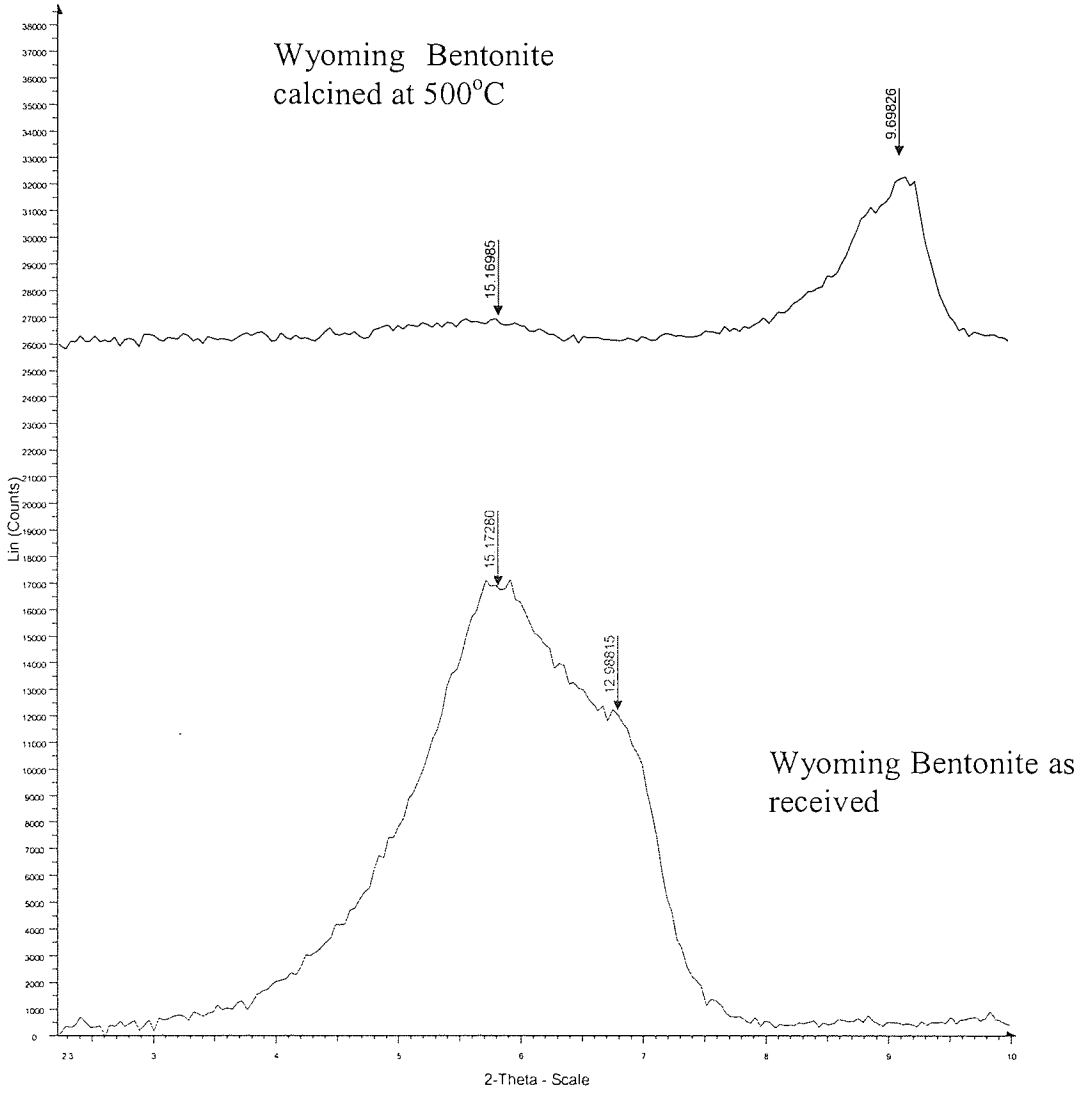

Figure 4.1 XRD patterns for Wyoming Bentonite

Table 4.1 Basal spacings for starting materials and their pillared derivatives

	Before calcination		After calcination	
Sample	**d_{001} (Å)**	**2θ**	**d_{001} (Å)**	**2θ**
W.B.	15.2 / 13	5.8 / 6.8	15.2 (w)/ 9.7	5.8 / 9.1
Ref. W.B.	16.0	5.5		
Na-mont	16.0 (w)/10	5.5 / 8.8	16.0 (vw)/ 9.7	5.5 / 9.1
CM1	16.9	5.2	15.6 (vw)	5.7
CM2	16.5	5.3	16.2 (vw)	5.4
CM3	16.5	5.3	15.4 (vw)	5.7
CM4	26.8	3.3	20.9	4.2
CM5	27.9	3.2	20.7	4.3
CM6	28.1	3.1	22.5	3.9
CM8	29.0	3.0	22.3	4.0
CM16	28.2	3.1	23.4 (vw)/ 15.9	3.8 / 5.5
CM7 (MW)	18.9	4.7		
CM9 (MW)	18.3	4.8		
CM10, CM11, CM12 (MW)	18.4	4.8		
CM13	18.4	4.8		
CM14 (MW)	18.9	4.7		
CM15 (MW)	20.0	4.4		
CM17 (MW)	20.2	4.4		
Cr/Ce mont	27.4 (vw)/15.3	3.2 / 5.8	no peak	
Ce-mont	15.7	5.6	15.6 (vw)	5.7
Eu-mont	15.4	5.7	15.5 (w)	5.7
SM1	15.7	5.6	15.7 (vw)/ 9.9	5.6 / 8.9
SM2 (MW)	15.3	5.7		
SM3 (MW)	13.8	6.4		
SM4 (MW)	14.6	6.0		
SM5 (MW)	15.6	5.6	15.7 (vw) / 10	5.6 / 8.8
SL7	no peak			
SL2	no peak			
CL	15.8	5.6	no peak	

W.B.: Wyoming Bentonite, mont: montmorillonite, CM: chromia pillared montmorillonite, SM: tin oxide pillared montmorillonite, SL: tin oxide pillared laponite, CL: chromia pillared laponite, w: weak, vw: very weak
Standard deviation in d_{001} measurements: 0.1 Å

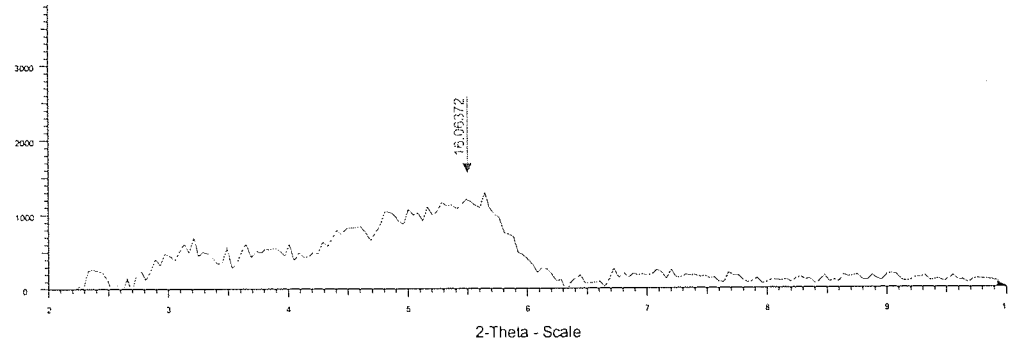

Figure 4.2 XRD pattern for refined Wyoming Bentonite

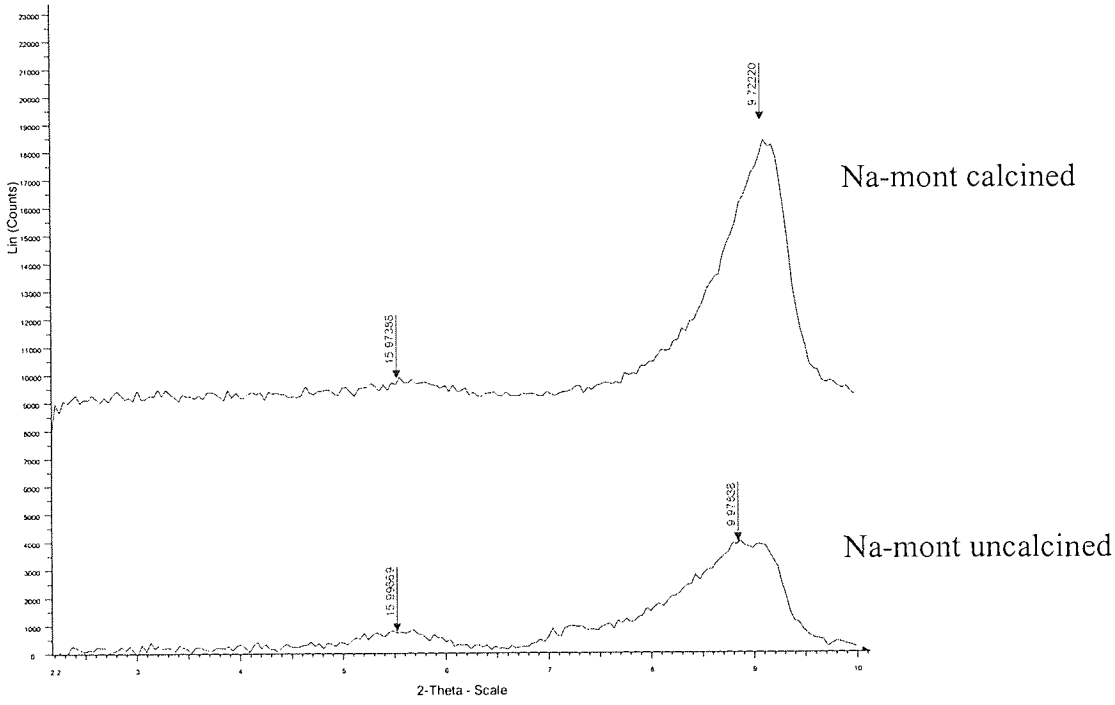

Figure 4.3 XRD patterns for sodium montmorillonite

4.1.2 Chromia pillared montmorillonites

As can clearly be seen from the measured basal spacings (d_{001}) for the starting materials and the prepared chromia pillared montmorillonites, in all cases there was an increase in d_{001} upon pillaring and a decrease during calcination (Table 4.1). However, the extent of the changes varied depending upon the experimental conditions.

Hydroxyl to chromium ratio

For CM1, CM2 and CM3 (OH/Cr =1) there was a slight increase in the basal spacing compared to the starting materials, which became even smaller after calcination (i.e. 1 h at 500°C under argon). An increase in refluxing time from 16 to 36h did not appear to

affect the basal spacing. These results are in the same range as those reported by Palinko et al. [116] (15.2Å uncalcined) and Pinnavaia et al. [117] (18.3Å uncalcined) for the same OH/Cr ratio of 1. However, they contradict the values presented by Bodman (27Å uncalcined and 23Å calcined) [2, 4].

In the case of CM4 and CM5, which were prepared following the patented method by Pinnavaia et al. for a OH/Cr ratio of 2, there was a significant increase in the basal spacing to ca. 27Å in agreement with the patent [117]. This decreased to 21Å after calcination. Clearly a higher OH/Cr ratio led to the production of higher pillaring units.

It should be noted that except the OH/Cr ratio which was changed to 2 for the preparation of CM4, the pillaring stoichiometry (moles of Cr per g of clay) and the clay concentration were also altered. This occurred because the patented method was reproduced exactly [117] Due to limited experimentation time it was not possible to change only one experimental parameter at a time.

Reactant concentration

Usually, diluted systems are employed in order to promote the diffusion of the pillaring species into the clay particles and provide a regular pillaring distribution. From an industrial point of view this process may be uneconomical, since manipulation of high volumes of aqueous pillaring solutions and clay slurries would require enormous equipment. Both the concentration of the pillaring agent and the use of dry powder clay rather than dilute slurry were investigated.

First, a highly concentrated pillaring solution consisting of aqueous solutions of 0.5M chromium nitrate and 0.75M sodium carbonate was used, keeping all the other experimental conditions unaltered (Table 3.1). CM6 and CM16, prepared from Wyoming Bentonite and sodium montmorillonite respectively, both exhibited basal spacings of 28Å. However, CM16 showed a broad and asymmetric peak in its XRD pattern consisting of two unresolved peaks, one weak corresponding to 28.2Å and another more intense corresponding to 16.1Å, indicating the existence of chromia oligomers of different composition between the sheets of montmorillonite (Figure 4.4). After calcination at 500°C the first peak decreased to 23.4Å while the second remained unaltered at 15.9Å because of the dehydroxylation of the pillars. Under the same

experimental conditions (Table 3.1), but with the exception of mixing the pillaring solution with the clay slurry before refluxing, the resulting clay CM13 exhibited limited pillaring (18.4Å). Therefore, the pillaring solution should be refluxed in advance for best results as described in the literature [117, 2, 121].

Secondly, Wyoming Bentonite was added as a powder to the highly concentrated pillaring solution again with success (CM8, 29Å). The addition of the clay as powder (100% w/v) overcame the handling difficulties of a highly concentrated clay paste, due to the thixotropy of the clay.

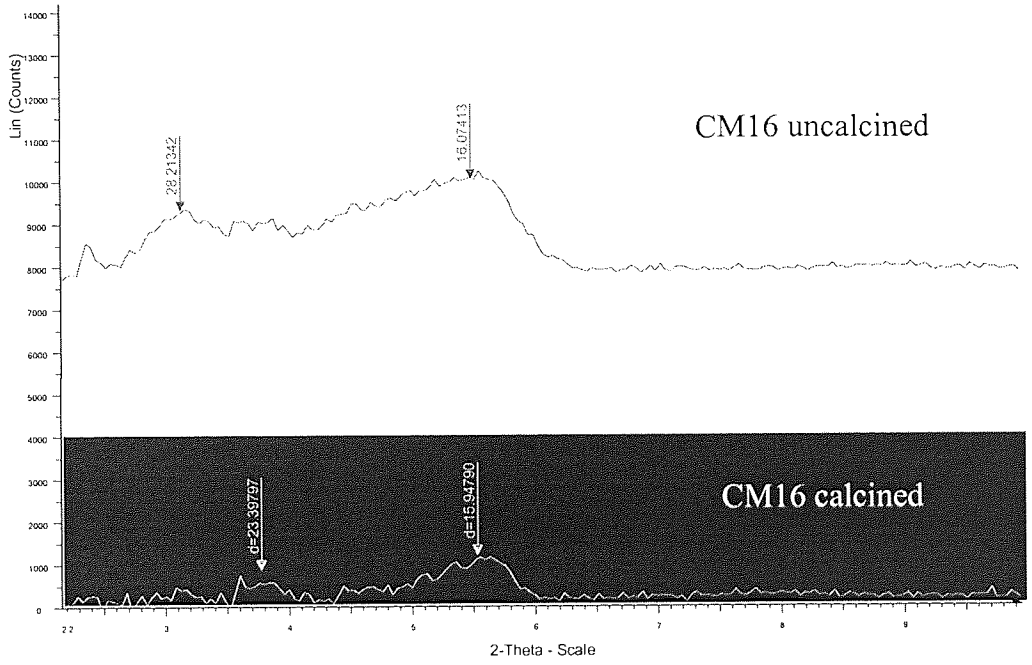

Figure 4.4 XRD patterns for chromia pillared montmorillonite CM16

Microwave method

With microwave irradiation a considerably faster preparation, possibly with highly concentrated clay suspensions and pillaring solutions, could be achieved, leading to large scale production of pillared clays.

The first approach was to mix the pillaring solution with the clay slurry before irradiation in contrast to the conventional method, because this procedure had been followed for the microwave preparation of an alumina pillared clay in the literature [52]. The same OH /Cr ratio and pillaring stoichiometry with those employed in the preparation of CM6 were used (Table 3.1, Table 3.2). However, higher clay

concentration (2%) and metal salts concentrations were employed imposed by the limited operational volume of the microwave (55ml). Power (100 W), temperature (95°C), hold time (2 min) and simultaneous cooling were set as starting point in the investigation. The basal spacing of the resulting clay CM7 was 18.9Å, which confirmed some pillaring, but was lower than that of CM6 (Table 4.1).

In the second step the power was increased to 165W and the effect of hold time without cooling was investigated keeping all the other parameters unaltered (Table 3.2).It was observed that as soon as the set temperature was reached, the microwave power was zeroed. That, in combination with the fact that CM9 to CM12 all displayed the same basal spacing, which was lower than the respective of CM7 under cooling, indicates that hold time without cooling has no effect in the basal spacing and that the application of simultaneous cooling is favourable.

The next approach was to support the necessity of irradiating the pillaring solution mixed with the clay slurry by conducting two experiments under exactly the same conditions. In the first experiment only the pillaring solution was irradiated and then mixed with the clay slurry (procedure similar to the conventional method), whereas in the second experiment the pillaring solution was mixed with the clay slurry before irradiation. The first experiment clearly led to lower basal spacing (CM14, 18.9Å) than the second (CM15, 20 Å).

Finally, the power and temperature settings were increased and the employed salt concentration decreased without any significant effect in the basal spacing of the produced pillared clay.

In conclusion, the results for the microwave assisted preparation of chromia pillared montmorillonites were promising (Figure 4.5). Although the achieved basal spacing of 20Å (CM17) may not have been as high as that following the conventional method by Pinnavaia, it was in agreement with other reports and confirmed some pillaring [121, 122]. Furthermore, the peaks were sharp and intense indicating a homogeneous distribution of chromia pillars assisted by microwave irradiation. A similar homogeneous distribution of alumina pillars was reported by Fetter et al. in the

respective microwave preparation of alumina pillared montmorillonites [52]. Further experimentation is required to optimise the microwave preparation method.

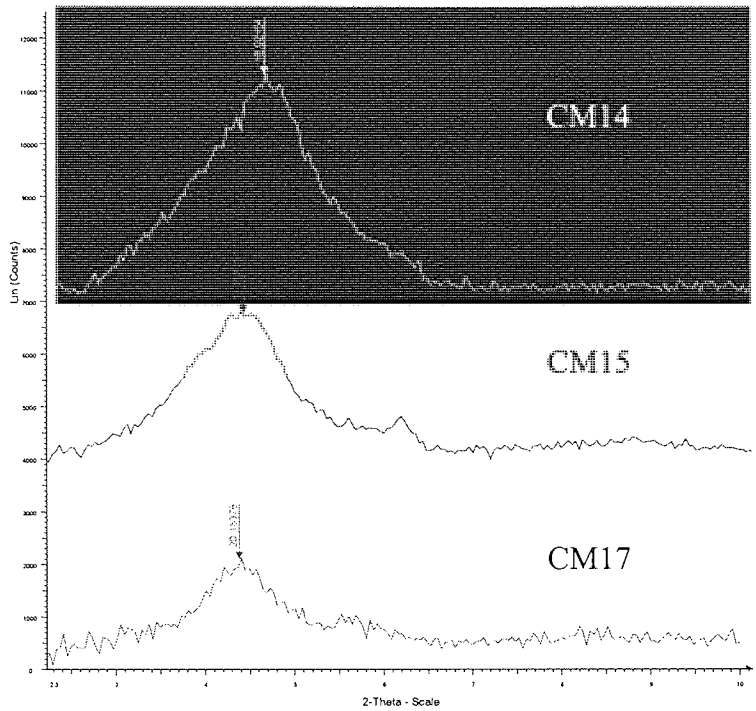

Figure 4.5 XRD patterns for chromia pillared montmorillonites prepared via a microwave assisted method (CM14, CM15 and CM17)

4.1.3 Tin oxide pillared montmorillonites

The basal spacing for conventionally prepared tin oxide pillared montmorillonite (air-dried) increased from 15.2Å (starting material Wyoming Bentonite) to 15.7Å which is not very significant. After heat-treatment for 1 h at 500°C the initially observed peak weakened in intensity, and a second peak appeared at 8.9° 2θ corresponding to ca 10Å (thickness of the montmorillonite layer) (Figure 4.6). This decrease in intensity was attributed to a low number of parallel layers with the same basal spacing indicating partial collapse of the tin oxide pillars.

These results are basically in agreement with those of Hannus et al. [123], although they have reported complete collapse of the pillars (10Å) after treatment for 2h at 500°C. They have suggested that the intercalated species are partially hydrated tin oxide species, most probably in trimeric form [124], whose degree of hydration depends on the temperature and possibly, the duration of heat treatment, and that moderately strong hydrogen bonds and van der Waals interactions keep the intercalated structure together.

When the tin oxide species dehydrate, they move to the outer surface of the clay. It is presumed that the longer refluxing (20h compared to 2h) undertaken during the current preparation has led to a higher degree of hydration of the tin oxide pillar. As a result the pillar was not completely dehydrated during the heat treatment, preserving some of the hydrogen bonds that keep the intercalated structure intact.

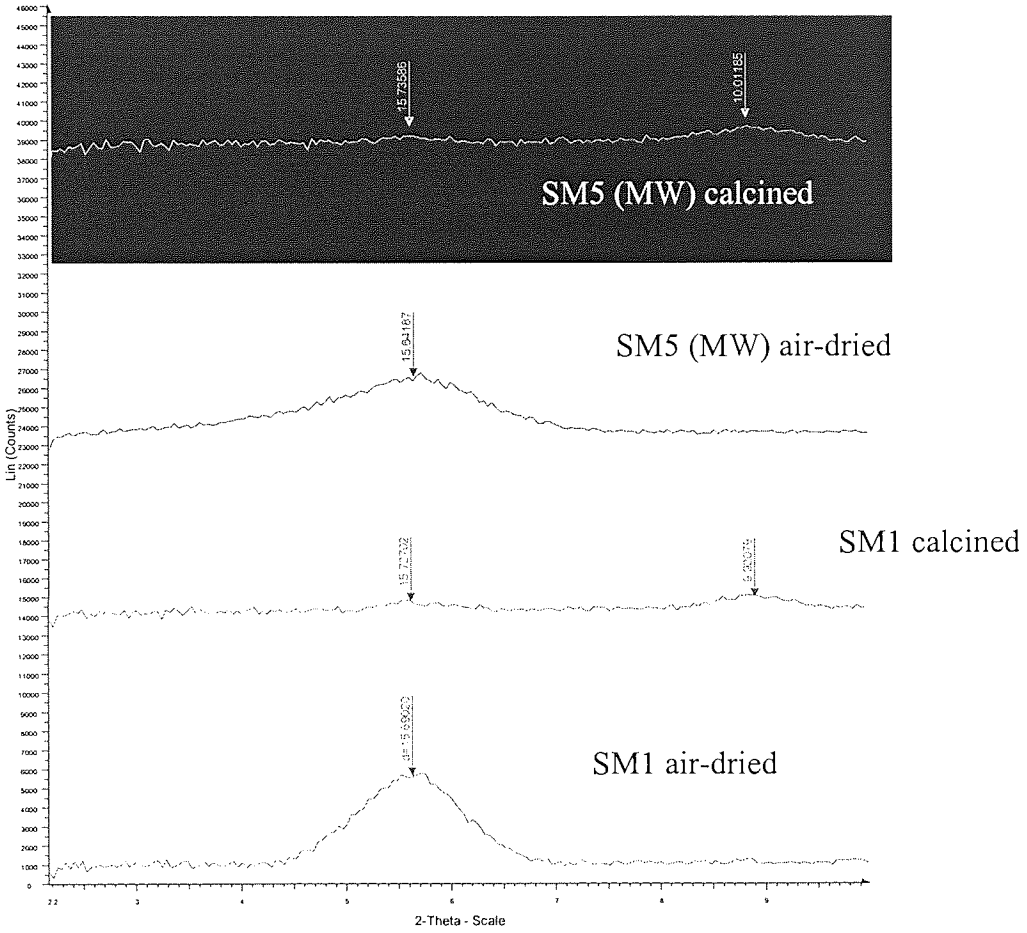

Figure 4.6 XRD patterns for tin oxide pillared montmorillonites

The XRD results for the tin oxide pillared montmorillonites prepared following microwave assisted methods showed similar values with those prepared by the conventional method. Therefore, microwave irradiation can be successfully applied for the synthesis of tin oxide pillared montmorillonites.

4.1.4 Cerium and europium oxide pillared montmorillonites

Pillaring of sodium montmorillonite with cerium or europium oxides did not significantly affect the basal spacing of the parent clay (Figure 4.7). This was attributed to the non-formation of polynuclear cationic complexes during hydrolysis of the salts of

the respective rare earth metals, since basal spacing is determined by the sizes and orientation of these complexes. In the case of cerium oxide pillared montmorillonite the observed basal spacing (15.7Å) is in agreement with that reported by Hernando et al. [35], whereas, according to the author's knowledge, no references are made in the literature regarding europium oxide pillared montmorillonite. In both cases the diffraction peaks were quite sharp indicating a relatively homogeneous pillaring process. Nevertheless, after calcination at 500°C the peaks were hardly observed indicating the collapse of the pillars. Before calcination occurs, it is still possible to exchange the pillars. Therefore, calcination is essential for the fixation of the metal oxide pillars and the stabilisation of the pillared clay, even if it leads to a decrease in its basal spacing or collapse of the pillars.

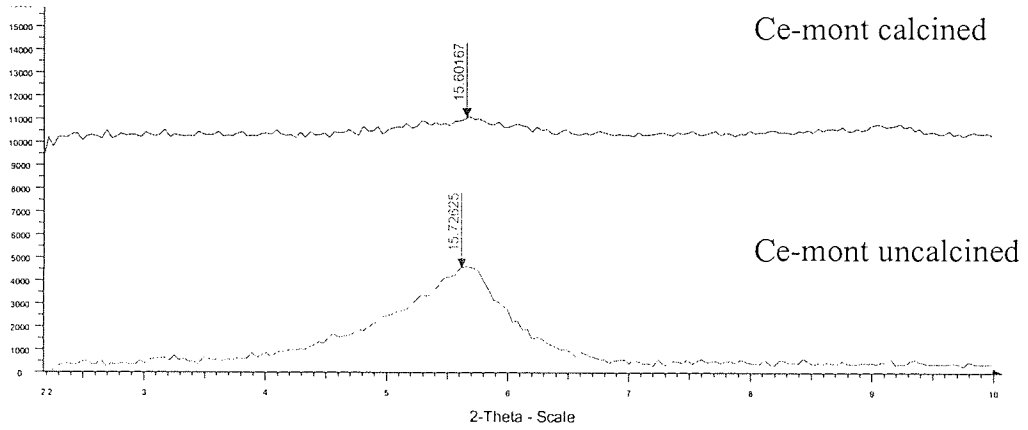

Figure 4.7 XRD patterns for cerium oxide pillared montmorillonite

4.1.5 Chromia pillared montmorillonite modified with cerium oxide

The incorporation of cerium in a chromia pillared montmorillonite decreased the basal spacing with respect to the analogous sample without cerium (CM16) from 28.2Å to 27.4Å and from 16.1Å to 15.6Å (Figure 4.4,Figure 4.8), which suggested that cerium was not found in the chromia pillars and may have been in another form such as an oligomeric cation. When the sample was calcined at 500°C the diffraction peaks were not observed indicating once again the collapse of the pillars. These results are in agreement with the work of Hernando et al. who reported that the introduction of cerium in an alumina pillared montmorillonite led to a decrease in the basal spacing with respect to the montmorillonite with single alumina pillars [35]. However, other authors have reported the synthesis of pillared clays with mixed alumina and cerium oxide pillars with higher basal spacings than those attributed to single alumina pillars

[119, 120] indicating that there is little consistency about the preparation and structure of this type of pillared clays.

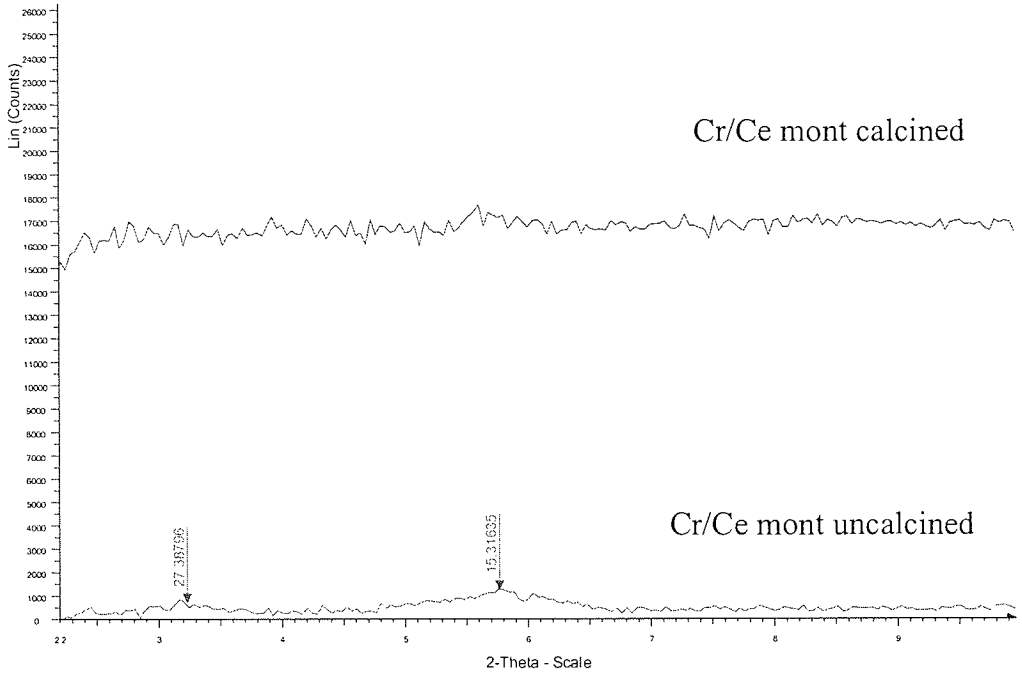

Figure 4.8 XRD patterns for chromia pillared montmorillonite modified with cerium oxide

4.2 Laponite and pillared laponites

In the case of laponite and tin oxide or chromia pillared laponite X-ray powder diffraction could not be used to determine the basal spacings as the XRD patterns did not contain a first order reflection between 2^{o} and 10^{o} 2θ. The absence of such a reflection is attributed to the small size of individual particles and the random rather than uniform face-to-face orientation of the clay platelets for both the starting material and the products.

4.3 Pillared clays after use as catalysts

Some of the pillared clays were characterized by XRD after their first and second use as hydrocracking catalysts following the same procedure with the fresh materials. The results are presented in Table 4.2.

Table 4.2 Basal spacings of pillared clays after use as hydrocracking catalysts

	Before use		After 1st use		After 2nd use	
Sample	**d_{001} (Å)**	**2θ**	**d_{001} (Å)**	**2θ**	**d_{001} (Å)**	**2θ**
CM3	15.4 (vw)	5.7	15.9	5.6	15.9	5.6
CM6	22.5	3.9	15.7	5.6	15.7	5.6
CM6 after HC	22.5	3.9	20.0 / 16.2	4.4 / 5.4		
Eu-mont	15.5 (w)	5.7			16.0	5.5
SL7	no peak		15.5	5.7	No peak	
SL2	no peak		15.5	5.7	15.4	5.7
CL	no peak		15.9	5.5	15.9	5.5
Blank	15.3	5.7				
Standard deviation in d_{001} measurements: 0.1 Å						

All catalysts exhibited similar basal spacings after the first and the second use. CM6, in particular, displayed a significant reduction of ca. 6.5Å in the basal spacing after the first use indicating that the hydrocracking conditions in the microbomb reactor (190 bars and 440°C) were very harsh causing the collapse of the chromia pillars. This assumption was supported by the lower basal spacing compared to the respective before use exhibited in the XRD pattern of CM6 after undergoing hydrocracking conditions in the absence of feed. CM3, which had initially a low basal spacing, was not affected by the hydrocracking conditions. The europium oxide pillared montmorillonite also exhibited similar basal spacing after its second use.

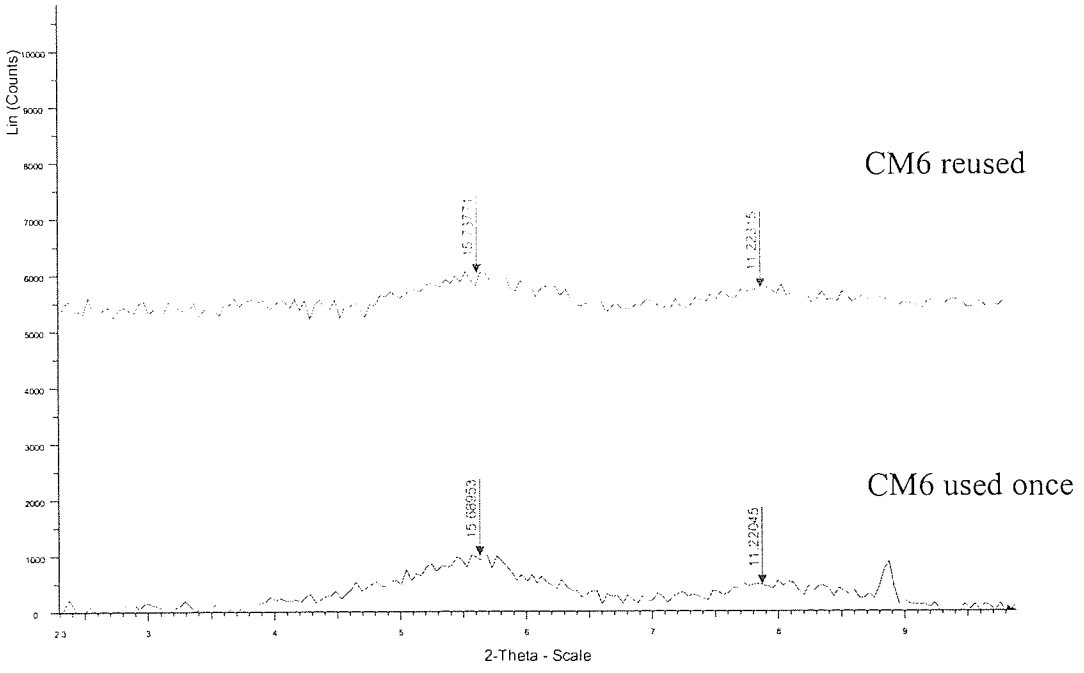

Figure 4.9 Chromia pillared montmorillonite CM6 after use as hydrocracking catalyst

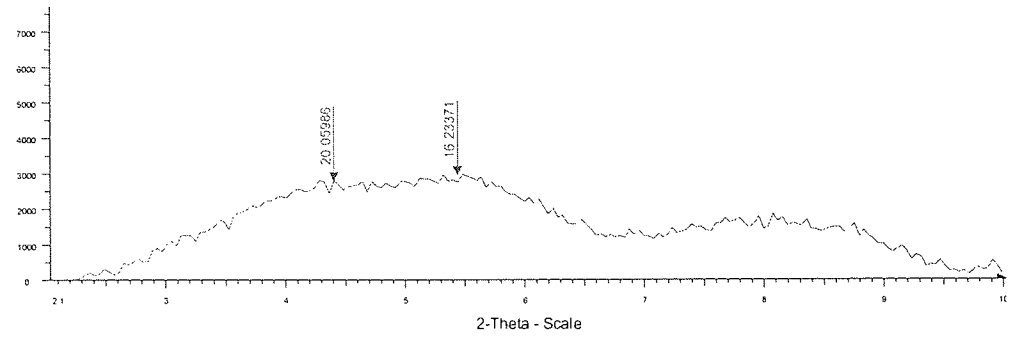

Figure 4.10 Chromia pillared montmorillonite CM6 after undergoing hydrocracking conditions in the absence of feed

However, special care should be taken when interpreting the peaks observed for the pillared montmorillonites after use as catalysts, since they all appeared at ca 5.7° 2θ, i.e. the region at which a weak peak appeared during a blank run (with an empty sample holder). Similar care should be taken with all the weak peaks observed after calcination.

A strange phenomenon was observed for the pillared laponites, which after use as catalysts exhibited a first order reflection and their basal spacing could be measured (Figure 4.11). This may be attributed to somehow better crystallization of the catalysts after use. The peaks observed were intense enough to be considered real and not be attributed to the sample holder.

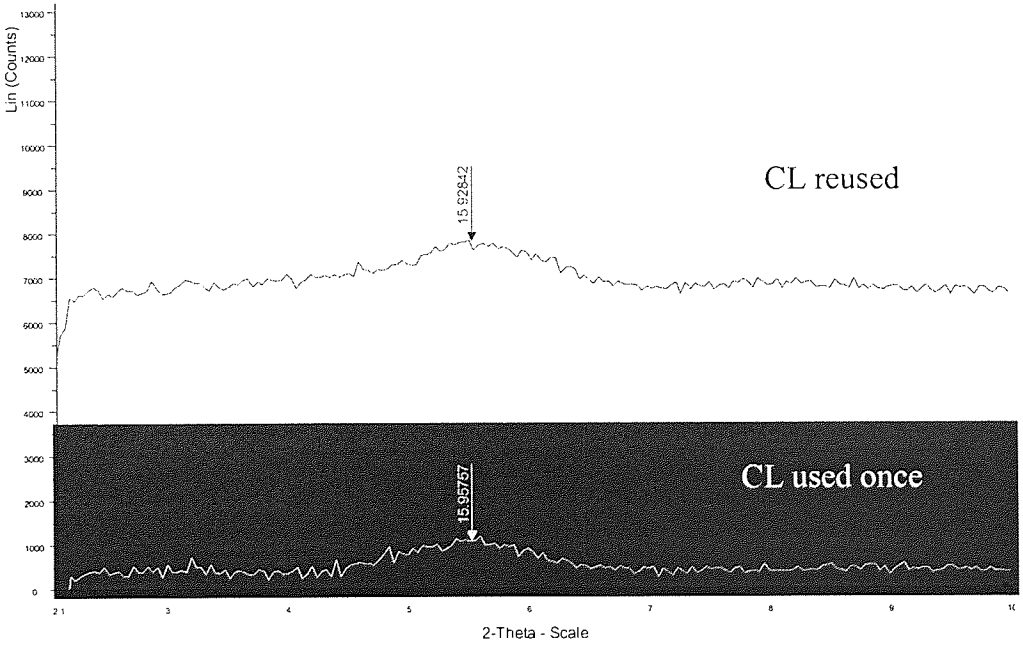

Figure 4.11 XRD pattern for chromia pillared laponite after use as hydrocracking catalyst

In order to gain more insight in the changes occurring to the pillared clays during their use as catalysts a series of XRD scans were performed on fresh sodium montmorillonite and reused chromia and europium oxide pillared montmorillonite, as well as laponite and reused tin oxide pillared laponite over a longer range (2 to 60° 2θ)(Figure 4.12, Figure 4.13). The pillared montmorillonites after use retained some crystallinity although the peaks of the clay layers decreased in intensity. However, this analysis is still inconclusive with regards to what takes place in the interlayer. Most likely the pillars have collapsed and the observed peaks are attributed to the sample holder. On the contrary, although laponite showed poor crystallinity before use, it presented first order reflection after use indicating higher order among the clay layers and possibly the existence of pillars.

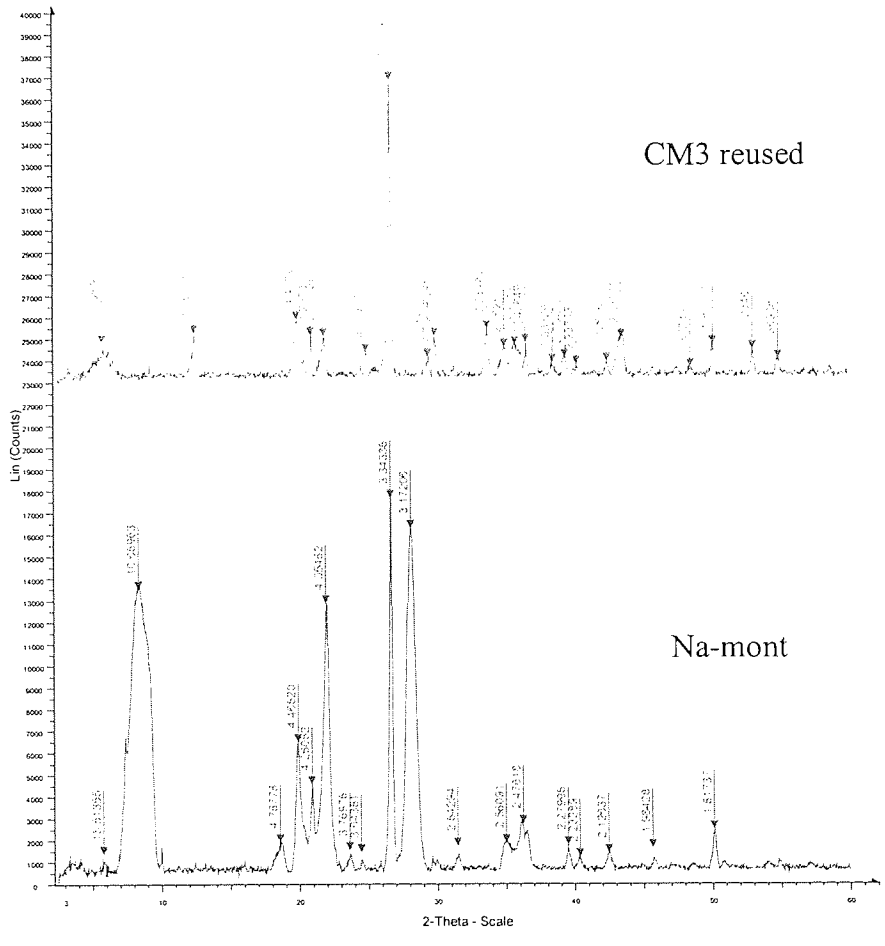

Figure 4.12 Long XRD scans for sodium montmorillonite and reused chromia pillared montmorillonite CM3

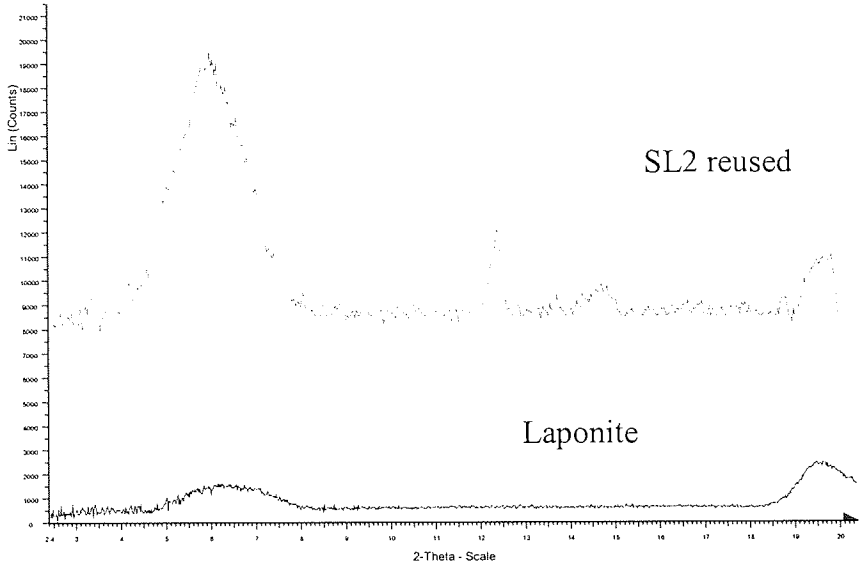

Figure 4.13 Long XRD scans for laponite and reused tin oxide pillared laponite SL2

4.4 Summary

X-ray powder diffraction was used as the principal method to study changes in the clays after pillaring reactions and calcination steps. All the prepared chromia pillared montmorillonites showed an increase in basal spacing upon pillaring and a decrease during calcination. However, the extent of the changes varied depending upon the experimental conditions, such as the OH/Cr ratio. The highest basal spacing (28 Å) was achieved at a OH/Cr ratio of 2. Furthermore, highly concentrated pillaring solutions and solid Wyoming Bentonite were employed successfully in the preparation despite the fears that this way diffusion of the pillaring species into the clay particles might be inhibited. The microwave assisted method led to lower basal spacing (20 Å) compared to the respective of the conventional method, but some pillaring was confirmed.

Tin, cerium or europium oxide pillared montmorillonites did not exhibit significant increase in basal spacing. This is probably due to the non-formation of polynuclear cationic complexes during hydrolysis of the salts of the respective metals. The incorporation of cerium in a chromia pillared montmorillonite decreased the basal spacing with respect to the analogous sample without cerium, indicating that cerium was not found in the chromia pillars and may have been in another form such as an oligomeric cation. After calcination at 500°C the diffraction peaks were barely or no longer observed indicating the collapse of the pillars in all the samples.

Some of the pillared clay materials that were used as hydrocracking catalysts were characterised by XRD and they all exhibited similar basal spacings. The used pillared montmorillonites retained some crystallinity although the peaks of the clay layers decreased in intensity. However, this analysis was inconclusive with regards to what took place in the interlayer. Most likely the pillars had collapsed during the hydrocracking process. On the contrary, although laponite showed poor crystallinity before use, it presented first order reflection after use indicating higher order among the clay layers and possibly the existence of pillars.

5 THERMOGRAVIMETRIC AND DERIVATIVE THERMOGRAVIMETRIC ANALYSIS; RESULTS & DISCUSSION

Thermogravimetric analysis (TGA) was selected as another characterisation method of the pillared clay materials and conducted in all three starting clay materials, i.e. Wyoming Bentonite, sodium montmorillonite and laponite, and their pillared derivatives before and after calcination. Derivative thermogravimetric analysis (DTG) curves were calculated using software provided by the manufacturer to elucidate the weight loss steps presented in the TGA curves and therefore aid characterisation. Weight loss is correlated with structural changes that occur during heating and these structural changes, in turn, indicate the thermal stability of the material.

TGA and DTG results are presented in this chapter and used to assess whether the preparation method (either conventional or microwave) plays any role in the thermal stability of the pillared clays and investigate how pillaring with different metal oxides and subsequent calcination influences the thermal behaviour of the starting materials.

5.1 Wyoming Bentonite, sodium montmorillonite and respective pillared clays

5.1.1 Wyoming Bentonite and sodium montmorillonite

Both thermograms for Wyoming Bentonite and sodium montmorillonite (Figure 5.1) consisted of two distinct weight loss steps. The first step over the temperature range 25 to 200°C corresponded to weight losses of about 6% and 1.5% for Wyoming Bentonite and sodium montmorillonite, respectively, and was due to mainly weakly adsorbed water molecules from the interlayer (25 to 100°C) and to hydration water from the exchangeable cations (100 to 200°C). Over the 200 to 550°C temperature range, the weights remained nearly constant. An additional 3% weight loss occurred between 550 and 750°C for both starting materials, indicating the removal of lattice water as the silicate frameworks began to be destroyed (dehydroxylation of the clay structure).

The derivative thermogravimetric analysis (DTG) curves express weight loss versus temperature (-dm/dT). The intensity of the peaks depends on the magnitude of the weight loss. In the case of starting materials the DTG curves consisted of two peaks in the ranges 25 to 150°C and 550 to 750°C (Figure 5.2). The first peak depicted

dehydration of the clay layers and the interlayer cations, whereas the second peak depicted dehydroxylation of the clay structure.

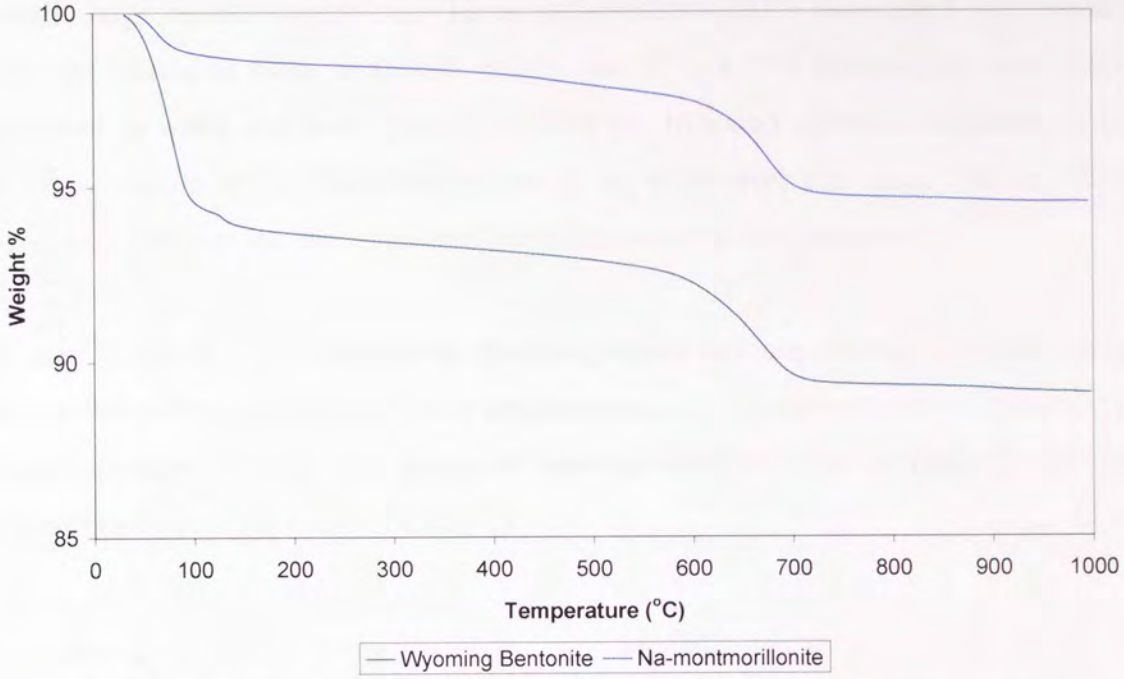

Figure 5.1 TGA curves for Wyoming Bentonite and sodium montmorillonite

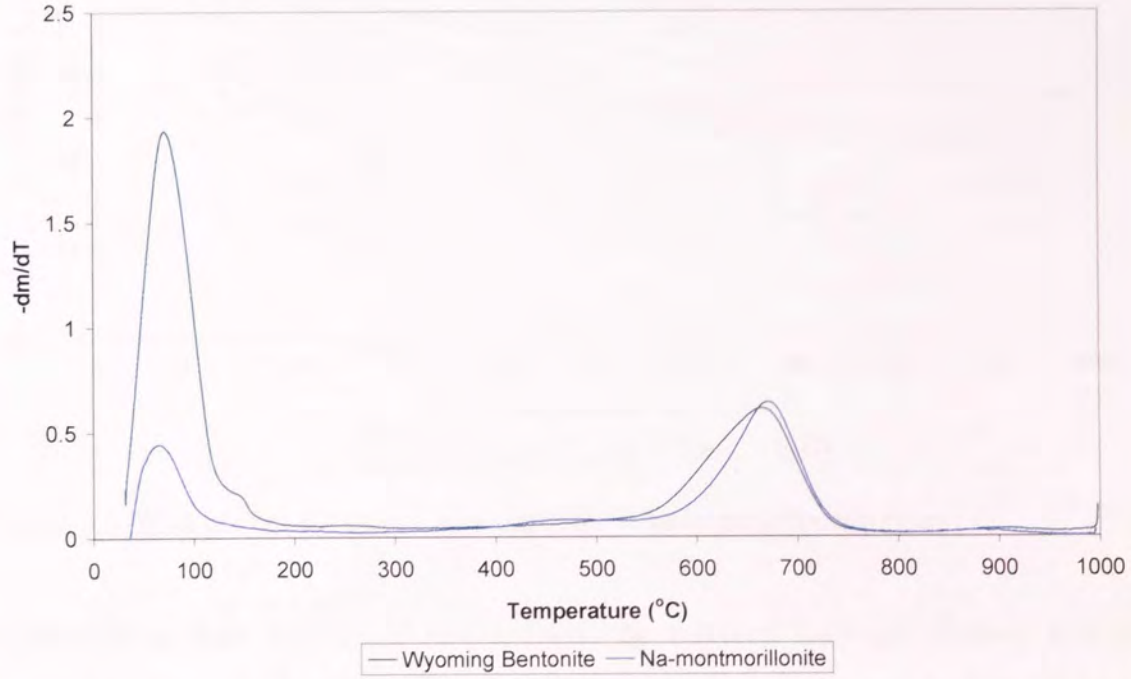

Figure 5.2 DTG curves for Wyoming Bentonite and sodium montmorillonite

5.1.2 Chromia pillared montmorillonites

The uncalcined chromia pillared montmorillonites exhibited three weight loss regions compared to the two regions of the starting materials (Figure 5.1 and Figure 5.3). These were a large initial weight loss (10 to 14%) below 200°C associated with weakly adsorbed interlayer water, a second weight loss (4 to 6.5%) between 200 and 500°C attributed to water and some hydroxyls from the hydrated chromia oligomers in the interlayer region and a final weight loss (3 to 4 %) over the range 500 to 750°C associated with the dehydroxylation of the pillars and the clay structure.

As seen in Figure 5.3 all uncalcined chromia pillared montmorillonites showed similar thermal behaviour regardless of their preparation method (conventional or microwave) or the experimental parameters employed (starting material, OH to Cr ratio, Cr and clay concentration etc.)(Table 3.1, Table 3.2).

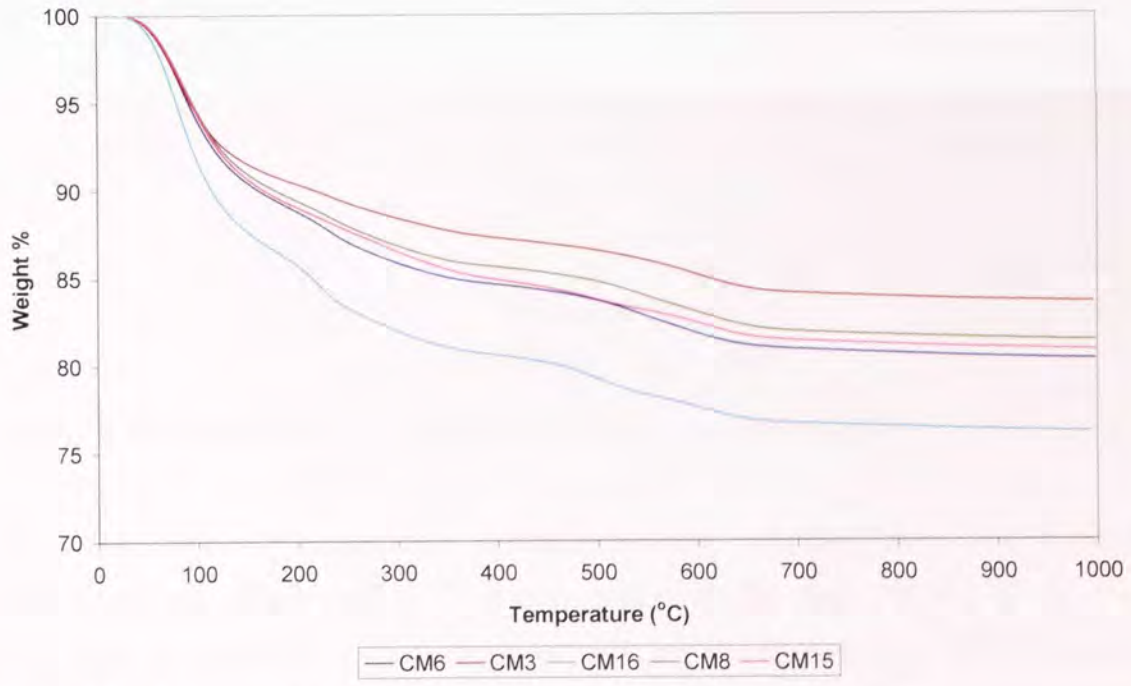

Figure 5.3 TGA curves for uncalcined chromia pillared montmorillonites

In contrast to their uncalcined counterparts, the calcined materials showed a small weight loss (2 to 4%) below 200°C followed by a nearly constant weight over the range 200 to 500°C (Figure 5.4). This indicates that structural changes that take place during calcination at 500°C are associated with the dehydration of the clay and the dehydration/dehydroxylation of chromia oligomers (which is supported by the basal

spacing reduction). These changes were minimised after calcination. The final ca. 2% weight loss over the range 500 to 700°C represented dehydroxylation of the pillar followed by dehydroxylation of the clay layer, leading to the collapse of the clay.

According to Figure 5.4 all calcined chromia pillared clays displayed the same thermal behaviour regardless of the experimental parameters employed during their conventional preparation (starting material, OH to Cr ratio, Cr and clay concentration etc.)(Table 3.1).

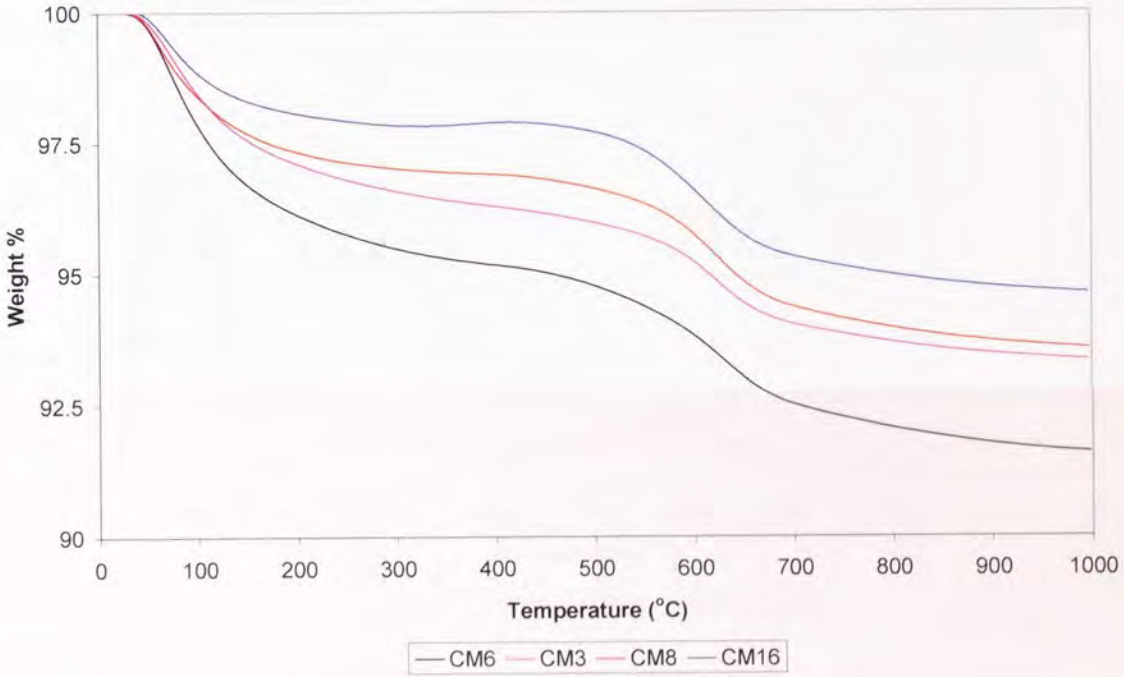

Figure 5.4 TGA curves for calcined chromia pillared montmorillonites

The DTG curves of uncalcined chromia pillared montmorillonites exhibited a dehydration peak with a shoulder (or smaller peak) over the range 200 to 400°C and an either broad or unresolved dehydroxylation peak over the range 400 to 700°C, whereas the respective curves of the calcined materials showed a single dehydration and a single dehydroxylation peak (Figure 5.5 and Figure 5.6). This supports the conclusion drawn earlier from the study of the TGA curves that structural changes occurring during calcination at 500°C are associated with the dehydration of the clay and the dehydration /dehydroxylation of chromia oligomers.

Comparison among the DTG curves of the chromia pillared montmorillonites with the respective of the starting materials showed that pillaring shifted the dehydration peak slightly towards higher temperature for both uncalcined and calcined samples, whereas the dehydroxylation peak shifted towards lower temperature (Figure 5.2, Figure 5.5 and Figure 5.6).The latter indicates that pillaring with chromium has decreased the temperature at which dehydroxylation begins leading to lower thermal stability, which is in accord with previous studies [116].

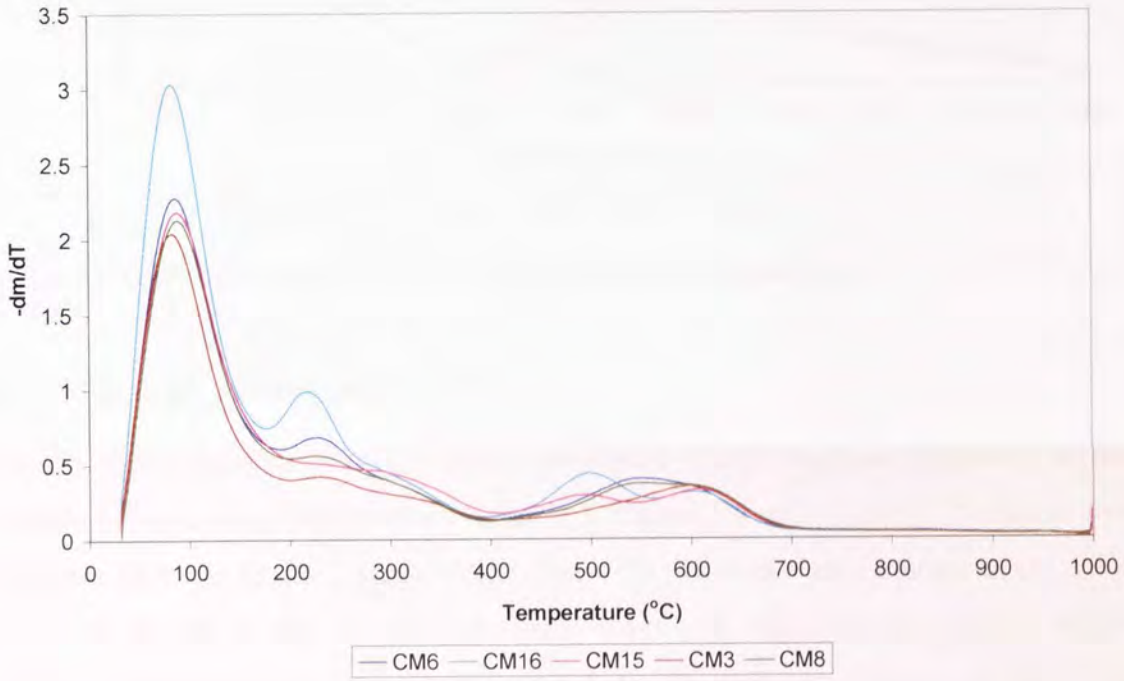

Figure 5.5 DTG curves for uncalcined chromia pillared montmorillonites

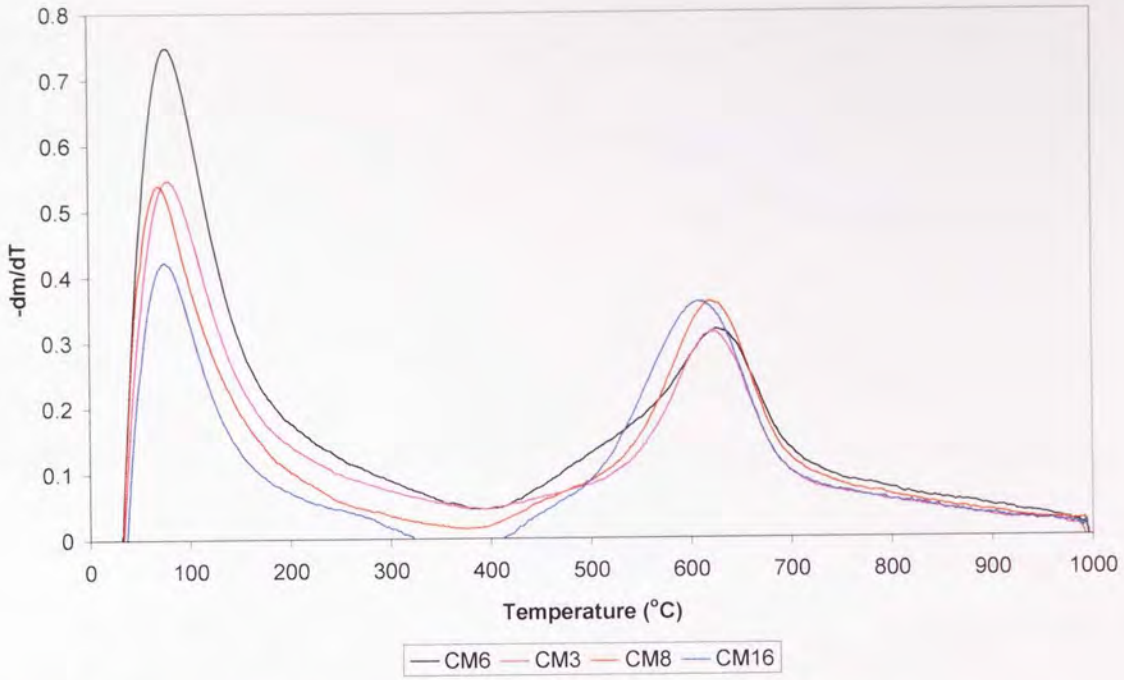

Figure 5.6 DTG curves for calcined chromia pillared montmorllonites

5.1.3 Tin oxide pillared montmorillonites

The tin oxide pillared montmorillonites exhibited similar thermal behaviour to the chromia pillared montmorillonites (Figure 5.3, Figure 5.4 and Figure 5.7). Before heat treatment they displayed a large weight loss (9%) over the temperature range 25 to 200°C attributed to the weakly adsorbed water and the hydration water of the exchangeable cations, which was reduced to about 3% after heat treatment at 500°C. An additional weight loss took place between 200 and 500°C, 2% for the untreated and 1% for the heat treated samples respectively associated with the hydration water of the tin oxide species and a final weight loss (2.5%) occurred for both untreated and heat treated samples over the range 500 to 730°C attributed to the dehydroxylation of the pillars and the clay structure.

As seen in Figure 5.7, tin oxide pillared montmorillonites, both before and after calcination, exhibited identical thermal behaviour in spite of their different preparation method (conventional or microwave).

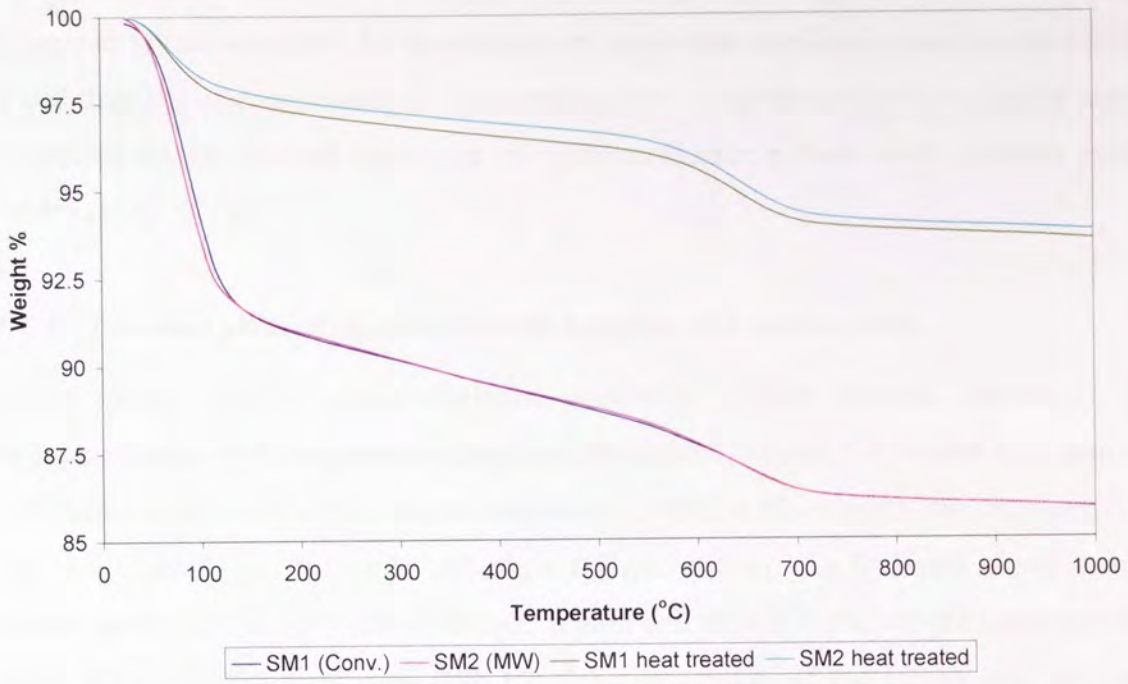

Figure 5.7 TGA curves for tin oxide pillared montmorillonites before and after heat treatment

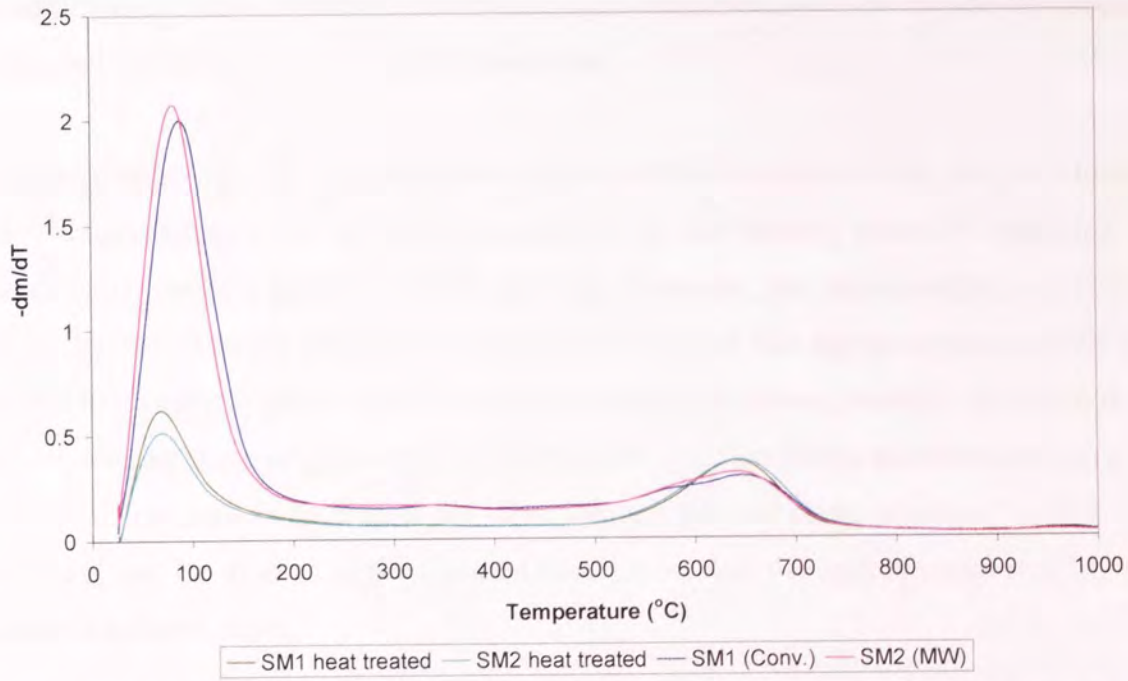

Figure 5.8 DTG curves for tin oxide pillared montmorillonites before and after heat treatment

The respective DTG curves consisted of two peaks, one for dehydration and one for dehydroxylation, for both uncalcined and calcined materials (Figure 5.8). For the tin

oxide pillared montmorillonites dehydroxylation began at a slightly higher temperature compared to the respective for the chromia pillared montmorillonites and at about 50°C lower than the starting material. These results are in agreement with an earlier study conducted on the thermal behaviour of montmorillonite pillared with different metal oxides [116].

5.1.4 Chromia pillared montmorillonite modified with cerium oxide

Mixed oxide pillared montmorillonite exhibited similar thermal behaviour to montmorillonite with single chromia pillars (Figure 5.3, Figure 5.4, Figure 5.9). Before calcination it showed a 9% weight loss below 200°C, a 6% weight loss between 200 and 500°C attributed to water and some hydroxyls from the hydrated chromia and cerium oxide oligomers in the interlayer region and a final 2.5% weight loss over the range 500 to 750°C associated with the dehydroxylation of the pillars and the clay structure. After calcination the weight losses decreased to 4% below 200°C, 1.5% over the range 200 to 500°C and 1.5% between 500 and 750°C respectively. The rather gradual incline of the curve between 200 and 500°C suggests that in this intermediate range there is loss of hydroxyls from the pillars concurrent with the release of residual adsorbed water (2% wt.) even after calcination.

As described earlier pillaring with chromia shifted the dehydroxylation peak to a lower temperature range (500 to 700°C) compared to the starting material indicating a decrease in thermal stability due to pillaring. However, the incorporation of cerium oxide in the chromia pillared montmorillonite shifted the dehydroxylation peak to higher temperatures (600 to 800°C) leading to increased thermal stability, similar to that of the starting material (Figure 5.10). Fetter et al. [125] reported that cerium played a similar thermostabilising role in modified alumina pillared clays, whereas Valverde et al. [126] and Booij et al. [119] reported that it increased the hydrothermal stability of alumina pillared clays.

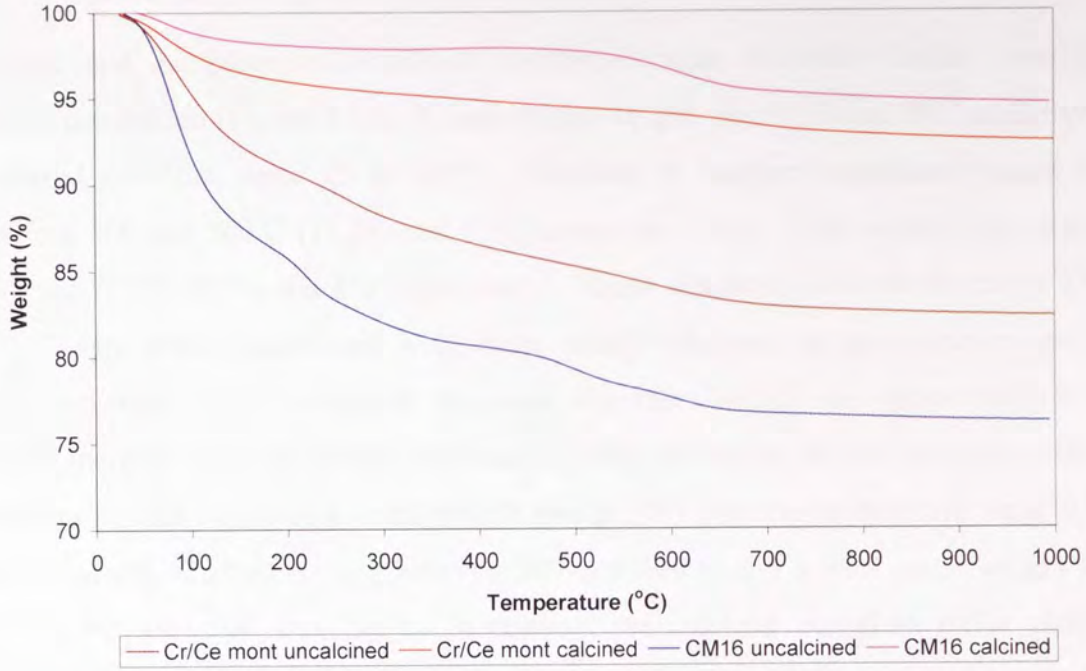

Figure 5.9 TGA curves for montmorillonite pillared with single chromia pillars and mixed chromia and cerium oxide pillars

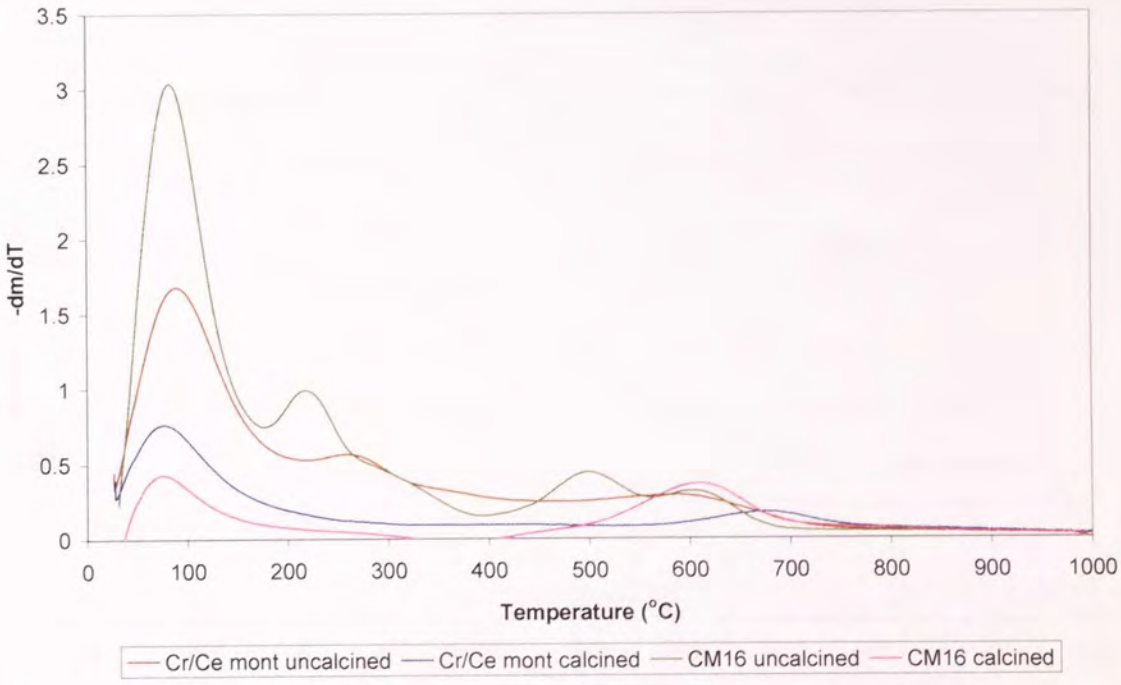

Figure 5.10 DTG curves for montmorillonite pillared with single chromia pillars and mixed chromia and cerium oxide pillars

5.1.5 Cerium and europium oxide pillared montmorillonites

Cerium and europium oxide pillared montmorillonites exhibited similar behaviour before calcination (Figure 5.11). A large initial weight loss (13% and 9% respectively) occurred over the range 25 to 200°C, followed by another significant weight loss between 200 and 500°C (11.5% and 11% respectively) and a final weight loss between 500 and 750°C (6.5% and 8% respectively). These weight losses over the range 25 to 500°C were mainly associated with water weakly adsorbed in the interlayer and the hydration water of the cerium or europium oligomers, which was responsible for the weight increase observed during preparation. After calcination the cerium oxide pillared montmorillonite exhibited a small weight loss (1.5%) over the temperature range 25 to 200°C, nearly constant weight between 200 and 500°C and a final small weight loss (1.5%) between 500 and 750°C. In contrast the calcined europium oxide pillared montmorillonite showed a small weight loss between 25 to 200°C, a higher weight loss (5%) between 200 and 500°C and a final weight loss (4.5%) over the range 500 to 750°C. This continuous weight loss exhibited by the europium oxide pillared montmorillonite even after calcination indicated that the europium oxide pillars were not thermally stable even at moderate temperatures.

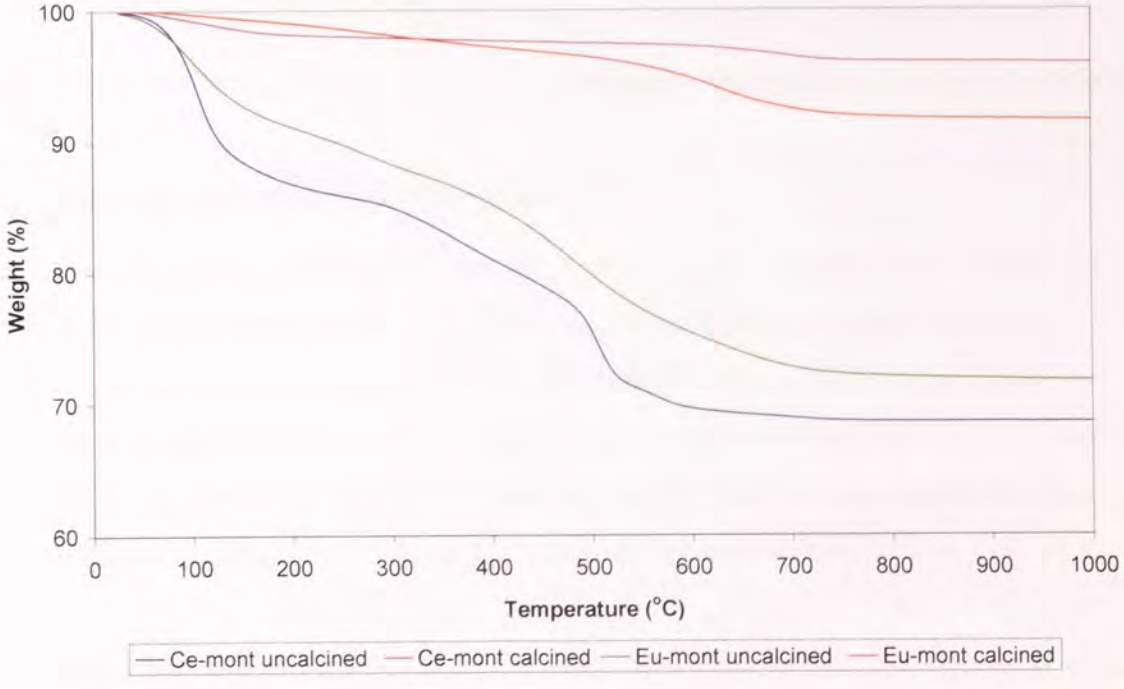

Figure 5.11 TGA curves for montmorillonite pillared with cerium and europium oxides

From the comparison of the DTG curves among sodium montmorillonite (Figure 5.2) and its pillared derivatives with cerium and europium oxides (Figure 5.12), it can be concluded that cerium oxide pillared montmorillonite after calcination exhibited similar thermal stability with the starting material, whereas europium oxide pillared montmorillonite showed lower thermal stability (the dehydroxylation peak became broader including lower temperatures).

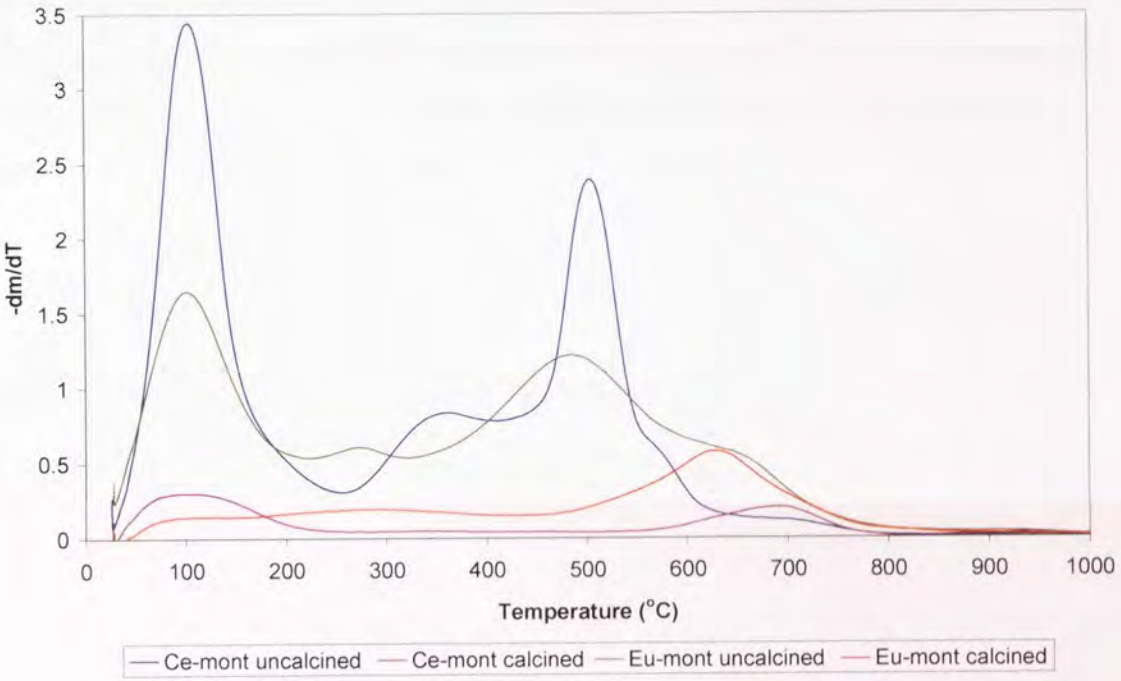

Figure 5.12 DTG curves for montmorillonite pillared with cerium and europium oxides

5.2 Laponite and respective pillared clays

For laponite (starting material) the weight loss occurred in three steps (Figure 5.13). Two of these were rapid, a 9% weight loss took place between 25 and 200°C and a 3% weight loss over 600 to 800°C. The rather gradual incline of the curve between the desorption of adsorbed water (25 to 200°C) and the release of structural hydroxyls (600 to 800°C) suggests that in this intermediate range there was a significant loss of structural hydroxyls concurrent with the release of residual adsorbed water (3% wt.).

Tin oxide pillared laponites exhibited the same behaviour as laponite regardless of the preparation method (conventional or microwave) and experimental parameters employed (Figure 5.13, Tables 3.1 and 3.2). A large initial weight loss (7 to 12%) occurred over the range 25 to 200°C and another one (3%) between 600 to 800°C,

whereas a slower but evident weight loss (3.5%) took place between 200 to 600°C. In contrast to pillared montmorillonites the second DTG peak associated with the dehydroxylation of the pillars and the clay structure did not shift to a lower temperature compared to the starting material (Figures 5.5, 5.6, 5.8 and 5.14).

Chromia pillared laponite exhibited a unique temperature profile (Figure 5.13). It consisted mainly of two temperature regions, 25 to 400°C (23% and 6% weight loss before and after calcination respectively) and 400 to 1000°C (ca. 5% weight loss in both cases), although after calcination the weight loss up to 500°C decreases significantly. This is probably a result of the combination of the hydrated chromia oligomers in the interlayer with the laponite structure.

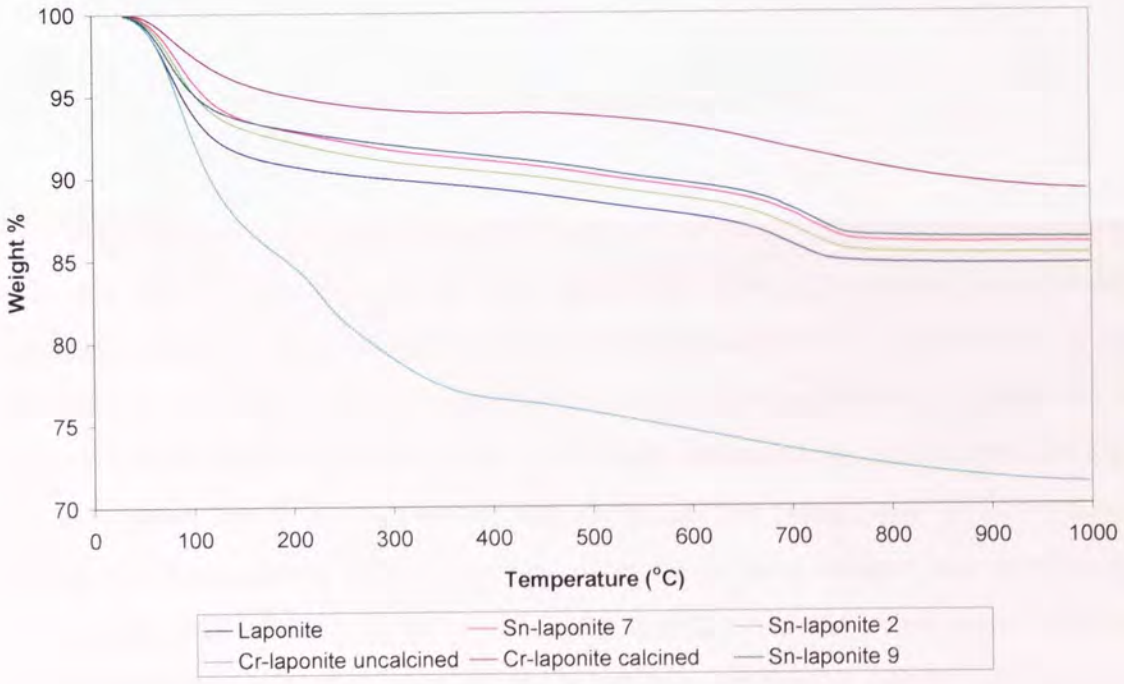

Figure 5.13 TGA curves for laponite and its pillared derivatives

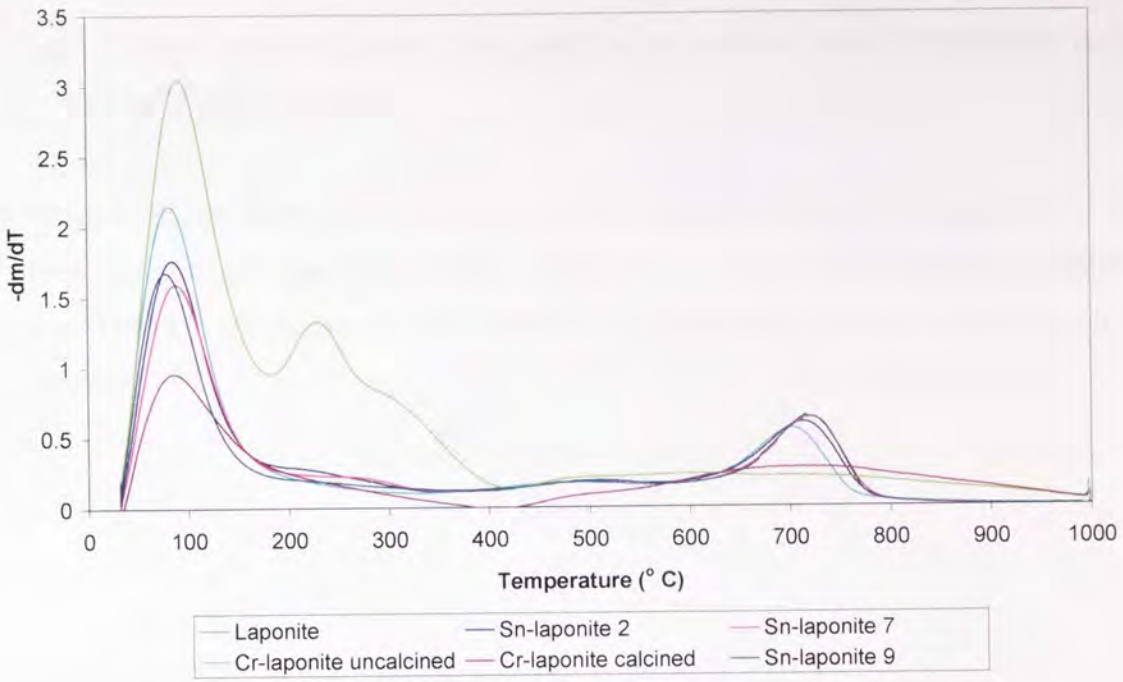

Figure 5.14 DTG curves for laponite and its pillared derivatives

5.3 Summary

TGA and DTG analysis showed that structural changes occurring in pillared montmorillonites during calcination at 500°C are associated with the dehydration of the clay and the dehydration /dehydroxylation of pillars. Pillaring Wyoming Bentonite or sodium montmorillonite with chromium or tin oxide decreased the temperature at which dehydroxylation begins in comparison with the respective temperature for the starting materials leading to lower thermal stability, whereas pillaring sodium montmorillonite with cerium oxide did not affect its thermal stability. On the other hand pillaring sodium montmorillonite with europium oxide led to lower thermal stability compared to that of the starting material (the dehydroxylation peak became broader including lower temperatures). Finally the incorporation of cerium in a chromia pillared montmorillonite shifted dehydroxylation to higher temperatures (600 to 800°C) compared to those for pillared montmorillonite with single chromia pillars leading to increased thermal stability, similar to that of the starting material.

Laponite seemed to be more thermally stable than montmorillonite. Tin oxide pillared laponites exhibited the same behaviour as laponite, whereas chromia pillared laponite displayed a unique temperature profile probably as a result of the combination of the

hydrated chromia oligomers in the interlayer with the laponite structure. For chromia pillared laponite dehydroxylation took place over a much wider temperature range compared to all other materials.

In conclusion, the starting material and the pillaring species influence significantly the thermal stability of the end product. However, no other experimental parameter appeared to have any influence, and neither did the preparation method (conventional of microwave).

6 X-RAY PHOTOELECTRON SPECTROSCOPY; RESULTS & DISCUSSION

X-ray photoelectron spectroscopy (XPS) was initially chosen as a complementary characterisation method to XRD for the pillared laponites in particular, since XRD patterns were not useful for proving the formation of tin oxide and chromia pillars in this case. XPS was used primarily to identify the composition of the materials, aiming to prove successful pillaring via the identification of the pillaring species in the form of metal oxide.

Apart from laponite and its pillared derivatives, XPS was also applied to Wyoming Bentonite, sodium montmorillonite and their pillared derivatives with chromium in order to support the obtained XRD results. It was also employed for the characterisation of some of these materials after being used as hydrocracking catalysts, aiming to collect information on their composition which could subsequently be related with their catalytic activity during reuse. All the XPS results are presented below.

6.1 Laponite and respective pillared clays

6.1.1 Laponite and tin oxide pillared laponites

Tin in the form tin(IV) oxide of has been detected in all the laponite samples treated with triphenyltin chloride (Table 6.1). The amount of tin varied among the different preparations (0.1 to 0.8%) and no clear trend with preparation conditions was observed. Even those samples that were prepared under identical conditions (SL2a and SL2b, SL7a and SL7b, SL9a and SL9d) displayed different contents of tin. This is attributed to inhomogeneous pillar distribution leading to different atomic concentrations in the same batch. An area of 0.3mm x 0.2 mm and 80 to 100Å in depth was irradiated with x-rays for each analysed sample and the quoted atomic concentrations are the mean values.

The presence of sodium in the pillared materials supports the assumption made earlier that hydrolysis of the organotin compound (Ph_3SnCl) occurs on the clay surface followed by aryl-tin bond breakage via proton attack thus leading to the formation of tin oxide pillars without the sacrifice of sodium cations from the interlayer. Benzene is a by-product remaining trapped within the clay lattice [127, 128, 55]. The chlorine detected in some of the samples was probably remaining from the precursor (Ph_3SnCl),

due to insufficient washing. Furthermore, the carbon detected in all the samples is attributed to adsorbed ethanol used for the swelling of the laponite, unreacted Ph_3SnCl, benzene trapped in the lattice, carbon dioxide absorbed from the atmosphere and instrument contamination.

Table 6.1 Atomic compositions (%) for laponite and tin oxide pillared laponites

Atomic Composition %	Laponite	SL1a	SL2a	SL2b	SL3b	SL4b
Na	3.1	2.4	1.3	2.5	2.8	3.4
O	52.3	54.0	43.8	48.9	51.6	52.2
Sn	-	0.5	0.4	0.5	0.3	0.4
C	3.6	2.3	15.1	10.2	6.3	5.1
Al	4.4	3.6	3.9	3.6	3.6	3.5
Si	22.6	24.6	22.3	22.0	22.5	22.8
Mg	14.0	12.6	13.0	12.4	13.0	12.5
Cl	-	-	0.3	-	-	-

Table 6.1 continued

Atomic Composition %	SL5b	SL6b	SL7a	SL7b	SL8b	SL9a	SL9d
Na	2.7	3.2	1.7	3.3	2.1	1.2	2.4
O	49.3	50.4	47.1	49.4	51.6	41.1	51.5
Sn	0.8	0.4	0.3	0.6	0.1	0.2	0.1
C	10.1	6.8	9.0	6.3	4.6	21.3	4.6
Al	4.0	4.4	3.5	4.4	4.3	2.3	4.8
Si	21.7	22.0	24.3	22.5	23.7	21.4	23.6
Mg	11.4	12.8	13.6	13.5	13.5	12.4	13.1
Cl	-	-	0.5	-	-	0.0	-

Atomic ratios were calculated from the atomic compositions (%) yielding the respective molecular formulas. The results are presented in Table 6.2.

Table 6.2 Atomic ratios for laponite and tin oxide pillared laponites

Atomic ratios	Laponite	SL1a	SL2a	SL2b	SL3b	SL4b	SL5b
Na/Si	0.14	0.10	0.06	0.12	0.12	0.15	0.13
O/Si	2.31	2.19	1.97	2.22	2.30	2.29	2.27
Sn/Si	-	0.02	0.02	0.02	0.01	0.02	0.04
C/Si	0.16	0.09	0.68	0.46	0.28	0.22	0.46
Al/Si	0.20	0.14	0.17	0.16	0.16	0.15	0.18
Si/Si	1.00	1.00	1.00	1.00	1.00	1.00	1.00
Mg/Si	0.62	0.51	0.58	0.56	0.58	0.55	0.52
Cl/Si	-	-	0.01	-	-	-	-

Table 6.2 continued

Atomic ratios	SL6b	SL7a	SL7b	SL8b	SL9a	SL9d
Na/Si	0.14	0.07	0.15	0.09	0.06	0.10
O/Si	2.29	1.94	2.20	2.18	1.92	2.18
Sn/Si	0.02	0.01	0.02	0.00	0.01	0.00
C/Si	0.31	0.37	0.28	0.19	0.99	0.19
Al/Si	0.20	0.15	0.20	0.18	0.11	0.20
Si/Si	1.00	1.00	1.00	1.00	1.00	1.00
Mg/Si	0.58	0.56	0.60	0.57	0.58	0.56
Cl/Si	-	0.02	-	-	0.00	-

According to literature laponite is a synthetic virtually iron-free trioctahedral smectite clay, in which all octahedral sites are occupied by Mg^{2+} and Li^{+} ions, with the tetrahedral layers composed in the same way as montmorillonite, with idealised composition $Na_{0.67}(Mg_{5.33}Li_{0.67})(Si_8O_{20}(OH)_4)$ [15]. For comparison purposes with the derived molecular formulas from the XPS results the empirical formula was reduced to one silicon atom ($Na_{0.084}Mg_{0.666}Li_{0.084}Si_1O_3H_{0.5}$). The calculated molecular formula for laponite ($Na_{0.14}$ $Mg_{0.62}$ $Al_{0.20}$ $Si_{1.00}$ $O_{2.31}$ $C_{0.16}$) deviated from the empirical formula, since no lithium was present, whereas aluminium was. XPS's inability to detect lithium is attributed to less lithium content than the detection limit (0.1%). The carbon content for untreated laponite is attributed to carbon dioxide absorbed from the atmosphere and instrument contamination.

The tin oxide pillared laponite samples showed variations in their atomic ratios. The C/Si ratio exhibited the highest variation range between 0.09 and 0.68, followed by the O/Si ratio which varied between 1.92 and 2.31.

6.1.2 Chromia pillared laponite

Chromium(III) coordinated with water and hydroxyl ligands (6.4%) was detected in the chromia pillared laponite proving the hydroxyl-oxy chromium composition of the pillars (Table 6.3).

Table 6.3 Atomic compositions (%) for laponite and chromia pillared laponite

Atomic composition %	Laponite	Cr-laponite uncalcined	Cr-laponite calcined
Na	3.1	0.4	0.6
Cr		7.4	6.4
O	52.3	53.6	59.4
C	3.6	8.5	5.5
Al	4.4	2.7	2.9
Si	22.6	21.2	18.4
Mg	14.0	6.3	6.7

The calculated atomic ratios are presented in Table 6.4. In the chromia pillared laponite samples the Na/Si ratio was nearly zero indicating ion-exchange between sodium and the pillaring species (i.e. Cr) during preparation in contrast to the preparation of tin oxide pillared laponites. However, according to the literature, ion-exchange is the principal method used for the preparation of pillared clays [13, 21]. The C/Si ratio reduced during calcination as expected. The presence of carbon is attributed to carbon dioxide absorbed from the atmosphere, carbonates from Na_2CO_3 and possible contamination of the instrument.

Table 6.4Atomic ratios for laponite and chromia pillared laponite

Atomic ratios	Laponite	Cr-laponite uncalcined	Cr-laponite calcined
Na/Si	0.14	0.02	0.03
Cr/Si		0.35	0.35
O/Si	2.31	2.53	3.23
C/Si	0.16	0.40	0.30
Al/Si	0.20	0.13	0.16
Si/Si	1.00	1.00	1.00
Mg/Si	0.62	0.30	0.37

6.2 Wyoming Bentonite, sodium montmorillonite and pillared clays with chromia and tin oxide

Wyoming Bentonite is a natural occurring material comprising of ca. 85% montmorillonite with the following idealised structural formula: $Na_{0.35}(Al_{1.65}Mg_{0.35})Si_4O_{10}(OH)_2.nH_2O$. Due to its natural origin isomorphous substitution of small amounts of Al and/or Fe^{3+} in the tetrahedral layer, and of Fe^{2+} in the octahedral layer are commonly encountered, along with carbonaceous deposits and particulate impurities such as quartz in the unrefined bulk material.

Wyoming Bentonite was refined and ion exchanged with sodium in order to yield monoionic sodium montmorillonite, which presented lower silicon and higher oxygen content compared with Wyoming Bentonite (Table 6.5). This is attributed to the removal of quartz, as well as to the higher degree of hydration of the sodium cations occurring after the refining and ion-exchange process. The chromia pillared montmorillonites prepared from sodium montmorillonite (CM3) exhibited similar silicon content to the respective of sodium montmorillonite. The lower silicon content of the chromia pillared montmorillonites prepared from Wyoming bentonite (CM6) compared to the respective of Wyoming Bentonite is again due to the removal of quartz that took place through partial refining before mixing the clay slurry with the pillaring solution.

Table 6.5 Atomic compositions (%) for Wyoming Bentonite, Na-montmorillonite and their pillared derivatives with chromium and tin oxides

Atomic compo/ sition %	W.B. (as received)	CM6 uncalc.	CM6 calc.	SM1 uncalc.	Na-mont	CM3 uncalc.	CM3 calc.
Na	2.3	-	-	-	2.6	-	-
Cr	-	4.1	4.5	-	-	2.7	2.6
Sn	-	-	-	2.8	-	-	-
O	44.5	57.3	49.4	57.9	60.6	55.0	54.0
C	3.9	14.2	20.4	6.3	3.1	12.4	11.8
Al	9.6	5.0	5.1	6.2	7.5	5.9	5.2
Si	39.7	19.4	20.0	26.8	26.2	23.9	26.4
F	-	-	0.6	-	-	-	-

No magnesium was detected in any of the montmorillonite samples (unpillared and pillared). It is assumed that the amount of magnesium was less than the detection limit (0.1%) of the analysed layer. On the other hand the carbon detected in all the samples is due to the carbonaceous deposits on the clay, in addition to carbon dioxide absorbed from the atmosphere, carbonates from Na_2CO_3 and possible contamination of the instrument.

Chromium(III) coordinated with water and hydroxyl ligands was detected in the chromia pillared montmorillonites supporting the XRD evidence for the existence of chromia pillars in the interlayer region. The higher amount of chromium intercalated in CM6 (4.6%) in combination with its higher basal spacing (22.5Å) compared to the

respective of CM3 (4.5% Cr and 15.4Å) indicates that chromium has formed higher pillars in CM6, instead of being dispersed in the interlayer. Specific surface area measurements also support this hypothesis (see chapter 7). Tin in the form of tin(IV) oxide was detected in the montmorillonite pillared with tin oxide at a much higher content (2.8%) compared to the respective for tin pillared laponites. The absence of sodium from all pillared montmorillonites indicates the occurrence of complete ion-exchange between sodium and chromium or tin during their preparation. If this is the case then the tin oxide pillars are retained in the interlayer by electrostatic forces and not hydrogen bonds as suggested earlier by Hannus et al. [123].

The atomic compositions measured by XPS were used for the calculation of atomic ratios in order to yield structural formulas for the materials (Table 6.6). For comparison purposes the montmorillonite's structural formula was reduced to one aluminium atom ($Na_{0.21}Al_1$ $Mg_{0.21}Si_{2.42}O_{13.33}H_{13.33}$). Since silicon is also present in quartz, reduction towards one silicon atom would have given erroneous results, because total separation of quartz impurities from the bulk of clay is not feasible via physical methods.

The derived structural formulas for Wyoming bentonite and sodium montmorillonite were $Na_{0.24}$ Al_1 $Si_{4.15}$ $O_{4.65}$ $C_{0.41}$ and $Na_{0.35}$ Al_1 $Si_{3.48}$ $O_{8.03}$ $C_{0.40}$ respectively. In both cases the Si/Al ratio is higher than the respective in montmorillonite's idealised formula indicating the presence of quartz.

Table 6.6 Atomic ratios for Wyoming Bentonite, sodium montmorillonite and their pillared derivatives with chromium and tin oxides

Atomic ratios	W.B. (as received)	CM6 uncalc.	CM6 calc.	SM1 uncalc.	Na-mont	CM3 uncalc.	CM3 calc.
Na/Al	0.24	-	-	-	0.35	-	-
Cr/Al	-	0.82	0.88	-	-	0.46	0.51
Sn/Al	-	-	-	0.44	-	-	-
O/Al	4.65	11.38	9.59	9.28	8.03	9.29	10.47
C/Al	0.41	2.82	3.96	1.01	0.40	2.09	2.29
Al/Al	1.00	1.00	1.00	1.00	1.00	1.00	1.00
Si/Al	4.15	3.85	3.88	4.29	3.48	4.04	5.12
F/Al	-	-	0.12	-	-	-	-

6.3 Reproducibility of the method

In order to ensure the validity of the XPS results presented so far, it was considered essential to check the reproducibility of method. Therefore, one of the analysed samples (CM6 uncalcined) was measured three extra times. The derived spectra were identical (Figure 6.1). The quantitative results for the atomic compositions (%) exhibited standard deviations over the range 0.5 to 1.3 (Table 6.7). Hence, it can be concluded that the method has very good reproducibility. It should be noted that the calculated atomic ratios (Table 6.8) exhibited variation up to 4.85 (O/Al ratio) indicating that variations in the same range observed in the atomic ratios of the analysed materials should not be alarming.

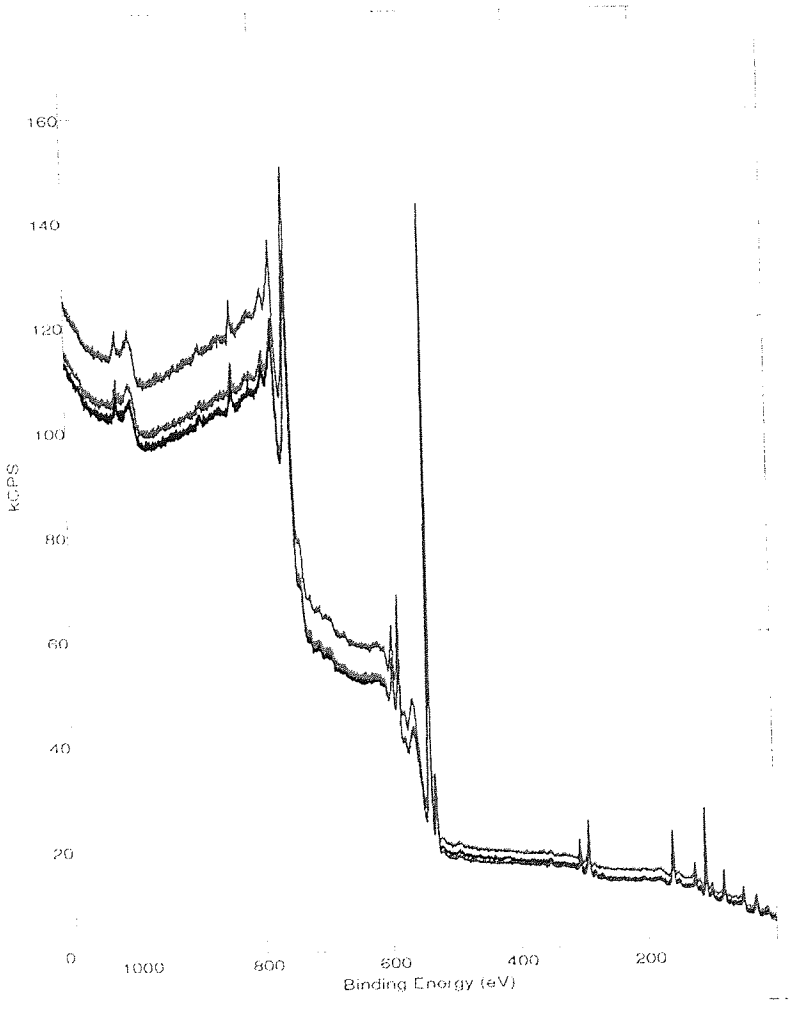

Figure 6.1 XPS spectra for the same sample (CM6)

Table 6.7 XPS reproducibility measurements

Atomic composition %	1	2	3	4	Average	Standard deviation
Cr	4.125	5.43	4.996	5.175	4.9	0.49
O	57.258	54.396	55.063	54.021	55.2	1.25
C	14.201	12.159	11.087	13.312	12.7	1.17
Al	5.032	7.595	8.431	6.983	7.0	1.25
Si	19.385	20.42	20.423	20.509	20.2	0.46
Total	100	100	100	100	100	

Table 6.8 Reproducibility of atomic ratios

Atomic ratios	1	2	3	4
Cr/Al	0.82	0.71	0.59	0.74
O/Al	11.38	7.16	6.53	7.74
C/Al	2.82	1.60	1.32	1.91
Al/Al	1.00	1.00	1.00	1.00
Si/Al	3.85	2.69	2.42	2.94

6.4 Pillared clays after use as hydrocracking catalysts

The atomic compositions (%) and the calculated atomic ratios of the laponites pillared with chromium and tin oxides after use as hydrocracking catalysts are presented in Table 6.9 and Table 6.10 respectively. Carbon dominated the composition of all the used catalysts leading to a significant increase in the C/Si ratio after the first and the second use, whereas no chromium or tin was detected. In addition the Mg/Si ratio increased after each use. This is attributed to the extensive carbon layer coating all the catalysts after use and probably occupying most of the 80 to 100Å depth of analysis of the x-ray beam. The beam might have penetrated the carbon layer, the first silicon tetrahedra up to the magnesium octahedra without reaching the adjusted silicon tetrahedra and the interlayer region. This assumption also justifies the increase in the Mg/Si ratio.

Table 6.9 Atomic compositions (%) for laponites pillared with chromium and tin oxides after use as hydrocracking catalysts

Atomic composition %	Cr-lap used	Cr-lap reused	SL2a used	SL2a reused	SL7a used	SL7a reused
Na	-	-	0.8	0.3	-	-
Cr or Sn	-	-	-	-	-	-
O	6.3	4.7	12.4	11.7	10.7	7.1
C	81.8	85.3	71.3	78.0	74.2	83.7
Al	-	-	0.9	0.4	1.2	0.6
Si	4.8	2.3	5.5	2.3	5.2	1.4
Mg	7.1	7.7	6.9	6.4	8.5	7.0
Cl	-	-	1.6	0.8	0.2	0.2
Fe	-	-	0.5	-	-	-

Table 6.10 Atomic ratios for laponites pillared with chromium and tin oxides after use as hydrocracking catalysts

Atomic ratios	Cr-lap used	Cr-lap reused	SL2a used	SL2a reused	SL7a used	SL7a reused
Na/Si	-	-	0.14	0.12	0.00	0.00
Cr/Si or Sn/Si	-	-	-	-	-	-
O/Si	1.33	2.09	2.24	4.99	2.08	5.12
C/Si	17.19	37.98	12.89	33.34	14.37	60.01
Al/Si	-	-	0.17	0.19	0.23	0.40
Si/Si	1.00	1.00	1.00	1.00	1.00	1.00
Mg/Si	1.48	3.43	1.25	2.76	1.65	5.01
Cl/Si	-	-	0.29	0.34	0.03	0.17
Fe/Si	-	-	0.09	-	-	-

The atomic compositions (%) and the calculated atomic ratios of the chromia pillared montmorillonites after use as hydrocracking catalysts are presented in Table 6.11 and Table 6.12 respectively. In accordance with the used pillared laponites, the C/Al ratio of the chromia pillared montmorillonites exhibited a big increase after the first use and kept increasing after the second use, while the Si/Al ratio decreased (Table 6.10, Table 6.12). It is presumed that due to the thickness of the carbon layer the x-ray beam does not reach the second silicon tetrahedra and the chromia pillars. Chromium is probably below the layer that can be detected by the x-ray beam.

Table 6.11 Atomic compositions (%) for chromia pillared montmorillonites after use as hydrocracking catalysts

Atomic composition %	CM6 used	CM6 reused	CM3 used	CM3 reused
Na	0.1		2.0	0.2
Cr				
O	11.3	9.0	13.3	12.3
C	84.2	87.6	76.1	83.3
Al	2.2	1.3	1.2	1.0
Si	2.2	2.1	2.8	1.7
Fe			1.2	0.3
Cl			3.4	1.3

Table 6.12 Atomic ratios for chromia pillared montmorillonites after use as hydrocracking catalysts

Atomic ratios	CM6 used	CM6 reused	CM3 used	CM3 reused
Na/Al	0.06		1.60	0.17
Cr/Al				
O/Al	5.21	6.84	10.66	12.39
C/Al	38.77	66.88	61.16	83.99
Al/Al	1.00	1.00	1.00	1.00
Si/Al	1.02	1.62	2.27	1.74
Fe/Al			0.98	0.25
Cl/Al			2.72	1.27

Iron and chlorine depositions detected in the used catalysts have derived from the feedstock and might have an effect in the activity of the used catalysts (Fe dehydrogenation reactions, coke formation)(Table 6.9, Table 6.11).

Cation Exchange Capacity (CEC) measurements and spectroscopic measurements of a Cu(II) exchanged laponite undergoing heating revealed that Cu ions migrate into the octahedral sheet where they replace Li and Mg ions [129]. In this respect another assumption could be made for the increasing Mg/Si ratio observed after use. Possibly under hydrocracking conditions (400°C and 190 bars) Mg has been exchanged with the interlayer cations in the trioctahedral sheet and therefore has moved closer to the surface. On the other hand the increasing Al/Si ratio observed for used montmorillonite catalysts might be attributed to some kind of structural alteration taking place transforming octahedral aluminium to tetrahedral aluminium. It is known that transition

from octahedrally bound aluminium to tetrahedrally coordinated aluminium occurs during the heating process and is a result of dehydroxylation [130]. In both cases it is assumed that under heating some kind of thermodynamically driven move of the cations belonging to the octahedral sheet towards the interlayer occurs.

6.5 Summary

Since XRD was not a suitable method for characterizing laponite or pillared laponites due to the lack of first order reflection, which was attributed to the small size of individual particles and the random rather than uniform face-to-face orientation of the clay platelets, it was replaced by XPS. The amount of tin in the form of tin(IV) oxide detected in the tin oxide pillared laponites varied among the different preparations (0.1 to 0.8%) and no clear trend with preparation conditions was observed. This is attributed to inhomogeneous pillar distribution leading to different atomic compositions (%) in the same batch. For each analysed sample an area of 0.3mm x 0.2 mm and 80 to 100Å in depth was irradiated with x-rays. Tin in the same form of tin(IV) oxide, but at a much higher content (2.8%) was also detected in tin oxide pillared montmorillonite. Furthermore, chromium(III) coordinated with water and hydroxyl ligands was detected in the chromia pillared clays (both laponites and montmorillonites) proving the hydroxyl-oxy chromium composition of the pillars.

XPS analysis of the used catalysts did not yield any significant information. Carbon dominated their composition, which is attributed to the extensive carbon layer coating of all the catalysts after use. The inability to detect any chromium indicated that it was probably located below the layer penetrated by the x-ray beam.

7 NITROGEN SORPTION; RESULTS & DISCUSSION

Nitrogen adsorption - desorption isotherms were obtained for the starting clay materials and their derivatives with single oxide or mixed oxide pillars after calcination, aiming to characterise them in terms of textural properties, such as specific surface area (total and microporous), pore volume (total and microporous) and pore size distribution.

The nitrogen sorption results presented in this chapter are correlated with the XRD results presented previously (Chapter 4) and used to assess the effect of the raw material and the pillaring species in the textural properties of the derived pillared clays. The reference catalyst NiMo on alumina was also included in the analysis for comparison purposes. Finally, the chromia pillared montmorillonite CM6 was also analysed after undergoing hydrocracking conditions in the absence of feed. The aim was to check the assumption made from the XRD analysis of the used pillared clay catalysts that harsh hydrocracking conditions in the microbomb reactor lead to partial collapse of the pillars (Section 4.3).

7.1 Wyoming Bentonite, sodium montmorillonite and respective pillared clays

The isotherms of Wyoming Bentonite and sodium montmorillonite were a combination of type II and IV in the IUPAC classification corresponding to macroporous and mesoporous materials respectively. The isotherm of Na-montmorillonite was shifted to higher volume of adsorbed nitrogen in the whole relative pressure region compared to the respective of Wyoming Bentonite as received (Figure 7.1). The hysteresis observed at higher relative pressures is due to capillary condensation in mesopores and corresponds to type H3 in the IUPAC classification. Among the materials showing H3 type of hysteresis are those having slit-shaped pores and plate-like particles with spaces between the parallel plates, such as clays [131, 132, 32, 126].

The isotherms of the calcined pillared derivatives with chromium and/or cerium oxides were a combination of types I and IV characteristic for microporous and mesoporous materials respectively with H3 hysteresis (Figure 7.2, Figure 7.3). The amount of nitrogen adsorbed at low pressures is the most important difference between isotherms corresponding to pillared clays obtained with different pillaring solutions. At $P/P_o<0.4$, where monolayer formation is produced, a parallelism between adsorption isotherm

curves of the pillared and raw clays is observed in agreement with Canizares et al. [131, 126]. On the contrary calcined montmorillonites pillared with tin or europium oxides exhibited isotherms closer to type II and III respectively (macroporous materials) (Figure 7.3, Figure 7.4). A similar type II isotherm has been displayed by an iron oxide pillared montmorillonite prepared by Maes et al. [133] and a titania pillared montmorillonite prepared by Chae et al. [134]. At $P/P_o<0.4$, the isotherm of europium oxide pillared montmorillonite coincided with the isotherm of the starting material, i.e. sodium montmorillonite (Figure 7.4).

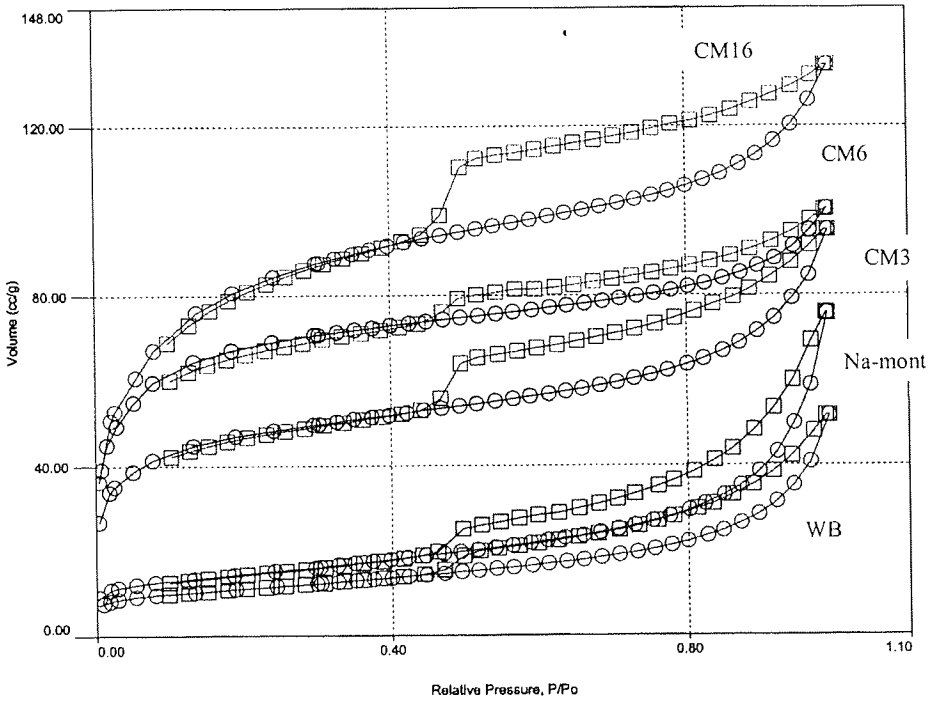

Figure 7.1 Nitrogen isotherms for Wyoming bentonite, sodium montmorillonite and chromia pillared montmorillonites

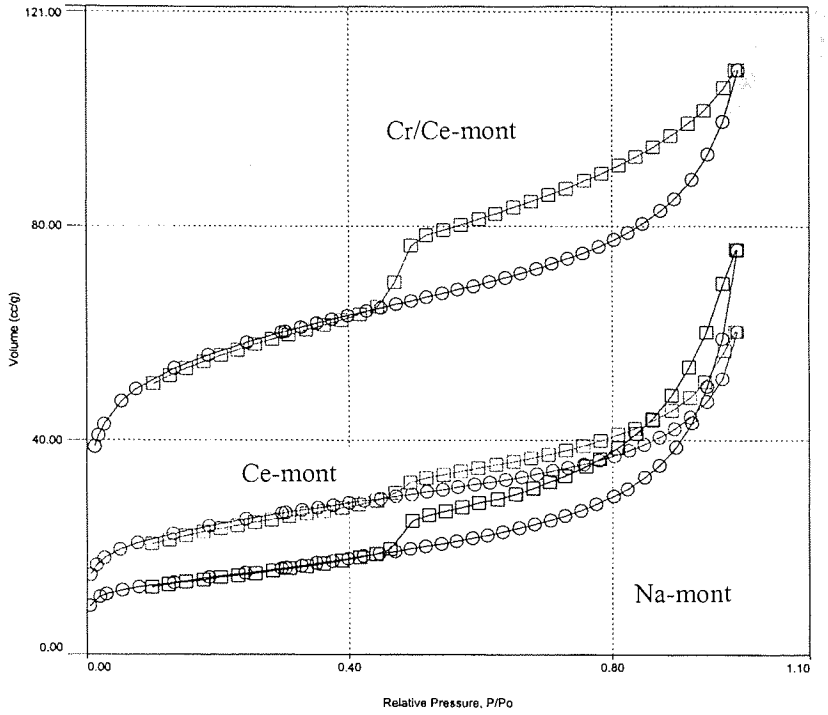

Figure 7.2 Nitrogen isotherms for sodium montmorillonite, cerium oxide and mixed chromium and cerium oxide pillared montmorillonites

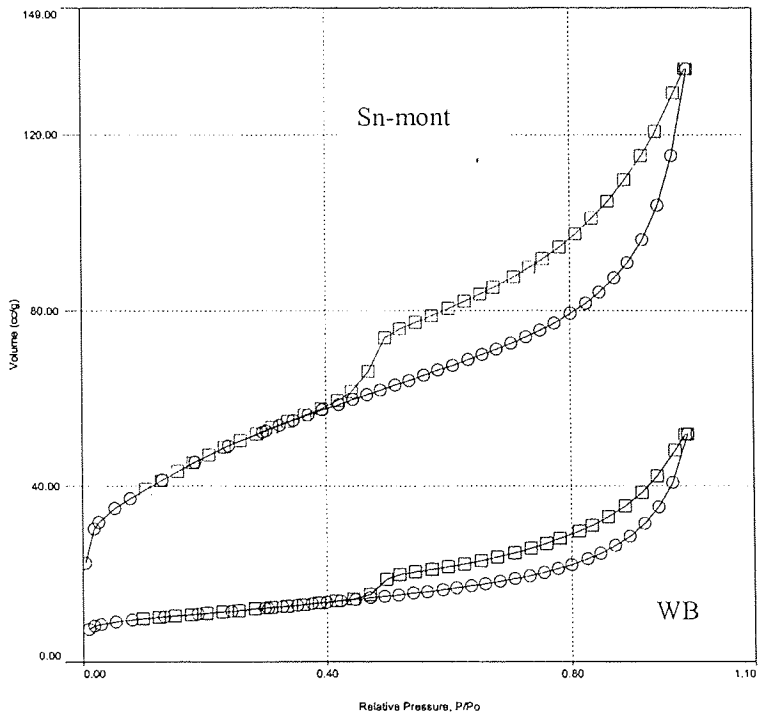

Figure 7.3 Nitrogen isotherms for Wyoming Bentonite and tin oxide pillared montmorillonite

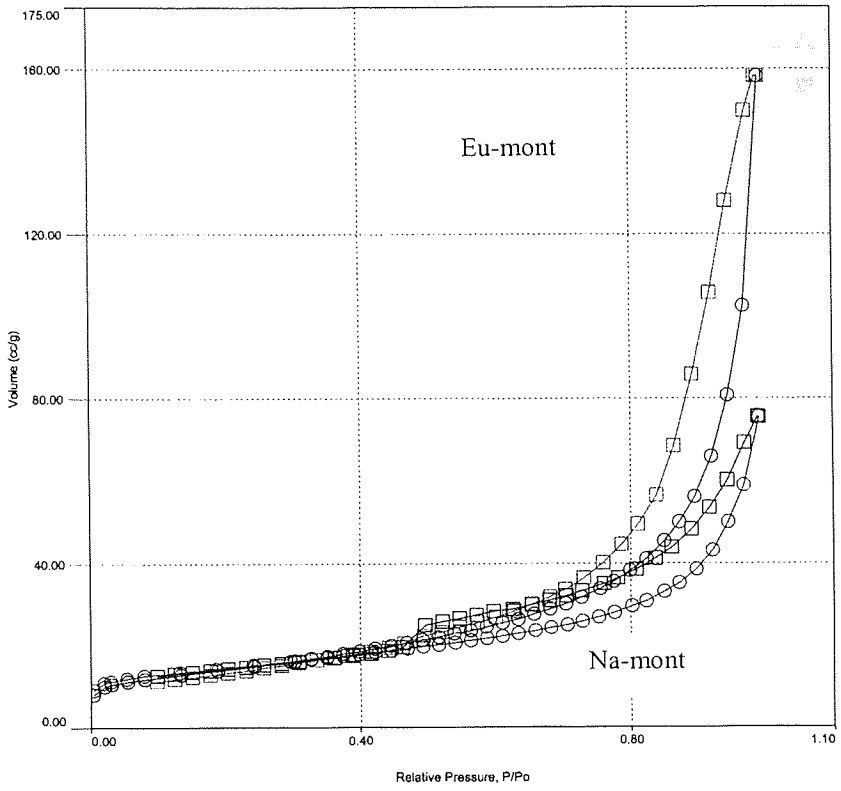

Figure 7.4 Nitrogen isotherms for sodium montmorillonite and europium oxide pillared montmorillonite

All surface areas were calculated using the multi point BET method as described in Section 3.2.4. The results are presented in Table 7.1. Table 7.2 shows the relative values with regard to the values for sodium montmorillonite. For clarity an example of the calculation of the surface area via the BET method for the chromia pillared montmorillonite CM3 is presented here. From the linear plot of $1/[W(P_o/P)-1]$ versus P/P_o in the range 0.02 to 0.13 (Figure 7.5) the slope and the intercept can be found (S = 20 and I = 0.08). As a result the weight of a monolayer of adsorbate W_m can be calculated 1/(S+I), 0.05g. Therefore the total surface area of the sample is:

$S_t = W_m \ N \ A_{cs} / M = 0.05g \ 6.023 \times 10^{23}$ molecules/mol $16.2 \ Å^2 / 28.013$ g/mol = $174 m^2$.

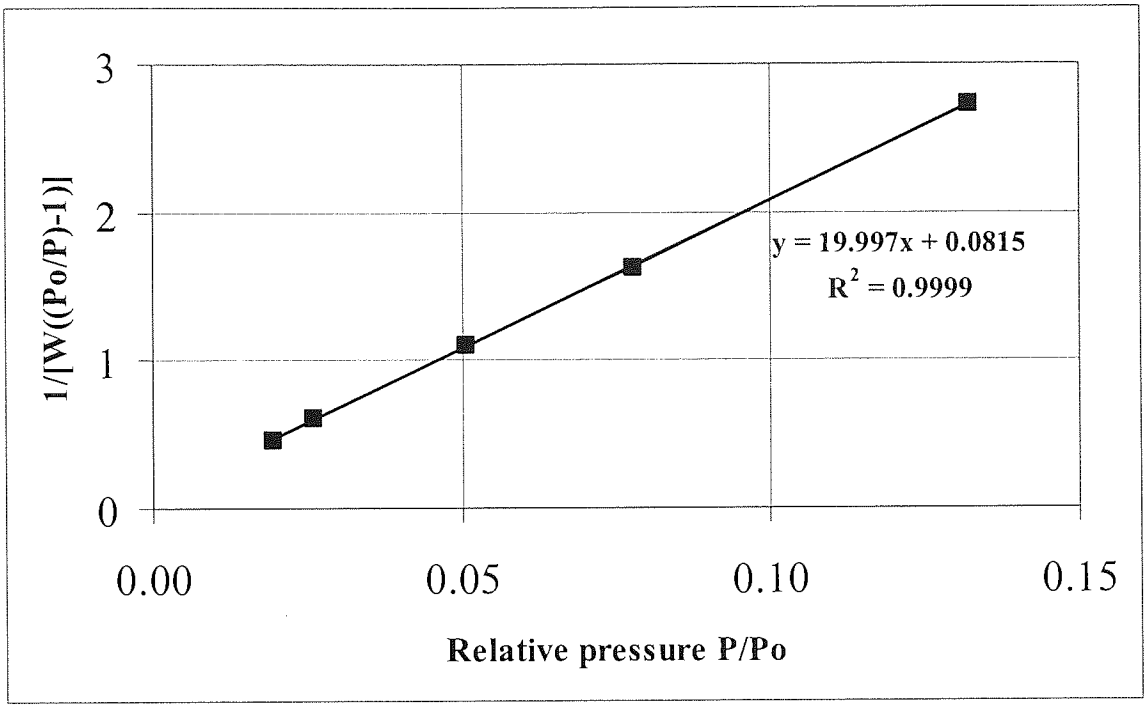

Figure 7.5 BET plot for the cancined pillared montmorillonite CM3

The composition, population (dimmers, trimers) and orientation of pillaring species influence surface area. Chromia pillared montmorillonites prepared from Wyoming Bentonite and sodium montmorillonite exhibited multi-fold increase in their surface area after calcination compared to their unpillared counterparts, which was attributed to the formation of chromia pillars expanding the clay layers. The increase in the surface area is correlated with the basal spacing of the respective materials which, in turn, is depended on the OH/Cr ratio used during the preparation. Similar results were reported by Pinnavaia et al. [118], Sychev et al. [135], Canizares et al. [131] and Volzone [122, 132]. It should be noted, however, that the results obtained from nitrogen sorption are an average of the accessibility of the materials (three dimensional) in contrast to the basal spacings obtained by XRD which provide only one-dimensional information.

Table 7.1 Nitrogen sorption results

					t-plot method			BJH method				
Sample	**d_{001} (Å)**	**Vtotal (cm^3/g) at P/Po=0.99**	**Mean pore diameter (Å)**	**S_{BET} (m^2/g)**	**Vmic (cm^3/g)**	**Smic (m^2/g)**	**Snon mic (m^2/g)**	**S (m^2/g)**	**Volume (cm^3/g)**	**Pore diameter (Å)**	**Vmic/ Vtot**	**Smic/ S_{BET}**
Na-mont	16.0	0.12	92	51	0.006	14	37	47	0.11	38.6	0.05	0.27
CM3 calc.	15.4	0.15	34	174	0.059	135	38	61	0.1	38.8	0.4	0.78
CM16 calc.	23.4	0.21	26	309	0.122	268	41	86	0.11	38.8	0.59	0.87
Ce-mont calc.	15.6	0.09	42	87	0.028	59	28	33	0.07	38.8	0.3	0.68
Cr/Ce mont calc.	n.a.	0.17	36	206	0.074	161	45	73	0.11	38.8	0.44	0.78
Eu-mont calc.	15.5	0.24	194	50	0.004	10	40	64	0.25	38.6	0.02	0.2
WB	15.2	0.08	80	39	0.005	11	28	35	0.08	39	0.06	0.28
CM6 calc.	22.5	0.16	24	253	0.098	226	27	41	0.07	38.8	0.63	0.89
CM6 calc. HC	20.0 / 16.2	0.15	28	211	0.072	171	40	43	0.07	38.8	0.48	0.81
Sn-mont calc.	15.7	0.21	50	167	0.056	103	65	96	0.17	39	0.27	0.61
Laponite	n.a.	0.29	30	383	0.276	378	5	174	0.16	36.6	0.97	0.99
Sn-lap	n.a.	0.27	30	361	0.264	357	4	177	0.17	36.8	0.97	0.99
Cr-lap calc.	n.a.	0.3	24	486	0.293	482	4	100	0.09	34.4	0.98	0.99
NiMo on alumina	n.a.	0.43	168	104	0	0	104	125	0.44	106.2	0	0

Table 7.2 Relative ratios to the values for Na-montmorillonite

				t-plot method			BJH method				
Sample	**Vtotal (cm^3/g) at P/Po=0.99**	**Mean pore diameter (Å)**	**S_{BET} (m^2/g)**	**Vmic (cm^3/g)**	**Smic (m^2/g)**	**Snon mic (m^2/g)**	**S (m^2/g)**	**Volume (cm^3/g)**	**Pore diameter (Å)**	**Vmic/Vtot**	**Smic/S_{BET}**
Na-mont	1	1	1	1	1	1	1	1	1	1	1
CM3 calc.	1.3	0.4	3.4	9.8	9.6	1.0	1.3	0.9	1.0	8	2.9
CM16 calc.	1.8	0.3	6.1	20.3	19.1	1.1	1.8	1.0	1.0	11.8	3.2
Ce-mont calc.	0.8	0.5	1.7	4.7	4.2	0.8	0.7	0.6	1.0	6	2.5
Cr/Ce mont calc.	1.4	0.4	4.0	12.3	11.5	1.2	1.6	1.0	1.0	8.8	2.9
Eu-mont calc.	2.0	2.1	1.0	0.7	0.7	1.1	1.4	2.3	1.0	0.4	0.7
WB	0.7	0.9	0.8	0.8	0.8	0.8	0.7	0.7	1.0	1.2	1.0
CM6 calc.	1.3	0.3	5.0	16.3	16.1	0.7	0.9	0.6	1.0	12.6	3.3
CM6 calc. HC	1.3	0.3	4.1	12.0	12.2	1.1	0.9	0.6	1.0	9.6	3.0
Sn-mont calc.	1.8	0.5	3.3	9.3	7.4	1.8	2.0	1.5	1.0	5.4	2.3
Laponite	2.4	0.3	7.5	46.0	27.0	0.1	3.7	1.5	0.9	19.4	3.7
Sn-lap	2.3	0.3	7.1	44.0	25.5	0.1	3.8	1.5	1.0	19.4	3.7
Cr-lap calc.	2.5	0.3	9.5	48.8	34.4	0.1	2.1	0.8	0.9	19.6	3.7
NiMo on alumina	3.6	1.8	2.0	0.0	0.0	2.8	2.7	4.0	2.8	0	0.0

Refined Wyoming Bentonite pillared with tin oxide after calcination for 1h at 500°C showed a four-fold increase in its surface area compared to the respective of the starting material as received (Table 7.1, Table 7.2). Nevertheless, a similarly prepared tin oxide pillared montmorillonite by Hannus et al. after calcination for 2h at 500°C displayed lower surface area (91 compared to 167 m^2/g) [123]. The same discrepancy has been observed in the basal spacings between the material prepared here and that reported by Hannus et al. (Section 4.1.3).

Sodium montmorillonite pillared with mixed chromium and cerium oxide pillars displayed a four-fold increase in its surface area, lower than the respective of the montmorillonite with single chromia pillars prepared using the same OH/Cr ratio of 2 (CM16), indicating in agreement with the XRD pattern that cerium was not found in the chromia pillars and may have been in another form such as an oligomeric cation in the interlayer region. Montmorillonite pillared with single cerium oxide pillars showed only a 1.7-fold increase in its surface area supporting the assumption of non-formation of polynuclear cationic complexes during hydrolysis of cerium nitrate leading to large cerium oxide pillars (Table 7.1, Table 7.2). Hernando et al. [35] have reported similar surface area for their cerium oxide pillared montmorillonite after calcination at 400°C (95 m^2/g). On the other hand, calcined europium oxide pillared montmorillonite did not show any change at all in its initial surface area. It is likely that the europium oxide pillars had completely collapsed during calcination filling the interlayer region in analogy with the sodium cations surrounded by their hydration spheres that fill the interlayer region of sodium montmorillonite.

The micropore volume and surface area of the starting materials, calculated by de Boer's t-plot method, were very small which is in accordance with their classification as meso-macroporous materials. Sodium montmorillonite displayed slightly higher pore volume and mean average diameter compared to Wyoming Bentonite as received (Table 7.1, Table 7.2). This may be due to the partial acid activation that took place during preparation of sodium montmorillonite leading to the formation of extra mesopores. Mishra and Parida have suggested the formation of extra mesopores in pillared materials derived from acid activated sodium montmorillonite displaying somewhat low basal spacings and surface areas but possessing significantly higher total pore volumes [32].

Pillaring of refined Wyoming Bentonite and sodium montmorillonite with chromium, tin and cerium oxides clearly induced microporosity (pores with diameter below 20Å), demonstrated by an increase in micropore volume and microporous surface area and a decrease in the average pore diameter, whereas pillaring with europium oxide did not. Europium oxide pillared montmorillonite exhibited a two-fold increase in its average pore diameter and total pore volume compared to sodium montmorillonite (194Å compared to 92Å) and no microposity. The increase in total pore volume observed in pillared clays can be normally justified by the added amount of microporosity to the total porosity of the starting clay material. However in the case of europium oxide pillared montmorillonite it cannot. It may be hypothesised instead that during calcination dexydroxylation of the pillars and the clay structure occurred resulting in the formation of large pores. Furthermore the total pore volume of sodium montmorillonite decreased after pillaring with cerium oxide, although microposity was induced. It may be assumed that some of the mesopores of the starting clay were filled with cerium oxide during pillaring. This assumption is supported by the significant weight increase of the clay observed after pillaring.

Similar lack of microporosity with europium oxide pillared montmorillonite has been displayed by a titania pillared montmorillonite prepared by Chae et al. [134] and two pillared bentonites with mixed alumina and lanthanum or cerium oxides prepared by Booij et al. [119]. The pillared bentonites exhibited large average pore diameter in the range between 60 and 70Å, which was attributed to the clay particle aggregation in a house of cards like structure (edge-to-face and edge-to-edge arrangements as observed by TEM) and corroborated by significant increase in their total surface area, which did not occur for europium oxide pillared montmorillonite. Hence, it appears that microporosity generated during the pillaring procedure differs with the type of the pillar, as evidenced by the XRD and nitrogen isotherm results.

All the mesopore size distributions obtained by the BJH method displayed one maximum at a pore diameter of ca. 38.8Å differing in the height of the peak, with the exception of europium oxide pillared montmorillonite that displayed a bimodal distribution with the first peak at a pore diameter of 38.6Å and the second broader at ca. 140Å elucidating its macroporosity (Figure 7.6, Figure 7.7).

Since no multiple samples of cerium and europium oxide pillared montmorillonites were prepared and analysed by nitrogen adsorption, there is a question of reproducibility. However, based on the experience gained during the preparation of the other pillared clay materials following similar methods, it is the researcher's belief that the differences observed were real and not due to factors related with the preparation procedure. If the experimentation time was longer reproducibility would have been validated.

From the XRD analysis of the used pillared clay catalysts it was assumed that harsh hydrocracking conditions in the microbomb reactor lead to partial collapse of the pillars (Section 4.3). This is supported by the nitrogen sorption analysis of the chromia pillared montmorillonite CM6 catalyst after undergoing hydrocracking conditions in the absence of feed. The catalyst showed a slight decrease in its BET surface area, as well as an increase in its average pore diameter compared with the respective of the fresh catalyst. In addition, the micropore surface area, micropore volume and the ratios of V_{mic}/V_{total} and S_{mic}/S_{total} of the used catalyst decreased compared to the respective of the fresh one. All the above observations illustrate the fact that harsh hydrocracking conditions indeed lead to partial collapse of the pillars in pillared clay catalysts.

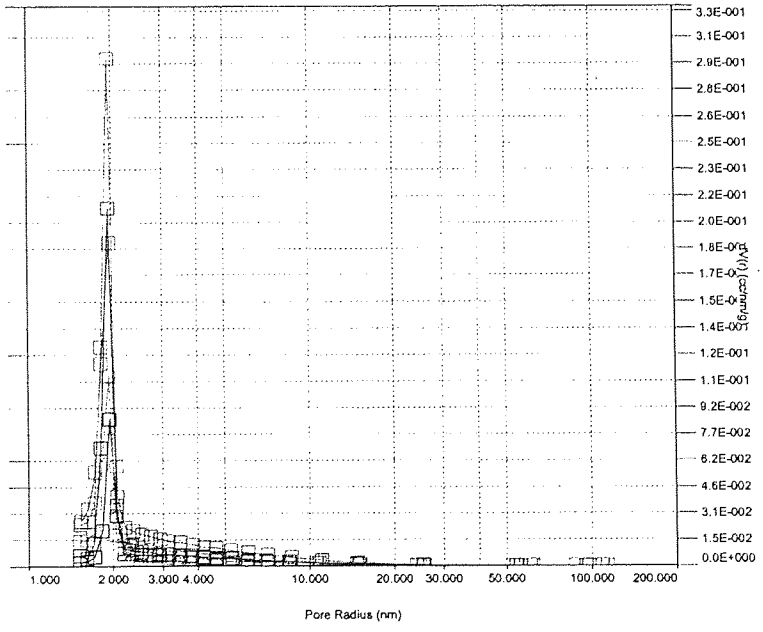

Figure 7.6 Mesopore size distributions for Wyoming Bentonite and chromia and tin oxide pillared montmorillonites

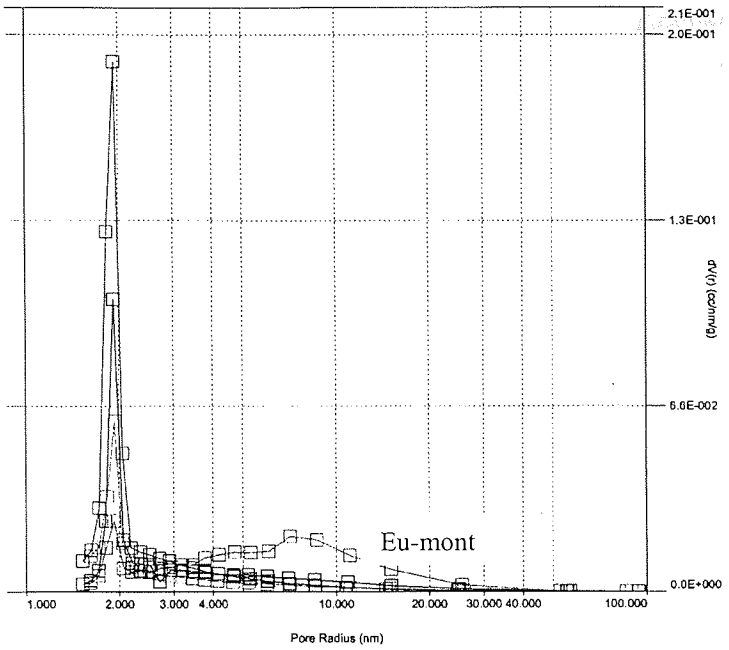

Figure 7.7 Mesopore size distributions for sodium montmorillonite and cerium, europium and mixed cerium and chromium oxide pillared montmorillonites

7.2 Laponite and respective pillared clays

The isotherm of laponite was a combination of type I (microporous materials) and IV (mesoporous materials). The hysteresis observed at higher relative pressures is due to capillary condensation in mesopores and corresponded to type H2 in the IUPAC classification. After its pillaring with either tin or chromium oxides, the isotherm retained its original shape and shifted to either lower or higher volume of adsorbed nitrogen respectively (Figure 7.8).

The pillaring of laponite did not have a significant effect in its total (BET) surface area or pore volume. Pillared laponite demonstrated either an increase or a slight decrease in its surface area depending on the pillaring species, chromium or tin respectively and almost constant pore volume. Similar results were reported by Volzone for chromia pillared laponite [132]. However, the surface area obtained here for chromia pillared laponite was nearly double compared to that reported by Pinnavaia et al. [117], although basically the same method was followed. This is probably due to the very high amount of chromium intercalated in their preparation, which is attributed to washing by dialysis instead of centrifugation, whereas in the current preparation washing was conducted by centrifugation. A tin oxide pillared laponite prepared by Occelli [136]

following a completely different method (via a colloidal suspension of tin oxide particles) compared to that followed here displayed surface area in the same order of magnitude (318 m^2/g).

It is clear that the pillaring of laponite did not influence much its porosity. Tin oxide pillared laponite actually displayed lower microporosity compared to the respective of the untreated laponite. This is in agreement with Maes et al. [133], who reported that the pillaring of laponite with titania, alumina and zirconia did not affect the porosity. In fact the microporosity of alumina pillared laponite even decreased.

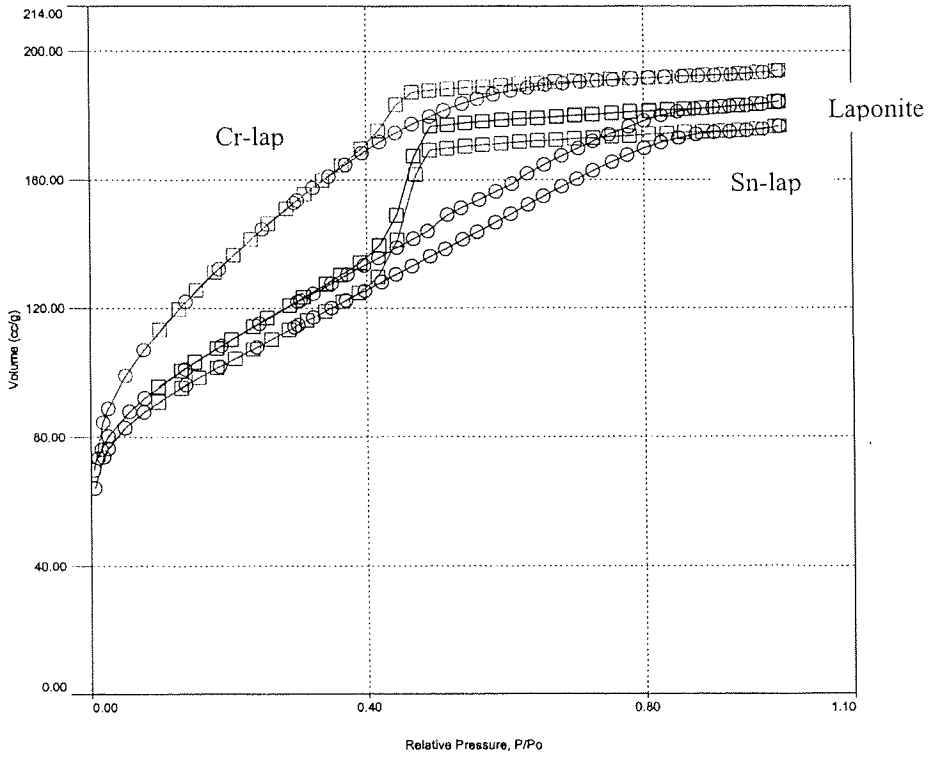

Figure 7.8 Nitrogen isotherms for laponite and chromia and tin oxide pillared laponites

Distortion was observed in the laponite isotherms (unpillared and pillared). It occurs due to the presence of pores on the border region between micro- and mesopores (15-35Å) and can shift the linear region in the t-plot to higher t-values. Consequently the micropore volumes calculated for these types of isotherms are high because they are composed of the volume of micropores as well as the volume of the small mesopores [133]. Therefore, the micropore volume obtained by the t-plot must be interpreted as the sum of the volume of micropores and small mesopores, which explains why the

micropore volume and surface area were almost equal to the total pore volume and surface area.

However, the pillars are not solely responsible for the pore system; the stacking of the clay layers into aggregates has a significant influence. The microporosity introduced by the pillaring of laponite is almost negligible compared to the volume formed by the delaminated stacking of the clay layers, but it will influence the catalytic behaviour [133].

The mesopore size distributions of both pillared laponites resembled that of the untreated laponite. All distributions displayed one maximum at a pore diameter of *ca.* 36.6Å, which is slightly lower than the respective displayed for pillared montmorillonites (Table 7.1).

7.3 Reference catalyst

The conventional catalyst NiMo/alumina used as a reference material in the hydrocracking runs was also analysed by nitrogen sorption in order to be compared with the other materials. It displayed, as expected, a type III isotherm typical for macroporous materials (Figure 7.9). Its BET surface area was double that of Wyoming bentonite, sodium montmorillonite and europium oxide pillared montmorillonite and its mean pore diameter (168Å) was higher compared to all the other materials (pillared and unpillared) except europium oxide pillared montmorillonite. Although it did not show any microporosity, it exhibited the highest total pore volume (Table 7.1, Table 7.2). Its mesopore size distribution showed a maximum at a pore radius of *ca.* 50Å, coinciding with the second peak displayed in the distribution of europium oxide pillared montmorillonite (Figure 7.10).

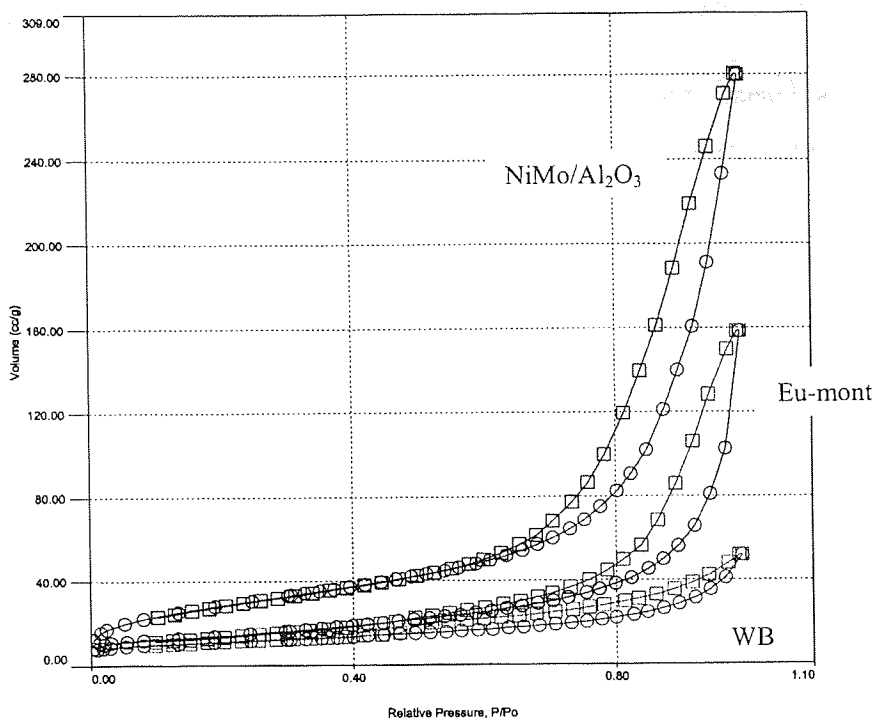

Figure 7.9 Nitrogen isotherms for Wyoming Bentonite, europium oxide pillared montmorillonite and NiMo supported on alumina

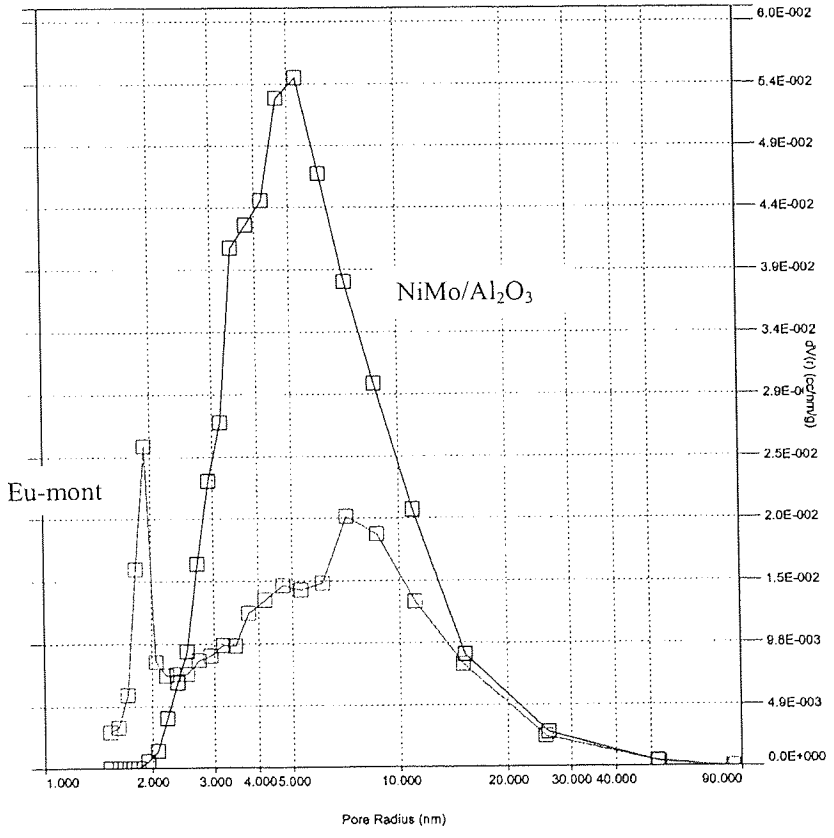

Figure 7.10 Mesopore size distributions for NiMo supported on alumina and europium oxide pillared montmorillonite

7.4 Summary

Pillaring of Wyoming Bentonite and sodium montmorillonite caused a multi-fold increase on the surface area, both total and microporous, and the pore volume, whereas pillaring of laponite only affected the total surface area as determined by this experimental technique. Moreover, the ratios of micropore volume to total pore volume and micropore surface area to total surface area (BET) increased after pillaring with respect to the ratios for Wyoming bentonite and sodium montmorillonite. However, the sodium montmorillonite pillared with europium oxide did not follow the general trend of the pillared montmorillonites. It did not display any microporosity or increase in its surface area and, in addition, showed higher macroporosity than the original montmorillonite. This could be attributed to the utilisation of europium oxide as pillaring species resulting in unconventional products behaving differently than the usual pillared clays deserving further investigation.

The unaltered surface area is likely to be due to the complete collapse of the europium oxide pillars during calcination filling the interlayer region in analogy with the sodium cations surrounded by their hydration spheres that fill the interlayer region of sodium montmorillonite. In addition the two fold increase in total pore volume may be attributed to the dexydroxylation of the pillars and the clay structure that may have occurred during calcination and resulted in the formation of large pores. In conclusion, it appears that microporosity generated during the pillaring procedure differs with the type of the pillar, as evidenced by the nitrogen sorption results.

8 MAGIC ANGLE SPINNING NUCLEAR MAGNETIC RESONANCE SPECTROSCOPY (MAS NMR); RESULTS & DISCUSSION

MAS NMR was the final characterisation method applied to the starting clay materials and their pillared derivatives after calcination. The recorded ^{29}Si and ^{27}Al MAS NMR spectra are presented herein aiming to identify weather pillaring with a range of species causes any changes in the aluminosilicate framework of the raw material. ^{29}Si and ^{27}Al MAS NMR spectra were also obtained for the chromia pillared montmorillonite CM6 after undergoing hydrocracking conditions in the absence of feed in an attempt to study the effect of hydrocracking conditions in the aluminosilicate framework of the catalyst.

However, it should be noted that although ^{29}Si MAS NMR provides information on the screening within, and hence the nature of, the silicate backbone, the formation of a charge-transfer complex in the interlayer may or may not cause a significant shift in electron density to be transmitted through the exchange sites to those silicon nuclei. ^{27}Al MASNMR can readily determine the coordination of aluminium, so that substitution of Al^{3+} into the tetrahedral silicate sheet, indicative of increased isomorphous substitution may be followed.

8.1 Wyoming Bentonite, sodium montmorillonite and respective pillared clays

Wyoming Bentonite's ^{29}Si spectrum consisted of two peaks, one corresponding to phyllosilicate silicon and the other, upfield of the first, corresponding to silica polymorphs, such as the quartz impurity (Figure 8.1). These chemical shift ranges of -91 to -98 ppm for phyllosilicate silicon, labelled Q^3, and -106 to -115 ppm for silica polymorphs, labelled Q^4, are well-known [137, 138].

The electronic environment of the nucleus influences significantly the ^{29}Si chemical isomer shift. For tetrahedral silicon there is good correlation between the isomer shift, the degree of polymerisation and the number of next nearest neighbour aluminium atoms. As the number of the next nearest neighbour Al atoms increases, polymerisation decreases leading to decreased shielding of the silicon nucleus and a less negative isomer shift with respect to tetramethyl silane. In montmorillonite, ideally, each silicon has a maximum of two next nearest neighbour aluminium atoms. However, isomorphous substitution of iron in the octahedral layer and aluminium and/or iron in

the tetrahedral layer, in combination with a random layer composition and edge effects can result in any number between none and four leading to rather broad resonances that overlap slightly.

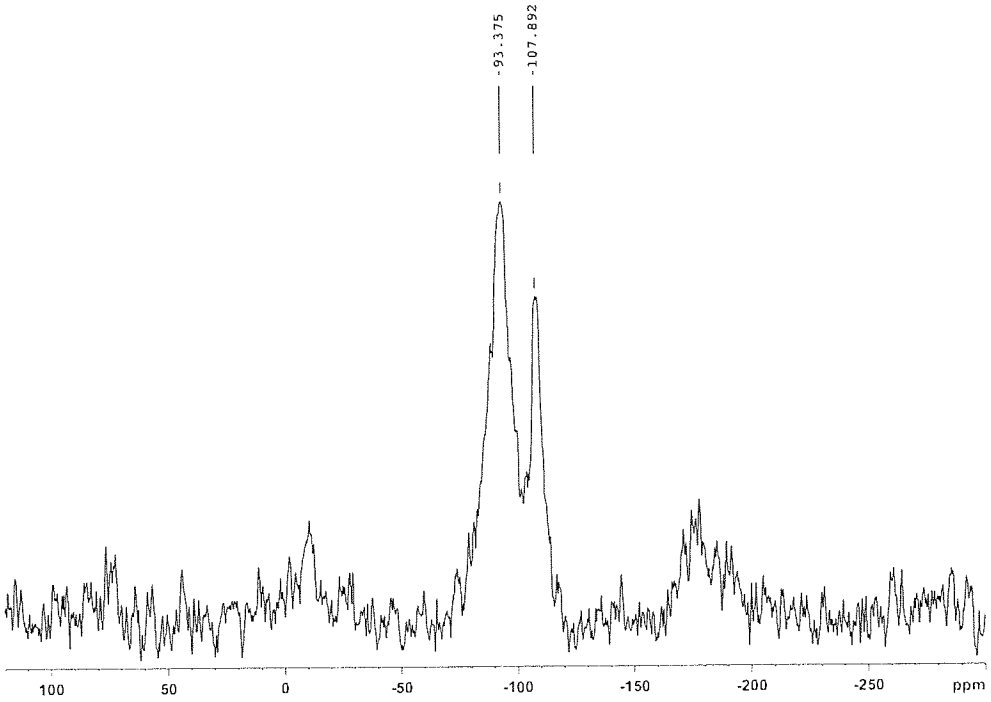

Figure 8.1 ^{29}Si MAS NMR spectrum of Wyoming Bentonite as received

The spectrum of monoionic sodium montmorillonite exhibited the same resonances with Wyoming Bentonite as received (Figure 8.2). Nevertheless, the first resonance decreased in intensity, whereas the second resonance remained almost unchanged indicating that a significant amount of quartz was still present in the clay despite the refining process undertaken. The lower intensity of the resonance at -93.6 ppm could be attributed to continuous stirring and centrifugation employed during the preparation of sodium montmorillonite, which led to the degradation of crystallinity of the original clay and also influenced the XRD pattern.

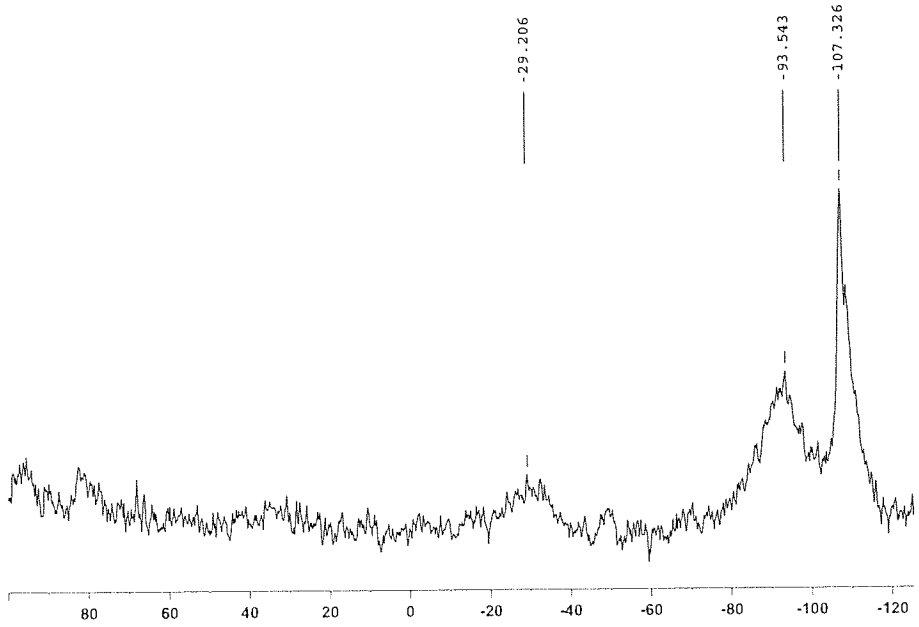

Figure 8.2 ^{29}Si MAS NMR spectrum of sodium montmorillonite

All silicon atoms of calcined pillared montmorillonite with chromium, tin, cerium or europium oxides continued to occupy two environments (Q^3 and Q^4) as indicated by the resonance peaks (Figures 8.3 to 8.8). The less negative ^{29}Si resonance (Q^3) shifted upfield for the calcined pillared derivatives compared with the respective resonance of the starting materials, while the ca. -107 ppm resonance attributed to quartz remained unaltered. A similar upfield shift observed on a calcined alumina pillared clay has been attributed to the diffusion of charge compensating protons generated during calcination to the octahedral layer [139]. In an improperly hydrolysed sample, shifts of the ^{29}Si signal could also result from the thermal diffusion to vacant octahedral sites of residual M^{3+} ions in the interlammellar space [140].

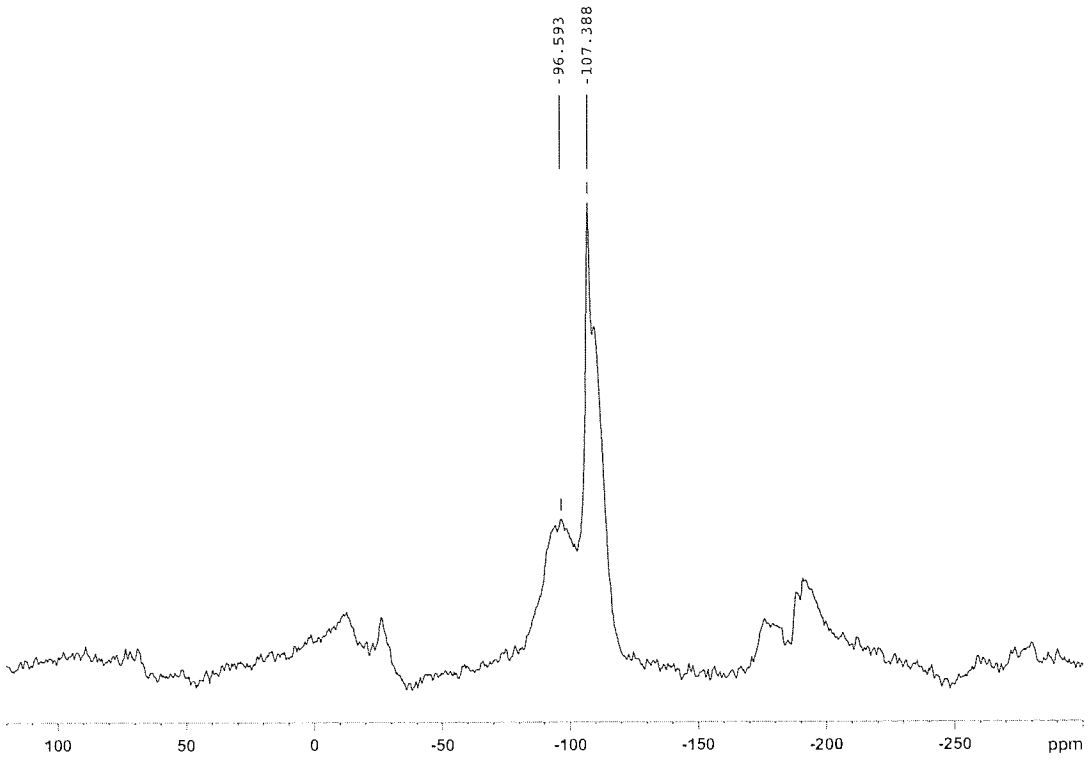

Figure 8.3 ^{29}Si MAS NMR spectrum of calcined chromia pillared montmorillonite CM3

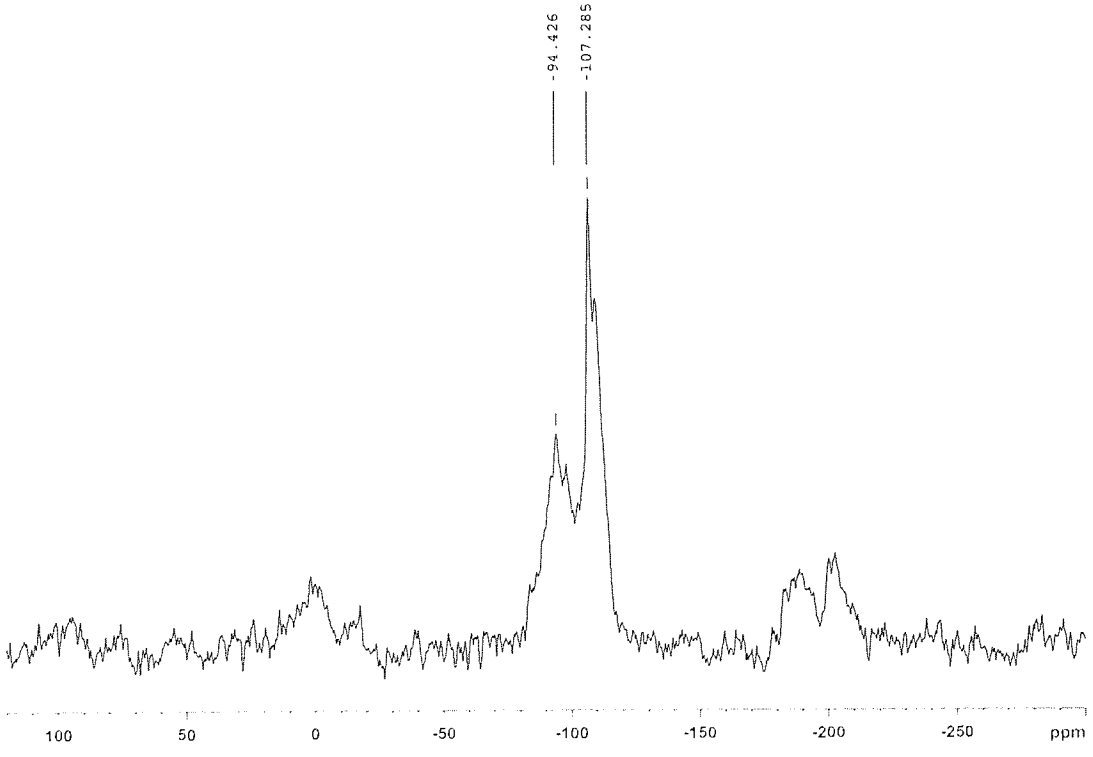

Figure 8.4 ^{29}Si MAS NMR spectrum of calcined chromia pillared montmorillonite CM6

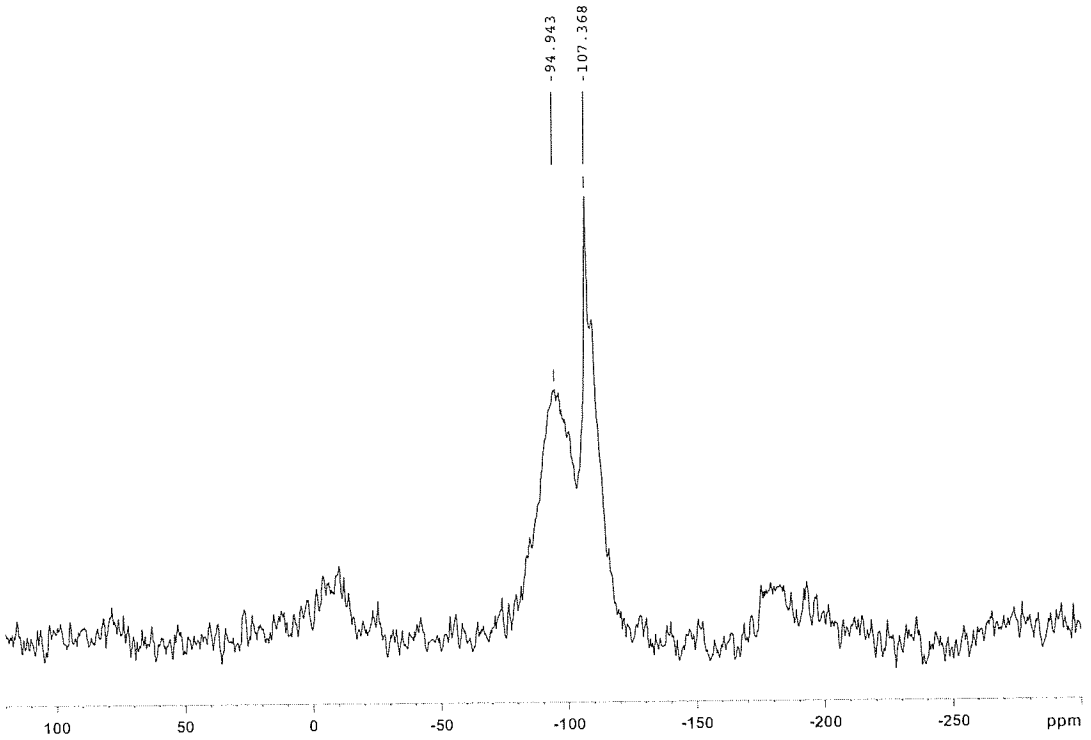

Figure 8.5 ^{29}Si MAS NMR spectrum of calcined tin oxide pillared montmorillonite SM1

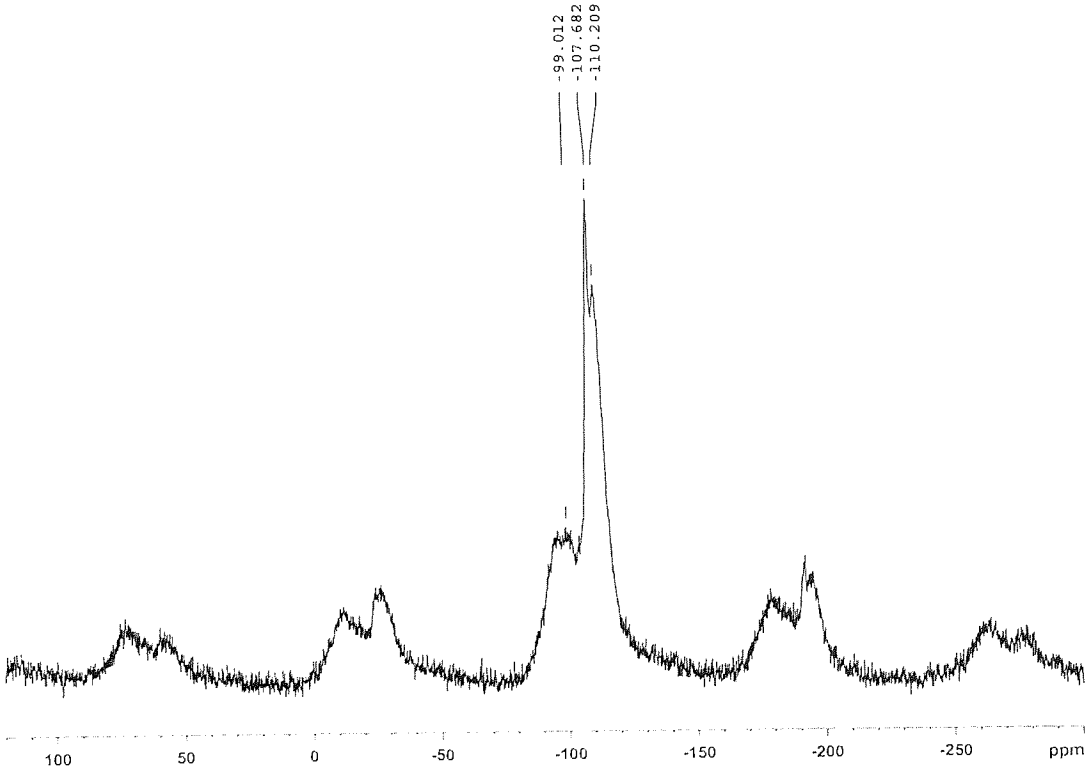

Figure 8.6 ^{29}Si MAS NMR spectrum of calcined montmorillonite pillared with mixed chromium and cerium oxides

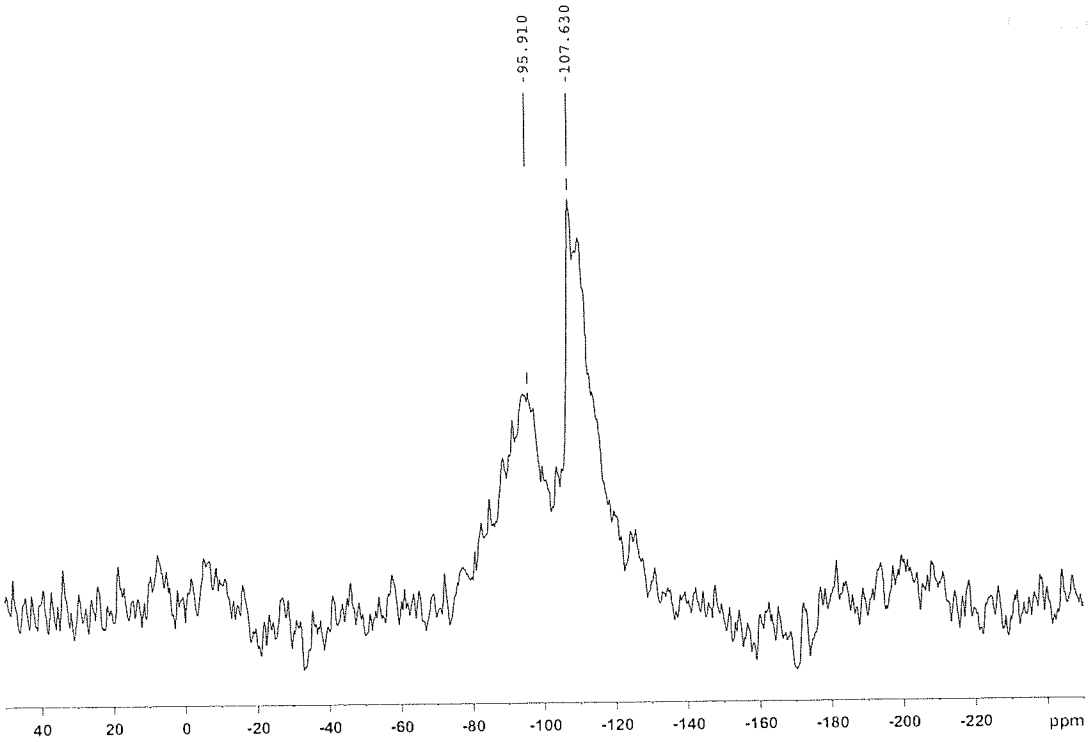

Figure 8.7 ^{29}Si MAS NMR spectrum of calcined cerium oxide pillared montmorillonite

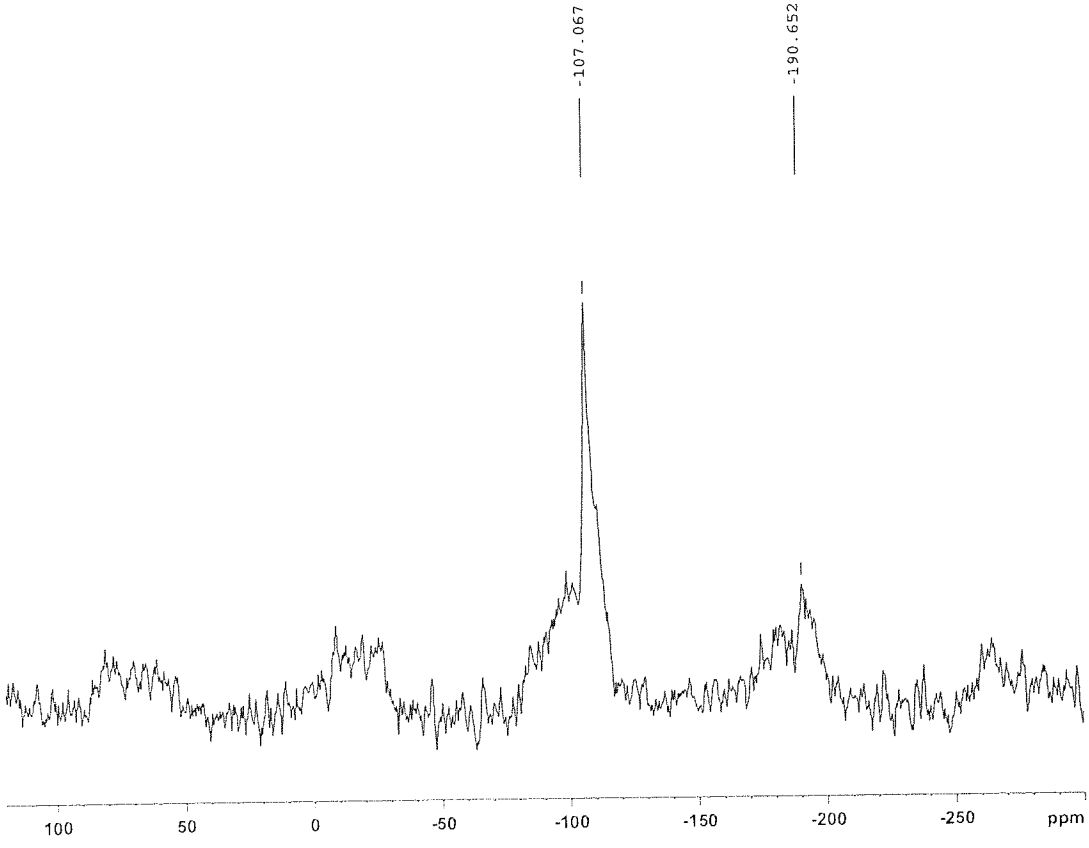

Figure 8.8 ^{29}Si MAS NMR spectrum of calcined europium oxide pillared montmorillonite

All the solid state ^{29}Si MAS NMR chemical shifts relative to tetramethyl silane are presented in Table 8.1.

Table 8.1 Solid state ^{29}Si MAS NMR chemical shifts for Wyoming Bentonite, sodium montmorillonite and their pillared derivatives

Samples	**δ (ppm)**	**δ (ppm)**
Wyoming Bentonite	-93.4	-107.8
Cr-mont calcined (CM6)	-94.4	-107.3
Sn-mont calcined	-94.9	-107.4
Na-montmorillonite	-93.6	-107.3
Cr-mont calcined (CM3)	-96.6	-107.4
Ce-mont calcined	-95.9	-107.6
Eu-mont calcined	-98.9	-107
Cr/Ce mont calcined	-98.9	-107.7, -110.2

Comparison of the ^{29}Si spectra among Wyoming Bentonite, sodium montmorillonite and their calcined pillared derivatives indicates that the silicate layer remained practically unchanged by the pillaring and calcination procedures. No relevant literature is available on calcined pillared montmorillonites with chromium, cerium or europium oxides. However, MAS NMR information on tin oxide pillared montmorillonite [123] is in agreement with the current work. Furthermore, an alumina pillared montmorillonite synthesised previously by Bodman also exhibited a practically unchanged ^{29}Si spectrum [4]. In contrast, the respective spectrum of an unpillared sodium montmorillonite heated to the temperature of calcination (500°C) showed two peaks over the range -106 to -115 ppm suggesting two slightly different Q^4 environments, indicative of different next-nearest neighbours [130].

Spinning sidebands are obvious in all the ^{29}Si spectra (Figures. 8.1 to 8.8) arising from modulation of the central transition by sample spinning and being enhanced by an increasing iron content in the sample due to magnetic susceptibility effects [141]. It is well known that randomly distributed paramagnetic ions in a naturally occurring mineral also have a significant broadening effect on its solid state MASNMR spectrum, due to both scalar electron-nuclear coupling, and modulation of the magnetic field experienced by the subject nucleus [142]. Increasing the content of paramagnetic ions reduces the quality of the spectrum. Nevertheless, no particular problem was encountered with the quality of the current spectra, regardless of the presence of

paramagnetic iron in all the samples and chromium in the chromia pillared montmorillonites.

The positions of ^{27}Al resonances are strongly influenced by co-ordination number and it is therefore easy to distinguish between tetrahedrally and octahedrally coordinated Al. The former presents chemical shift over the range 50 to 80 ppm, whereas the latter between -10 and 20 ppm. Hence, substitution of Al^{3+} into the tetrahedral silicate sheet, indicative of increased isomorphous substitution may be followed. However, there are problems associated with obtaining quantitative ratios of tetrahedral: octahedral aluminium from ^{27}Al MAS NMR spectra not only due to the inconvenient position of spinning sidebands resulting from octahedral aluminium when observing the central transition of tetrahedral aluminium or vice versa, but also associated with different quadrupolar interactions in the two structural environments [143]. Consequently, only the variation in the magnitude of the ratio should be taken into consideration.

The transition from octahedrally bound aluminium to tetrahedrally coordinated aluminium occurs during the heating process and is a result of dehydroxylation. More recent reports have shown peaks in the range of 31 to 37 ppm which have been assigned to 5-coordinate aluminium [140]. The difficulties in detecting 5-coordinate aluminium have been associated with the overall instability of this coordination environment combined with a ca. 90% loss in intensity of ^{27}Al NMR signal intensity upon dehydroxylation [130].

Wyoming Bentonite's ^{27}Al NMR spectrum presented an intense peak at 56.4 ppm and a less intense peak at -2.2 ppm representing tetrahedrally and octahedrally coordinated aluminium respectively (Figure 8.9). However, the high intensity of the peak at around 55 ppm indicates major isomorphous substitution of aluminium in the tetrahedral layer in contrast to the literature [4, 130, 140].

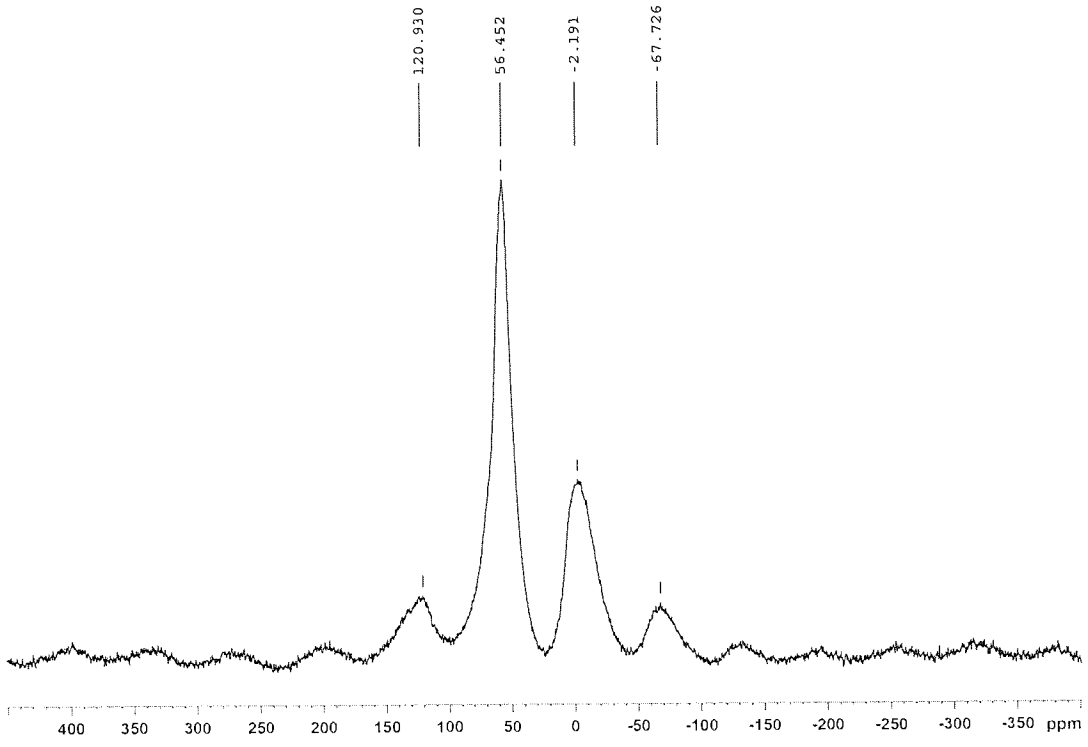

Figure 8.9 ^{27}Al MAS NMR spectrum of Wyoming Bentonite

Due to the practically unchanged ^{29}Si MAS NMR spectra by the pillaring and calcination procedures, only one ^{27}Al MAS NMR spectrum was obtained for chromia pillared montmorillonite in order to investigate if the same trend with the ^{29}Si MAS NMR spectra is followed by the ^{27}Al MAS NMR spectra (Figure 8.10). Again the ^{27}Al MAS NMR spectrum appeared relatively unchanged after pillaring and calcination. All the results are presented in Table 8.2. However, the ^{27}Al NMR spectrum of a Texas sodium montmorillonite after calcination at 500°C for 10h in air, displayed changes in coordination of structural aluminium attributed to partial dehydroxylation of the lattice and formation of 5-coordinate aluminium, which did not occur in the current work [140].

Table 8.2 Solid state ^{27}Al MAS NMR results of Wyoming Bentonite and its chromia pillared derivative CM6

Samples	δ (ppm)	δ (ppm)
Wyoming Bentonite	56.4	-2.2
Cr-mont calcined (CM6)	55.2	0

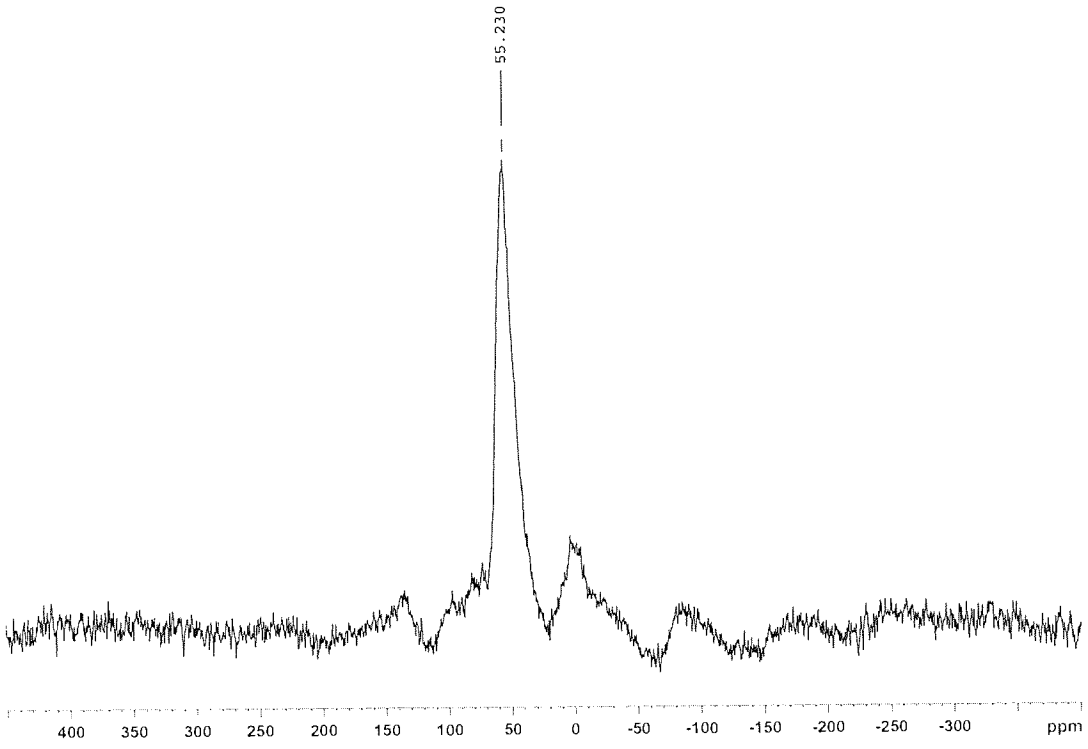

Figure 8.10 ^{27}Al MAS NMR spectrum of calcined chromia pillared montmorillonite CM6

An attempt was undertaken to characterize by MAS NMR the pillared clays after they had been used as hydrocracking catalysts with the aim to collect information on the impact of the hydrocracking procedure in their structure. However, spinning the sample at a rate of thousands of revolutions per second led to leakage of the oil (i.e. product from the hydrocracking of coal liquids) that was occluded in the coke coated catalyst causing short circuiting of the probe's coil. As an alternative the chromia pillared montmorillonite CM6 that was treated under hydrocracking conditions in the absence of feed was analysed by MAS NMR (Figure 8.11, Figure 8.12). Nevertheless no significant changes appeared in either the ^{29}Si or ^{27}Al MAS NMR spectrum compared to the respective ones before use (Table 8.3)

Table 8.3 Solid state ^{29}Si and ^{27}Al MAS NMR results of the chromia pillared montmorillonite CM6 before and after undergoing hydrocracking conditions

Samples	**^{29}Si δ(ppm)**		**^{27}Al δ(ppm)**	
Cr-mont calcined (CM6)	-94.4	-107.3	55.2	0
Cr-mont calcined (CM6) after HC	-95.2	-110.9	85.2, 57.4	3.9

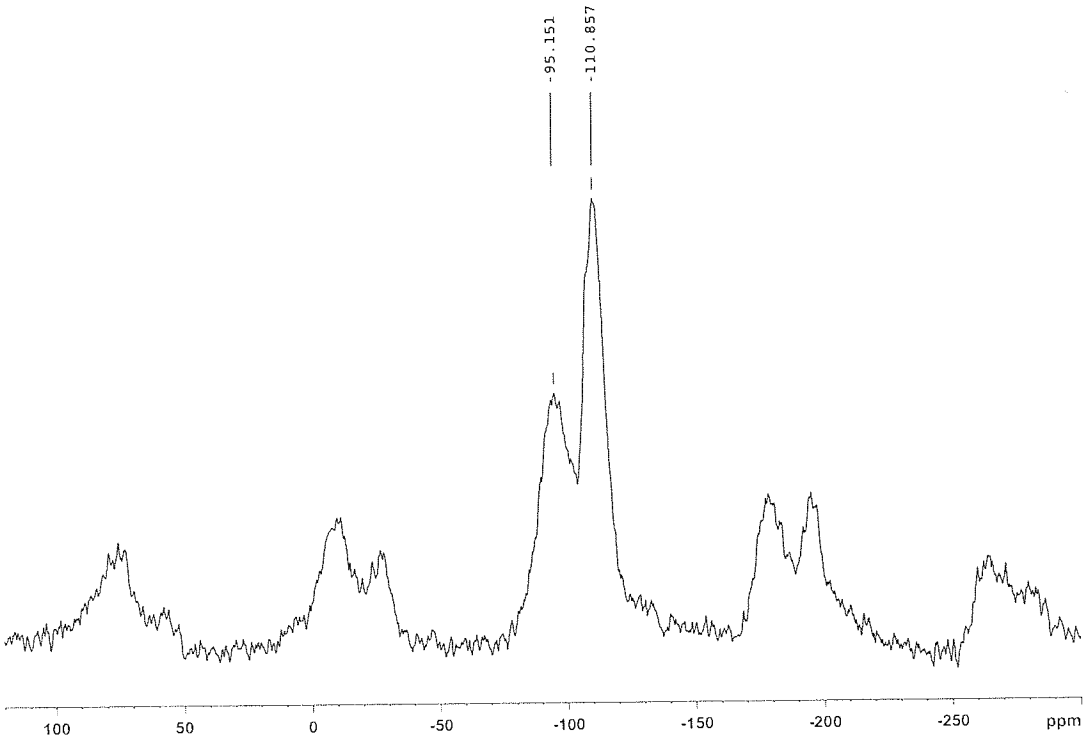

Figure 8.11 ^{29}Si MAS NMR spectrum of calcined chromia pillared montmorillonite CM6 after undergoing hydrocracking conditions in the absence of feed

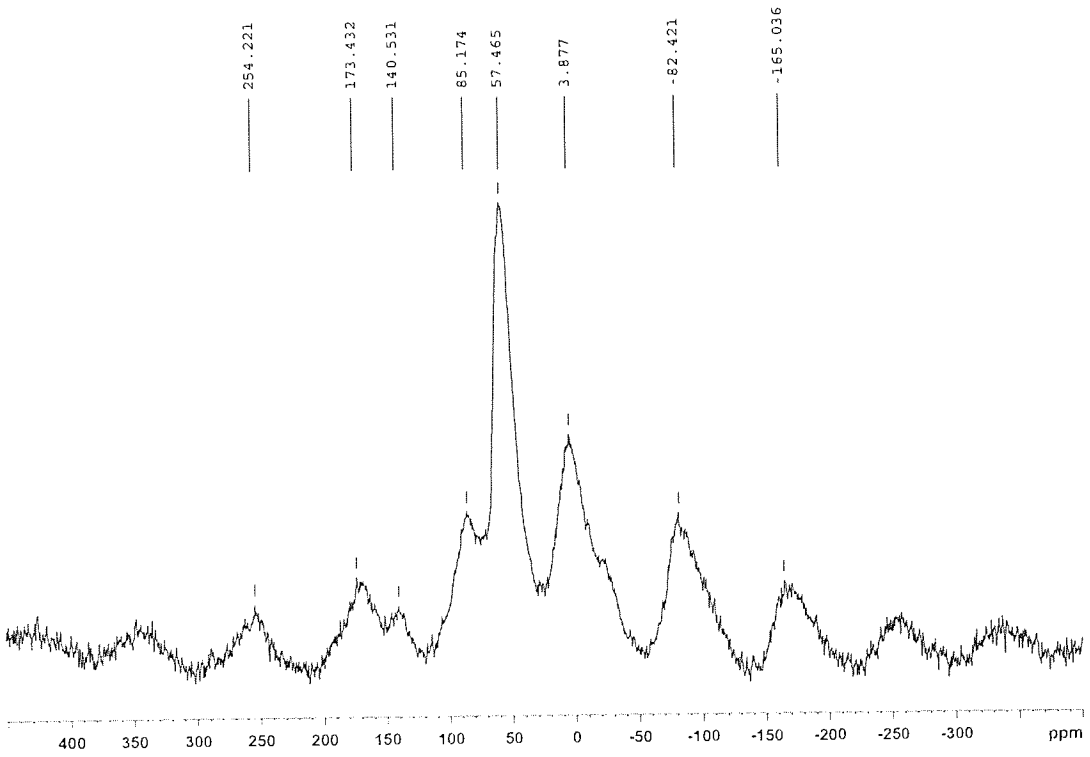

Figure 8.12 ^{27}Al MAS NMR spectrum of calcined chromia pillared montmorillonite CM6 after undergoing hydrocracking conditions in the absence of feed

8.2 Laponite and respective pillared clays

The ^{29}Si MAS NMR spectrum of laponite showed two resonances at -94.3 and -85.1 ppm respectively in agreement with the literature (Figure 8.13) [127, 144]. The data are interpreted with regards to the number of SiO_4 tetrahedra linked to a central SiO_4 tetrahedron via bridging oxygen atoms. Therefore Q^3 represents a SiO_4 group with one terminal oxygen and three forming common vertices with three other SiO_4 tetrahedra. The dominant resonance at -94.3 ppm is derived from the Q^3 silicons. The weak resonance at -85.1 ppm is caused by the Q^2 silicon which must occur at the silicate sheet edges. This component is visible with laponite RD because of the very small particle size of the clay, leading to a significant proportion of edge sites.

After pillaring with tin oxide the ^{29}Si MAS NMR spectrum of laponite remained unaltered (Figure 8.13, Figure 8.14). However, pillaring with chromium oxide and calcination at 500°C under argon, modified the spectrum. Only one resonance was exhibited at -96.9 ppm (Figure 8.15). In addition, large spinning sidebands appeared in the spectrum attributed to the paramagnetic character of chromium.

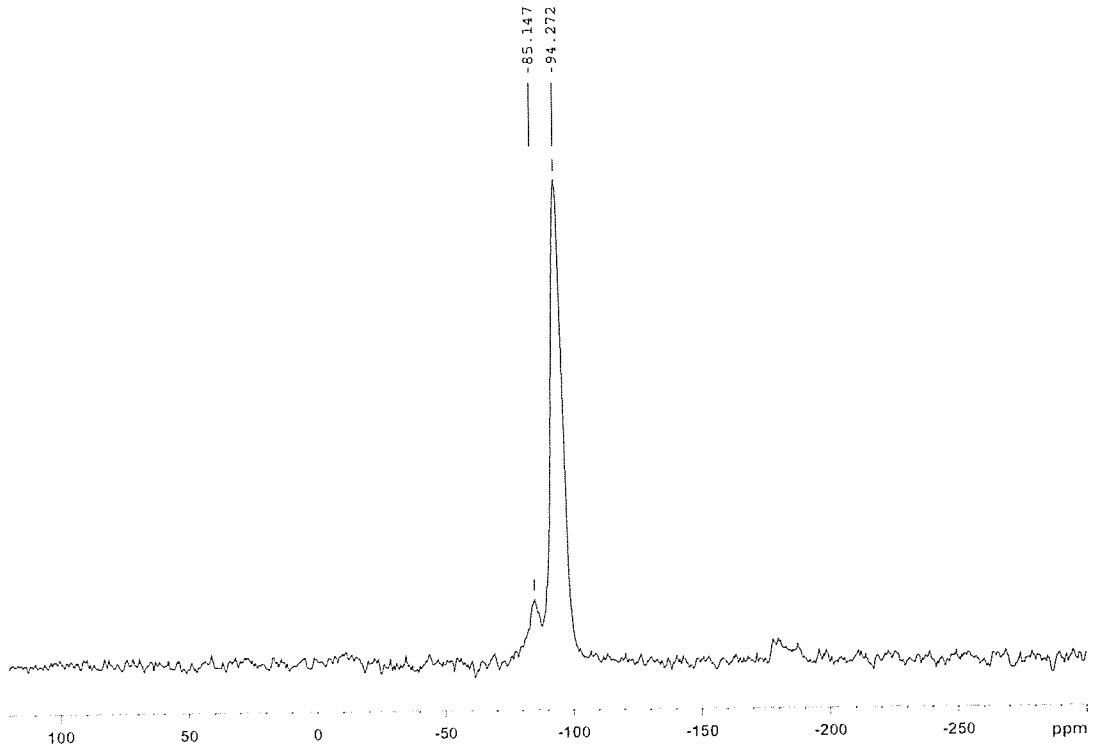

Figure 8.13 ^{29}Si MAS NMR spectrum of laponite

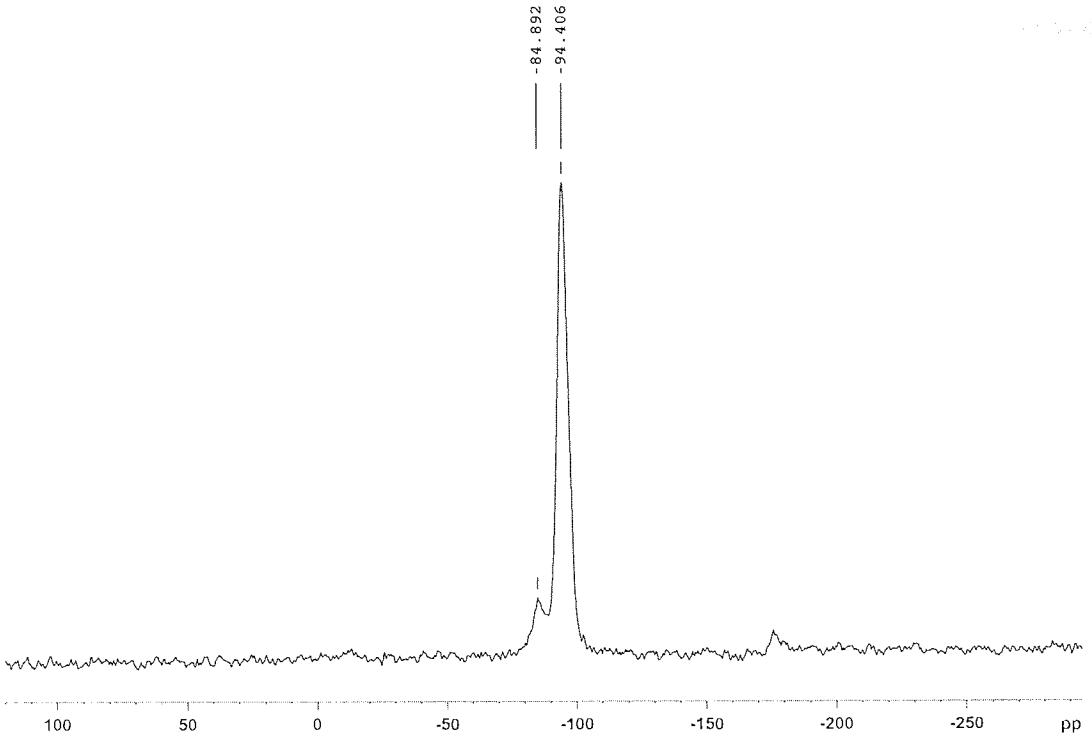

Figure 8.14 ^{29}Si MAS NMR spectrum of tin oxide pillared laponite

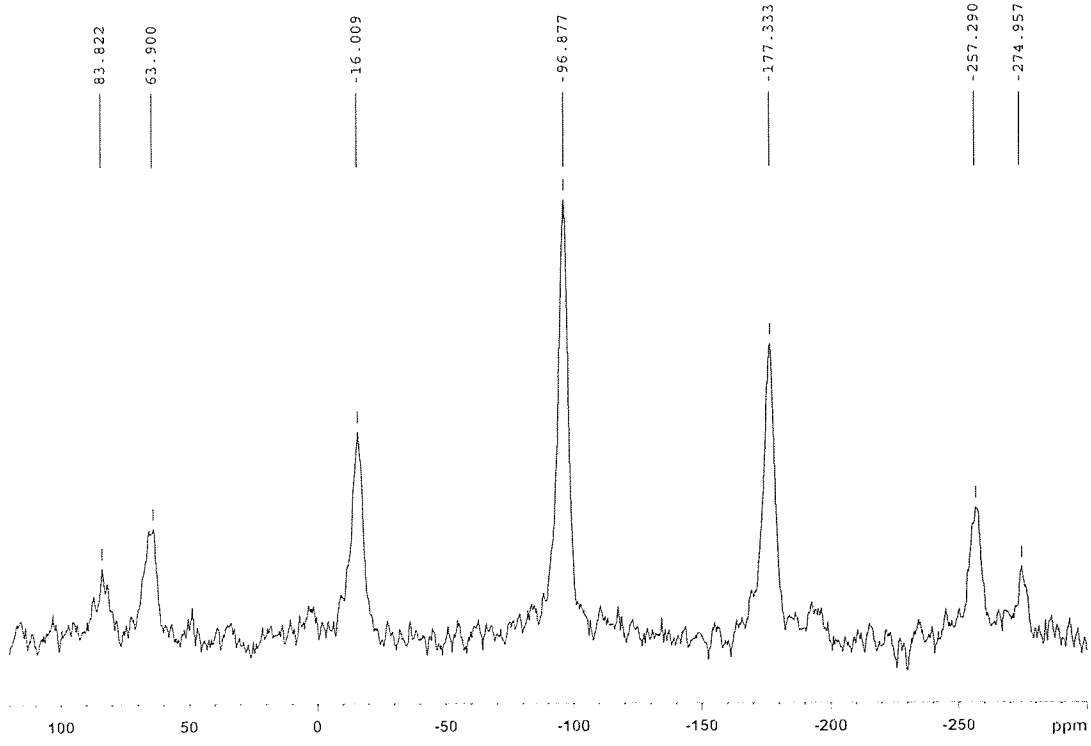

Figure 8.15 ^{29}Si MAS NMR spectrum of chromia pillared laponite

Table 8.4 Solid state ^{29}Si MAS NMR results for laponite and its pillared derivatives

Samples	δ (ppm)	δ (ppm)
Laponite	-85.1	-94.3
Sn-laponite	-84.9	-94.4
Cr-laponite calcined		-96.9

The change observed in the ^{29}Si MAS NMR spectrum for the calcined chromia pillared laponite is in agreement with the work by Mandair et al. on the thermolysis of laponite [144]. They reported that after heating laponite at 600°C the Q^2 resonance was not resolved and only a relatively sharp resonance was seen at -97.7 ppm and suggested that the lithium ions had become labile and been removed from their structural octahedral sites to edge sites and that was reflected in the shielding of the silicon Q^3 sites. In this respect, the change in the ^{29}Si spectrum for the calcined chromia pillared laponite should be attributed to the calcination procedure and not the pillaring, which is supported by the unaltered ^{29}Si spectrum for the uncalcined tin oxide pillared laponite.

8.3 Summary

The ^{27}Al MAS NMR spectra of Wyoming bentonite and its derived pillared montmorillonites all showed a dominant resonance at *ca.* 56 ppm and a weak resonance at *ca.* -2 ppm representing tetrahedrally and octahedrally coordinated aluminium respectively. This indicates major isomorphous substitution of aluminium in the tetrahedral layer in contrast to the literature. With respect to the pillaring procedure, the ^{29}Si and ^{27}Al MAS NMR spectra of the prepared materials did not exhibit any significant changes before and after pillaring signifying that the aluminosilicate structure of the materials remained basically unaltered. The appearance of only a sharp Q^3 resonance in the ^{29}Si MAS NMR spectrum of chromia pillared laponite whilst the Q^2 resonance was unresolved is attributed to the calcination procedure. During calcination the lithium ions became labile and were removed from their structural octahedral sites to edge sites and that was reflected in the shielding of the silicon Q^3 sites.

9 CATALYSTS HYDROCRACKING PERFORMANCE; RESULTS & DISCUSSION

This chapter presents the conversions achieved during two series of hydrocracking runs in a microbomb reactor at Imperial College utilising a range of clay materials (pillared and unpillared) as catalysts and coal liquids as feed. In the first series fresh feed and fresh catalysts were employed, whereas in the second series a selection of recovered coated catalysts and fresh feed were in use.

Based on these results the performance of the catalysts is assessed in comparison to the respective performance of a conventional catalyst (NiMo on alumina). An attempt is undertaken to correlate the catalyst's performance with their properties, which were identified previously via the characterisation route. The effect of coke deposition on the catalysts' activity is taken into consideration.

This chapter also presents the commissioning of a microwave hydrocracking reactor operating at moderate conditions (13.8 bar and 190°C) and the results from a test with coal derived liquids as feed and NiMo on alumina as catalyst. These results are used to appraise weather microwave irradiation enables conversion to occur at milder conditions than those conventionally used, coupled with a more effective use of hydrogen.

9.1 Hydrocracking conversions in the microbomb reactor

According to colleagues working at Imperial College, 'conversion' is defined as the proportion of material in the initial feed of boiling point above 450°C, which has been converted to lower boiling products. The calculation depends on the determination of the mass of product mixture after hydrocracking and the proportion of it boiling above 450°C by TGA. Conversions have been calculated both with (total conversion) and without (liquid conversion) inclusion of the carbonaceous deposits as above 450°C boiling material. Material deposited on the catalyst and not removed with chloroform/methanol was classed as boiling above 450°C. This correction was performed in order to distinguish between catalysts with high hydrocracking activity from those which merely remove the above 450°C fraction as coke on catalyst. The exact formulas are presented below:

$$\text{Liquid conversion \%} = \frac{\text{Amount of BP>450°C in the feed – Amount of BP>450°C in the product}}{\text{Amount of BP>450°C in the feed}} \times 100$$

Solids (Catalyst weight loss, %): determined by thermogravimetric analysis

$$\text{Total conversion \%} = \frac{\text{Amount of BP>450°C in the feed – (Amount of BP>450°C in the product + Solids)}}{\text{Amount of BP>450°C in the feed}} \times 100$$

BP: boiling point

A better factor than the total conversion for assessing the hydrocracking performance of the catalysts, bearing in mind that in a commercial process the liquid phase would be recycled infinitely to yield the desired product, is the ratio of the liquid phase towards the sum of the liquid and solid phase:

$$\frac{\text{Liquid conversion \%}}{\text{Liquid conversion \% + Solids \%}} \times 100$$

The abbreviation [L/(L+S)]% will be used herein to describe this factor.

All the results are presented in Table 9.1 and Table 9.2. The respective mass balances are presented in Appendix 2. The conversion calculations for the first run conducted with the chromia pillared montmorillonite CM3 are presented below as an example.

Feed (mg) = 1015.7

Ash free feed (mg) = 963.9

Amount with boiling point >450°C in the ash free feed (%) = 46.5

Amount with boiling point >450°C in the ash free feed (mg) = 448.2

Recovered product (mg) = 709.8

The percentage of the recovered product with boiling point above 450°C was determined by TGA. The temperature was kept at 30°C for 15 min followed by a 4°C/min ramp up to 247°C (corresponding to 450°C boiling point) where it was held for 10 min. The profile is presented in Figure 9.1.

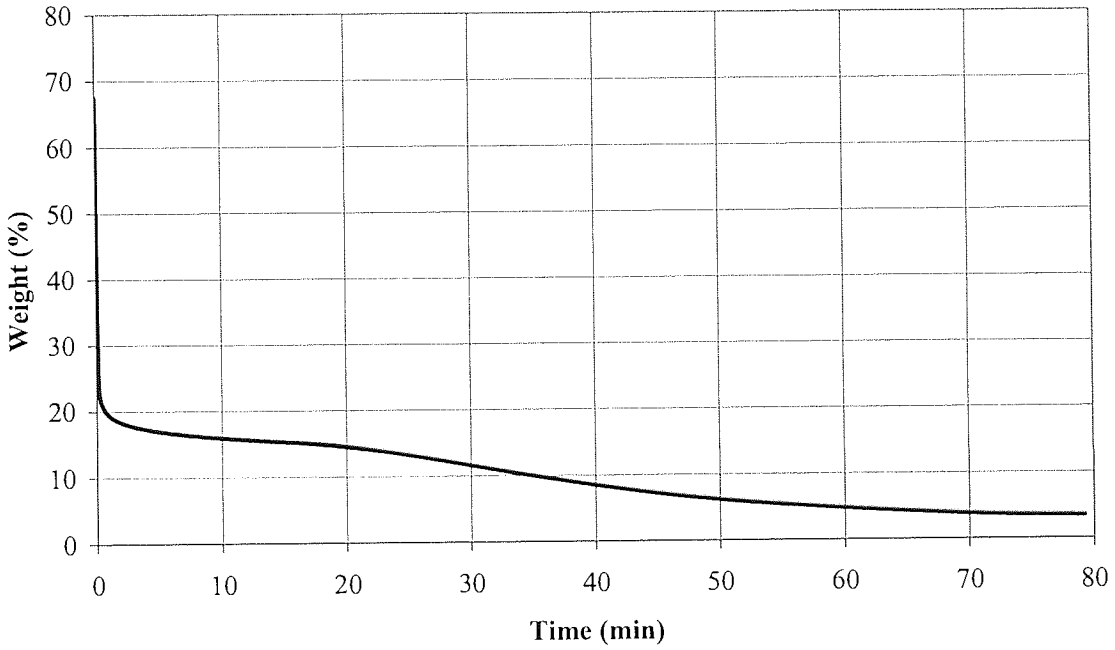

Figure 9.1 TGA profile for the first run conducted with the chromia pillared montmorillonite CM3

The percentage of the recovered product with boiling point above 450°C was obtained by dividing the weight at the end of the run (only material with boiling point above 450°C remained on the TGA pan) by that at 15 minutes ($CHCl_3$/MeOH has been completely evaporated).

Amount of product with boiling point above 450°C (%) = 3.49/ 15.31 = 22.8

Amount of product with boiling point above 450°C (mg) = 161.8

Recovered catalyst (mg) = 453.4

Catalyst weight loss (by TGA, %) = 34.5

Catalyst weight loss (solids, mg) = 156.4

As a result for the first run conducted with CM3 the conversions are:

Liquid conversion % = (448.2 – 161.8)*100 / 448.2 = 63.9

Total conversion % = [448.2 – (161.8+156.4)]*100 / 448.2 = 29

[L/(L+S)]% = {63.9 / (63.9 + 34.5)]*100 = 64.9

The blank run that was conducted under the same conditions with all the other runs but in the absence of any catalyst displayed considerable hydrocracking attributed to a thermal effect. In order to distinguish catalytic hydrocracking from thermal hydrocracking, relative conversion factors were calculated by subtracting the total conversion and the [L/(L+S)]% of the blank run from the respective of all the catalytic hydrocracking runs. The results are presented in Table 9.3.

The hydrocracking runs employing the chromia pillared montmorillonite CM3 and unpillared laponite as catalysts were duplicated in order to check the reproducibility of the process and assess the magnitude of experimental error. Liquid conversion and solids values presented variation in the range 6 to 11% and 3 to 8% respectively (Table 9.1 and Table 9.2). However, the calculated total conversion displayed a much lower variation of 1 to 3%, whereas the [L/(L+S)]% showed only 1% variation. Therefore, in the assessment of the results an experimental error of 8% and 5% will be taken into account for the liquid conversion and the solids respectively, while a 2% error will be considered for the total conversion and the [L/(L+S)]%.

Table 9.1 Hydrocracking conversions for Wyoming Bentonite, sodium montmorillonite and their pillared derivatives

		1st use				2nd use			
Catalyst	**Basal spacing (Å)**	**Liquid conversion %**	**Solids (% of filter cake)**	**Total conversion %**	**[L /(L + S)] %**	**Liquid conversion %**	**Solids (% of filter cake)**	**Total conversion %**	**[L /(L + S)] %**
Na-mont	15.9	47	28	**24**	**63**	45	10	**40**	**82**
Cr-mont CM3	15.5	64	35	**29**	**65**	48	4	**45**	**92**
	15.5	53	27	**30**	**66**				
Cr-mont CM16	23.4	50	29	**23**	**63**				
Eu-mont	15.7	51	23	**33**	**69**	34	13	**24**	**72**
Ce-mont	15.7	47	23	**30**	**67**	43	14	**31**	**75**
Cr/Ce-mont	no peak	50	28	**25**	**64**	47	13	**37**	**78**
W. B.	15.2	44	26	**23**	**63**	48	14	**38**	**77**
Cr-mont CM2b	15.7	41	28	**20**	**59**				
Cr-mont CM2c	15.7	55	30	**26**	**65**				
Cr-mont CM2d	15.7	43	26	**21**	**62**				
Cr-mont CM6	22.5	50	27	**27**	**65**	39	9	**33**	**81**
Cr-mont B61		62	38	**26**	**62**				
$NiMo/Al_2O_3$		55	26	**36**	**68**	59	16	**45**	**79**
No catalyst		41	64	**21**	**39**				

Table 9.2 Hydrocracking conversions for laponite and its pillared derivatives

	1st use				2nd use			
Catalyst	**Liquid conversion %**	**Solids (% of filter cake)**	**Total conversion %**	**[L /(L + S)] %**	**Liquid conversion %**	**Solids (% of filter cake)**	**Total conversion %**	**[L /(L + S)] %**
Laponite	55	24	**33**	**70**	53	19	**38**	**74**
	49	21	**30**	**70**				
Sn-lap SL3a	50	34	**21**	**60**				
Sn-lap SL4a	48	35	**15**	**58**				
Sn-lap SL5a	46	24	**25**	**66**				
Sn-lap SL6a	48	21	**29**	**70**				
Sn-lap SL9a	45	20	**27**	**69**				
Sn-lap SL9b	55	25	**30**	**69**				
Sn-lap SL9c	52	34	**21**	**60**				
Sn-lap SL2a	59	43	**18**	**58**	40	3	**38**	**93**
Sn-lap SL2b	54	32	**23**	**63**				
Sn-lap SL7a	55	21	**37**	**72**	51	37	**20**	**58**
Sn-lap SL7b	45	27	**21**	**63**				
Sn-lap B71	50	28	**22**	**64**				
Cr-laponite CL1	54	29	**28**	**65**	45	18	**34**	**71**
Cr-lap B14	48	31	**23**	**61**				
$NiMo/Al_2O_3$	55	26	**36**	**68**	59	16	**45**	**79**
No catalyst	41	64	**21**	**39**				

9.1.1 First series of hydrocracking runs

The first series of hydrocracking runs was conducted with both fresh catalysts and fresh feed. The liquid conversions obtained ranged between 41 and 64%. The chromia pillared montmorillonite CM3, which was prepared from sodium montmorillonite exhibited the highest liquid conversion (64%) followed by the tin oxide pillared laponite SL2a (59%). However, considering the experimental error (±8%) no one of the catalysts appeared to supersede the others with regards to liquid conversion. The majority of catalysts including the reference catalyst $NiMo/Al_2O_3$ and the pillared clay catalysts prepared earlier by Bodman (B61, B14, B71) displayed liquid conversion over the range 64 ± 8%, whereas a smaller number of catalyst showed lower liquid conversion over the range 41 ± 8% (Na-mont, Ce-mont, W.B., Cr-mont CM2b, Cr-mont CM2d, SL5a, SL7b, SL5a) (Figures 9.2 and 9.3).

Sodium montmorillonite, Wyoming Bentonite and their pillared derivatives displayed a narrower distribution of coke deposition over the range 23 to 38% compared to the respective for laponite and its pillared derivatives (21 to 43%). Taking into account the experimental error (±5%) once again most of the catalysts fall into the same category. The europium and cerium oxide pillared montmorillonites, the unpillared laponite and the tin oxide pillared laponites SL6a, SL9a, SL7a exhibited the lowest amount of coke deposition (20 to 23%) (Figures 9.2 and 9.3).

The reference catalyst ($NiMo/Al_2O_3$), the europium oxide pillared montmorillonite, the unpillared laponite and the tin oxide pillared laponite SL7a displayed the highest relative total conversion (12 to 16%) bearing in mind the experimental error (±2%). On the contrary the chromia pillared montmorillonite CM2b and the tin oxide pillared laponites SL2a and SL4a showed negative relative total conversion, whereas the chromia pillared montmorillonite CM2d and the tin oxide pillared laponites SL3a and SL7b showed zero relative total conversion indicating only thermal and no catalytic hydrocracking.

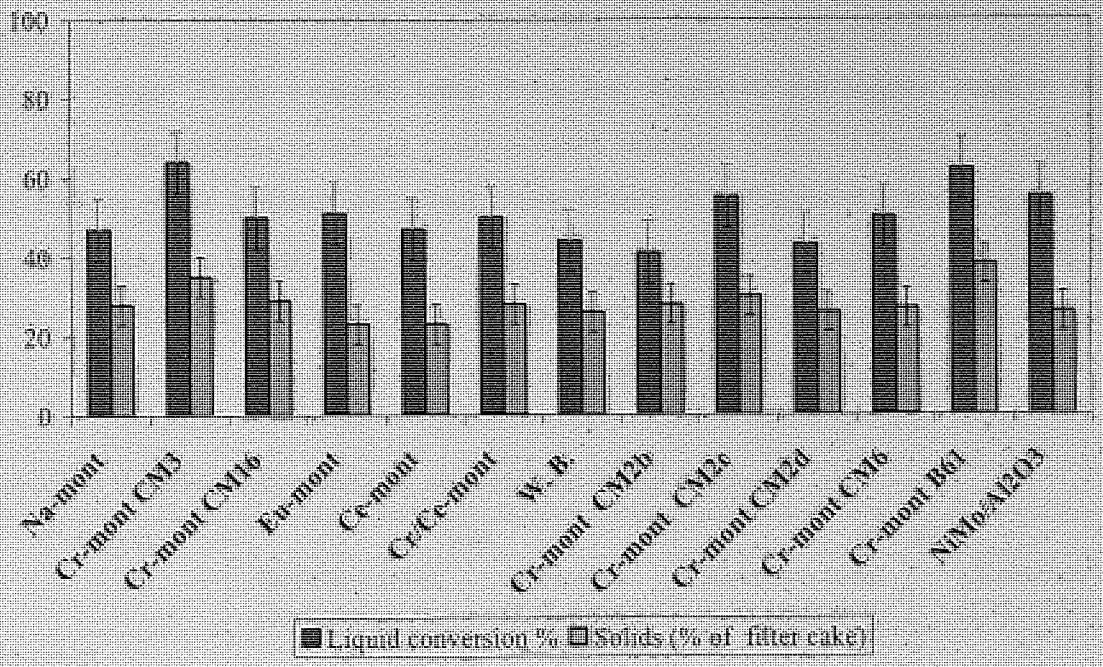

Figure 9.2 Liquid conversion and solids for the first series of hydrocracking runs employing sodium montmorillonite, Wyoming Bentonite and their pillared derivatives as catalysts

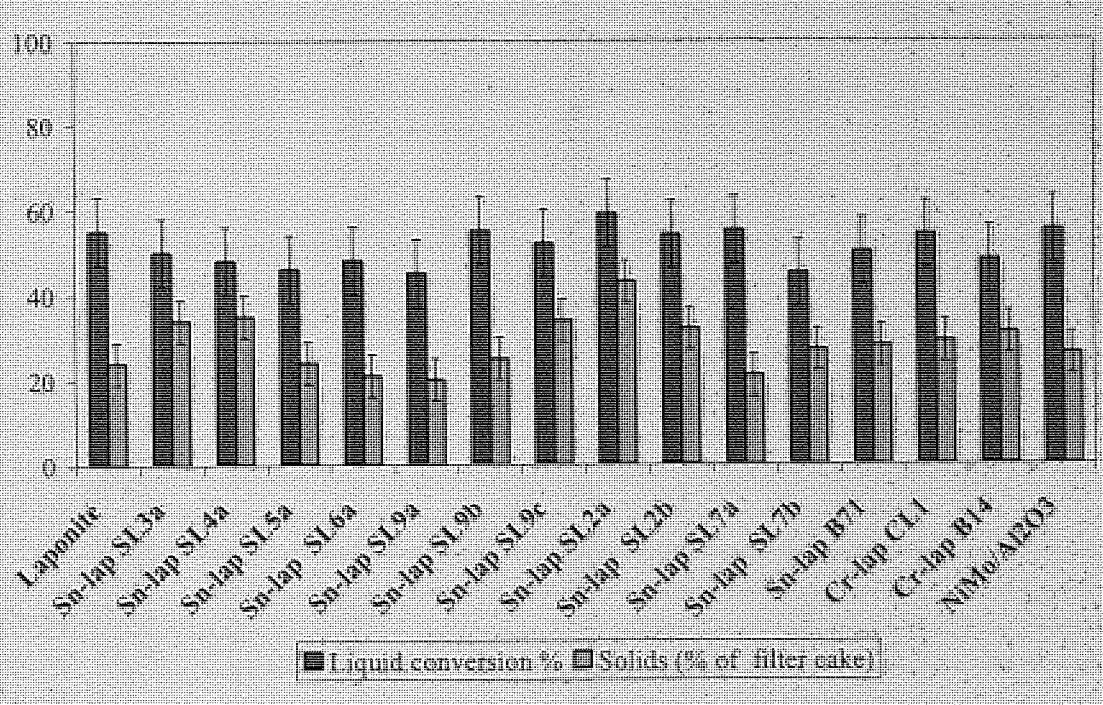

Figure 9.3 Liquid conversion and solids for the first series of hydrocracking runs employing laponite and its pillared derivatives as catalysts

With regards to the preferred relative conversion factor L/(L+S) all the catalysts exhibited positive relative conversion and a large number of catalysts was classified in the top range. These catalysts were those that exhibited the highest relative total conversion in addition to the tin oxide pillared laponites SL5a, SL9a, SL9b SL6a and the cerium oxide pillared montmorillonite (Table 9.3, Figure 9.4 and Figure 9.5). Nevertheless, due to the rapid initial carbon deposition which occured as soon as the fresh catalysts came in contact with the coal liquids, no real comparison of the catalysts performance can be performed from the first series of hydrocracking runs.

Table 9.3 Relative hydrocracking conversions for all catalysts

Catalyst	1st use		2nd use	
	Relative total conversion %	Relative (L/L+S)%	Relative total conversion %	Relative (L/L+S)%
Na-mont	3	24	19	43
Cr-mont CM3	8	26	24	53
	9	27		
Cr-mont CM16	2	24		
Eu-mont	12	30	3	33
Ce-mont	9	28	10	36
Cr/Ce-mont	4	25	16	39
W. B.	2	24	17	38
Cr-mont CM2b	-1	20		
Cr-mont CM2c	5	26		
Cr-mont CM2d	0	23		
Cr-mont CM6	6	26	12	42
Cr-mont B61	5	23		
Laponite	12	31	17	35
	9	31		
Sn-lap SL3a	0	21		
Sn-lap SL4a	-6	19		
Sn-lap SL5a	4	27		
Sn-lap SL6a	8	31		
Sn-lap SL9a	6	30		
Sn-lap SL9b	9	30		
Sn-lap SL9c	0	21		
Sn-lap SL2a	-3	19	17	54
Sn-lap SL2b	2	24		
Sn-lap SL7a	16	33	-1	19
Sn-lap SL7b	0	24		
Sn-lap B71	1	25		
Cr-laponite CL1	7	26	13	32
Cr-lap B14	2	22		
$NiMo/Al_2O_3$	15	29	24	40

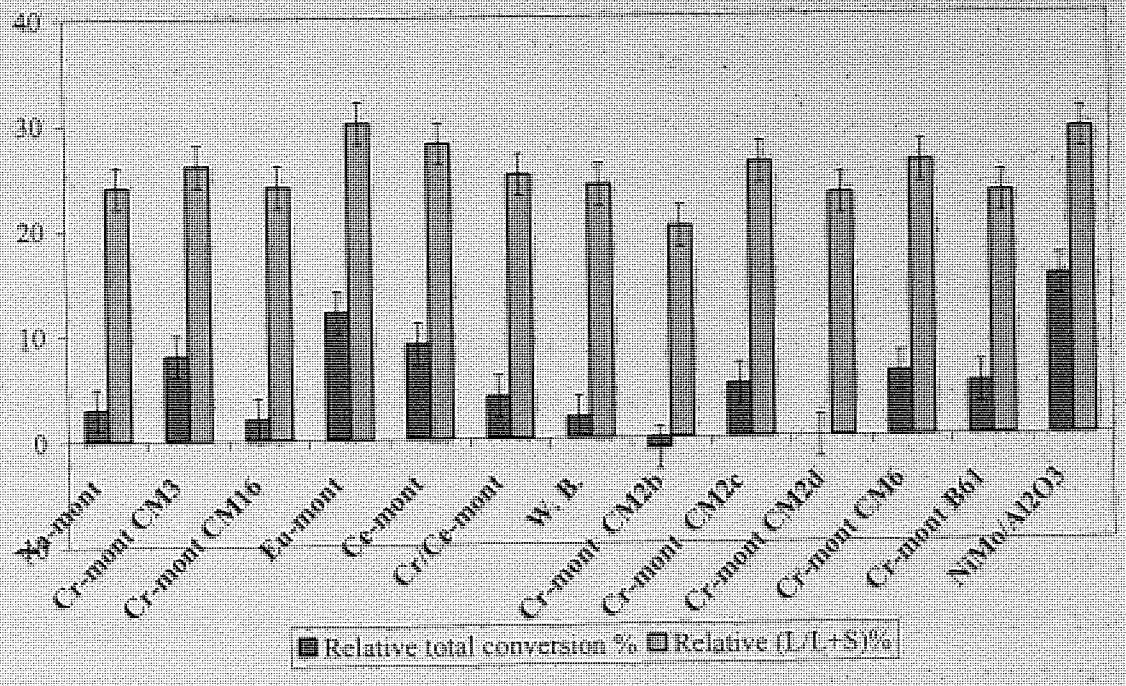

Figure 9.4 Relative conversions for the first series of hydrocracking runs with sodium montmorillonite, Wyoming Bentonite and their pillared derivatives as catalysts

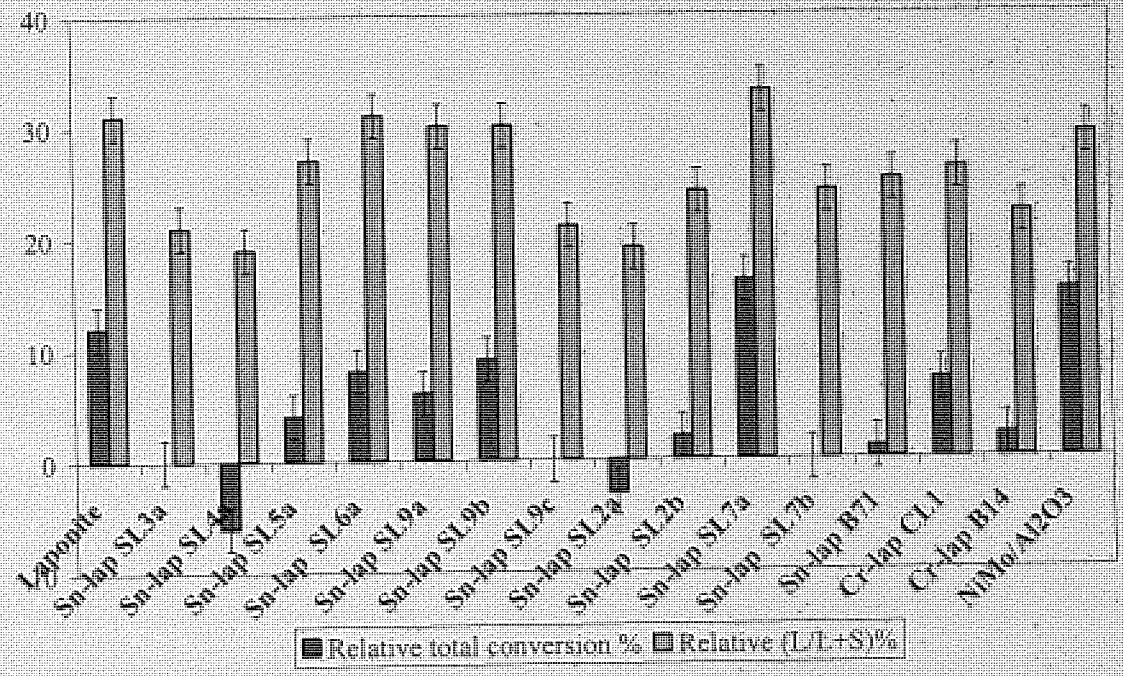

Figure 9.5 Relative conversions for the first series of hydrocracking runs with laponite and its pillared derivatives as catalysts

9.1.2 Second series of hydrocracking runs

The second series of hydrocracking runs was conducted using fresh feed and a selection of the coated catalysts recovered from the first series, which consisted of the starting materials, some of the pillared clays and the reference catalyst. The comparison of the catalysts performance was based on the results from this series of runs.

A range of liquid conversions was obtained between 34 and 59%. The reference catalyst $NiMo/Al_2O_3$ exhibited the highest liquid conversion (59%) followed by the unpillared laponite (53%). Most of the other catalysts showed similar liquid conversions, taking into account the experimental error (±8%). Only three catalysts showed lower liquid conversion, the europium oxide pillared montmorillonite, the chromia pillared montmorillonite CM6 and the tin oxide pillared laponite SL2a (34 to 40%) (Figure 9.6). With regards to coke deposition, the tin oxide pillared laponite SL2a exhibited the lowest amount (3%) followed by the chromia pillared montmorillonite CM3 (4%), whereas SL7a showed an excessive amount (37%).

The tin oxide pillared laponite SL7a was the only catalyst that exhibited negative relative total conversion indicating no catalytic hydrocracking effect, whereas the reference catalyst $NiMo/Al_2O_3$ and the chromia pillared montmorillonite CM3 displayed the highest relative total conversion (24%). When the conversion factor [L/(L+S)]% was taken into account for the assessment of the catalysts the chromia pillared montmorillonite CM3 still remained on the top range displaying conversion of 53%, while the reference catalyst (40%) fell in the same category with most of rest of the catalysts. The tin oxide pillared laponite SL2a was upgraded in the top range (Figure 9.7).

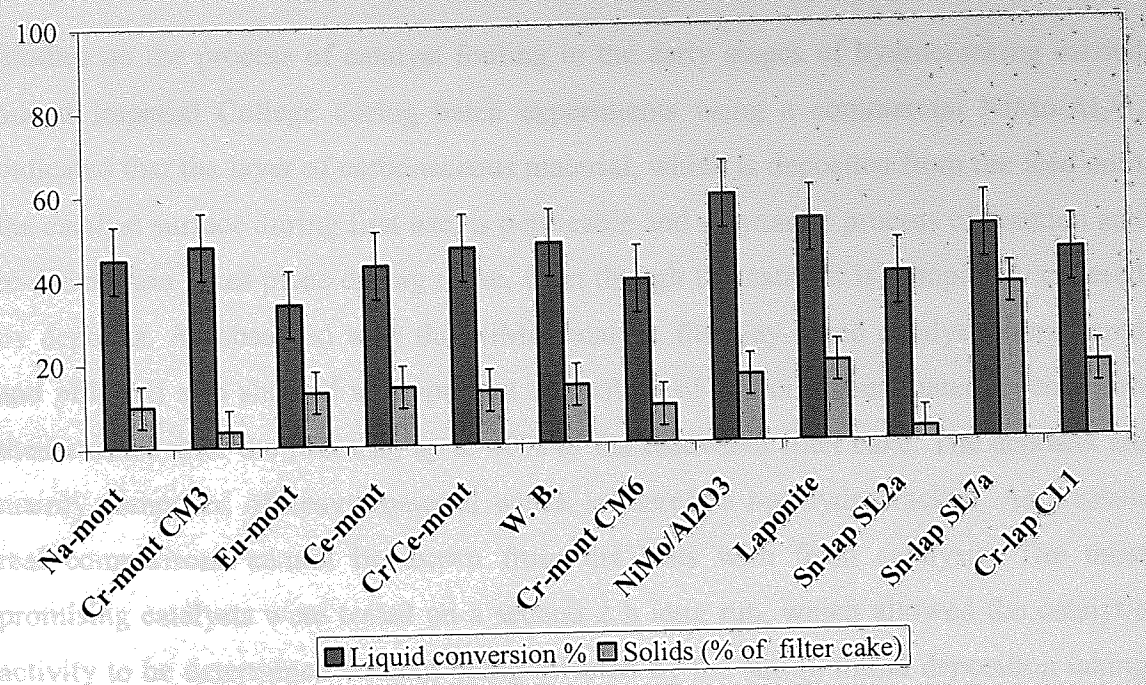

Figure 9.6 Liquid conversion and solids for the second series of hydrocracking runs

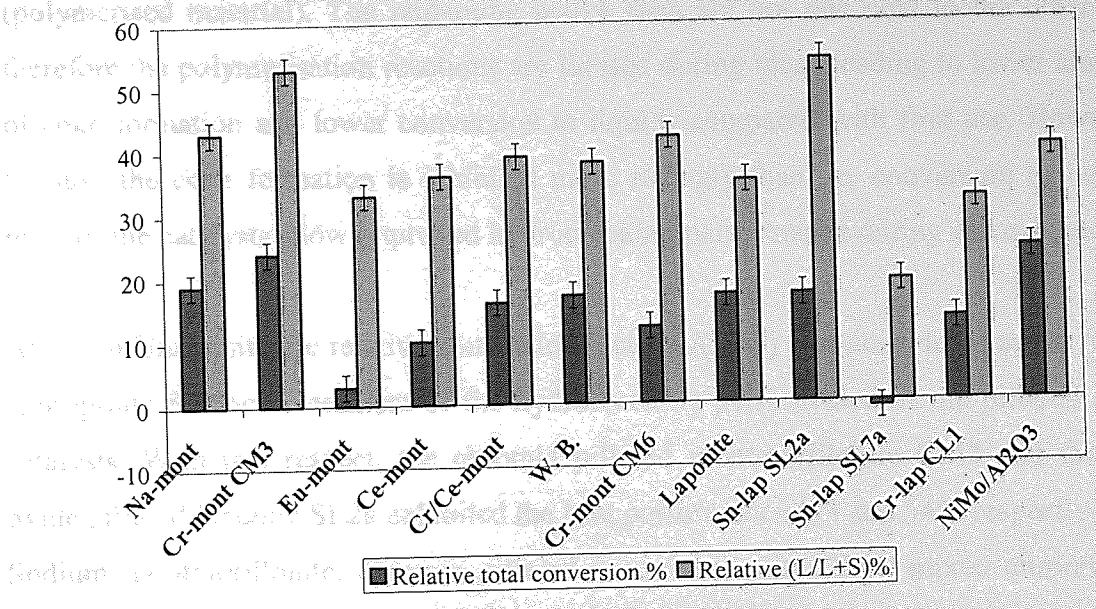

Figure 9.7 Relative conversions for the second series of hydrocracking runs

9.1.3 Discussion

Studies on the process of catalyst fouling in the early stages of hydrocracking carried out at Imperial College during batch experiments using a commercial $NiMo/Al_2O_3$ indicated that the layer of carbonaceous material, which is deposited from the feed onto the catalyst surface during first use, is permeable and a dynamic process of reaction and re-dissolution takes place during reuse, even though the catalyst is completely covered by deposits. As observed with the NiMo catalyst, the clay-based catalysts (unpillared and pillared) also showed an important deposition of carbonaceous material (coke) on their surface after the first use, up to 40% of the recovered filter cake. The deposits are mainly composed of heavy material which is therefore not hydrocracked. As a result real comparisons cannot be drawn from the tests with fresh catalysts. The most promising catalysts were tested on a second 2 h long run, which allowed the catalytic activity to be determined without being affected by the strong initial deposition taking place at the early stages of hydrocracking. During catalyst reuse, the new deposition was significantly lower and, thus, a more realistic assessment of catalyst activity was achieved [145].

It is assumed that during first use some of the catalysts' active sites are blocked by coke (polymerised material). The remaining active sites are not one next to the other and therefore the polymerisation reactions are limited during reuse leading to lower amount of coke formation and lower conversion to liquids compared with first use. However, because the coke formation is inhibited more strongly than the conversion to liquids most of the catalysts show improved hydrocracking performance during second use.

At Aston University the relative conversion factor L/(L+S) was considered as the most appropriate for the assessment of the hydrocracking performance of the pillared clay catalysts. With this respect, the chromia pillared montmorillonite CM3 and the tin oxide pillared laponite SL2a exhibited the best performance (53 and 54% respectively). Sodium montmorillonite, chromia pillared montmorillonite CM6, mixed chromium-cerium oxide pillared montmorillonite and Wyoming Bentonite as received displayed similar conversions with the reference catalyst $NiMo/Al_2O_3$ (40%), but slightly lower than the respective for CM3 and SL2a. However, the small amounts of catalyst and feed employed in the runs might have compromised the ability of the test programme

to provide definitive trends by increasing the experimental error. Moreover, some information on heteroatom removal (by elemental analysis) in the products would have resulted in a better assessment of catalytic performance.

The situation between the tin oxide pillared laponites SL2a and SL7a was completely reversed between first and second use. They both exhibited very high deposition of carbonaceous materials (coke) indicating the removal of the fraction boiling above 450°C as insoluble products and deposits on the catalyst and no relevant hydrocracking activity during either first or second use. The minor differences in the preparation method and the resulting intercalated tin content between the two catalysts cannot account for the totally different catalytic performance observed. Therefore, the real effectiveness of SL2a should be questioned. Given more research time, repeated experiments would have been carried out.

The intercalation of chromium in the clay clearly increased conversion, although the increase was not proportional to the increase in chromium content or basal spacing, since the high chromium - high basal spacing montmorillonite (CM6) showed lower conversion than the low chromium - low basal spacing one (CM3). Increasing pillar density (higher chromium content) is expected to increase overall activity. However, high pillar density could reduce accessibility of the active sites and, therefore, reduce activity. The latter is in agreement with Pinnavaia et al. who attributed the greater activity exhibited by a chromia pillared montmorillonite with low chromium content compared to the respective activity of a chromia pillared montmorillonite with high chromium content in the dehydrogenation of cyclohexane to benzene to the higher degree of chromium's dispersion in the interlayer. Nevertheless, these chromia pillared montmorillonites both exhibited similar basal spacings [118].

No correlation was observed among the conversions achieved during first use and the structural properties of the catalysts, such as basal spacing, total pore volume and surface area, micropore volume and surface area, which were manipulated via pillaring (Figures 1 to 15 - Appendix 3). This indicates that the structural properties of the catalysts did not influence the conversions, possibly because under operating conditions the pillars had collapsed as indicated by XRD analysis conducted on the used catalysts (all catalysts showed similar basal spacings after use (15.5Å to 16Å)).

The collapsed pillars in those chromia pillared montmorillonites with initially high basal spacing (high chromium content) possibly reduced accessibility of the active sites and reduced activity regardless of the higher chromium content.

Even if the pillared structure was partially retained under hydrocracking conditions, there is another reason why it may not have affected conversion. The reason is that coal liquids are highly complex consisting of a wide range of molecular weights varying from a few hundreds to 100,000 daltons (MALDI analysis), leading to a significant proportion of these liquids being unable to enter the micropores induced by pillaring in order to reach the active sites (pillar related active sites).

Since the original clays showed high conversions when reused, even higher than the respective conversions for cerium and europium oxide pillared montmorillonites, it is presumed that the clay's Bronsted acid sites are mainly responsible for the hydrocracking activity. However, the high activity of sodium montmorillonite and Wyoming Bentonite contradict the lack of catalytic activity for sodium montmorillonite or monoionic cerium montmorillonite in contrast to cerium oxide pillared montmorillonite in n-heptane reaction reported by Hernando et al. [35]. These authors suggested that cerium needs to be in the form of cerium oxide to be active and that the introduction of cerium in an alumina pillared clay increases the Bronsted / (Bronsted + Lewis) ratio via increasing the number and/or the strength of the Bronsted acid sites and leads to a shift in the selectivity towards cracking [35].However, the incorporation of cerium in the chromia pillared montmorillonite performed here did not affect its activity.

Initially it was hypothesised that the catalytic behaviour observed during second use is attributed to a change in the oxidation state of the pillaring species, which occurred during first use and was triggered by the hydrogen atmosphere in the microbomb reactor. Hence, the first run could be considered as a preparatory-activation step to convert the catalyst to its final form. However, this change in oxidation state did not have a favourable effect in the performance of the cerium and europium oxide pillared montmorillonites. Furthermore, this hypothesis could not explain the improved conversions observed for the original clays, since they did not contain any metal oxides whose oxidation state could be manipulated.

As mentioned in Chapter 2 (Literature and theory) during earlier work at Aston University and Imperial College chromia and alumina pillared montmorillonites, a tin oxide pillared laponite, layered double hydroxides based on polyoxo-vanadate and –molybdate, as well as a standard NiMo catalyst supported on alumina and a dispersed $Mo(CO)_6$ catalyst were compared in hydrocracking a coal extract for a short contact time of 10 min in the same microbomb reactor used for the current work (440°C, 190 bar of H_2), but in the presence of tetralin as a hydrogen donor solvent [2]. The chromia montmorillonite and the tin oxide pillared laponite outperformed all the other catalysts during the short runs and were further compared with the supported catalyst and the dispersed catalyst in the repeated hydrocracking of fresh coal extract over three sequential periods of 1h. In addition, they were compared with the supported catalyst and in the absence of a catalyst in hydrocracking of a petroleum distillation residue with 10 min and 2h reaction times [3]. The performances of both catalysts at short, long or repeated reaction times were better than that of the conventional NiMo catalyst for the hydrocracking of coal-derived materials and a petroleum residue in terms of conversions, molecular mass reduction, polynuclear aromatic ring system reduction, heteroatom removal and resistance to rapid deactivation [2, 3], which is in accordance with the current results. It should be noted that during this earlier study no hydrocracking runs were conducted with the parent clays as catalysts for comparison purposes.

Bodman suggested that the activity of chromia pillared montmorillonite is largely due to the redox activity of the intercalated polyoxochromia oligomer, which promotes reduction of the organic material in the presence of pressurised hydrogen, coupled with the further increased basal spacing which allows improved access to the active sites [4]. However, although the redox activity of the chromia pillars is in agreement with the current findings, the assumption that the increase in the basal spacing allows better access to the catalytic sites has been proven wrong because of the collapse of the pillars under hydrocracking conditions. Nevertheless, Bodman had not conducted XRD analysis on any of the used catalysts.

In the case of tin oxide pillared laponite, it was assumed again by Bodman that the catalytic activity was a result of better access to the active sites due to the delaminated nature of laponite, further enhanced by the presence of tin oxide, promoting the activity

of these sites [4]. The edge-to-edge and edge-to-face orientation of the laponite platelets is generating a "house of cards" structure containing macropores of a size typically found in amorphous aluminosilicates in addition to the micropores found in pillared clays. According to Occelli [28] relatively large size organic molecules, such as aromatic compounds, which are normally too large to enter the micropores formed by the pillars, can penetrate the macropores of the delaminated clays where the acidity introduced by the metal oxide clusters causes the conversion to occur. All these are in agreement with the high performance exhibited by the tin oxide pillared laponite SL2a, but do not justify the low performance displayed by SL7a. Unpillared laponite also displayed relatively good performance which is attributed to the better access to the clay's acid sites, since no metal oxides were intercalated introducing further acid sites.

Occelli also suggested that pillared laponites (delaminated) exhibit higher resistance to coke formation compared to pillared montmorillonites, probably due to the weaker acidity and the macroporosity of the catalyst which facilitate desorption of aromatics which otherwise would be retained (occluded) as coke [28]. However, the current findings do not show any significant difference between the amount of coke formed on the pillared montmorillonites and the pillared laponites (delaminated structure).

In conclusion, valid comparisons could not be drawn from the tests with fresh catalysts due to the rapid lay down of carbon. A more realistic assessment of catalytic activity was achieved during catalyst reuse, while the new carbon deposition was significantly lower. However, the small amounts of catalyst and feed employed in the runs might have compromised the ability of the test programme to provide definitive trends due to higher experimental error. It appears that the chromia pillared montmorillonite CM3 and the tin oxide pillared laponite SL2a exhibited slightly better performance (53 and 54% respectively) than the other catalysts. However, some information on heteroatom removal (by elemental analysis) in the processed feed would have improved the assessment of catalytic performance.

The intercalation of chromium in the form of chromia (Cr_2O_3) in the montmorillonite's interlayer clearly increased conversion attributed to the redox activity of the chromia pillar, although the increase was not proportional to the increase in chromium content or basal spacing. In the case of tin oxide pillared laponite, the catalytic activity might

be a result of better access to the acid sites due to the delaminated nature of laponite, whose activity is promoted by the presence of tin oxide. However, the structural properties of the catalysts which were manipulated via pillaring did not seem to have any effect on activity. The relatively good performance of all the parent clays is attributed to their acid sites, coupled with their macropores which are able to accommodate the clay liquids.

9.2 Hydrocracking conversion in the microwave reactor

A run with coal liquids (1g), a (4:1 v/v) mixture of chloroform and methanol as solvent and NiMo supported on alumina (250 mg) as catalyst was performed under argon (131 psig) in order to assure the safety of the system before the introduction of hydrogen, because of its high flammability. The exact experimental conditions are presented in Table 9.4. Chloroform/methanol was used as solvent, on the ground that the hydrocracking products would be sent to Imperial College for analysis and their products were collected in chloroform/methanol.

Approximately 19 min after irradiation began and while the temperature was 156°C (bulk temperature, see Section 3.4.2) and the pressure 153 psig, part of the tubing was blown off and the run was aborted. There was no liquid left in the reactor, just solid coal on the walls. All the solvent had evaporated. The low temperature achieved during the run is attributed to the low absorption of microwave energy by coal although the inorganics present in its ash content (5%) are receptive to microwave energy.

In an attempt to explain the failure of that run, a series of runs was performed with chloroform and/or methanol in sealed vials to study the behaviour of these solvents under microwave irradiation. During the chloroform/methanol runs significant pressure increase occurred quickly attributed to the evaporation of the solvent. During the chloroform run relatively higher temperature was achieved (182°C, bulk temperature) compared to the respective during the chloroform/methanol runs and the pressure build-up was lower as well. During the run with methanol the vial ruptured at 165°C (bulk temperature) and 227 psig. These conditions are below the operational limits of the vials (250°C bulk temperature, 300 psig). Therefore, the rupture is attributed to a microexplosion occurring in the vial caused by the very low flash point of methanol

(12°C). Presumably the same thing occurred during the run with coal. Hence, due to the required use of hydrogen during the hydrocracking run and in order to ensure safety, instead of a mixture of chloroform and methanol only chloroform was further used as a solvent for the coal extract.

Another series of runs was conducted with chloroform under argon to investigate the effect of microwave power in the final temperature and pressure. Maximum power (300 W) caused temperature and pressure fluctuations. However, it was necessary in order to achieve the relatively high temperature and pressure required for hydrocracking. Still the pressure increase was very small. During the chloroform run in a sealed vial a pressure increase of 94 psig was exhibited, attributed to the evaporation of chloroform. During the run under argon, the same pressure increase plus the increase attributed to argon's thermal expansion would have been expected. Since very low pressure increase was displayed and in one case the final pressure was lower than the initial pressure, it is clear that there was small leak in the system, allowing an amount of the solvent vapours and the pressurised argon to escape. Despite all the efforts undertaken this leak could not be eliminated, because the equipment was not originally designed for a gaseous reactant. However, a suitable system could be designed in the future.

Two more runs were performed with coal extract and chloroform at 160 and 190 psig argon (initial pressure) to assess the operation of the system before the introduction of hydrogen. Regardless of the leak a ca. 14 bar (200 psig) final pressure was attained. The low pressure employed was expected to hinder the system from achieving maximum conversion, although it could allow some mild hydrocracking to occur.

Table 9.4 Experimental conditions for the runs in the microwave reactor

Solvent	Feed	Catalyst	Head-space gas	Charged P (psig) at room T	Set T (°C)	Ramp t (min)	Hold t (min)	T_{final} (oC)	P_{final} (psig)	Power (W)	Comments
$CHCl_3$/MeOH	Coal	NiMo	Ar	131	200	10	30	156	153	200 to 300	Fitting failure at t=19.4 min
$CHCl_3$/MeOH	n/a	n/a	Air	0	200	10	5	150	114	250	
$CHCl_3$/MeOH	n/a	NiMo	Air	0	200	10	0	167	198	300	
$CHCl_3$	n/a	n/a	Air	0	200	10	22	182	94	300	
MeOH	n/a	n/a	Air	0	200	10	0	163	227	250	Ruptured vial at t= 4 min
Water	n/a	n/a	Ar	155	130	10	2	143	155	250	
$CHCl_3$	n/a	n/a	Ar	150	150	10	20	151	157	300	
$CHCl_3$	n/a	n/a	Ar	150	200	10	30	170	200	300	P, power fluctuations
$CHCl_3$	n/a	n/a	Ar	190	200	10	30	185	204	250 to 300	P, T fluctuations
$CHCl_3$	n/a	n/a	Ar	200	200	10	30	185	177	300	P, T fluctuations, $P_{final} < P_{initial}$
$CHCl_3$	n/a	n/a	Ar	207	200	10	5	191	206	300	P, T fluctuations
$CHCl_3$	Coal	n/a	Ar	196	200	10	30	152	199	300	Small P, T fluctuations at the start
$CHCl_3$	Coal	n/a	Ar	157	200	10	30	165	154	300	
$CHCl_3$	Coal	NiMo	H_2	165	200-185-190	10	30	187	201	300	

During the hydrocracking run the temperature increased faster compared to the run under argon, leading to rapid pressure increase. The temperature was then set to 185°C to stop any further pressure increase (pressure limit 250 psig). Due to the leak a slow pressure decrease was observed which was partially counteracted by setting the temperature at 190°C (Figure 9.8). After the run the system was depressurised and the products recovered and sent to Imperial College for analysis. The results are presented in Table 9.5.

Table 9.5 Conversion for $NiMo/Al_2O_3$ in the microwave reactor

Catalyst	Liquid conversion %	Solid (% of filter cake)	Total conversion %	[L/(L+S)]%
$NiMo/Al_2O_3$	70	62	-10	53

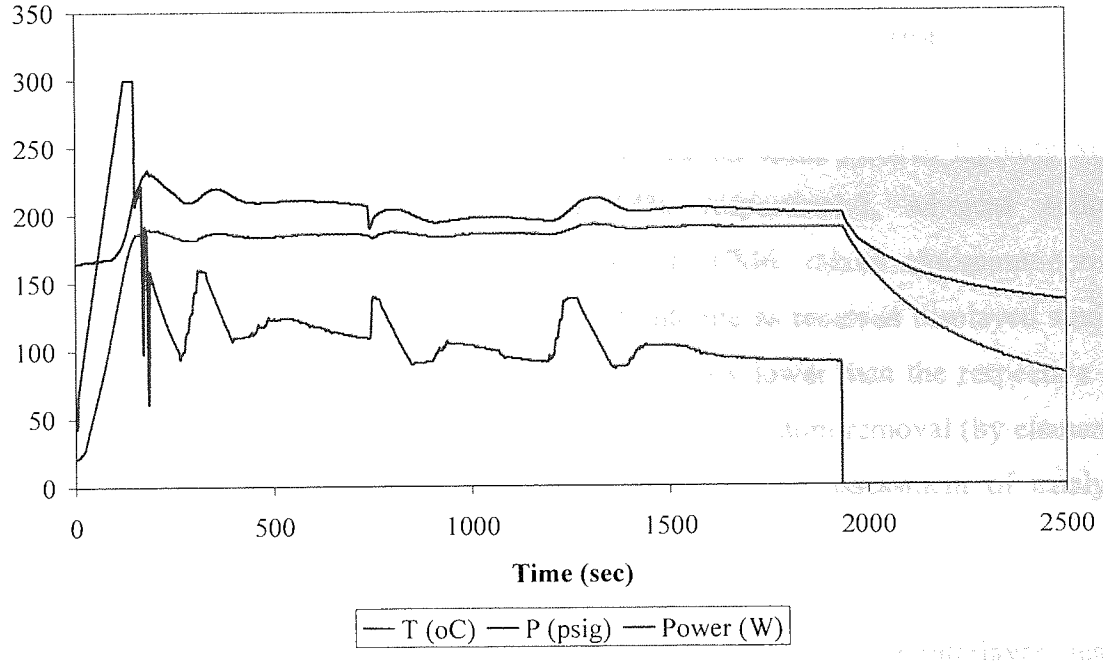

Figure 9.8 Temperature, pressure and power profiles during the hydrocracking run

It was thought that microwave irradiation could enable some hydrocracking to occur at milder conditions (temperature and pressure) than those conventionally used with more effective use of hydrogen leading to lower operating costs. However, in practice excessive coke deposition occurred leading to negative total conversion. Similar behaviour had been observed in runs in the microbomb reactor under helium instead of

hydrogen [146]. Apparently, the very low hydrogen pressure attained in the microwave reactor compromised its ability to achieve good hydrocracking conversion.

9.3 Summary

The performance of the pillared clay catalysts was mainly assessed in terms of their ability to hydrocrack the fraction of the feed with boiling points above 450°C and convert it into materials with lower boiling points. All the catalysts tested (original clays, pillared clays and NiMo on alumina) showed a significant deposition of carbonaceous material on their surface after the first use, and therefore valid comparisons with regards to their catalytic activities could not be drawn. These deposits are mainly composed of heavy material with boiling points above 450°C. The most promising catalysts were reused showing a significantly lower deposition leading to a more realistic assessment of catalytic activity. However, the small amounts of catalyst and feed employed in the runs might have compromised the ability of the test programme to provide definitive trends due to higher experimental error.

The chromia pillared montmorillonite CM3 and the tin oxide pillared laponite SL2a showed the best conversions (53 and 54% respectively), whereas sodium montmorillonite, chromia pillared montmorillonite CM6, mixed chromium-cerium oxide pillared montmorillonite and Wyoming Bentonite as received displayed similar conversions with the NiMo catalyst (40%), but slightly lower than the respective for CM3 and SL2a. Nevertheless, some information on heteroatom removal (by elemental analysis) in the processed feed would have improved the assessment of catalytic performance.

The intercalation of chromium in the form of chromia (Cr_2O_3) in the interlayer clearly increased conversion attributed to the redox activity of the chromia pillar. However this increase was not proportional to the increase in chromium content or basal spacing. In the case of tin oxide pillared laponite, the catalytic activity might be a result of better access to the acid sites due to the delaminated nature of laponite, whose activity is promoted by the presence of tin oxide.

The manipulation of the structural properties of the catalysts via pillaring did not seem to have any effect on the catalysts' activity. This is probably due to the collapse of the pillars under hydrocracking conditions. The relatively good performance of all the parent clays is attributed to their acid sites, coupled with their macropores which are able to accommodate the very high molecular mass clay derived liquids.

A microwave reactor operating at moderate conditions (13.8 bar and 190°C) was adapted for the hydrocracking of coal derived liquids and tested with the conventional catalyst, NiMo on alumina. The concept was that microwave irradiation could enable conversion to occur at milder conditions than those conventionally used, coupled with a more effective use of hydrogen. The latter could lead to lower operating costs making the process cost effective. However, in practice excessive coke deposition took place leading to negative total conversion. It is thought that the very low hydrogen pressure attained in the microwave reactor compromised its ability to achieve good hydrocracking conversion even under microwave irradiation.

10 DECOMPOSITION OF BIO-OIL UNDER MICROWAVE IRRADIATION

This chapter studies the decomposition of bio-oil under microwave irradiation, aiming to identify the extent to which the properties of bio-oil change as a function of time, temperature, mode of heating, presence of char and catalyst. The change in bio-oil's properties was measured by means of visual observation (physical appearance), water content determination (Karl Fisher titration), molecular weight distribution (GPC) and functional groups composition (FTIR).

Bio-oil contains many reactive organic compounds that form higher molecular weight species during storage at ambient temperature. This phenomenon is known as ageing and is intensified with increasing temperature. As a result an increase in bio-oil's viscosity and a decrease in its volatility occur, which are both unfavourable for fuel applications [86]. Furthermore, like coal derived liquids and petroleum residues, bio-oil requires high temperatures and pressures in order to be upgraded to transport fuel and the conventional catalysts employed until now are rapidly deactivated and unable to handle its high water content (*ca.* 25% wt). Hence, any information on the effect of parameters such as temperature, time, char content etc. in the properties of bio-oil would be helpful for any potential end user.

10.1 Effect of temperature and hold time

A series of microwave runs was performed with bio-oil irradiated (with simultaneous cooling) at different temperatures (50, 75, 100, 125, 150 and 175°C) and hold times (0 and 30 min) in order to investigate the effect of these two factors on bio-oil's decomposition. Temperature, pressure and power were monitored throughout the runs and during the cooling down process. The temperature was measured via the infrared sensor as described in Section 3.4.2. The pressure was measured directly by a load-cell sensor and connector mounted to the reaction vessel located in the instrument cavity and plugged into the rear of the instrument. The pressure at the end of the run (Pfinal) and the pressure after cooling down to ambient temperature (Pambient) were recorded. The conditions are presented in Table 10.1.

Furthermore, it was aimed to investigate whether microwave irradiation *per se* and not temperature played a role in bio-oil's decomposition. In this respect another series of

runs was performed with bio-oil heated conventionally at 50, 100, 125, 150 and 175°C for 30 min in a mineral oil bath (Table 10.2). However, in this case it was not possible to monitor the actual temperature or pressure, only the temperature of the mineral oil bath.

Table 10.1 Experimental conditions for the bio-oil runs conducted under microwave irradiation

Run No	Feed (g)	T (°C)	Power (W)	Hold time (min)	Pfinal (psig)	Pambient (psig)	Recovered product (g)	Unconverted bio-oil %
9	8.22	50	75	30	3			
17	8.04	50	75	30	4	3	8.04	100
18	8.03	75	100	30	8	3	8.02	99.9
3	8.85	100	200	30	20			
12	8.73	100	200	30	17			
19	8	100	200	30	24	13	7.99	99.9
35	8.24	100	200	18	17	8	8.22	99.8
13	8.18	125	200	30	39			
20	8.09	125	200	30	70	40	8.04	99.4
31	8.19	125	200	30	59	32	8.13	99.3
4	8.1	150	250	30	107			
14	8.74	150	200-250	30	122	60		
21	7.96	150	200-250	30	162	90	7.9	99.2
30	8.09	150	250	30	181	96	8.02	99.1
5	8.24	175	250	30	218			
16	7.4	175	250	30	224	140		
36	6.1	175	250	30	258	158	5.95	97.5
38	6.02	175	250	30	231	136	5.89	97.8
29	7.99	175	250	10	288	139	7.87	98.5
32	8.09	150	250	10	123	62	8.04	99.4
33	8.01	150	250	20	134	74	7.94	99.1
34	8.09	150	250	40	174	93	8.02	99.1
22	7.97	50	75	0	3	2	7.97	100
23	7.99	75	100	0	6	2	7.99	100
24	7.94	100	200	0	18	3	7.94	100
25	8.07	125	200	0	41	8	8.05	99.8
26	7.99	150	250	0	98	20	7.97	99.7
27	7.84	175	250	0	214	86	7.76	99.0
28	7.63	175	250	0	212	95	7.56	99.1
15	7.65	175	250	0	139	51		

Table 10.2 Experimental conditions for the bio-oil runs conducted under conventional heating

T (°C)	Bio-oil (g)	Recovered bio-oil	Unconverted bio-oil %
50	8.23	8.23	100
100	8	8	100
125	8.09	8.09	100
150	8	7.81	97.6
175	8.02	7.23	90.1

It was observed that the pressure profile in the microwave runs was not always reproducible. This was attributed to slight variations in the properties of the bio-oil employed in the runs due to ageing over the experimentation period. However, in general the pressure appeared to increase with heating (microwave or conventional) and decrease after cooling down at ambient temperature. It was assumed that pressure was generated via the evaporation of water contained in the bio-oil in addition to the production of gases as a result of bio-oil decomposition reactions due to heating. The decrease in pressure after cooling down at ambient temperature was attributed to the condensation of the water vapours reducing the amount of gases generating pressure in the reaction vessel. This was also supported by means of visual observation. After the runs water droplets were observed on the walls of the reaction vessel. Therefore, the final pressure at ambient temperature is the one representing the production of permanent gases due to bio-oil decomposition and consequently used in this study.

As shown in Figure 10.1, there is a correlation between the temperature of the run and the final pressure at ambient temperature (after cooling down) for the 30 min hold time runs. The fit of the linear plot was improved when Run 17 (50°C, temperature of run too low to have an effect on bio-oil) and Run 14 (150°C, this run showed a different temperature curve compared to Runs 21 and 30 conducted at the same temperature) were not taken into consideration (Figure 10.2). A similar correlation was noticed between the temperature of the run and the final pressure at ambient temperature (after cooling down) for the zero hold time runs (Figure 10.3). Again, the fit of the linear plot was enhanced when Run 22 (50°C), Run 23 (75°C) (both temperatures were too low to have an effect at zero hold time) and Run 15 (175°C, this run showed a different P curve compared to Runs 27 and 28 conducted at the same temperature) were not taken into account (Figure 10.4).

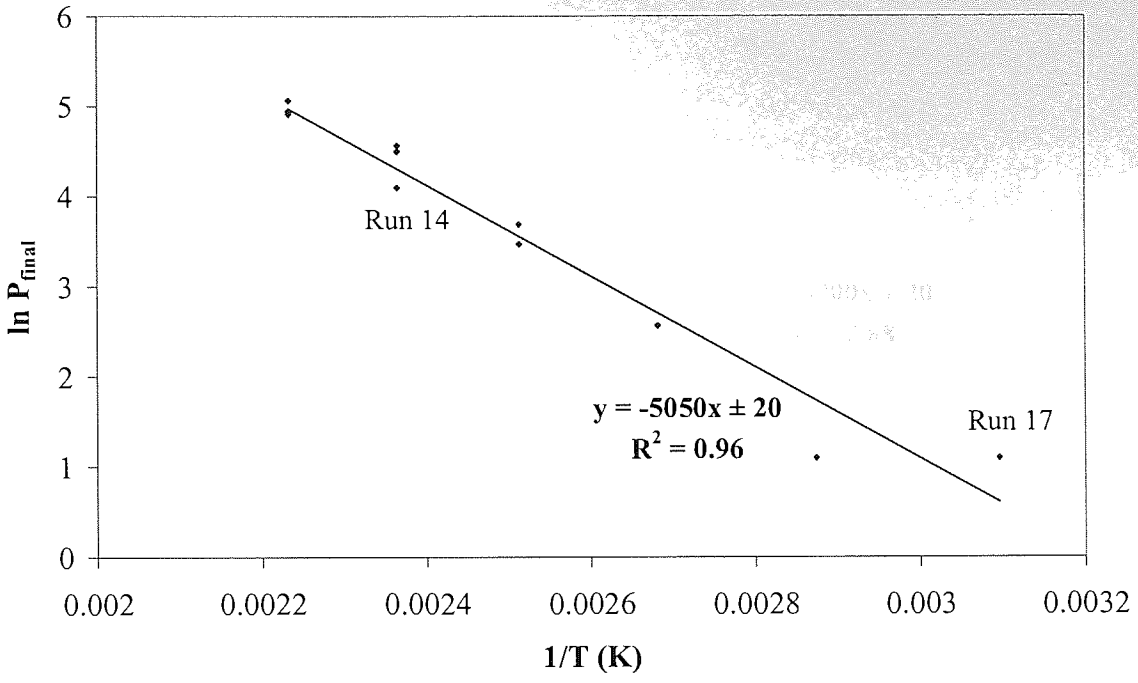

Figure 10.1 Plot of 1/T (K) versus $\ln P_{final}$ at ambient temperature for the 30 min hold time microwave runs (Runs 14, 17, 18, 19, 20, 31, 21, 30, 16, 36, 38)

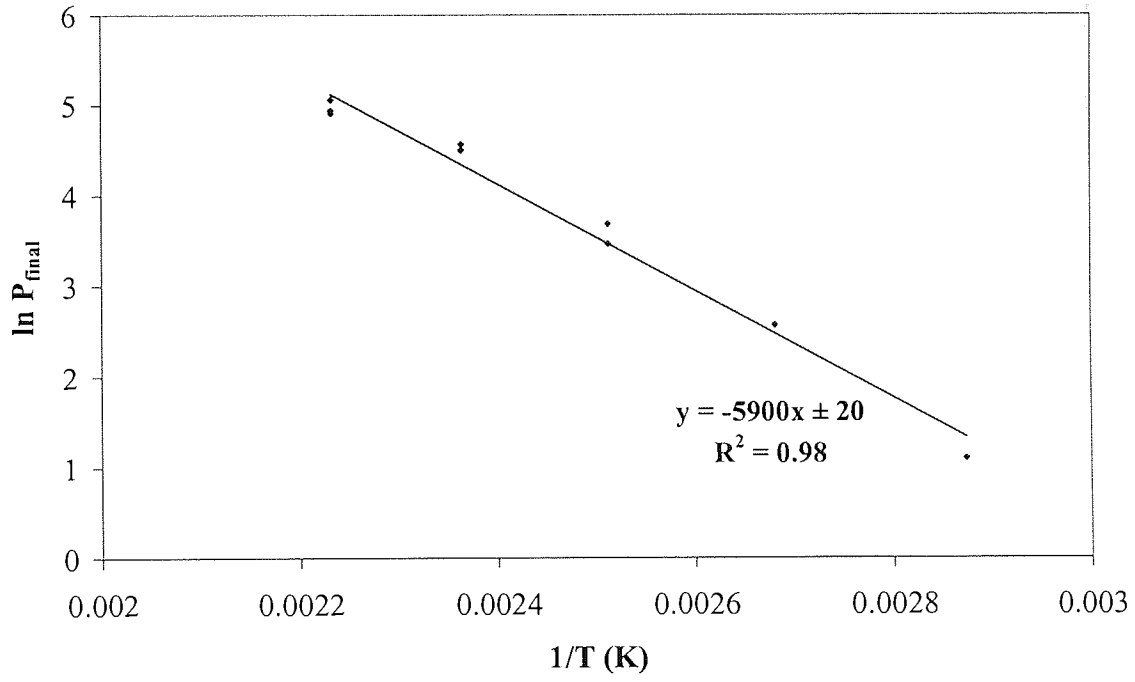

Figure 10.2 Plot of 1/T (K) versus $\ln P_{final}$ at ambient temperature for the 30 min hold time microwave runs (Runs 18, 19, 20, 31, 21, 30, 16, 36, 38)

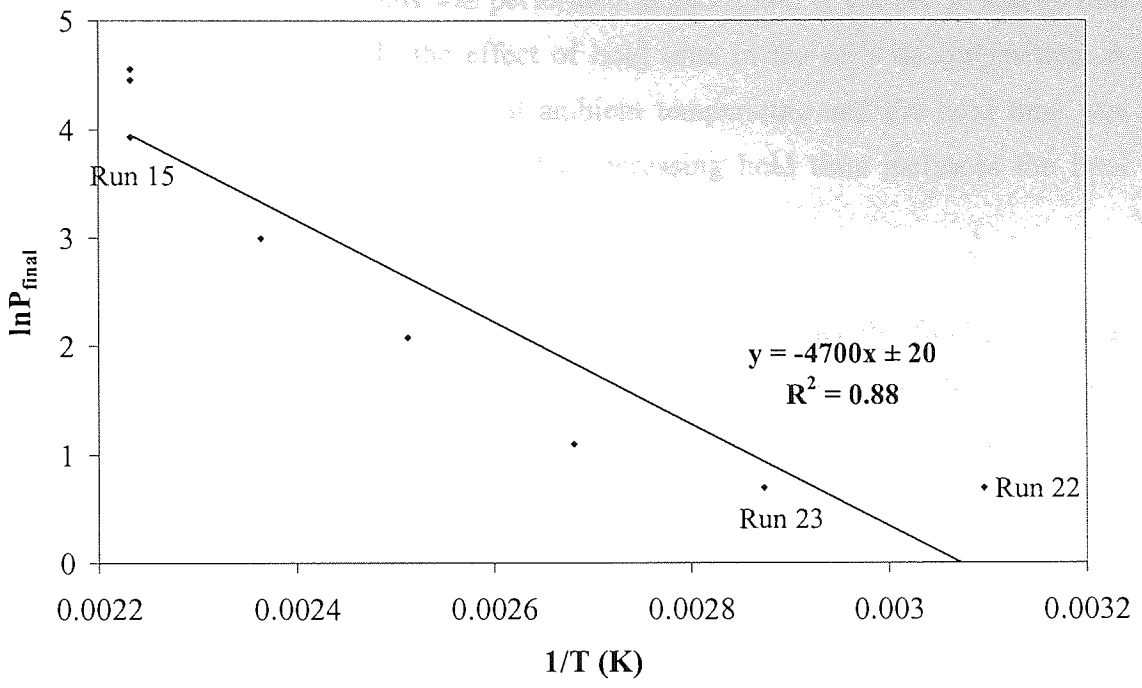

Figure 10.3 Plot of 1/T (K) versus lnP_{final} at ambient temperature for the microwave runs with zero hold time (Runs 22 to 28 and 15)

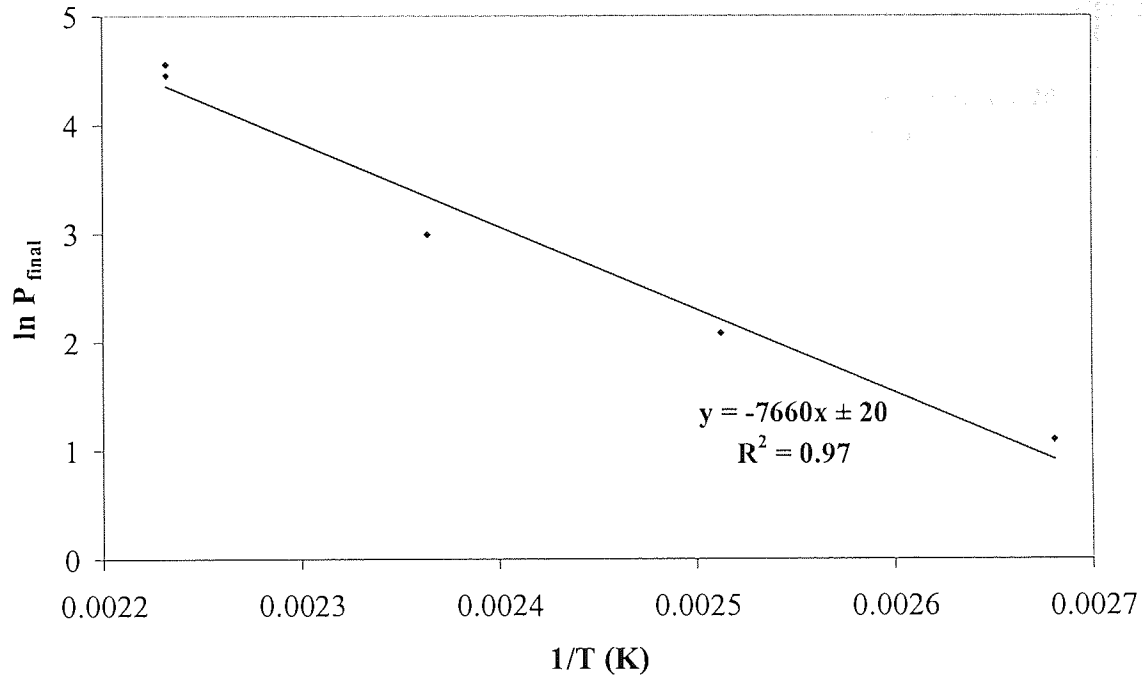

Figure 10.4 Plot of 1/T (K) versus lnP_{final} at ambient temperature for the microwave runs with zero hold time (Runs 24 to 28)

Another series of microwave runs was performed at 150°C and 0, 10, 20, 30 and 40 min hold time respectively to study the effect of hold time in bio-oil's decomposition. A correlation between the final pressure at ambient temperature and the hold time was derived from these runs. It was shown that increasing hold time increases the final pressure (Figure 10.5).

The percentage of unconverted bio-oil was plotted versus either the final pressure at ambient temperature (Figure 10.6 and Figure 10.7) or the temperature of the run (Figure 10.8 and Figure 10.9) for a hold time of 30 or 0 min respectively aiming to identify a relationship between these factors. No appropriate best fit line was identified for the data points in the graphs versus temperature. Given that the error bars in all these figures are relatively large, it can be assumed that the unconverted bio-oil remained nearly constant (*ca.* 100%) for the whole pressure and temperature range.

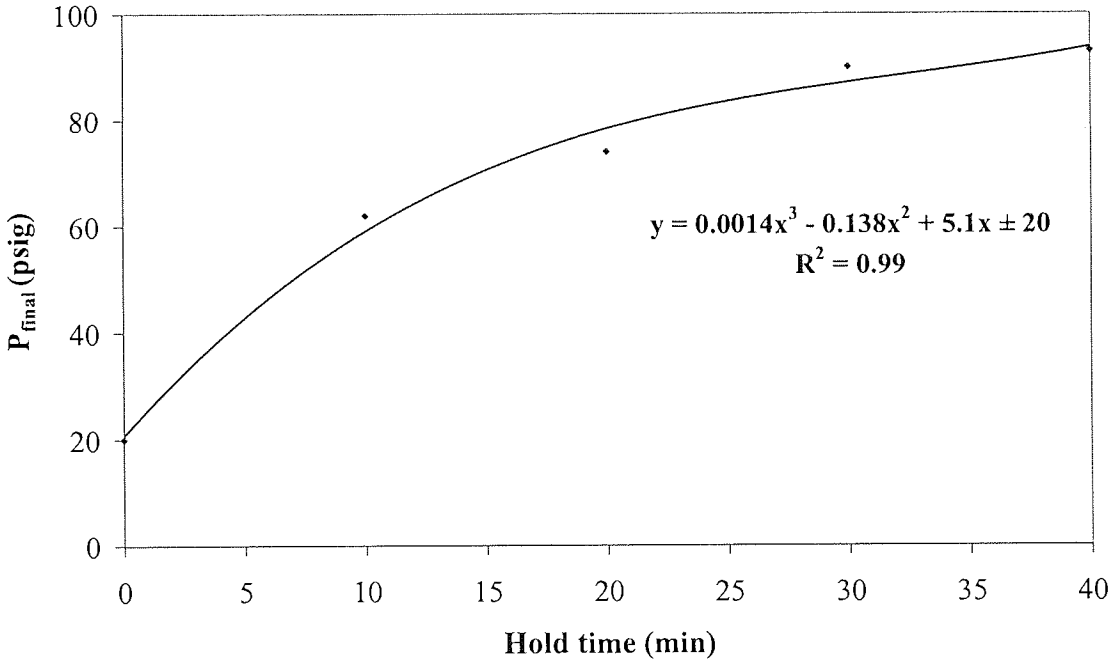

Figure 10.5 Plot of P_{final} at ambient temperature versus hold time for the runs performed at 150°C (Runs 32 to 34, 24 and 26)

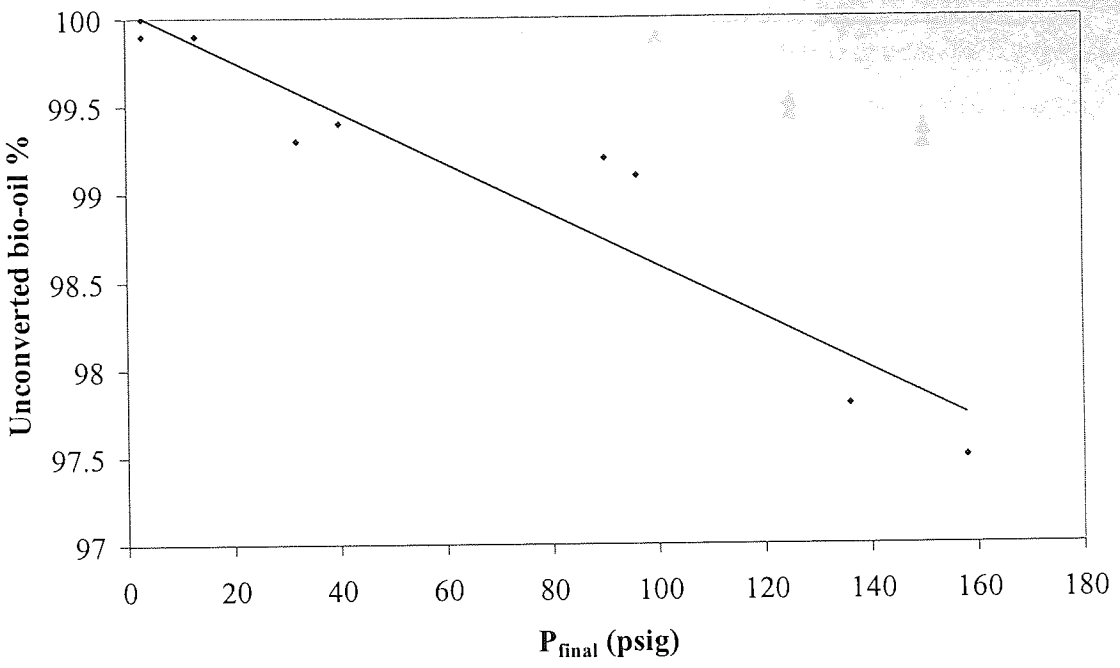

Figure 10.6 Plot of P_{final} at ambient temperature versus unconverted bio-oil % for the 30 min hold time runs (Runs 17 to 21, 30, 31, 36, 38)

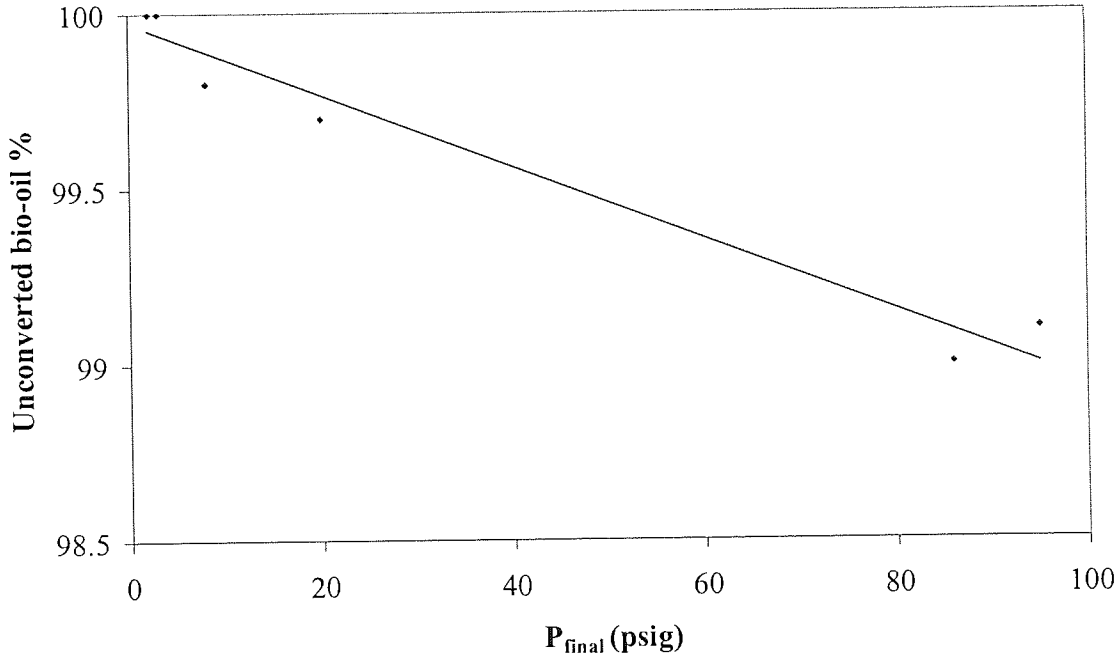

Figure 10.7 Plot of P_{final} at ambient temperature versus unconverted bio-oil % for the zero hold time runs (Runs 22 to 28)

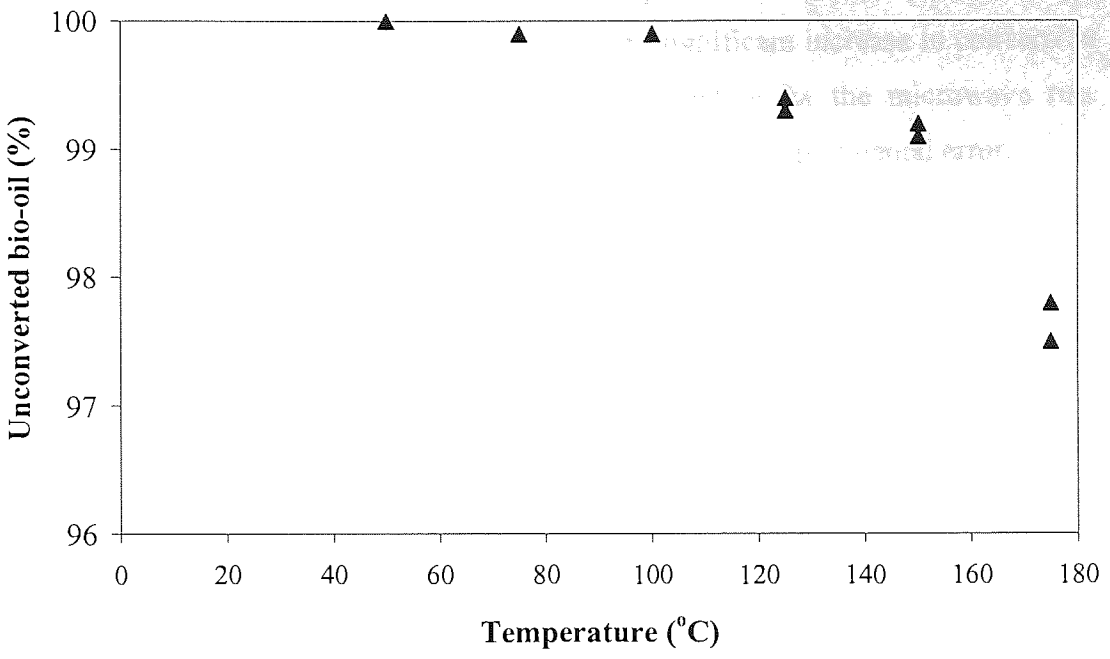

Figure 10.8 Plot of temperature of run versus unconverted bio-oil % for the 30 min hold time runs (Runs 17 to 21, 30, 31, 36, 38)

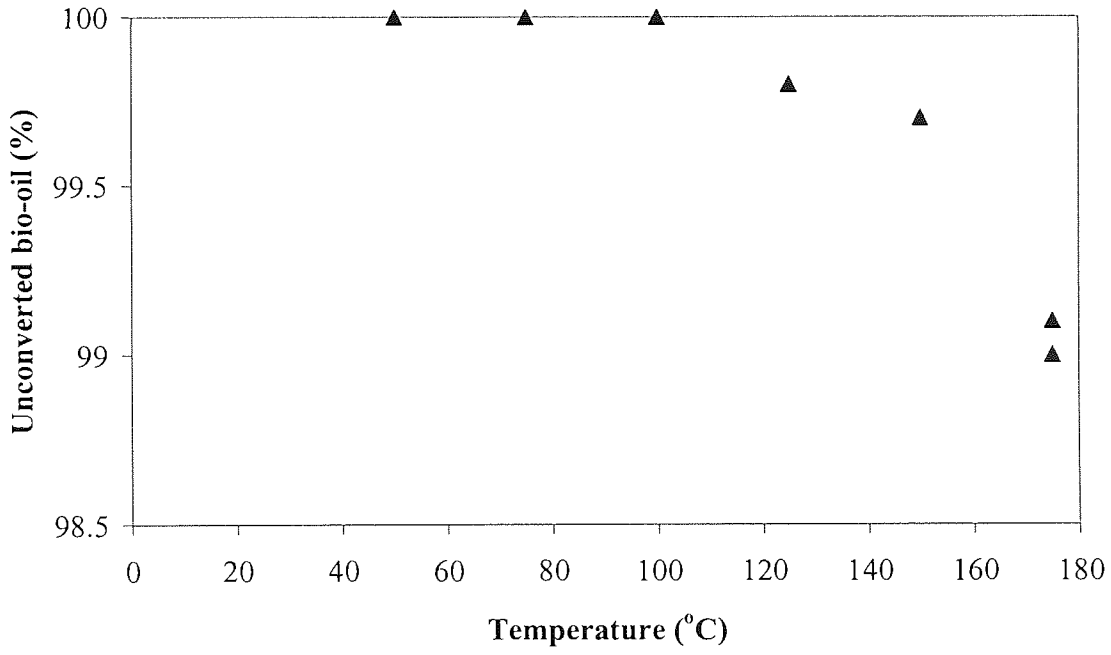

Figure 10.9 Plot of temperature of run versus unconverted bio-oil % for the zero hold time runs (Runs 22 to 28)

Comparison of the graphs of percentage of unconverted bio-oil versus the temperature of the runs between microwave and conventional runs (Figure 10.8 and Figure 10.10)

showed that the unconverted bio-oil remained nearly 100% for the temperature range 50 to 150°C in both cases. However at 175°C a more significant increase in conversion was observed for the conventional run than the respective for the microwave run. Nevertheless this difference was in the order of maginitude of experimental error.

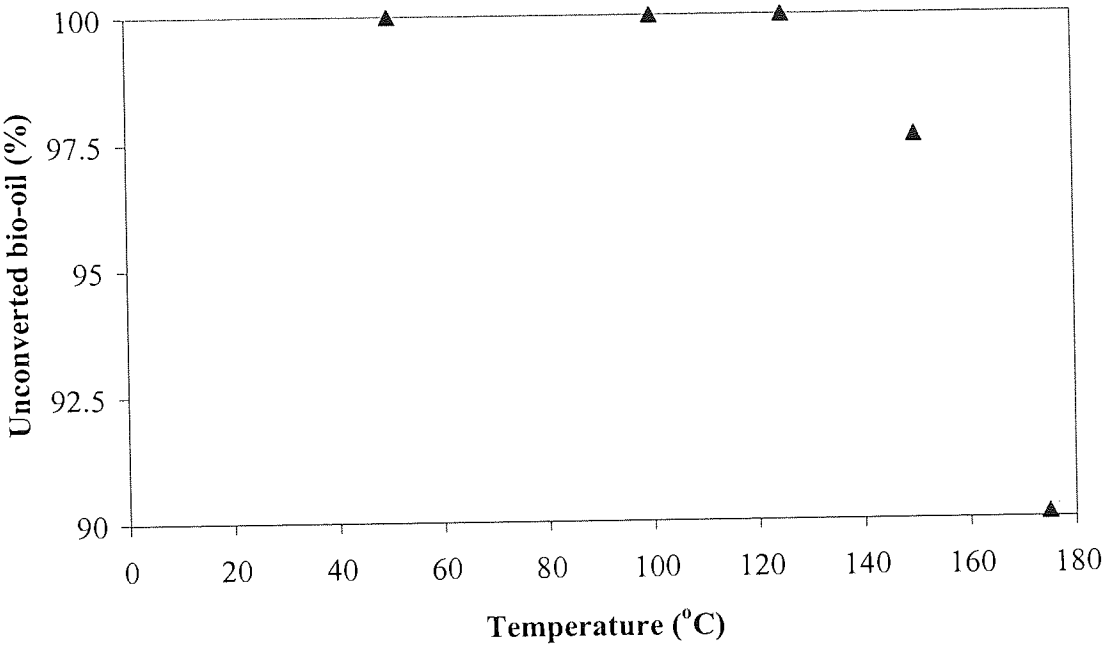

Figure 10.10 Plot of temperature of run versus unconverted bio-oil % for 30 min hold time conventional runs

10.1.1 Water content and physical appearance

Bio-oil samples from the 30 min hold time runs conducted under either microwave irradiation or conventional heating at 50, 100, 125, 150 and 175°C, as well as from the zero and 10 min hold time microwave runs at 175°C were analysed via Karl Fisher titration to determine their water content. The results, which are presented in Tables 10.3 and 10.4, were used to assess whether temperature, mode of heating (conventional or microwave) and hold time had any effect on bio-oil's water content. The original bio-oil used for all the runs was also analysed for comparison purposes. The standard deviation of the measurements is included in the tables as an error indicator. From these values a general standard deviation of *ca.* 0.5 may be deducted.

No significant differences were observed in the water content of bio-oil heated either under microwave irradiation or conventionally at the same temperature and hold time indicating no effect of the mode of heating. However, it was shown that the water content of bio-oil increased with increasing temperature and duration of heating (hold time) (Table 10.3 and Table 10.4), which is in accordance with Czernik et al. [86]. They conducted a study on the effect of storage conditions on the properties of an oak bio-oil exposed to elevated temperatures over extended periods of time. They reported a water content increase with the time and temperature of storage and attributed this increase to some condensation or dehydration reactions occurring in the bio-oil, especially when exposed to higher temperatures. On the other hand in a similar study conducted by Boucher et al. [147] on bio-oil obtained by vacuum pyrolysis (water content 5.3%) the water content measurements did not show any clear tendency that would allow any conclusions to be drawn on the water content variation.

Table 10.3 Water content of bio-oil after 30 min of conventional heating

T (°C)	Water content %
50	27.3 ± 0.7
100	27.8 ± 0.7
125	29.3 ± 0.7
150	29.8 ± 0.5
175	30.6 ± 0.6
Bio-oil as received	27.2 ± 0.2

Table 10.4 Water content of bio-oil after microwave irradiation

Run No	T (°C)	Power (W)	Hold time (min)	Water content %
9	50	75	30	27.2 ± 0.4
12	100	200	30	27.7 ± 0.3
13	125	200	30	29.0 ± 0.4
31	125	200	30	28.8 ± 0.4
4	150	250	30	28.5 ± 0.5
14	150	200-250	30	29.8 ± 0.5
30	150	250	30	31.7 ± 0.2
16	175	250	30	33.0 ± 0.5
38	175	250	30	34.4 ± 0.1
29	175	250	10	30.8 ± 0.4
28	175	250	0	29.1 ± 0.5
Bio-oil as received				27.2 ± 0.2

The mode of heating (microwave or conventional) did not appear to affect the physical appearance of bio-oil either, whereas the temperature and duration of heating (hold time) did. After each run water droplets appeared on the walls surrounding the head space of the vial. Each vial was shaken well before visual observation.

- Thirty minute runs (microwave or conventional) conducted at 50, 100 and 125°C did not cause any change in bio-oil's appearance. It remained one phase, free flowing liquid without any apparent increase in viscosity. However, the 30 min run conducted at 150°C caused phase separation in the bio-oil. It became thicker and consisted of a light fluid "watery" phase and a "tarry" sticky phase resembling paste and adhering on the vial's walls. The 30 min run conducted at 175°C led to further phase separation. The same two phases that were observed for the 150°C run appeared, plus another very dense phase stuck on the bottom of the vial.
- Zero hold time microwave runs conducted at 75, 100, 125 and 150°C did not alter the physical appearance of bio-oil (i.e. one phase free flowing liquid), while the respective run at 175°C caused bio-oil to separate into a light fluid phase and a viscous slow flowing phase.
- Ten and twenty minutes hold time microwave runs conducted at 150°C showed initiation of phase separation during the 10 min hold time run and total phase separation during the 20 min run.

From the observations mentioned above it can be concluded that increasing hold time had lowered the temperature at which phase separation occurred.

10.1.2 Gel permeation chromatography (GPC)

Duplicate bio-oil samples (for reproducibility purposes) from the 30 min hold time runs under either microwave or conventional heating and the zero and 10 min hold time microwave runs at 175°C were prepared by dissolution in THF and subsequently analysed by GPC. The aim was to assess the effect of temperature, mode of heating and hold time on bio-oil's average molecular weight. Possible interactions through hydrogen bonding between the OH-groups in the bio-oil with the oxygen in THF should be taken into consideration [148]. However, in this case the phenomenon was irrelevant as all samples were treated under comparable conditions. Moreover, GPC yields 'apparent' or linear molecular weight, because all the results are relevant to the polystyrene standards (linear and not branched compounds) which were used for the

calibration of the column. Therefore, the molecular weight values presented in this thesis can not be regarded as absolute. A GPC report for the original bio-oil used in all the runs is presented in Appendix 4 as an example. All calculations were conducted using the Cirrus software.

The GPC results have been quoted to the nearest ten in Table 10.5. Up to 100°C there was no significant change in any of the expressions of average molecular weight. At 125°C a slight increase in the average molecular weight was observed without any apparent change in the physical appearance of the bio-oil. Upon shaking it remained one phase free flowing liquid. At higher temperatures the molecular weight increase observed was accompanied by phase separation, which originally led to irreproducible GPC results due to the difficulty to acquire representative samples (Run 4 and Run 5 in italics, Table 10.5). The recovered bio-oil was homogenised with the addition of THF before re-sampling and reanalysis exhibiting better reproducibility. In particular, the results from Run 4 after homogenisation were in agreement between them and with the results from Run 14. The same occurred with the results from Run 5. They were in a narrower range and slightly lower than the results from Run 16.

As shown in Table 10.5, all the expressions of average molecular weight, M_p, M_n, M_w and M_z, as well as polydispersity (PD), i.e. the ratio of M_w and M_n, which is a measure of the spread of the molecular masses, increased with increasing temperature and hold time. These results are in agreement with those reported by Boucher et al. [147] and Czernik et al. [86]. They all attributed the increase in the average molecular weight of the bio-oil with the time and temperature of storage to the intensification of the condensation and polymerisation reactions induced by its high content of reactive organic compounds.

The average molecular weight calculated for the conventional runs showed the same trend with the respective for the microwave runs (i.e. M_w increased with increasing T), but the actual changes in average molecular weight (ΔM_w) were lower. However, before attributing any differences to a "microwave" effect it should be noted that the lack of monitoring the actual bio-oil temperature during the conventional runs has introduced in the results a factor of uncertainty.

Table 10.5 Average molecular weight of bio-oil after microwave or conventional heating

Sample	Run No	Mp	Mn	Mw	Mz	PD
BTG bio-oil	N/A	230	360	610	1100	1.68
	N/A	220	360	600	1080	1.68
	N/A	230	350	590	1100	1.70
Microwave runs						
50°C, 30 min	9	220	370	620	1120	1.67
	9	220	370	610	1100	1.65
100°C, 30 min	3	220	360	620	1150	1.72
	3	230	360	630	1200	1.74
	12	220	360	620	1150	1.72
	12	220	360	620	1130	1.72
125°C, 30 min	13	220	390	680	1300	1.76
	13	220	390	680	1290	1.76
	31	230	350	670	1360	1.9
	63	220	380	660	1250	1.76
	63	220	380	670	1260	1.76
150°C, 30 min	*4*	*230*	*360*	*640*	*1330*	*1.80*
	4	*230*	*400*	*830*	*1800*	*2.08*
	4	230	430	840	1680	1.98
	4	230	430	850	1700	1.98
	14	220	400	810	1710	2.04
	14	220	400	810	1690	2.03
	30	230	360	740	1610	2.08
175°C, 0 min	15	230	380	700	1380	1.86
	15	220	380	720	1420	1.89
	28	240	370	810	1770	2.15
175°C, 10 min	29	240	380	940	2280	2.51
175°C, 30 min	*5*	*290*	*340*	*580*	*1290*	*1.73*
	5	*290*	*409*	*950*	*2200*	*2.33*
	5	280	450	1000	2060	2.21
	5	280	460	1050	2280	2.28
	5	280	470	1100	2450	2.33
	5	280	460	1050	2230	2.27
	16	280	450	1110	2480	2.48
	16	280	450	1180	2820	2.64
Conventional runs						
50°C, 30 min	N/A	220	340	570	1070	1.70
		230	340	580	1110	1.71
100°C, 30 min	N/A	230	340	570	1090	1.71
		230	340	580	1110	1.73
125°C, 30 min	N/A	230	350	630	1240	1.8
		230	350	630	1250	1.81
150°C, 30 min	N/A	240	380	840	1960	2.19
		240	380	830	1870	2.15
175°C, 30 min	N/A	240	380	870	2050	2.28
		240	390	880	2090	2.29

Overlays of the GPC curves obtained from the 30 min hold time runs under microwave or conventional heating are presented in Figure 10.11 and Figure 10.12 respectively. In case of the microwave runs the 175°C curve clearly shifted to lower retention times exhibiting a distribution of higher molecular weights, since there is an inverse relationship between retention time and molecular weight (Figure 10.11). The third peak at high retention time observed for the 50°C and 150°C curves belonged to an impurity and not bio-oil. In the conventional runs the 150°C and 175°C curves shifted slightly to lower retention times (Figure 10.12), but the change was not as significant as that in the microwave runs.

Overlays of the GPC curves obtained from the 0, 10 and 30 min hold time microwave runs at 175°C are shown in Figure 10.13. A clear shift to lower retention times is exhibited by the 30 min hold time curve. The proportion of low molecular weight material (high retention times) decreased while that of high molecular weight material (low retention times) increased. The increase in the amount of high molecular weight fraction resulted in an increase in the average molecular weight (M_w) of the bio-oil.

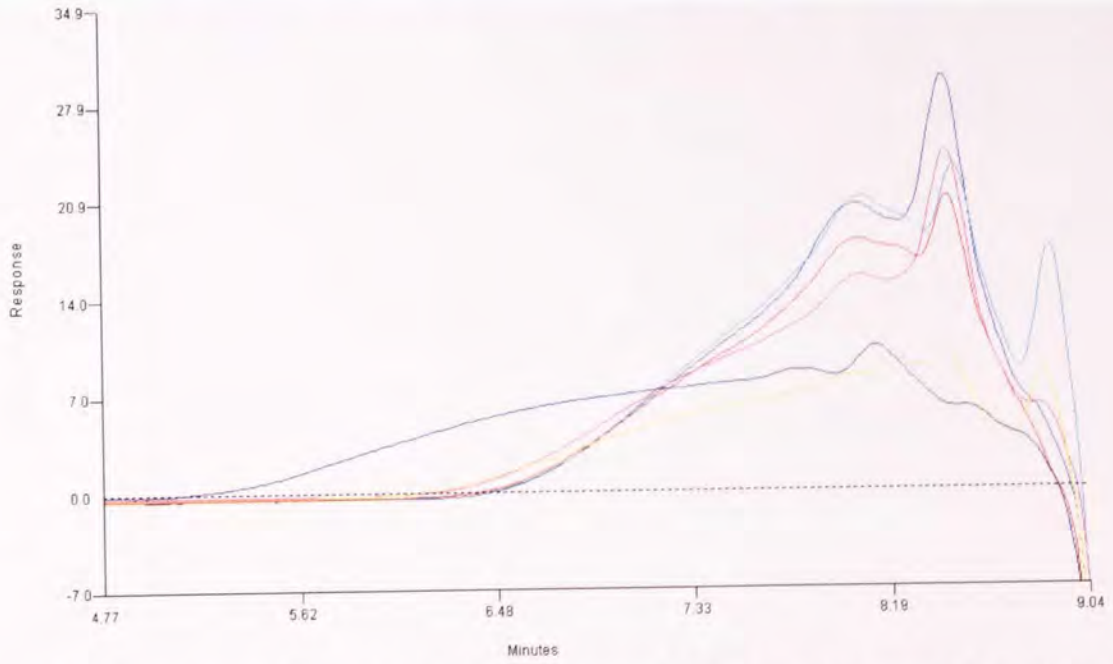

--- bio-oil (untreated), --- 50°C (Run 10), --- 100°C (Run 12), --- 125°C (Run 31), --- 150°C (Run 4), ---175°C (Run 16)

Figure 10.11 GPC curves for untreated bio-oil and bio-oil irradiated at 50, 100, 125, 150 and 175°C for 30 min

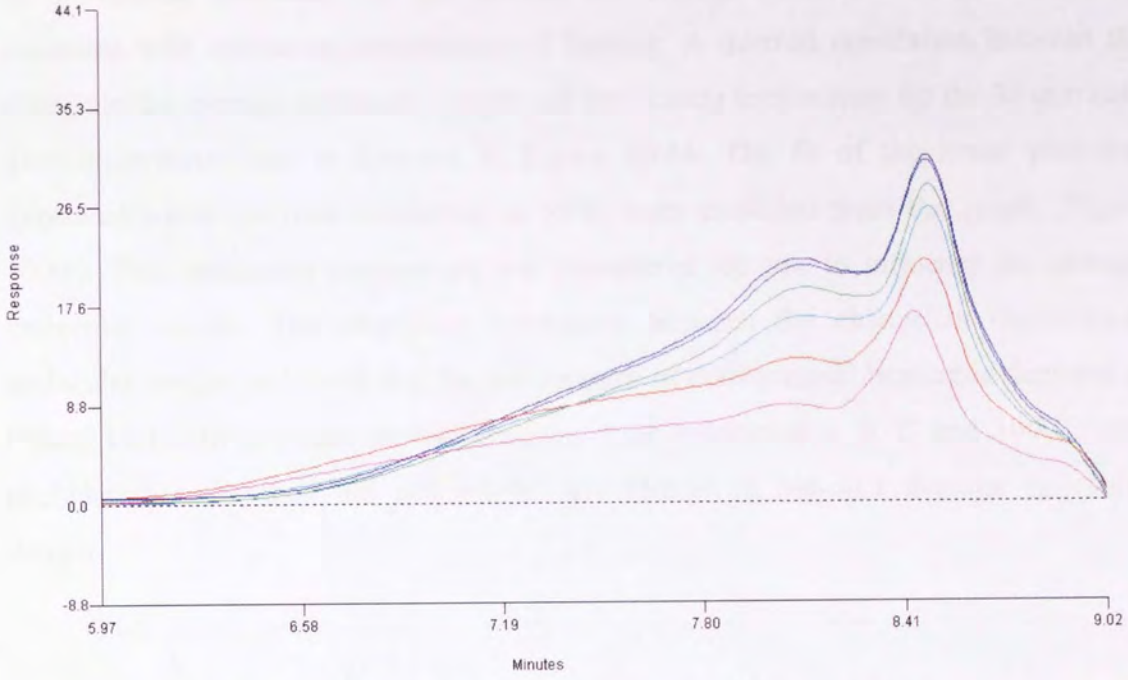

--- untreated bio-oil, --- 50°C, --- 100°C, --- 125°C, --- 150°C, --- 175°C

Figure 10.12 GPC curves for untreated bio-oil and bio-oil heated at 50, 100, 125, 150 and 175°C in a mineral-oil bath

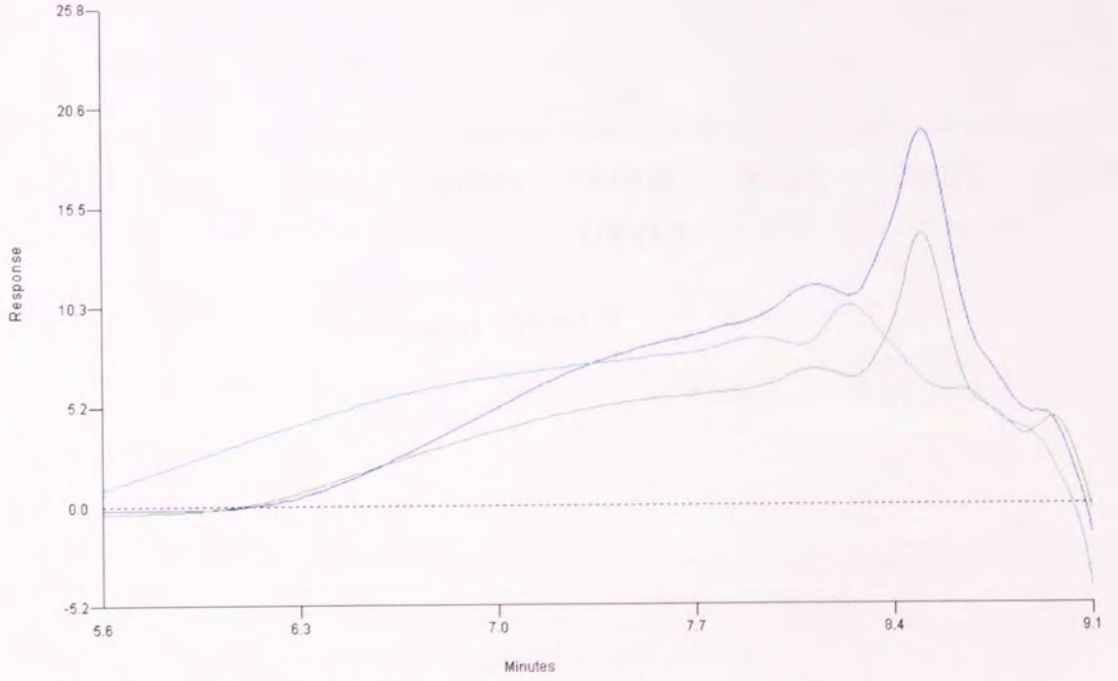

--- 0 min (Run 28), --- 10 min (run 29), --- 30 min (Run 16)

Figure 10.13 GPC curves for bio-oil irradiated at 175°C for 0, 10 and 30 min

As mentioned previously in this section the average molecular weight of bio-oil increased with increasing temperature of heating. A derived correlation between the change in the average molecular weight and the heating temperature for the 30 min hold time microwave runs is depicted in Figure 10.14. The fit of the linear plot was improved when the runs conducted at 50°C were excluded from the graph (Figure 10.15). This irradiation temperature was considered too low to influence the average molecular weight. The respective correlation between the change in the average molecular weight of bio-oil and the temperature of conventional heating is depicted in Figure 10.15. In this case the conventional runs conducted at 50°C and 100°C were excluded because they did not exhibit any change in bio-oil's average molecular weight.

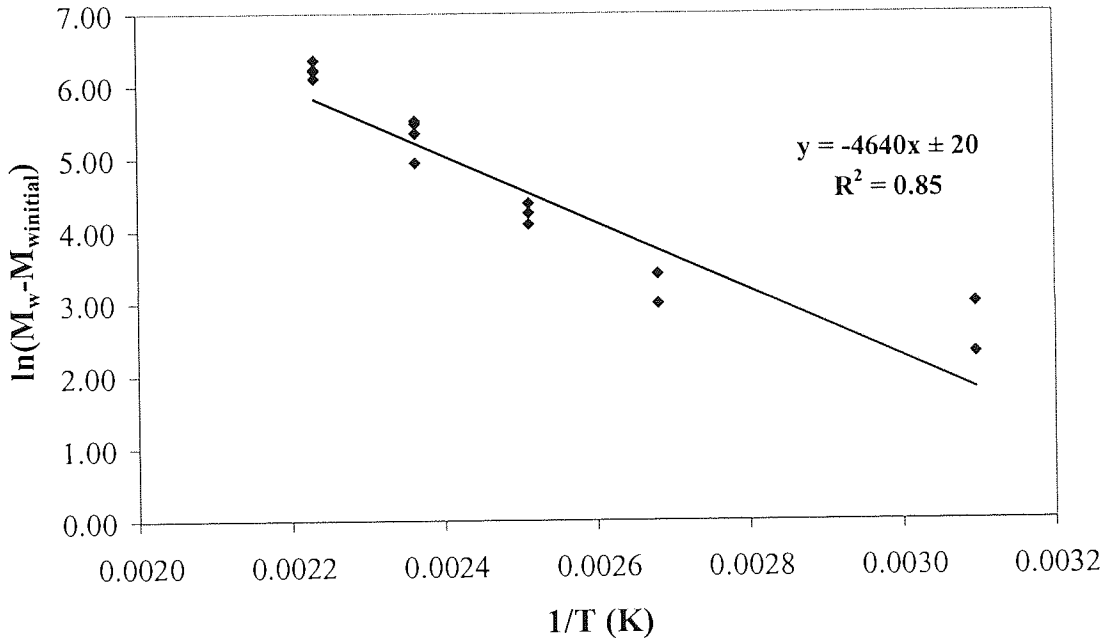

Figure 10.14 Plot of $\ln(M_w-M_{winitial})$ versus 1/T

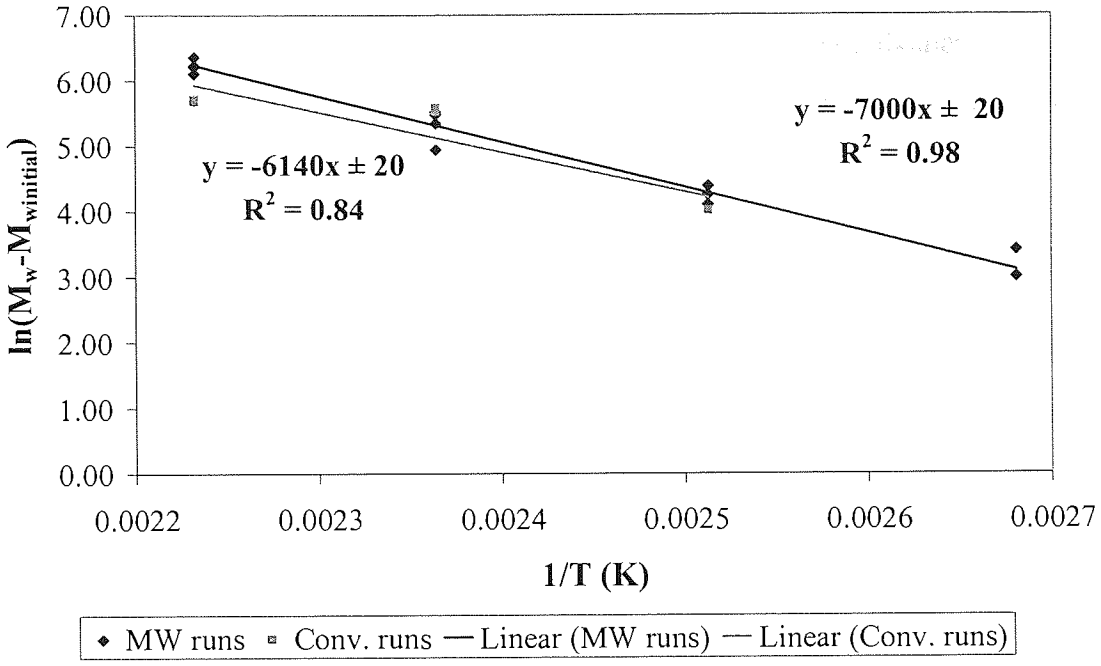

Figure 10.15 Plot of $\ln(M_w-M_{winitial})$ versus 1/T for microwave and conventional runs

10.1.3 FTIR spectroscopy

Bio-oil samples from the 30 min hold time runs (conventional or microwave) (Figure 10.16) and the zero and 10 min hold time microwave runs conducted at 175°C (Figure 10.17) were analysed by FTIR spectroscopy. The obtained spectra were compared on a qualitative basis, i.e. providing information on the presence or absence of specific functional groups, aiming to investigate the influence of temperature, mode of heating and hold time on bio-oil's functional group composition. Because the bio-oil samples contained THF in different amounts (due to homogenisation) a spectrum for THF was also collected for comparison purposes (Figure 10.18).

The following functional groups were identified in the bio-oil from the FTIR spectra in agreement with the literature [149, 150, 151].

- The O-H stretching band between 3650 and 3250 cm^{-1} indicates the presence of phenols and alcohols. The broad band shows the existence of hydrogen bonding and water. In the case of THF the sharp band at 3584 cm^{-1} indicates a compound containing non-hydrogen bonded hydroxy group, often an alcohol or phenol with a sterically hindered OH group.

- The C-H stretching vibrations between 3000 and 2800 cm^{-1} and C-H bending vibrations between 1475 and 1350 cm^{-1} point out the presence of alkanes.
- The C=O stretching vibrations between 1750 and 1650 cm^{-1} indicate a simple carbonyl compound such as a ketone or an aldehyde, which in combination with the O-H stretching shows an ester or a carboxylic acid.
- The C=C stretching at approximately 1650 cm^{-1} in combination with the C=O stretching indicates conjugation with a double bond (olefinic unsaturation).
- Bands above 1510 cm^{-1} result from carbonyl and aromatic skeletal vibrations.
- Below 1500 cm^{-1} all bands are complex and have their origin in a variety of vibrational modes. The bands between 1300 and 950 cm^{-1} are due to alcohols, phenols, ethers and esters showing the C-O stretching and O-H bending vibration. In particular for THF the band at 1070 cm^{-1} indicates a cyclic ether showing C-O stretching.
- Absorbance bands between 900 and 650 cm^{-1} are attributed to the presence of aromatic groups which in combination with the C=O and C-O stretching vibrations indicate the presence of aromatic esters.

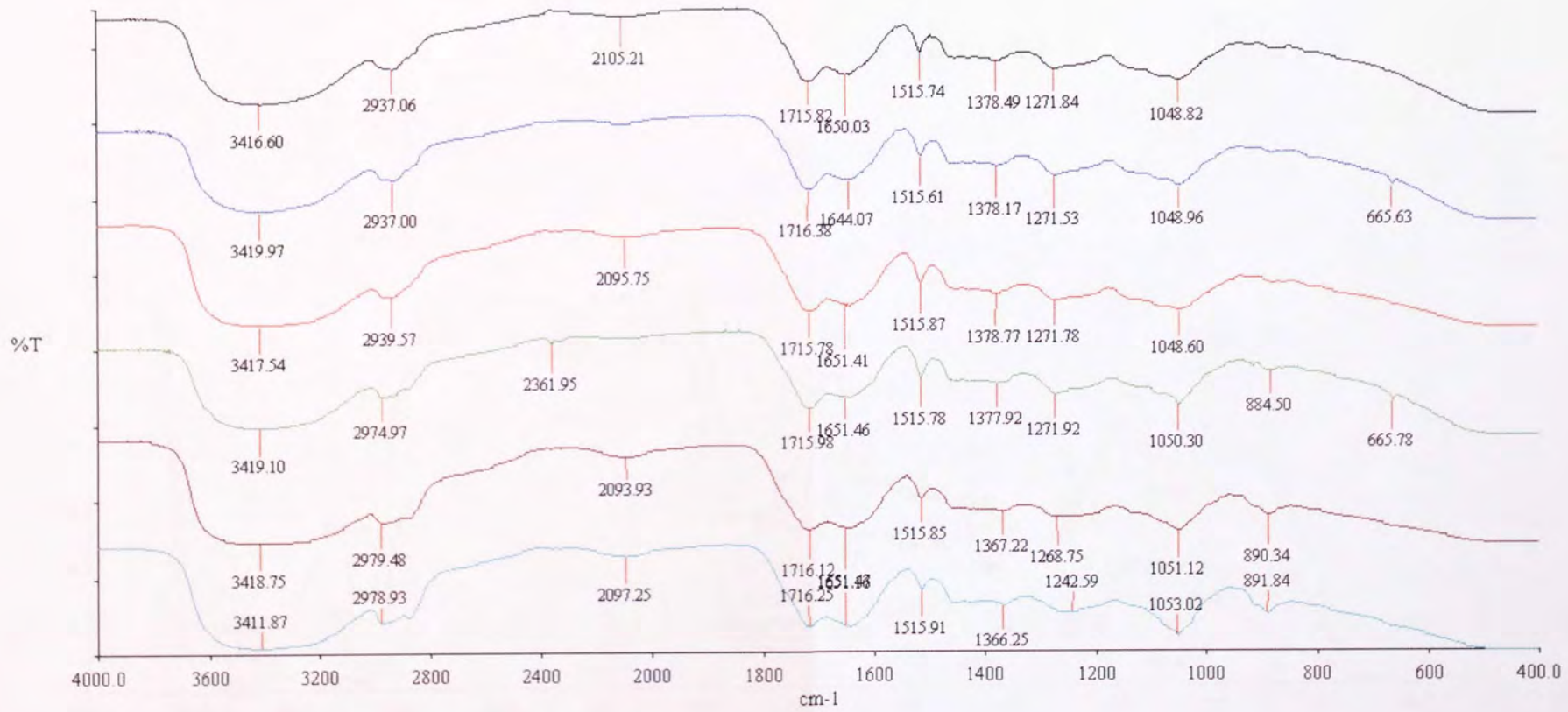

__ bio-oil untreated, ___ 50°C, ___ 100°C, ___ 125°C, ___ 150°C, ___ 175°C

Figure 10.16 FTIR spectra collected from bio-oil heated at 50, 100, 125, 150 and 175°C in a mineral oil bath

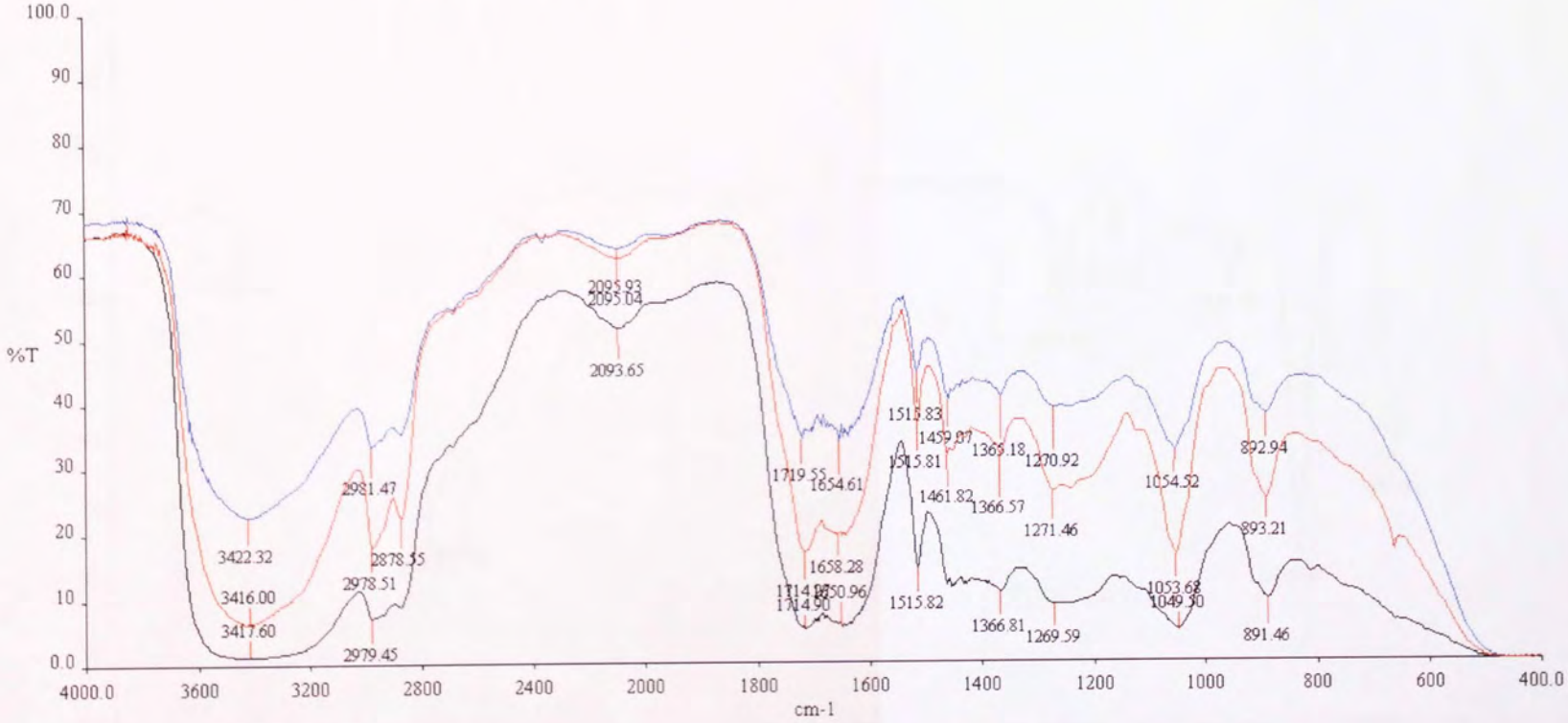

___ 0 min, ___ 10 min, ___ 30 min

Figure 10.17 FTIR spectra from bio-oil irradiated at 175°C for 0, 10 and 30 min hold time

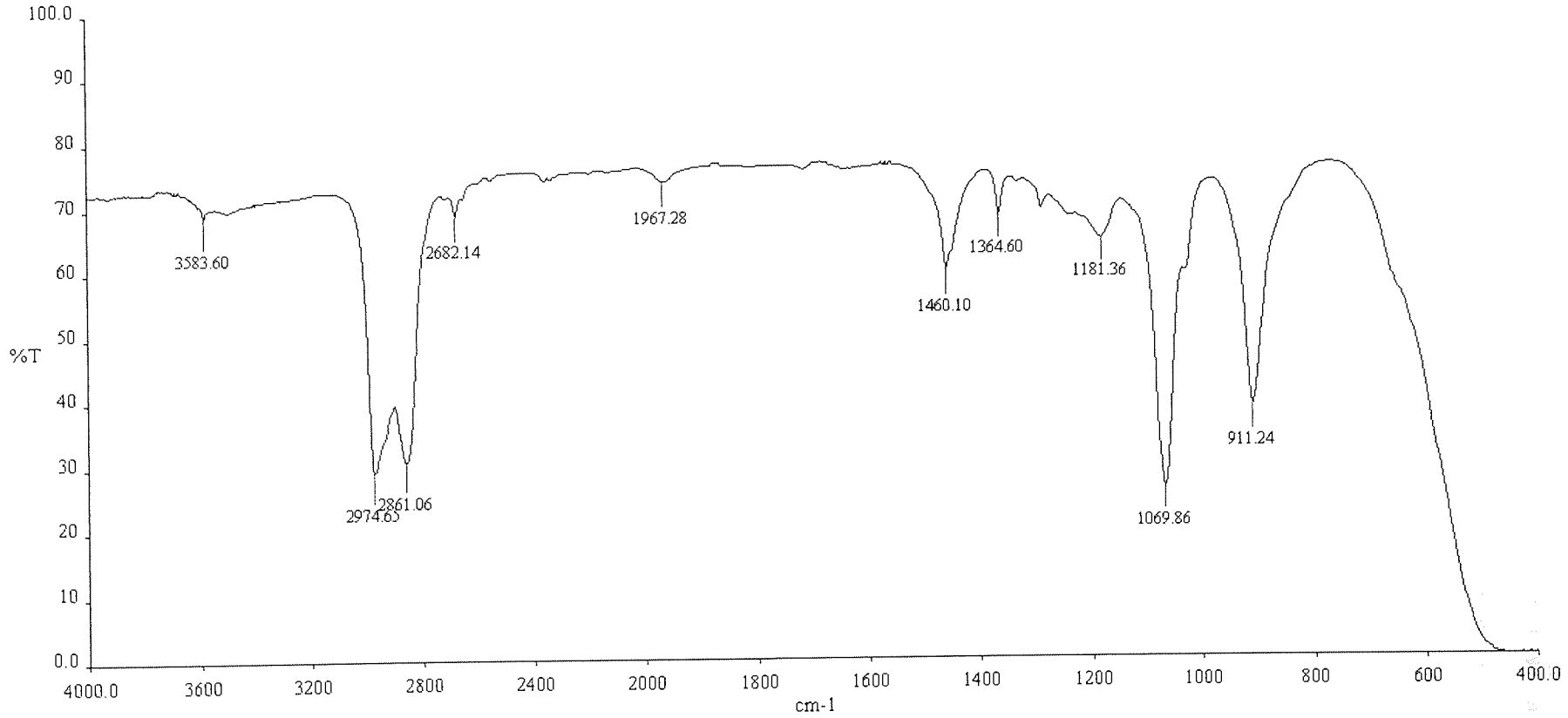

Figure 10.18 FTIR spectrum collected from THF

Comparison of the obtained FTIR spectra did not yield any functional group differences in the bio-oil that could be attributed to heating mode (microwave or conventional), temperature or hold time. However, it should be noted that it is extremely difficult to interpret the bio-oil spectra with complete certainty because they consist of a set of overlapping peaks, not separately resolved, due to the high complexity of the sample comprising of hundred different compounds.

10.1.4 Rate constants of bio-oil's decomposition

A correlation between the final pressure at ambient temperature and the hold time was derived from a series of runs conducted at 150°C showing that increasing hold time increases the final pressure (Figure 10.5).

The rate constant k of bio-oil's decomposition at 150°C was calculated from the data of final pressure and hold time assuming first order kinetics, since the unconverted bio-oil remained nearly constant (*ca.* 100%) for the whole pressure and temperature range:

$$(P_\infty - P) = (P_\infty - P_0)\, e^{-kt}$$

where P is the final pressure at ambient temperature after t hold time, P_0 is the final pressure after zero hold time (Run 26, 20 psig) and P_∞ is the final pressure after infinite hold time.

As shown in Figure 10.5 after 40 min hold time the final pressure reached 95 psig. A slightly higher value of 105 psig was given to P_∞. As a result:

$(P_\infty - P) = (P_\infty - P_0)\, e^{-kt} \rightarrow$

$(105 - P) = (105 - 20)\, e^{-kt}$

$-\ln [(105 - P)/85] = kt$

By fitting a linear plot on the data (Figure 10.19) the rate constant of bio-oil's decomposition at 150°C was calculated as the slope of the linear curve, i.e. k=0.05 min^{-1}.

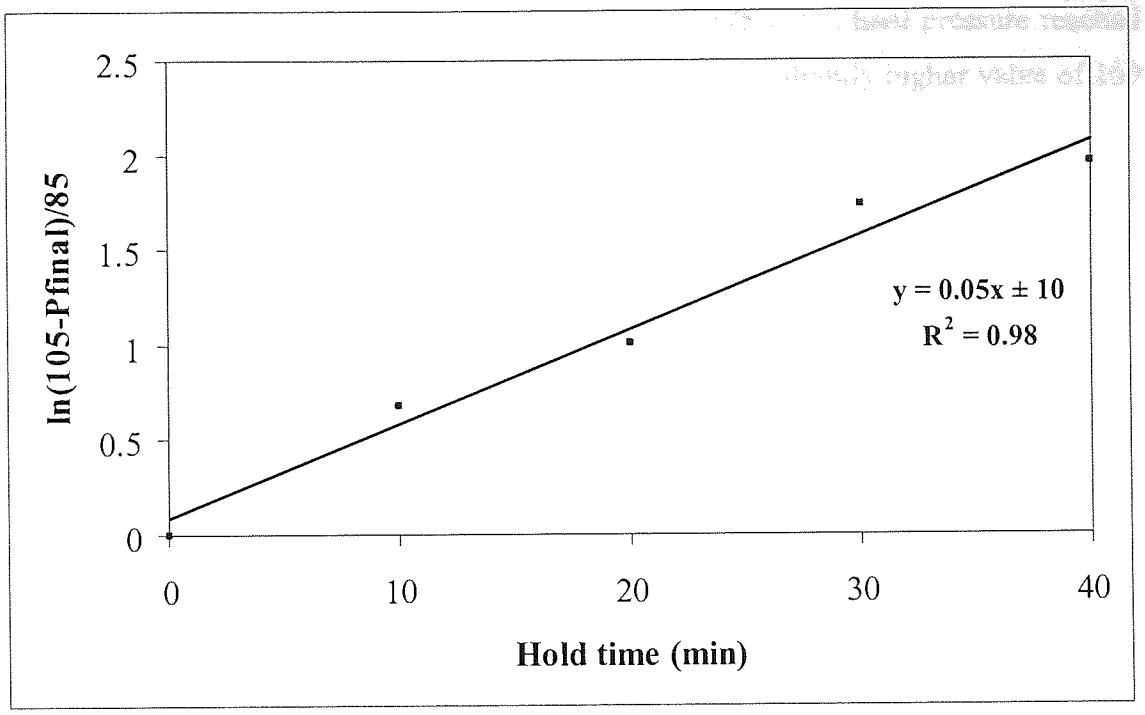

Figure 10.19 Rate constant of bio-oil's decomposition at 150°C under microwave irradiation

During the microwave runs it was observed that increasing hold time at a particular temperature leads to an increase in final pressure at ambient temperature, as well as in the average molecular weight and water content (%) of the treated bio-oil. Therefore it would have been worthwhile to determine the rate constant of bio-oil's decomposition based on both the increase of its average molecular weight and water content versus hold time and compare these values with the rate constant determined from the increase of final pressure. However no analysis was performed on the bio-oil treated at 150°C except for the 30 min hold time runs. In retrospection the treated bio-oil should have been analysed and the data used for the determination of the rate constant. Nevertheless, limited data on final pressure, average molecular weight and water content were available for the runs conducted at 175°C and 0, 10 and 30 min hold time and used for the determination of the rate constant at 175°C. Because only three data points were available, the determined rate constants at 175°C require validation via further experimentation and should be treated as no more than rough estimates of true values.

As shown in Figure 10.20 after 30 min hold time at 175°C the final pressure reached 145 psig (average value of P_{final} for runs 16, 36 and 38). A slightly higher value of 160 psig was specified to P_∞(P_∞ = 160psig)

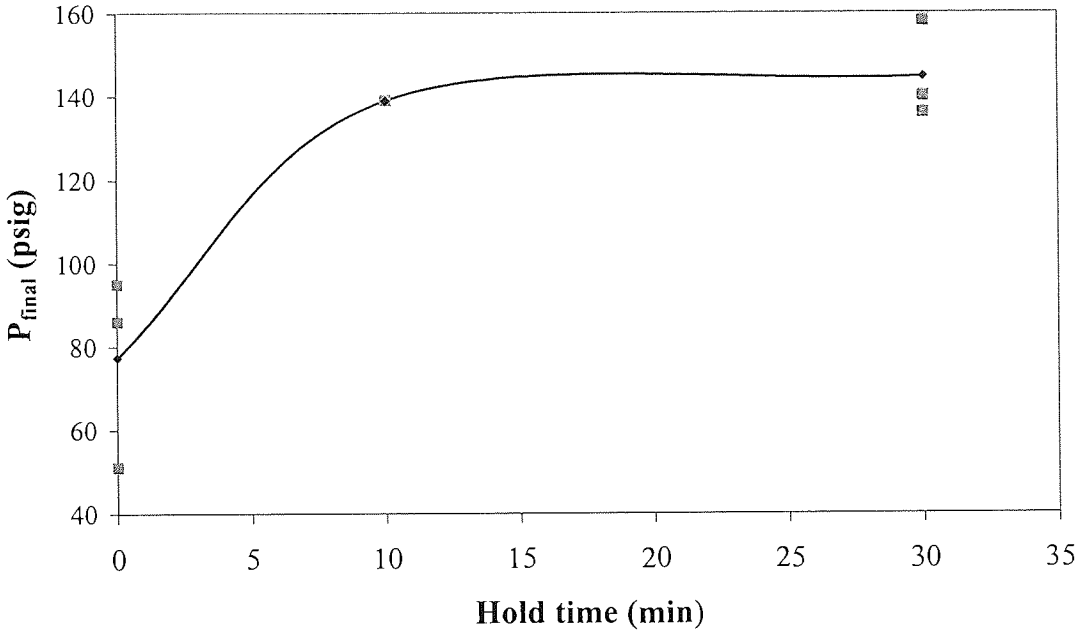

Figure 10.20 Plot of final pressure (P_{final}) at ambient temperature versus hold time for the runs performed at 175°C (Runs 15, 16, 27 to 29, 36, 38)

Similarly the average of the final pressure at ambient temperature for the 3 runs conducted at 175°C and zero hold time (runs 27, 28 and 15) was assigned to P_o.

Po = average (86, 95, 51) psig = 77 psig

Assuming first order kinetics:

$(P_\infty - P) = (P_\infty - P_o)\, e^{-kt} \rightarrow$

$(160 - P) = (160 - 77)\, e^{-kt}$

$-\ln [(160-P)/83] = kt$

For the hold time of 30 min the average value of the final pressure at ambient temperature for runs 16, 36 and 38 was taken into account.

P_{30}= average (140, 158, 136) psig = 145 psig

A linear curve was fitted on the data (Figure 10.21) and the rate constant of bio-oil's decomposition at 175°C was calculated as the slope, i.e. k= 0.05 min^{-1}. However it should be noted that the fit of the linear curve was poor.

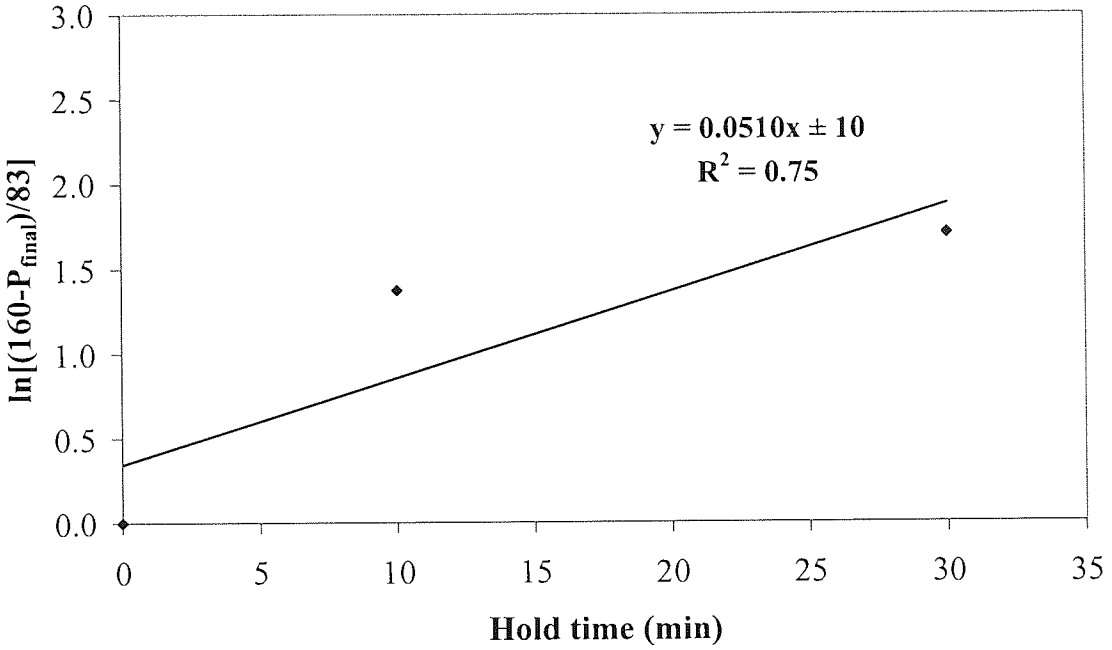

Figure 10.21 Rate constant of bio-oil's decomposition at 175°C under microwave irradiation based on the increase of P_{final} vs hold time

The rate constant k of bio-oil's decomposition at 175°C was also derived from the data of average molecular weight (Mw) and hold time assuming first order kinetics:

$$[(Mw)_\infty - Mw] = [(Mw)_\infty - (Mw)_o)\, e^{-kt}$$

As shown in Figure 10.22 after 30 min hold time the average molecular weight of bio-oil reached 1110 daltons (average value of Mw for runs 5 and 16). A slightly higher value of 1200 daltons was assigned to $(Mw)_\infty$

$(Mw)_\infty = 1200$ daltons

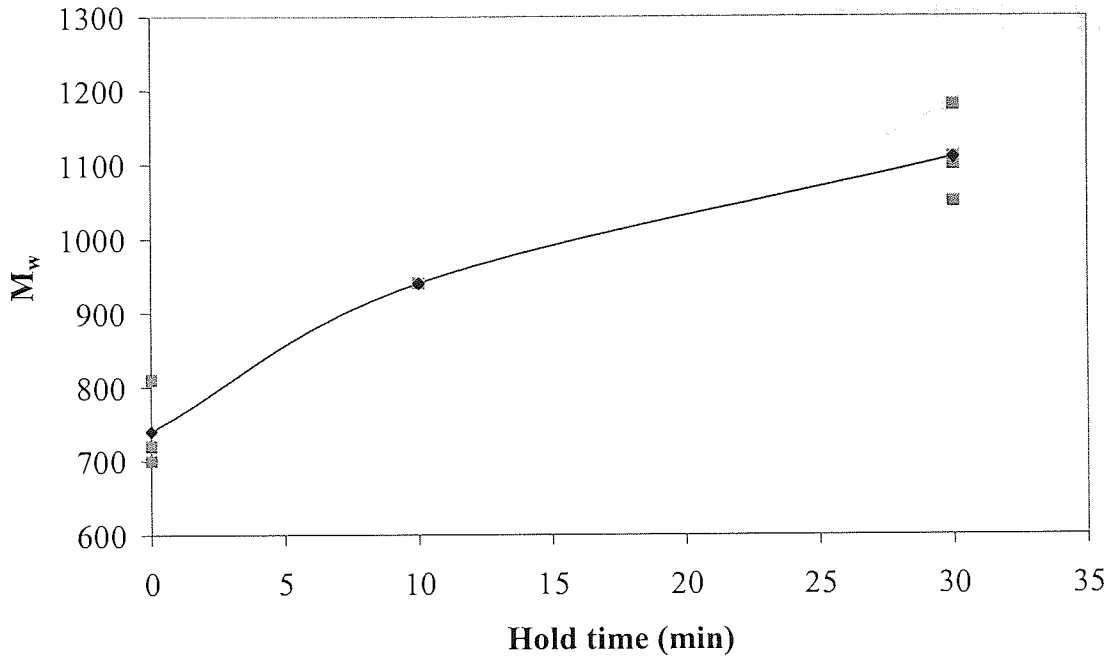

Figure 10.22 Plot of average molecular weight (Mw) versus hold time for the runs performed at 175°C (Runs 5, 15, 16, 28, 29)

The mean value of the average molecular weight for the two runs conducted at 175°C and zero hold time was given to $(Mw)_o$.

$(Mw)_o$= average (700, 720, 810) daltons = 740 daltons

Thus,

$[(Mw)_\infty - Mw] = [(Mw)_\infty - (Mw)_o)\ e^{-kt} \rightarrow$

$(1200-Mw) = (1200-740)\ e^{-kt}$

$-\ln [(1200-Mw)/460] = kt$

For the hold time of 30 min the mean value of bio-oil's average molecular weight for runs 5 and 16 was considered.

$(Mw)_{30}$ = average (1100, 1050, 1110, 1180) daltons= 1110 daltons

Again a linear plot was fitted on the data (Figure 10.23) and the rate constant was calculated as the slope, i.e. k= 0.054 min^{-1}. The fit of the linear curve was excellent, but with only three points this could be fortuitous. This value of k was close to the respective calculated based on the increase of final pressure versus hold time.

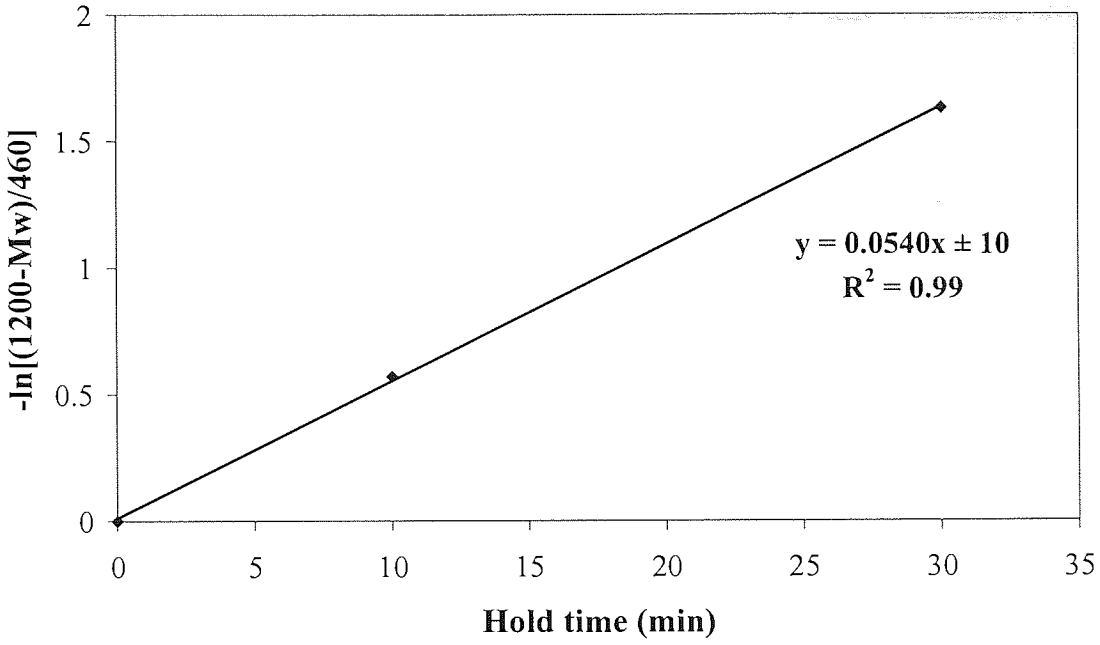

Figure 10.23 Rate constant of bio-oil's decomposition at 175°C under microwave irradiation based on the increase of Mw vs hold time

Finally the rate constant k of bio-oil's decomposition at 175°C was calculated from the data of water content ($H_2O\%$) and hold time assuming first order kinetics:

$$[(H_2O\%)_\infty - (H_2O\%)] = [(H_2O\%)_\infty - (H_2O\%)_o]\, e^{-kt}$$

As shown in Figure 10.24 after 30 min hold time the water content (%) of bio-oil reached 33.7 (average value of bio-oil's water content for runs 16 and 38). A slightly higher value of 35 was set to $(H_2O\%)_\infty$

$(H_2O\%)_\infty = 35$

The water content (%) measured for the 175°C and zero hold time run was considered as $(H_2O\%)_o$.

$(H_2O\%)_o = 29.1$

Therefore,

$[(H_2O\%)_\infty - (H_2O\%)] = [(H_2O\%)_\infty - (H_2O\%)_o]\, e^{-kt} \rightarrow$

$[35-(H_2O\%)] = (35-29.1)\, e^{-kt}$

$-\ln \{[35-(H_2O\%)]/5.9\} = kt$

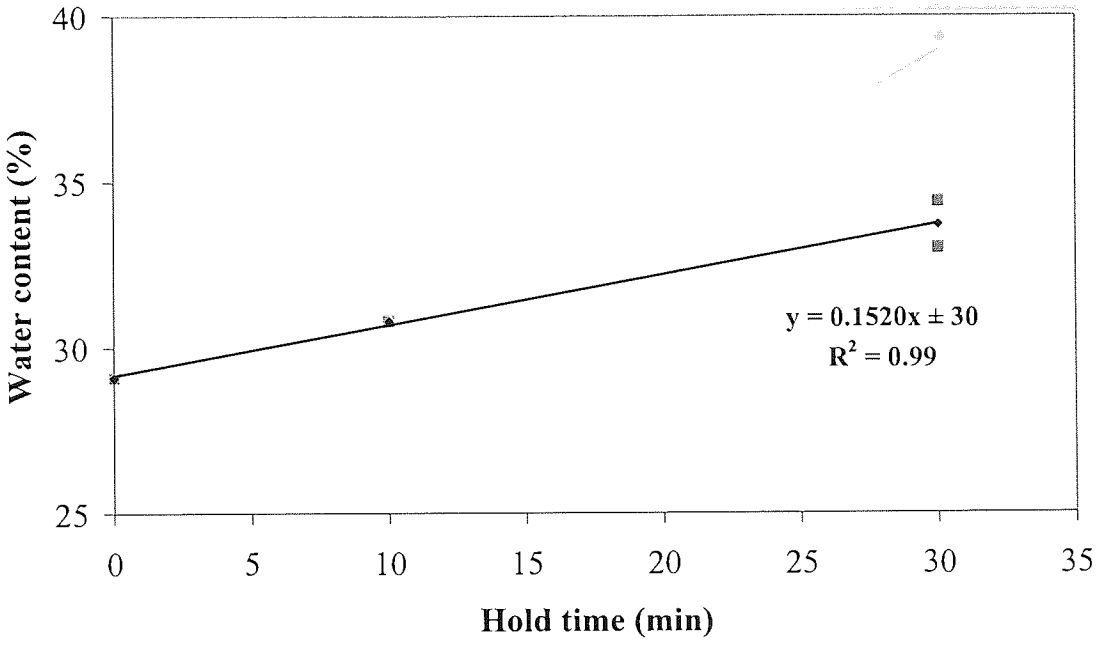

Figure 10.24 Plot of water content (%) versus hold time for the runs performed at 175°C (Runs 16, 28, 29, 38)

For the hold time of 30 min the average value of water content (%) for the runs 16 and 38 was used.

$(H_2O\%)_{30}$= average (33, 34.4)= 33.7

By fitting a linear plot on the data (Figure 10.25) the rate constant was calculated as the slope of the linear curve, i.e. k= 0.051 min^{-1}. The fit of the linear plot was again very good. This value of k was equal to that calculated from the increase of the final pressure versus hold time.

As mentioned previously, caution should be taken when considering these quoted rate constants at 175°C because the calculations were based on three data points only. Nevertheless the indicated rate could be validated by further experimentation. In addition, the proximity of the calculated rate constants based on the increase of final pressure, average molecular weight and water content % versus hold time respectively, assuming first order kinetics, strongly indicates that this approach was correct.

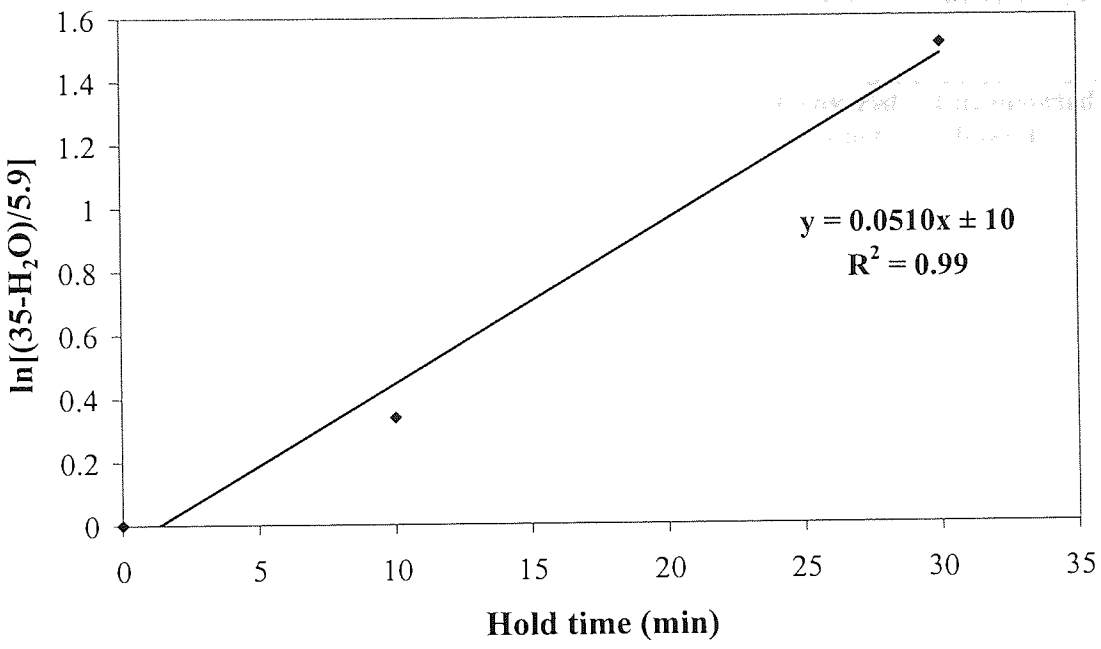

Figure 10.25 Rate constant of bio-oil's decomposition at 175°C under microwave irradiation based on the increase of water content (%) vs hold time

The fact that the calculated rate constants at 175°C were in the same range with the one calculated at 150°C is indicative of a pre-equilibrium with a negative enthalpy change leading to a negative activation energy for the observed rate constant.

10.2 Effect of char

A series of microwave runs was performed at 125°C and 30 min hold time (under simultaneous cooling) with bio-oil containing different amounts and types of char. The aim was to examine how the content of char and its origin (woody or grassy feedstock) influences bio-oil decomposition under microwave irradiation at a particular temperature. This temperature (125°C) was considered of interest because it was the one at which a significant change in bio-oil's average molecular weight had been observed (Section 10.1.2). The experimental conditions are presented in Table 10.6.

Table 10.6 Experimental conditions for the bio-oil runs conducted at 125°C, 200W and 30 min hold time in the presence of char

Run No	Feed (g)	Char (%)	Origin of char	Pfinal (psig)	Pambient (psig)	Recovered product (g)	Unconverted bio-oil %
64	8.00	0.14 (>11μm)	softwood	45	25	7.98	99.8
65	7.50	(<11μm)	softwood	43	25	7.46	99.5
66	8.03	+2	beech	68	38	8.00	99.7
67	8.01	+2	switchgrass	70	42	7.97	99.4

It should be mentioned that the level of char separation (>11 μm) did not leave a clean char-free oil. Therefore a char effect was possible even in the filtered bio-oil.

Again there is no apparent correlation between the final pressure after each run (at ambient temperature) and the percentage of unconverted bio-oil, as it was observed in section 10.1. The unconverted bio-oil remained nearly constant (ca. 100%) regardless of the final pressure, indicating that its decomposition under these conditions still follows first order kinetics.

10.2.1 Water content and physical appearance

Bio-oil samples were analysed via Karl Fisher titration aiming to investigate the effect of char content and origin on bio-oil's water content. The original bio-oil employed in all the runs was also analysed for comparison purposes.

The water content measurements are presented in Table 10.7, including the standard deviation as an error indicator. From these values a general standard deviation of *ca.* 0.3 may be deducted. Water content showed an increase in accordance with the char content (Run 65< Run 64< Run 66 < Run 67). This increase indicated a catalytic effect of char enhancing the condensation or dehydration reactions, which according to Czernik et al. occur in bio-oil, especially when exposed to higher temperatures [86]. The char originating from switchgrass led to slightly higher water content than the char from beech, probably due to its higher catalytic activity, which is attributed to its higher ash and alkalimetal content. However, taking into account the standard deviation of these measurements (0.3%) and the proximity of the results, no definitive conclusions on the effect of the type of char should be drawn.

Table 10.7 Water content of bio-oil irradiated at 125°C for 30 min hold time in the presence of char

Run No	Char (%)	Origin of char	Water content (%)
64	0.14 (>11μm)	softwood	29.1 ± 0.3
65	<11μm	softwood	28.7 ± 0.3
66	+2	beech	29.5 ± 0.3
67	+2	switchgrass	29.7 ± 0.3
Bio-oil non-irradiated			28.3 ± 0.1

The char content also influenced the physical appearance of the irradiated bio-oil. As in the previous series of runs (section 10.1.1) water droplets appeared on the walls surrounding the head space of the vial. In addition, phase separation was observed. However, upon shaking the two phases were completely miscible resulting in a one phase free flowing liquid. This initial phase separation was more severe for the bio-oil with the added char, leading to slightly higher viscosity upon mixing (the bio-oil appeared to adhere more strongly on the walls).

10.2.2 Gel permeation chromatography

Bio-oil samples before and after irradiation at 125°C in the presence of char were analysed by GPC. The aim was to assess the effect of the content and type char on bio-oil's molecular weight distribution.

The GPC results have been quoted to the nearest ten in Table 10.8. It was observed that the change in average molecular weight after irradiation at 125°C increased with increasing char content (Table 10.9). These results indicate that char has a mild catalytic effect and enhances the polymerisation /polycondesation reactions which are responsible for the formation of higher molecular weight species. This is in agreement with Abglevor et al. who reported that the char particles present in the bio-oil seem to catalyse polymerisation and viscosity increase [85]. Trace element analysis of biomass pyrolysis chars in the literature has showed that the inorganic elements present in bio-oil (i.e. the same elements that are found in the biomass) and in particular the alkali metals, which are catalytically active, are concentrated in the chars [152]. This could explain the catalytic effect of char. In this respect, the slightly stronger catalytic effect of the char originating from switchgrass could be attributed to its higher ash and alkalimetal content. However, the change in average molecular weight between the two

different types of char is minor and, hence, no hasty conclusions should be drawn about the effect of the type of char.

Another interesting point is the average molecular weight of the filtered bio-oil, which was a bit higher (*ca.* 20 daltons) than the respective of the original bio-oil, although upon visual observation it looked thinner. A lower or unchanged average molecular weight was expected after filtration. It is likely that some compounds of low molecular weight were adsorbed on the char particles and retained during filtration.

Table 10.8 Average molecular weight of bio-oil after microwave irradiation at 125°C and 30 min hold time in the presence of char

Samples	Run No	Mp	Mn	Mw	Mz	PD
Original bio-oil	N/A	230	370	640	1190	1.75
	N/A	230	370	640	1190	1.74
Filtered bio-oil	N/A	240	380	660	1240	1.74
Microwave runs 125°C, 30 min						
Original bio-oil	64	240	390	720	1420	1.85
	64	240	390	720	1410	1.85
Filtered bio-oil	65	240	390	720	1450	1.86
	65	240	390	720	1410	1.85
+ 2% beech char	66	240	390	730	1450	1.88
	66	240	390	730	1450	1.88
+ 2% switchgrass char	67	240	390	740	1510	1.89
	67	240	390	730	1460	1.89

Table 10.9 Changes in bio-oil's average molecular weight after irradiation at 125°C and 30 min hold time

Sample	ΔMw
Original bio-oil	80
Filtered bio-oil	60
+ 2% beech char	90
+ 2% switchgrass char	95

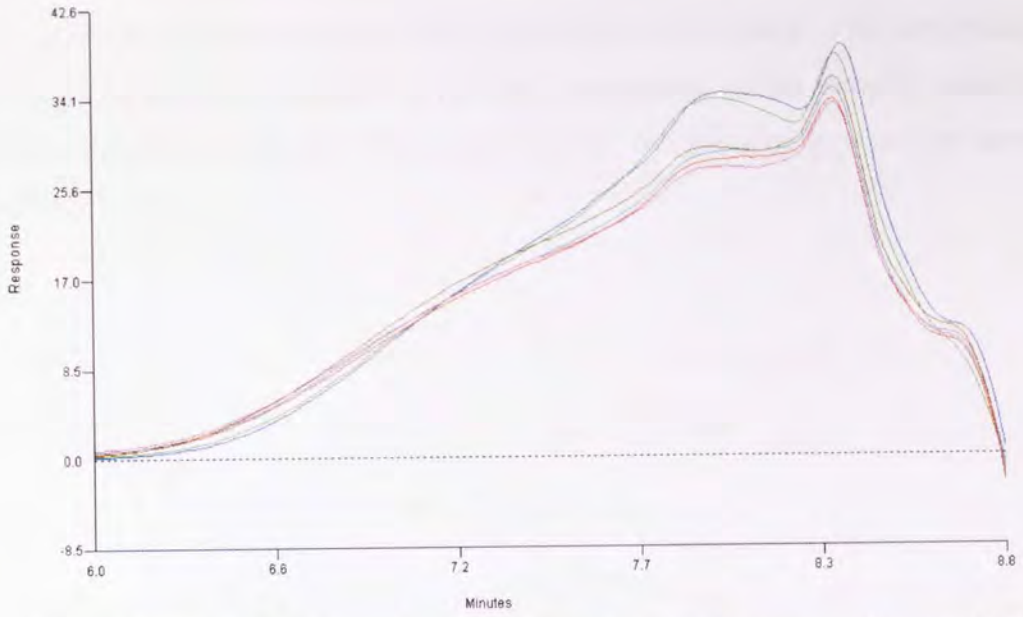

___ bio-oil non-irradiated, ___ filtered bio-oil non-irradiated, ___ bio-oil 125°C, ___ filtered bio-oil 125°C, ___ bio-oil (+2% wood char) 125°C, ___ bio-oil (+2% grass char) 125°C

Figure 10.26 GPC curves of non-irradiated original and filtered bio-oil and bio-oil with different amounts of char irradiated at 125°C

Overlays of the GPC curves show a slight shift to lower retention times for all the irradiated samples (Figure 10.26). However this shift was slightly more intense for the bio-oil with 2% added char from switchgrass, indicating a higher molecular weight distribution. Char might have a more significant effect in bio-oil's molecular weight distribution at higher irradiation temperatures.

10.2.3 FTIR spectroscopy

Bio-oil samples from the 30 min hold time microwave runs conducted at 125°C in the presence of different amounts and types of char were analysed by FTIR spectroscopy. All the bio-oil samples except the non-irradiated bio-oil contained a small portion of THF to ensure homogeneity. The collected FTIR spectra were used to examine whether the content and type of char had any effect on bio-oil's functional groups.

From the obtained FTIR spectra the same functional groups composition with the respective discussed in Section 10.2.3 was derived (Figure 10.27). No structural

differences were observed in the bio-oil that could be attributed to the content or type of char. However, it should be taken into account that the accuracy of the interpretation of the bio-oil's spectra is limited by the high complexity of the sample comprising of hundred different compounds which leads to a set of overlapping peaks, not separately resolved.

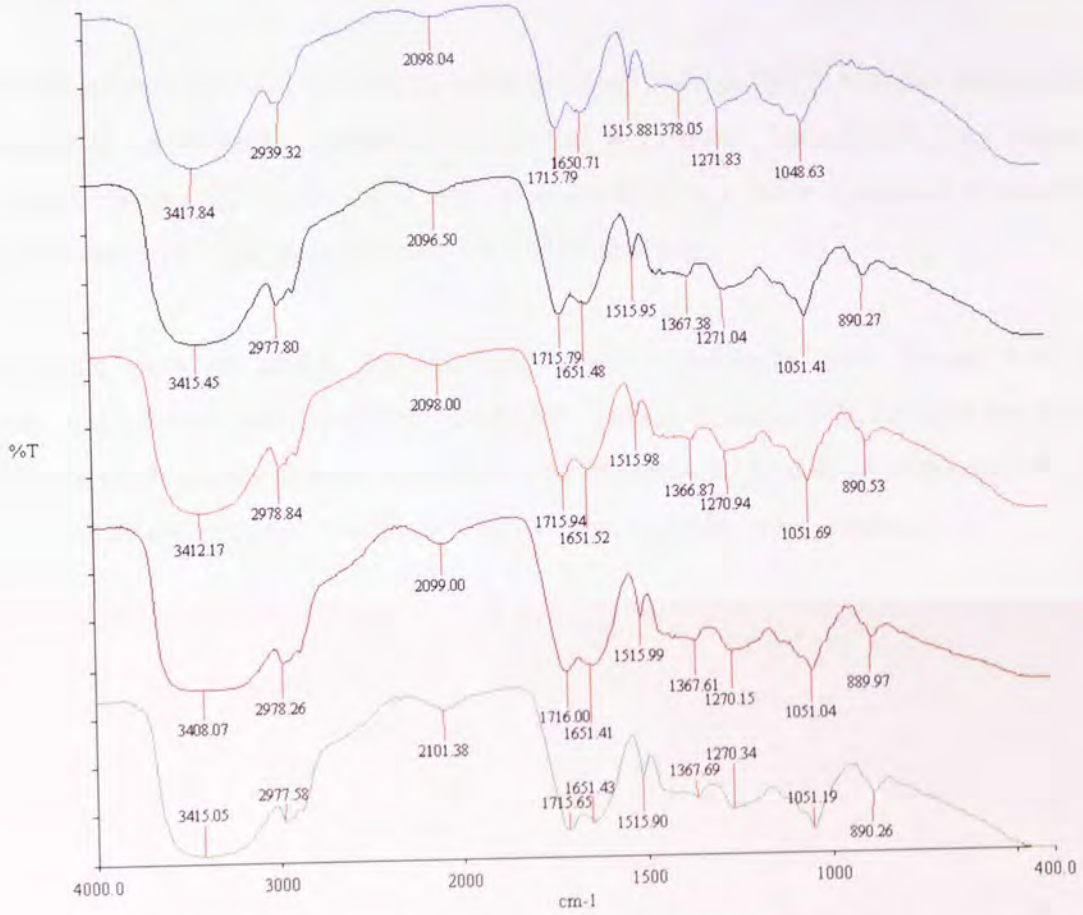

___ non-irradiated bio-oil, ___ bio-oil 125°C, ___ filtered bio-oil 125°C, ___ +2% wood char bio-oil 125°C, ___ 2% grass char bio-oil 125°C

Figure 10.27 FTIR spectra collected from bio-oil with different amounts and types of char irradiated at 125°C

10.3 Effect of catalyst

The aim of this series of runs was to study the effect of the presence of catalyst in bio-oil's decomposition under microwave irradiation. At first, a series of runs was conducted with bio-oil and laponite as catalyst, with and without simultaneous cooling, in order to determine the conditions under which 30 min reproducible runs could be performed (Table 10.10).

During the runs conducted under cooling at 175°C, excessive pressure was built up which led to abortion of the runs before the completion of 30 min hold time (Table 10.10). The temperature of the runs was then decreased to 150°C aiming to prolong them to 30 min hold time. Although the runs were prolonged compared to those conducted at 175°C, they still did not reach the 30 min hold time limit. In addition, the behaviour of the system with regards to temperature and pressure was not reproducible.

The next approach was to conduct another set of runs at 160°C without simultaneous cooling in an attempt to achieve the 30 min hold time (Table 10.10). As expected without cooling the power input was lower leading to a more controlled temperature and pressure rise. The final pressure was below 200 psig.

Duplicate runs (to check reproducibility) were performed with bio-oil and Na-montmorillonite as catalyst at 160°C without cooling, but at 150W, because the system required more energy in order to achieve 160°C compared to that with laponite. Similar temperature and pressure profiles with those from laponite were obtained.

Table 10.10 Experimental conditions for the microwave bio-oil runs conducted in the presence of catalyst

Run No	Feed (g)	Catalyst (g)	Type of catalyst	T (°C)*	Power (W)	Ramp time (min)	Hold time (min)	Pfinal (psig)	Pambient (psig)	Recovered product (g)	Unconverted bio-oil %
With cooling											
37	7.8	0.7807	Laponite	125 (175)	250	1.5	0	292	65	7.73	99.1
40	5.52	0.551	Laponite	175	150	5.2	5.7	288	134	5.4	97.8
41	4.85	0.485	Laponite	175	100-110-125	18.6	5.5	226	VIAL RUPTURED		
42	5.79	0.576	Laponite	175	125	12.9	3.5	270	124	5.65	97.6
43	5.98	0.592	Laponite	145 (160)	125	11.9	0	287	124	5.77	96.5
45	5.57	0.556	Laponite	150	125	5.5	11.8	276	VIAL RUPTURED		
46	5.92	0.592	Laponite	147 (150)	125	16.9	0	267	126	5.82	98.3
48	5.66	0.558	Laponite	150	125	7.6	17.6	263	146	5.53	97.7
49	4.05	0.401	Laponite	150	125	6.4	29.1	89	53	3.98	98.3
50	5.24	0.513	Na-mont	150	125-150-200	23.6	13.5	267	106	5.16	98.5
Without cooling											
39	5	0.496	Laponite	160	100	9.7	21.8	118	73	4.87	97.4
44	5.49	0.545	Laponite	160	100	3.4	29.5	184	117	5.4	98.4
47	5.34	0.529	Laponite	160	100	5.3	30.3	164	97	5.22	97.8
51	5.72	0.561	Na-mont	160	150	2.85	30	148	86	5.61	98.1
52	5.41	0.538	Na-mont	160	150	2.8	30	188	90	5.28	97.6
53	5.48	0	None	160	150	3.2	30	80	45	5.43	99.1
54	5.39	0.536	Eu-mont	160	150	2.1	30	166	119	5.24	97.2
55	5.4	0.532	Ce-mont	160	150	3	30	146	106	5.27	97.6
56	5.39	0.532	Cr-mont	160	150	6	30	190	103	5.26	97.6
57	5.42	0.536	Sn-lap	170 (160)	150	2.2	30	226	114	5.23	96.5
58	5.33	0.529	Laponite	160	150	2.8	30	175	102	5.22	97.9
59	5.32	0.529	Sn-lap	160	150	4.7	30	201	128	5.18	97.4
60	5.18	0.51	NiMo	160	150	3.1	30	123	76	5.09	98.3

(T): Set temperature if different than the achieved temperature

Since both aims of 30 min hold time and reproducibility were attained, the experimental conditions employed in the Na-montmorillonite runs (160°C, 150W, no cooling) were then applied in a series of runs with Eu-, Ce- and Cr-montmorillonites, Laponite, Sn-laponite and NiMo on alumina as catalysts. A blank run was also performed with bio-oil only to act as a reference for the analysis.

A bar chart depicting the percentage of unconverted bio-oil coupled with the final pressure at ambient temperature (after cooling down) for each catalyst run is presented in Figure 10.28. It is shown that the percentage of unconverted bio-oil is not dependent on the final pressure. The same conclusion is drawn from Figure 10.29, which displays a plot of the percentage of unconverted bio-oil versus the final pressure at ambient temperature.Given that the error bars for the quoted percentages of unconverted bio-oil are large, it can be assumed that bio-oil remains constant, and its decomposition under these conditions follows first order kinetics.

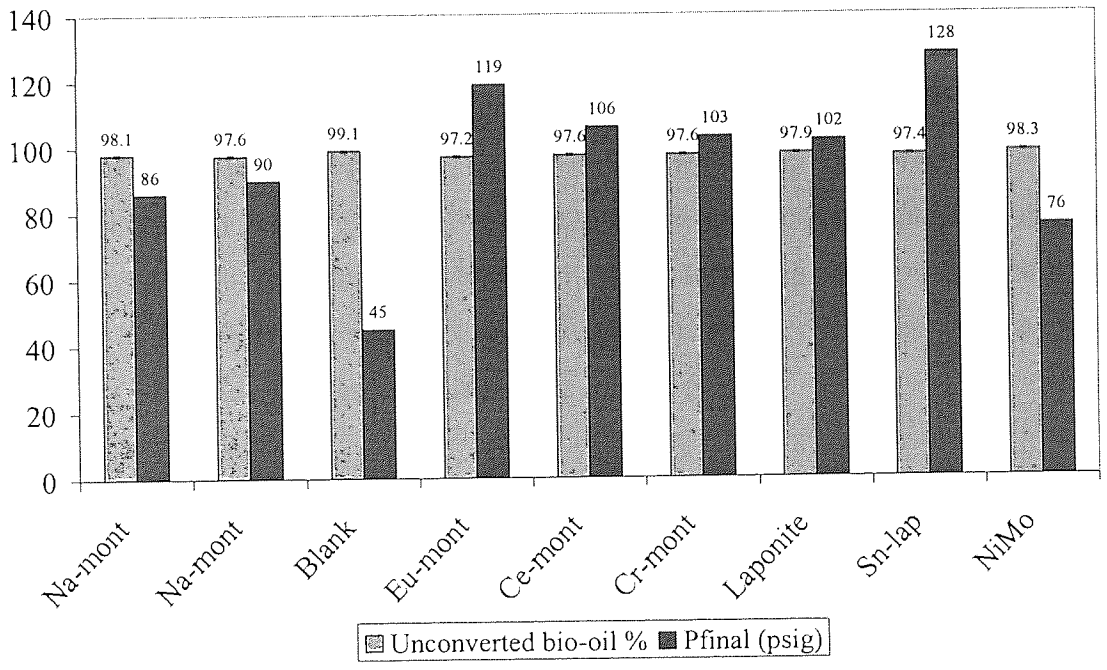

Figure 10.28 Unconverted bio-oil% and P_{final} for the series of microwave runs with different catalysts

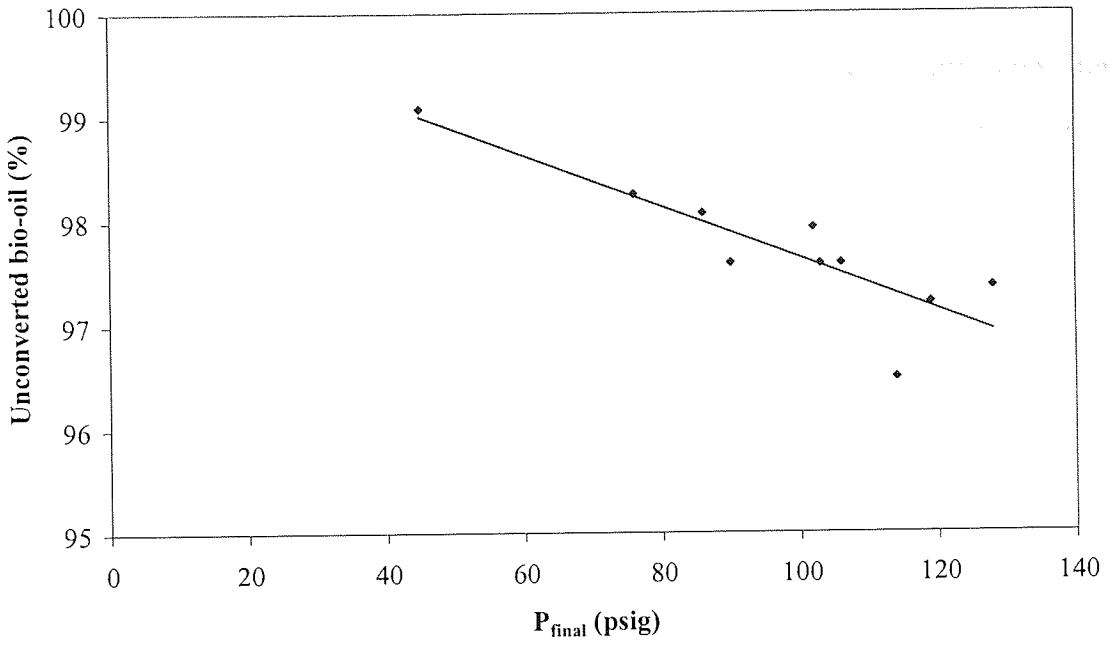

Figure 10.29 Unconverted bio-oil (%) versus final pressure at ambient temperature for the microwave runs in the presence of catalyst

10.3.1 Water content and physical appearance

Volumetric Karl Fisher titration is employed in the analysis of high level water content samples, such as bio-oil. However, after the catalyst runs, the recovered bio-oil was highly diluted in THF causing the water content of the samples to decrease significantly. As a result volumetric Karl Fisher was not an appropriate method for analysis. Nonetheless, the reference sample (blank), which contained only a limited amount of THF, was analysed yielding water content of 33%.

With regards to physical appearance, the microwave runs in the presence of catalyst made bio-oil to separate in a light fluid "watery" phase and a "tarry" sticky phase resembling paste. Catalyst sedimentation was observed on the bottom of the vial. For Cr-montmorillonite CM3, in particular, the amount of the "watery" phase was very small. However, during the runs with Na- montmorillonite all the bio-oil was converted to a semi-solid, paste-like material. All the catalysts during irradiation obtained darker colour than their original but not black.

10.3.2 Gel permeation chromatography

Duplicate bio-oil samples (for reproducibility purposes) from the 30 min hold time microwave runs in the presence of catalyst were analysed by GPC aiming to investigate whether catalyst has an effect in bio-oil's average molecular weight.

The GPC results have been quoted to the nearest ten and are presented in Table 10.11. All the expressions of average molecular weight for the catalyst runs, M_p, M_n, M_w and M_z, as well as polydispersity (PD), displayed higher values than the respective of the blank run (bio-oil only). These results indicate that the presence of catalyst enhances polymerisation and polycondensation, since the increase in average molecular weight has been attributed to this type of reactions. Cr-montmorillonite was the catalyst that caused the most significant change in average molecular weight, followed by NiMo on alumina and Sn-laponite (Figure 10.30).

Table 10.11 Bio-oil microwave runs with catalyst at 160°C and 30 min

Run	Catalyst	Mp	Mn	Mw	Mz	PD
53	Blank	320	390	850	1860	2.19
	Blank	320	410	990	2560	2.44
51	Na-mont	320	460	1130	2640	2.48
	Na-mont	320	460	1140	2630	2.47
52	Na-mont	320	470	1260	3310	2.67
	Na-mont	320	470	1220	2890	2.6
54	Eu-mont	440	440	1240	3790	2.83
	Eu-mont	450	450	1270	3880	2.8
55	Ce-mont	430	440	1290	4180	2.91
	Ce-mont	440	450	1290	3880	2.84
56	Cr-mont	320	510	1690	4520	3.32
	Cr-mont	320	550	1970	5540	3.55
58	Laponite	450	470	1210	2890	2.6
	Laponite	460	460	1200	2860	2.58
59	Sn-lap	450	500	1460	3640	2.93
	Sn-lap	450	500	1490	4200	2.99
60	NiMo	330	500	1500	4040	3
	NiMo	450	490	1540	4600	3.15

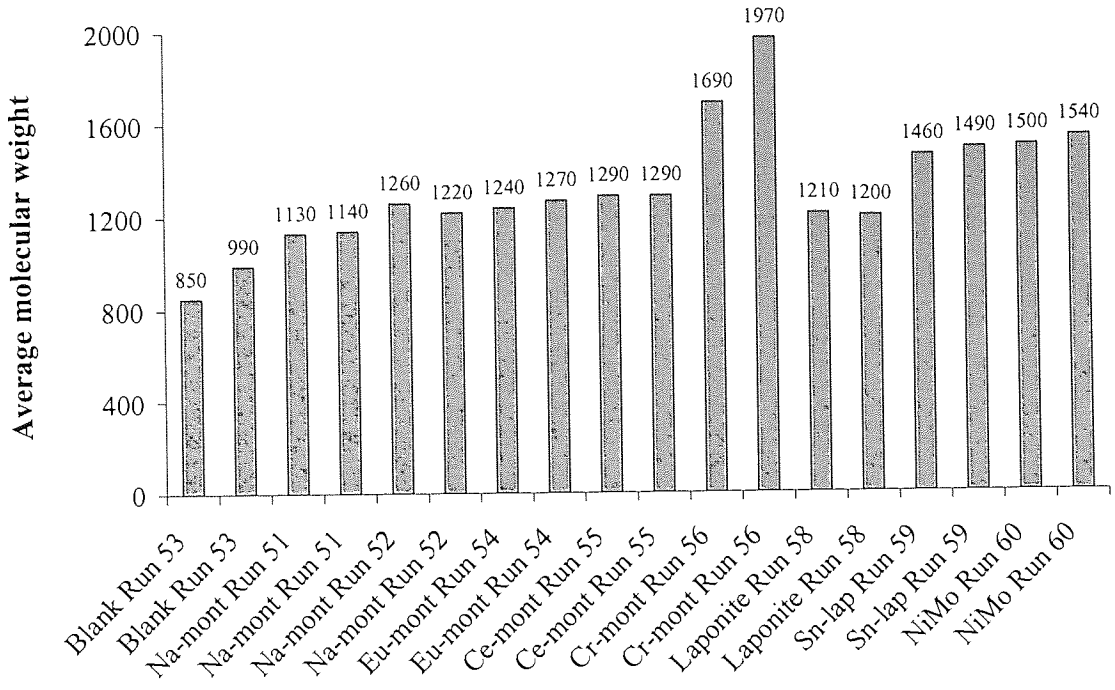

Figure 10.30 Average molecular weights for the series of bio-oil microwave runs with catalyst

Overlays of the GPC curves obtained from the microwave runs in the presence of catalyst are presented in Figure 10.31. The GPC curve of the reference run is also included for comparison purposes. The R56 Cr-montmorillonite curve clearly shifted to lower retention times. In every case there was a shift to lower retention times compared to the reference run R53 (blank) indicating a distribution of higher molecular weight.

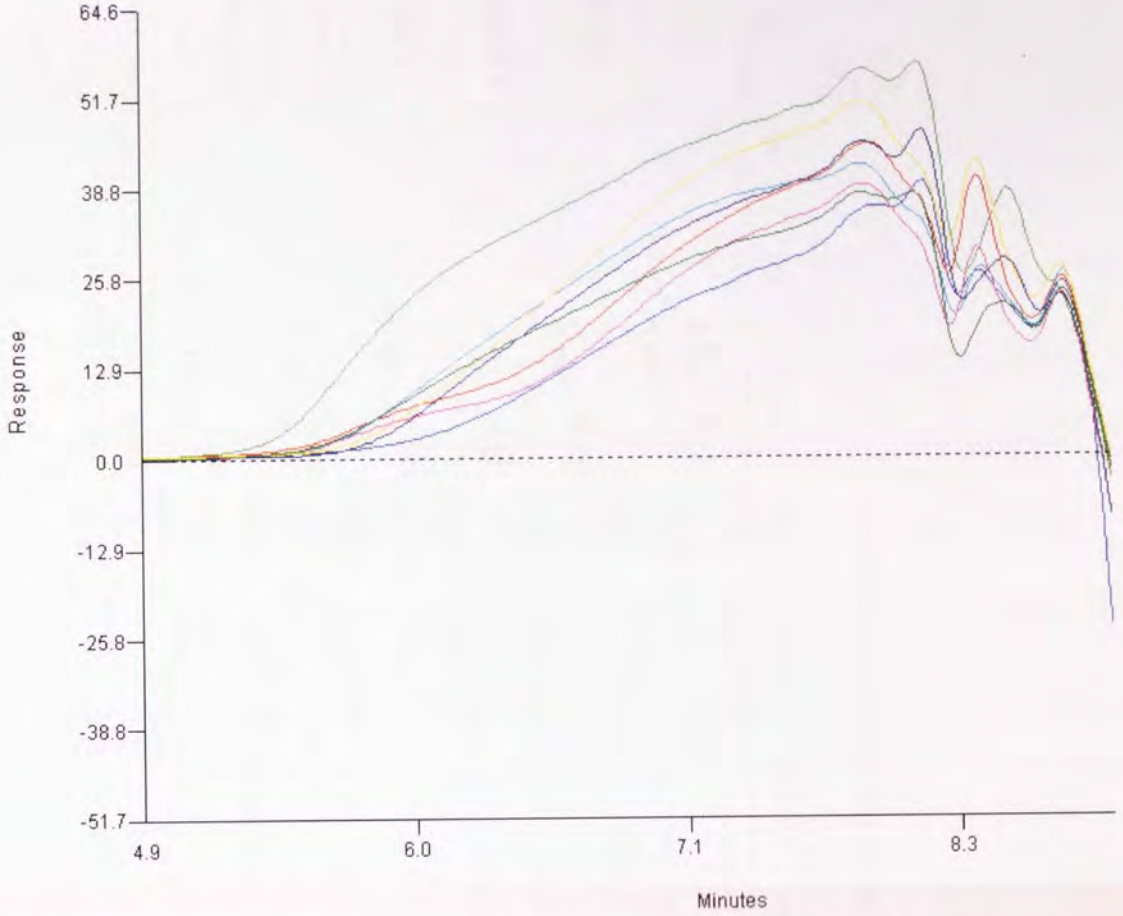

--- R53 blank, --- R56 Cr-mont, --- R59 Sn-lap, --- R55 Ce-mont, --- R54 Eu-mont, --- R58 Laponite, --- R 52 Na-mont, --- R60 NiMo

Figure 10.31 GPC curves for the series of microwave runs with bio-oil and catalyst

10.3.3 FTIR spectroscopy

Bio-oil samples from the 30 min hold time microwave runs in the presence of catalyst were analysed by FTIR spectroscopy. The collected FTIR spectra were used to study whether the presence of catalyst had any effect on bio-oil's functional group composition.

The FTIR spectra were dominated by the peaks attributed to THF, due to the high dilution in THF. The band attributed to C=O (1750-1650 cm^{-1}) was still present, whereas that attributed to C=C (ca. 1650 cm^{-1}) was very broad and weak (Section 10.1.3). Comparison of the FTIR spectra did not show any functional group differences that could be attributed to the presence of catalyst.

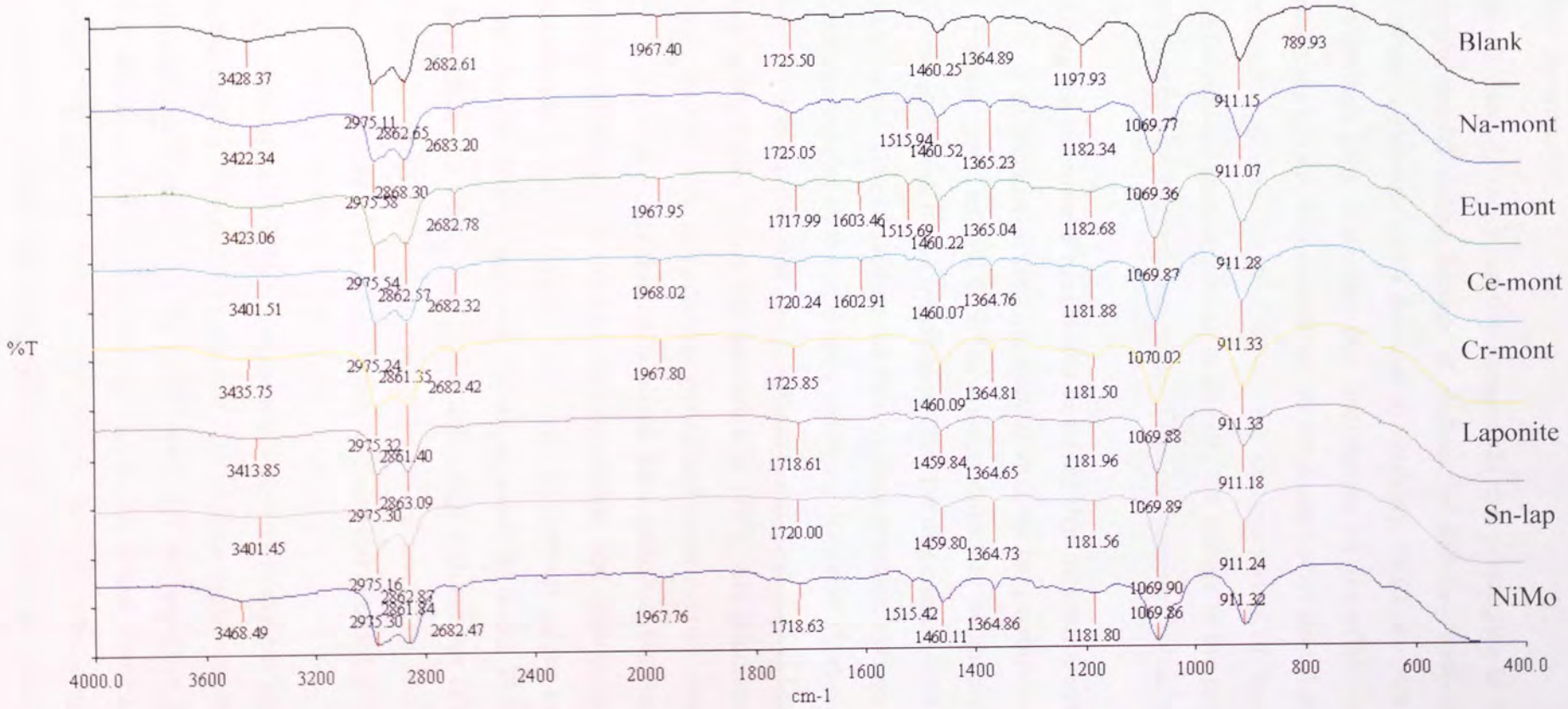

Figure 10.32 FTIR spectra from bio-oil recovered from the microwave runs in the presence of catalyst

10.4 Summary

Bio-oil contains many reactive compounds that polymerise to form higher molecular weight species during storage at ambient or elevated temperature, resulting in an increase in viscosity and a decrease in volatility, which are both unfavourable for fuel applications [86]. Therefore any information on the effect of parameters such as temperature, time, char content etc. in the properties of bio-oil would be useful for any potential end user. In this respect the decomposition of bio-oil under microwave irradiation was studied, aiming to identify the change in the properties of bio-oil as a function of time, temperature, mode of heating, presence of char and catalyst.

During the microwave runs it was observed that increasing temperature or hold time leads to an increase in final pressure at ambient temperature due to the formation of permanent gases, as well as in the average molecular weight and water content (%) of the treated bio-oil. It was hypothesised that the rate constant of bio-oil's decomposition could be calculated based on the data of final pressure, average molecular weight and water content (%) versus hold time, assuming first order kinetics. The rate constant k of bio-oil's decomposition at 150°C was calculated from data of final pressure versus hold time ($k=0.05\ min^{-1}$). The rate constant k at 175°C was calculated from limited data on final pressure, average molecular weight and water content versus hold time. Because in the latter case only three data points were available, the determined rate constants require validation via further experimentation and should be considered as rough estimations of the true values. However, the derived values are very close (*ca.* 0.05 min^{-1}), which strongly indicates that the approach is correct. The fact that the calculated rate constants at 175°C were in the same range with the one calculated at 150°C could signify a negative activation energy for the observed rate constant which, in turn, is usually indicative of a pre-equilibrium with a negative enthalpy change.

The mode of heating (microwave or conventional) did not appear to affect bio-oil's water content or physical appearance. The average molecular weight calculated for the conventional runs showed the same trend with the respective for the microwave runs (i.e. M_w increased with increasing T), but the actual changes in average molecular weight (ΔM_w) were lower. However, the lack of monitoring of the actual bio-oil temperature during the conventional runs should be taken into account before

attributing any differences to a "microwave" effect.

Char content or type and presence of catalyst did not appear to have any significant effect on bio-oil's physical appearance. However, increasing char content increased bio-oil's water content. The char originating from switchgrass led to slightly higher water content than the char from beech, probably due to its higher catalytic activity, which is attributed to its higher ash and alkali metal content. Still, taking into account the standard deviation of these measurements and the proximity of the results, no definitive conclusions should be drawn on the effect of the type of char in the water content.

The change in bio-oil's average molecular weight after irradiation at 125°C increased with increasing char content. The change was slightly higher for the bio-oil with added char originating from switchgrass compared to the bio-oil with char from beech. However, it was a minor change and, hence, no hasty conclusions should be drawn about the effect of the type of char in bio-oil's average molecular weight. Char might have a more significant effect in bio-oil's molecular weight distribution at higher irradiation temperatures. The average molecular weight of the bio-oil recovered from the catalyst runs was higher than the respective from the blank run (bio-oil only). Bio-oil recovered from the runs conducted in the presence of Cr-montmorillonite as catalyst exhibited the highest average molecular weight, followed by that from the runs in the presence of NiMo on alumina and Sn-laponite.

Thus the condensation and polymerisation reactions, which are induced by the high content of reactive organic compounds in bio-oil and leading to an increase in its average molecular weight, were intensified by increasing temperature, hold time, and char content, as well as by introducing a catalyst. Char originating from a grassy feedstock may have a stronger catalytic effect attributed to its higher ash and alkali metal content.

Comparison of the obtained FTIR spectra did not yield any differences in bio-oil's functional group composition. Yet, it should be noted that the accurate interpretation of the bio-oil spectra is very difficult due to the complexity of the sample comprising of hundreds of compounds leading to a set of overlapping peaks, not separately resolved.

11 SUMMARY & CONCLUSIONS

11.1 Synthesis and characterisation of pillared clays

11.1.1 Summary

Two sets of pillared clay catalysts were prepared from Wyoming bentonite and laponite by initially intercalating chromium and tin oxides via both conventional and microwave assisted techniques. Laponite as synthetic clay with no impurities was used as received, whereas Wyoming bentonite as a natural clay required some refining or else some refining plus pre-exchange with sodium to yield monoionic sodium montmorillonite. Then cerium, europium and a mixture of chromium and cerium oxides (5/1 w/w) were intercalated conventionally in sodium montmorillonite under the concept that the oxidation states of cerium and europium could be manipulated during calcination and hydrocracking, leading to possible improvement of the performance of the pillared clays as catalysts. The pillared clays containing chromium were calcined under argon (inert atmosphere) in order to avoid chromium oxidation and subsequent loss of chromium in the form of volatile oxides leading to decomposition, whereas the others were calcined under air. Tin oxide pillared laponites were the only materials that did not require calcination prior to utilisation.

11.1.2 Conclusions

Novel microwave assisted methods of preparing chromium and tin oxide pillared montmorillonites were developed; tin oxide pillared laponites were prepared using a literature microwave method. The application of microwave irradiation resulted in significant reductions in preparation time compared to that of the respective conventional methods. More specifically, the chromia pillared montmorillonite preparation time was reduced from 36 h to 15 min, the respective for tin oxide pillared montmorillonite from 23 h to 15 min, and for tin oxide pillared laponite from 1 week to 5 min.

X-ray powder diffraction (XRD) was used as the principal method to study changes in the clays after pillaring reactions and subsequent calcination steps. Since basal spacing is the measure of the distance between the silicate layers, addition or changes of pillaring agents will directly affect its value. As chromia pillared montmorillonites were

the most promising catalysts in early tests [2, 3], these were investigated more thoroughly leading to the following conclusions:

- Basal spacing depends on the experimental conditions employed with the most important being the OH/Cr ratio. An OH/Cr ratio of 2 led to the highest basal spacing (28Å).
- Highly concentrated pillaring solutions and dry powder Wyoming bentonite can be employed successfully in the preparation, despite the fears that diffusion of the pillaring species into the clay particles may be inhibited. This is very significant from an economic point of view, since it does not require manipulation of high volumes of both aqueous pillaring solutions and clay slurries, which involves very large equipment with high capital costs.
- The novel microwave assisted method for the synthesis of chromia pillared montmorillonite led to basal spacing of 20Å, which is not as high as that following the conventional method (28Å), but is in agreement with other references and confirms that some pillaring occurred. It is not clear whether microwave irradiation affects catalytic activity since these catalysts were not tested for hydrocracking efficacy.

Upon pillaring with tin, cerium and europium oxides there was a slight increase in basal spacing, which decreased during calcination. This was probably due to the non-formation of polynuclear cationic complexes during hydrolysis of the salts of the respective rare earth metals. However, in all cases the diffraction peaks were quite sharp indicating a relatively homogeneous pillaring process. Incorporation of cerium oxide in a chromia pillared montmorillonite decreased the basal spacing with respect to the analogous sample without cerium oxide, indicating that cerium oxide was not found in the chromia pillars and may have been in another form such as an oligomeric cation. After calcination at 500°C the diffraction peaks were barely or no longer observed indicating the collapse of the pillars.

XRD was not suitable for the characterisation of laponite or pillared laponites due to the lack of first order reflection. This was attributed to the small size of individual particles and the random rather than uniform face-to-face orientation of the clay platelets. However, pillared laponite after use presented first order reflection indicating higher order among the clay layers and possibly the existence of pillars. The used pillared

montmorillonites retained some crystallinity, although the peaks of the clay layers decreased in intensity, and exhibited similar basal spacings. However, this analysis was inconclusive with regards to what took place in the interlayer. Most likely the pillars had collapsed during the hydrocracking process.

Thermogravimetric analysis (TGA) and differential thermogravimetric analysis (DTG) showed that structural changes occurring in pillared montmorillonites during calcination at 500°C are associated with the dehydration of the clay and the dehydration /dehydroxylation of pillars. Pillaring Wyoming bentonite or sodium montmorillonite with chromium or tin oxide decreased the temperature at which dehydroxylation begins in comparison with the respective temperature for the starting materials leading to lower thermal stability. This behaviour was observed for all the chromium and tin oxide pillared clays regardless of the experimental conditions, e.g. OH/metal ratio, or preparation method (conventional or microwave). Pillaring sodium montmorillonite with cerium oxide did not affect its thermal stability; yet pillaring with europium oxide led to lower thermal stability compared to that of the starting material (the dehydroxylation peak became broader including lower temperatures). Finally the incorporation of cerium oxide in a chromia pillared montmorillonite shifted dehydroxylation to higher temperatures compared to those for pillared montmorillonite with single chromia pillars leading to increased thermal stability, similar to that of the starting material. Addition of cerium thus improves thermal stability.

Laponite appeared to be more thermally stable than montmorillonite, with tin oxide pillared laponites exhibiting the same thermal behaviour. Chromia pillared laponite displayed a unique temperature profile probably as a result of the combination of the hydrated chromia oligomers in the interlayer with the laponite structure. For chromia pillared laponite dehydroxylation took place over a much wider temperature range compared to all other materials.

X-ray photoelectron spectroscopy (XPS) was used to verify pillaring of laponites, since XRD proved inappropriate. Tin in the form of tin(IV) oxide was detected in the tin oxide pillared laponites. The amount of tin varied among the different preparations (0.1 to 0.8%), although no clear trend was observed relating it with the preparation conditions. It was hypothesised that this was due to inhomogeneous pillar (i.e. tin

oxide) distribution leading to different atomic compositions (%) in the same batch. Tin in the same form of tin(IV) oxide, but at a much higher content (2.8%) was also detected in tin oxide pillared montmorillonite. Furthermore, chromium(III) coordinated with water and hydroxyl ligands was detected in the chromia pillared clays (both laponites and montmorillonites) proving the hydroxyl-oxy chromium composition of the pillars.

XPS analysis of the used catalysts did not yield any significant information. Carbon dominated their composition, which was attributed to the extensive carbon layer coating all the catalysts after use. The inability to detect any chromium indicated that it was probably located below the layer penetrated by the x-ray beam.

Nitrogen adsorption was undertaken to measure the textural properties, such as surface area and pore volume of the starting materials and their pillared derivatives. Pillaring of Wyoming bentonite and sodium montmorillonite with chromium, tin or cerium oxides caused a multi-fold increase in surface area, both total and microporous. Moreover, the ratios of micropore volume to total pore volume and micropore surface area to total surface area (BET) also increased after pillaring with respect to the ratios for the starting materials. However, europium oxide pillared montmorillonite did not follow the general trend of pillared montmorillonites. It did not display any microporosity and, in addition, showed higher macroporosity than the parent sodium montmorillonite. This could be attributed to the utilisation of europium as pillaring species resulting in an unconventional non-microporous product behaving differently than the usual pillared clays. It is likely that during calcination dexydroxylation of the europium oxide pillars and the clay structure occurred resulting in the formation of large pores. Further investigation is required on this matter. On the other hand laponite had higher surface area and higher total pore volume than all the pillared montmorillonites, which was credited to its delaminated nature and small particles. Pillaring of laponite did not affect significantly either its surface area or its pore volume.

MAS NMR was applied to the starting clay materials and their pillared derivatives after calcination to investigate whether pillaring with a range of species affects their aluminosilicate framework. Since no significant changes were exhibited between the recorded ^{29}Si and ^{27}Al MAS NMR spectra, it can be concluded that the aluminosilicate

structure of the materials remained basically unaltered regardless of being pillared or unpillared.

11.2 Catalytic performance

11.2.1 Summary

The catalytic performance of the pillared clays synthesised was mainly assessed in terms of their ability to hydrocrack the fraction of the coal derived liquids with boiling points above 450°C and convert it into materials with lower boiling points. All the catalysts tested (parent clays, pillared clays and NiMo on alumina) showed a significant deposition of carbonaceous material on their surface after the first use and as a result valid performance comparisons could not be drawn from these tests. The deposits are mainly composed of heavy material with boiling points above 450°C. A more realistic assessment of catalytic activity was achieved during reuse of the most promising catalysts, while the new carbon deposition was significantly lower. However, the small amounts of catalyst and feed employed in the runs might have compromised the ability of the test programme to provide definitive trends due to higher experimental error.

11.2.2 Conclusions

The chromia pillared montmorillonite CM3 (d_{001}=15.4 Å, 2.6% Cr) and the tin oxide pillared laponite SL2a showed slightly better "conversions" (53 and 54% respectively) than the other catalysts. Sodium montmorillonite, the chromia pillared montmorillonite CM6 (d_{001}=22.5 Å, 4.5% Cr), the mixed chromium-cerium oxide pillared montmorillonite and Wyoming bentonite as received displayed similar "conversions" with the conventional catalyst (NiMo on alumina) (40%). However, some information on heteroatom removal (by elemental analysis) in the processed feed would have improved the assessment of catalytic performance.

The intercalation of chromium in the form of chromia (Cr_2O_3) in the interlayer clearly increased conversion. This was attributed to the redox activity of the chromia pillar. However, this increase was not proportional to the increase in chromium content or basal spacing. In the case of tin oxide pillared laponite, the catalytic activity might

have been a result of better access to the acid sites due to the delaminated nature of laponite, whose activity was promoted by the presence of tin oxide.

The manipulation of the structural properties of the catalysts via pillaring did not seem to have any effect on the catalysts' activity. This was probably due to the collapse of the pillars under hydrocracking conditions as indicated by the similar basal spacing of the catalysts after use. However, the type of the pillaring species had a significant effect on conversion. Whereas pillaring with chromium and tin oxides increased the conversion exhibited by the parent clays, pillaring with cerium and europium oxides appeared to have a detrimental effect. The relatively good performance of the parent clays was attributed to their acid sites, coupled with their macropores which are able to accommodate the very high molecular mass of coal derived liquids.

The catalytic behaviour observed during the second series of hydrocracking runs might be attributed to a change in the oxidation state of chromium and tin, which occurred during the first series of runs and was triggered by the hydrogen atmosphere in the microbomb reactor. Hence, the first run could be considered as a preparatory-activation step to convert the catalyst to its final form. However, in the case of cerium and europium oxide pillared montmorillonites the improvement in the hydrocracking performance during second use was small, indicating that this preparatory-activation step works favourably only for certain metals. The improved performance exhibited in most cases during reuse may indicate that the coke layer has a catalytic effect.

The catalysts were tested in a microbomb reactor under conventional hydrocracking conditions involving high temperatures and high hydrogen pressures. It was thought that microwave irradiation could enable conversion to occur at milder conditions than those conventionally used, coupled with a more effective use of hydrogen. The latter could lead to lower operating costs making the process cost effective. In this framework a CEM Focused Microwave™ Synthesis System, Model Discover was adapted for the hydrocracking of coal derived liquids and tested with the conventional catalyst NiMo on alumina at moderate conditions (13.8 bar and 190°C). However, in practice excessive coke deposition took place leading to negative total conversion. This was probably due to a very low hydrogen pressure, unable to have any hydrocracking effect even under microwave irradiation.

11.3 Bio-oil decomposition under microwave irradiation

11.3.1 Summary

Bio-oil contains many reactive organic compounds that polymerise to form higher molecular weight species during storage at ambient or elevated temperature, resulting in an increase in viscosity and a decrease in volatility, which are both unfavourable for fuel applications. Like coal derived liquids and petroleum residues, it requires high temperatures and pressures in order to be upgraded to transport fuel and the conventional catalysts (NiMo and CoMo on alumina) employed until now are rapidly deactivated and unable to handle its high water content (*ca.* 25% wt). Therefore any information on the effect of parameters such as temperature, time, mode of heating, presence of char and catalyst in the properties of bio-oil would be beneficial for any potential end user.

11.3.2 Conclusions

Increasing temperature at constant hold time or increasing hold time at constant temperature had similar effects on bio-oil. They both led to an increase in the final pressure (at ambient temperature) during the runs, as well as in the water content and average molecular weight of the treated bio-oil and influenced its physical appearance. The lowest temperature at which phase separation was observed was 150°C for the 30 min hold time runs and 175°C for the zero hold time runs. Therefore, increasing hold time had lowered the temperature at which phase separation occurred. No effect of temperature or hold time was observed in the functional group composition.

The rate constant of bio-oil's decomposition at 175°C was calculated based on the data of final pressure, average molecular weight and water content (%) versus hold time, assuming first order kinetics. Because only three data points were available, the determined rate constants require validation via further experimentation and should be considered as rough estimations of the true values. However, the derived values are very close (*ca.* 0.05 min^{-1}), which strongly indicates that the approach is correct. The calculation of the rate constant at 150°C from data of final pressure versus hold time ($k=0.05\ min^{-1}$) was more accurate using several data points. The same calculated rate constants at 175°C and 150°C may point to a negative activation energy for the

observed rate constant which, in turn, is usually suggestive of a pre-equilibrium with a negative enthalpy change.

The mode of heating (microwave or conventional), which was investigated at constant temperature and hold time, appeared to have no effect in bio-oil's water content, physical appearance or functional group composition. The increase in average molecular weight calculated for the conventional runs (ΔM_w) was lower than the respective for the microwave runs. However, it is important to appreciate the lack of monitoring of the actual bio-oil temperature during the conventional runs before attributing these differences to a "microwave" effect. A possible lower temperature during the conventional runs could explain the lower increase in average molecular weight.

Increasing bio-oil's char content at constant temperature and hold time increased its water content and average molecular weight, but did not affect its physical appearance or functional group composition. The char originating from switchgrass led to slightly higher water content and average molecular weight than the char from beech, probably due to its higher catalytic activity, which is attributed to its higher ash and alkalimetal content. However, because those differences were minor and could render in the order of magnitude of experimental error, no definitive conclusions should be drawn on the effect of the type of char in bio-oil's water content or average molecular weight.

Bio-oil irradiated at constant temperature and hold time in the presence of a range of catalysts exhibited an increase in its average molecular weight compared to the respective from the blank run (bio-oil only). The biggest increase was displayed by the the bio-oil recovered from the run conducted in the presence of chromia pillared montmorillonite, followed by those from the runs in the presence of NiMo on alumina and tin oxide pillared laponite, indicating that the condensation and polymerisation reactions, which are responsible for the formation of higher molecular weight species in bio-oil, are enhanced by these catalysts.

12 RECOMMENDATIONS

During the current work several areas requiring further investigation were identified, but it was not possible to follow them due to time limitations. These areas formed the basis of the recommendations for further work presented in this chapter.

With regards to 'conversion' of coal derived liquids, the chromia pillared montmorillonite CM3 (d_{001}=15.4Å, 2.6% Cr) and the tin oxide pillared laponite SL2a were the best catalysts. Sodium montmorillonite, the chromia pillared montmorillonite CM6 (d_{001}=22.5Å, 4.5% Cr), the mixed chromium-cerium oxide pillared montmorillonite and Wyoming bentonite as received displayed similar 'conversions' with the conventional catalyst (NiMo on alumina), but slightly lower than the respective for CM3 and SL2a. The intercalation of chromium in the form of chromia (Cr_2O_3) in the interlayer clearly increased conversion but not proportionally to the increase in chromium content or basal spacing. Initial basal spacing did not seem to be related to the catalysts' activity, probably due to the collapse of the pillars under hydrocracking conditions as indicated by the similar low basal spacing of the catalysts after use. The high 'conversion' of the chromia pillared montmorillonite was attributed to the redox activity of the chromia pillar. On this basis it would be of particular interest to:

- Utilise a chromia pillared montmorillonite as support for NiMo, in order to combine on a molecular level the two catalysts that displayed high conversions in hydrocracking coal, which is expected to further increase conversion. This combination will yield a hydrotreating catalyst, i.e. a dual function catalyst where hydrogenation-dehydrogenation reactions will occur on the metal centres comprising Ni-Mo, whereas cracking reactions will occur on the acid sites provided by the chromia pillared clay.
- Utilise a moderate acidity aluminosilicate as substrate for chromium oxide, ensuring good dispersion of the active phase, and compare the activity of the resulting catalyst with that of a chromia pillared clay. The fact that the chromia pillared montmorillonite exhibited high conversion in hydrocracking coal derived liquids although the pillars had probably collapsed implies that pillaring may not be necessary.

Neither of the above mentioned catalyst formulations has been investigated so far.

The effectiveness of the tin oxide pillared laponite SL2a should be questioned. SL2a and SL7a exhibited a completely reversed catalytic behaviour between first and second use, for which the minor differences in the preparation method and the resulting intercalated tin content between the two catalysts can not account. Therefore:

- More experiments assessing the reproducibility of the production and the performance of tin oxide pillared laponites should be carried out.

The tin oxide pillared montmorillonite was the only catalyst that could not be tested in hydrocracking coal derived liquids. Hence:

- Hydrocracking experiments employing tin oxide pillared montmorillonite in order to provide information on the catalytic effect of the tin oxide pillar in connection to the nature of the parent clay would be helpful.

A 144-fold reduction was achieved in the preparation time of the microwave assisted chromia pillared montmorillonite compared to that of the conventional method. However the basal spacing of the resulting material was lower than that of the conventional method. Thus:

- Optimisation of the microwave preparation of chromia pillared montmorillonite in order to yield a material with higher basal spacing of *ca.* 28Å to match that from the conventional method is recommended.
- Testing of chromia montmorillonites synthesised under microwave irradiation in hydrocracking coal liquids to assess whether microwave irradiation improves catalytic activity as suggested by the literature for other catalytic applications would be of interest.

Cerium and europium were intercalated conventionally in sodium montmorillonite in the belief that their oxidation states could be manipulated during calcination and hydrocracking, leading to possible improvement of the catalytic performance of the derived pillared clays. Hence:

- XPS analysis of cerium and europium oxide pillared montmorillonites before and after calcination to identify the oxidation state of the metal cation and check the validity of the assumption of possible manipulation should be carried out.

The derived europium oxide pillared montmorillonite did not follow the general trend of the pillared montmorillonites. It did not display any microporosity or increase in its surface area and, in addition, showed higher macroporosity than the original montmorillonite. This could be attributed to the utilisation of europium oxide as pillaring species resulting in an unconventional product with different properties than the usual pillared clays. As a result:

- Repetition of experiments to prove reproducibility of the production and further characterisation in order to investigate the validity of the assumptions made in the attempt to explain these different properties would be valuable.

The catalytic behaviour observed during the second series of hydrocracking runs might be attributed to a change in the oxidation state of the metal during the first series of runs, triggered by the hydrogen atmosphere in the microbomb reactor. Hence, the first run could be considered as a preparatory-activation step to convert the catalyst to its final form. However, in the case of cerium and europium oxide pillared montmorillonites the improvement in the hydrocracking performance during second use was small, indicating that this preparatory-activation step works favourably only for certain metals. In order to shed more light into the catalytic behaviour of the pillared materials:

- Depth resolved XPS should be performed on all the used catalysts, if it is possible to overcome the problem of the carbon layer and still detect the metal cation and its structure, in order to identify the oxidation state of the metal cation and check whether any change occurs during hydrocracking as assumed. Alternatively, subjecting the catalysts to hydrocracking conditions in the absence of feed and subsequent performance of XPS analysis could be employed. This should be indicative of any changes in the oxidation state of the metal cation, if carbon deposition does not play a role in the process.

Further information on the used catalysts would improve the understanding of the catalytic process.

- Scanning electron microscopy (SEM) or atomic force microscopy (AFM) conducted on the used catalysts would provide information for the nature of surface coking.
- Performance of nitrogen sorption on the used catalysts could elucidate the real

effect of hydrocracking conditions on the textural properties of pillared clay catalysts.

Evidence from the XRD analysis of the used catalysts (similar low basal spacing) and the nitrogen sorption analysis of a chromia pillared montmorillonite subjected to hydrocracking conditions in the absence of feed (smaller surface area, larger mean pore size) suggest that the pillars collapse under these conditions. Hence:

- Performance of a series of hydrocracking runs at milder conditions (i.e. lower temperatures and/or pressures) followed by catalysts characterisation to assess the impact of the employed conditions on the catalysts aiming to identify the conditions at which the pillars collapse would be useful.

Whether the most active pillared clays represent an advantage over the commercial catalysts in terms of overall performance should be assessed over longer periods. In this respect it would be helpful to:

- Utilise a continuous reactor instead of the batch microbomb reactor used at Imperial College with higher amount of catalyst to conduct long hydrocracking runs in order to assess better catalytic activity.
- Perform elemental analysis in the processed feed to measure heteroatom removal.
- Consider catalyst regeneration due to the high level of coking in addition to develop catalysts that suffer from much lower levels of carbon deposition.

Although a range of catalysts with different structural properties was prepared, varying in preparation, nature of parent clay, nature of active metal, texture, etc., the selected hydrocracking reaction did not show any particular sensitivity to these factors. Therefore, it would be of particular interests to:

- Use the same catalysts in shape-selective reactions to investigate the effect of structure upon catalytic performance.
- Employ the same catalysts in the field of other acid-catalysed reactions, such as cracking, hydroisomerisation, dehydration, dehydrogenation, hydrogenation, aromatisation, disproportionation, esterification, alkylation and selective catalytic reduction. These reactions usually employ milder conditions than those in the hydrocracking reactor (i.e. 440°C and 190 bar).

During the study of bio-oil's decomposition it was shown that rate constants can be calculated from data of final pressure, average molecular weight and water content versus hold time. Very limited work has previously been done on assigning kinetic parameters to the effect of heating on bio-oil [86]. This could be useful both as a general approach and as a means of systematising experimental information. Therefore there is a need to refine the technique and its results and demonstrate their reproducibility and limitations. In this respect it would be useful to:

- Perform a series of runs at different hold times for each irradiation temperature to calculate more accurately the rate constants of bio-oil decomposition and assess reproducibility.

The presence of char during microwave irradiation at 125°C influenced bio-oil's water content and average molecular weight. Char originating from switchgrass led to slightly higher water content and average molecular weight than char from beech, probably due to its higher catalytic activity, which is attributed to its higher ash and alkali metal content. However, those differences were minor, of the order of magnitude of experimental error. Therefore:

- Performance of a series of microwave runs to investigate the effect of char content and origin on bio-oil at temperatures higher than 125°C would be recommended. It is possible that the catalytic effect of char is stronger at higher temperatures.

Bio-oil irradiated in the presence of a range of catalysts exhibited an increase in its average molecular weight compared to the respective from the blank run (bio-oil only), indicating that the condensation and polymerisation reactions, which are responsible for the formation of higher molecular weight species in bio-oil, are enhanced by these catalysts. In this respect:

- Performance of a series of bio-oil and catalyst runs conducted in the presence of tetralin (hydrogen donor) to investigate whether any deoxygenation takes place would be of interest.
- Performance of a series of bio-oil catalytic hydrotreating runs in the developed microwave reactor to assess the potential of bio-oil upgrading under microwave irradiation would be helpful.

REFERENCES

1 EPSRC final report, New Catalysts for the Hydrocracking of High RMM Fractions of Coal Derived Liquids and of Heavy Hydrocarbon Liquids, GR/R27464/01 and GR/R27471/01.

2 S.D. Bodman, W.R. McWhinnie, V. Begon, I. Suelves, M.-J. Lazaro, T.J. Morgan, A.A. Herod, R. Kandiyoti, Metal-ion pillared clays as hydrocracking catalysts (I): Catalyst preparation and assessment of performance at short contact times, *Fuel*, **81**, 2002, 449-459.

3 S.D. Bodman, W.R. McWhinnie, V. Begon, M. Millan, I. Suelves, M.-J. Lazaro, A.A. Herod, R. Kandiyoti, Metal-ion pillared clays as hydrocracking catalysts (II): effect of contact time on products from coal extracts and petroleum distillation residues, *Fuel* , **82**, 2003, 2309-2321.

4 S.D. Bodman, Novel Catalytic Methods for the Upgrading of Coal Liquids, PhD Thesis, Aston University, 1999

5. Z. Ding, J.T. Kloprogge, R.L. Frost, Porous clays and pillared clays-based catalysts. Part 2: A review of the catalytic and molecular sieve applications, *J. Porous Mat.*, **8**, 2001, 273-293.

6. E. Kikuchi, T. Matsuda, Shape selective acid catalysis by pillared clays, in R. Burch (Ed.), Catal. Today, Pillared Clays, Elsevier, 1988, 2 (no. 2-3), p. 297.

7. S. Cheng, From layer compounds to catalytic materials, *Catal. Today*, **49**, 1999, 303-312.

8 A.V. Bridgwater, Catalysis in thermal biomass conversion, *Appl. Catal. A*, **119**, 1994, 5-47.

9 Glossary of Clay Terms, Virginia Division of Mineral Resources, Department of Mines, Minerals and Energy
http://www.mme.state.va.us/DMR/DOCS/MinRes/CLAY/glos.html

10 C.J.B. Mott, Clay minerals an introduction. In: Catalysis Today, Pillared Clays, R. Burch (Ed), Elsevier, 1988, 2 (no. 2-3), pp. 199-208.

11 I.E. Odom, Smectite clay minerals: properties and uses, *Phil. Trans. R. Soc. Lond.* A **311**, 1984, 391-409.

12 G.W. Brindley, G. Brown, Crystal structures of clay minerals and their X-ray identification, London, Mineralogical society, 1980.

13 J.T. Kloprogge, Synthesis of smectites and porous pillared clay catalysts: A review, *J. Porous Mat.*, **5**, 1998, 5-41.

14 S.W. Bailey, Reviews in Mineralogy, Vol. 19, Hydrous Phyllosilicates (Exclusive of Micas), Mineralogical Society of America, 1988.

15 F.J. Berry, M.S. Beevers, S.P. Bond, W.R. McWhinnie, Tin-119 mössbauer spectroscopic studies of novel tin oxide pillared clays, *Hyperfine Interact.*, **68**, 1991, 181-184.

16 T.J. Pinnavaia, Intercalated clay catalysts, *Science*, **220**, 1983, pp. 365-371.

17 H. van Olphen, J.J. Fripiat, Data handbook for clay materials and other non-metallic minerals, Pergamon Press, 1979.

18 H. van Olphen, An Introduction to Clay Colloid Chemistry, A Wiley-Interscience Publication, John Wiley and Sons Inc., 2nd Edition, 1977.

19 A. Vaccari, Clays and catalysis: a promising future, *Appl. Clay Sci.*, **14**, 1999, 161-198.

20 M.S. Tzou, T.J. Pinnavaia, Chromia pillared clays. In: Catalysis Today, Pillared Clays, Burch R (Ed), Elsevier, 1988, 2 (no. 2-3)

21 F. Figueras, Pillared clays as catalysts, *Catal. Rev.- Sci. Eng.*, **30 (3)**, 1988, 457-499.

22 D. Tichit, F. Figueras, Preparation and modification of the thermal stabilities and acidities of Al, Zr and Si pillared smectites. In: Pillared layered structures, Current trends and applications, Mitchell IV (Ed.), Elsevier Applied Science, London and New York, 1990, pp.149-158.

23 A. Sanchez, M. Montes, Influence of the preparation parameters (particle size and aluminium concentration) on the textural properties of Al-pillared clays for a scale up process, *Micropor. Mesopor. Mat*, **21**, 1998, 117-125.

24 G. Fetter, G. Heredia, L.A. Velazquez, A.M. Maubert, P. Bosch, Synthesis of aluminum-pillared montmorillonites using highly concentrated clay suspensions, *Appl. Catal. A*, **162**, 1997, 41-45.

25 S.L. Jones, The preparation and solution chemistry of Al(III) and Zr(IV) pillaring species. In: Catalysis Today, Pillared Clays, R. Burch (Ed), Elsevier, 1988, 2 (no. 2-3), pp. 209-217.

26 G.J.J. Bartley, Zirconium pillared clays. In: Catalysis Today, Pillared Clays, Burch R (Ed), Elsevier, 1988, 2 (no. 2-3), pp.233-241.

27 J. Sterte, Hydrothermal treatment of hydroxycation precursor solutions. In: Catalysis Today, Pillared Clays, Burch R (Ed), Elsevier, 1988, 2 (no. 2-3), pp. 219-231.

28 M.L. Occelli, Surface properties and cracking activity of delaminated clay catalysts, In: Catalysis Today, Pillared Clays, Burch R (Ed), Elsevier, 1988, pp.339-355.

29 D. Zhao, Y. Yang, X. Guo, Synthesis and characterization of hydroxy-CrAl pillared clays, *Zeolites*, **15**, 1995, 58-66.

30 M. Sychev, N. Kostoglod, E.M. van Oers, V.H.J. de Beer, R.A. van Santen, J. Kornatowski, M. Rozwadowski, Synthesis, characterisation and catalytic activity of chromia pillared clays. In: Catalysis by Microporous Materials, Studies in surface science and catalysis, H.K. Beyer, I. Kiricsi, J.B. Nagy (Eds.), Vol. 94, 1995 Elsevier Science, pp. 39-46.

31 S.M. Bradley, R.A. Kydd, Ga_{13}, Al_{13}, $GaAl_{12}$ and chromium pillared montmorillonites: Acidity and reactivity for cumene (C_9H_{12}) conversion, *J. Catal.*, **141**, 1993, 239-249.

32 T. Mishra, K. Parida, Transition metal pillared clay 4. A comparative study of textural, acidic and catalytic properties of chromia pillared montmorillonite and acid activated montmorillonite, *Appl. Catal. A: Gen.*, **166,** 1998, 123-133.

33 K.A. Carrado, S.L. Suib, N.D. Skoularikis, R.W. Coughlin, Chromium(III)-doped pillared clays, *Inorg. Chem.*, **25**, 1986, 4217-4221.

34 F. Gonzalez, C. Pesquera, I. Benito, S. Mendioroz, G. Poncelet, High conversion and selectivity for cracking of n-heptane on cerium-aluminium montmorillonite catalysts, *J. Chem. Soc., Chem. Commun.*, 1992, 491-493.

35 M.J. Hernando, C. Pesquera, C. Blanco, I. Benito, F. Gonzalez, Effect of Ce on catalytic properties of pillared montmorillonite with Al- and GaAl-polyoxocations, *Appl. Catal. A: Gen.*, **141**, 1996, 175-183.

36 A. De Stefanis, G. Perez, E. Illa, O. Ursini, A.A.G. Tomlinson, Conversions of resins and asphaltenes in porous catalysts, *J. Anal. Appl. Pyrolysis*, **57**, 2001, 37-44.

37 M.L. Occelli, R.J. Rennard, Hydrotreating catalysts containing pillared clays. In: Catalysis Today, Pillared Clays, Burch R (Ed.), Elsevier, 1988, pp.309-319.

38 C.E. Ramos-Galvan, G. Sandoval-Robles, A. Castillo-Mares, J.M. Dominguez, Comparison of catalytic properties of $NiMo/Al_2O_3$ with NiMo supported on Al-, Ti-pillared clays in HDS of residual oils, *Appl. Catal. A*, **150**, 1997, 37-52.

39 W.Q. Liu, L. Zhao, G.D. Sun, E.Z. Min, Saturation of aromatics and aromatization of C3 and C4 hydrocarbons over metal loaded pillared clay catalysts, *Catal. Today*, **51**, 1999, 135-140.

40 A. Louloudi, N. Papayannakos, Hydrogenation of benzene on Ni/Al-pillared montmorillonite catalysts, *Appl. Catal A*, **204**, 2000, 167-176.

41 R. Issaadi, F. Garin, C.E. Chitour, G. Maire, Catalytic behaviour of combined palladium-acid catalysts: use of Al and Zr-pillared montmorillonite as supports Part I. Reactivity of linear, branched and cyclic hexane hydrocarbons, *Appl. Catal A*, **207**, 2001, 323-332.

42 A.C. Metaxas, R.J. Meredith, Industrial Microwave Heating, IEE Power Engineering Series 4, Peter Peredrinus Ltd., London, UK, 1983.

43 B. L. Hayes PhD, Microwave Synthesis, Chemistry at the speed of light, CEM publishing, 2002.

44 C.R. Strauss, R.W. Trainor, Invited Review. Developments in Microwave-Assisted Organic Chemistry, *Aust. J. Chem.*, **48**, 1995, 1665-1692.

45 F. Chemat, E. Esveld, Microwave Assisted Heterogeneous and Homogeneous Reactions, Fifth International Electronic Conference on Synthetic Organic Chemistry (ECSOC-5), http://www.mdpi.org/ecsoc-5.htm, 1-30 September 2001.

46 D.R. Baghurst, D.M.P. Mingos, Superheating effects associated with microwave dielectric heating, *J. Chem. Soc., Chem. Commun.*, 1992, 675-677.

47 G.I. Ghin, Y.K. Yeo, B.W. Jo , H.Y. Kim, V.V. Levdansky, Analysis on effects of microwave heating in porous catalysts, *J. Chem. Eng. Jpn.*, **34**, 2001, 1567-1574..

48 S. Leskovsek, A. Smidovnik, T. Koloini, Kinetics of catalytic transfer hydrogenation of soybean oil in microwave and thermal field, *J. Org. Chem.*, **59**, 1994, 7433-7436.

49 R.N. Gedye, F.E. Smith, K.C. Westaway, The rapid synthesis of organic compounds in microwave ovens, *Can. J. Chem.*, **66**, 1988, 17-26.

50 P.S. Sai Prasad, N. Lingaiah, P. Kanta Rao, F.J. Berry, L.E. Smart, The influence of microwave heating on the morphology and benzene hydrogenation activity of alumina- and silica-supported palladium catalysts, *Catal. letters*, **35**, 1995, 345-351.

51 G. Roussy, S. Hilaire, J.M. Thiebaut, G. Maire, F. Garin, S. Ringler, Review Permanent change of catalytic properties induced by microwave activation on 0.3% Pt/Al2O3 (EuroPt-3) and on 0.3% Pt – 0.3% Re/Al2O3 (EuroPt-4), *Appl. Catal. A*, **156**, 1997, 167-180.

52 G. Fetter, G. Heredia, A.M. Maubert, P. Bosch, Synthesis of Al-intercalated montmorillonites using microwave irradiation, *J.Mater.Chem.*, **6** (11), 1996, 1857-1858.

53 G. Fetter, V. Hernandez, V. Rodriguez, M.A. Valenzuela, V.H. Lara, P. Bosch, Effect of microwave irradiation time on the synthesis of zirconia-pillared clays, *Mater. Letters*, **57**, 2003, 1220-1223.

54 M.J. Martinez-Ortiz, G. Fetter, J.M. Dominguez, J.A. Melo-Banda, R. Ramos-Gomez, Catalytic hydrotreating of heavy vacuum gas oil on Al- and Ti-pillared clays prepared by conventional and microwave irradiation methods, *Micropor. Mesopor. Mat.*, **58**, 2003, 73-80.

55 R.C. Ashcroft, S.P. Bond, M.S. Beevers, M.A.M. Lawrence, A.Gelder, W.R. McWhinnie, 119Sn Mossbauer and X-ray photoelectron studies of novel tin oxide pillared laponite formed under ambient conditions from aryltin precursors. Rapid intercalation reactions using microwave heating, *Polyhedron*, **11** (9), 1992, 1001-1006.

56 A.K. Bose, B.K. Banik, K.J. Barakat, M.S. Manhas, Simplified rapid hydrogenation under microwave irradiation- Selective transformation of beta-lactams, *Synlett*, **8**, 1993, 575-576.

57 B. Dayal, N.H. Ertel, K.R. Rapole, A. Asgaaonkar, G. Salen, Rapid hydrogenation of unsaturated sterols and bile alcohols using microwaves, *Steroids*, **62**, 1997, 451-454.

58 M.E. Gordon, D.C. Gaba, K.A. Jebber, D.M. Zacharias, Catalytic transfer hydrogenation of benzaldehyde in a microwave oven, *Organometallics*, **12**, 1993, 5020-5022.

59 J.K.S. Wan, Microwave induced catalytic conversion of methane to ethylene and hydrogen, **US Patent 4,574,038**, 1986.

60 M.S. Ioffe, S.D. Pollington, J.K.S. Wan, High-power pulsed radio-frequency and microwave catalytic processes: Selective production of acetylenene from the reaction of methane over carbon, *J. Catal.*, **151**, 1995, 349-355.

61 D.H. Bradhurst, H.K. Worner, Evaluation of oil produced from the microwave retorting of Australian shales, *Fuel*, **75**, 1996, 285-288.

62 S.I. Al-Mayman, S.M. Al-Zahrani, Catalytic cracking of gas oils in electromagneticfields: reactor design and performance, *Fuel Process. Technol.*, **80**, 2003, 169– 182.

63 World Coal Institute - What is coal? http://www.worldcoal.org

64 P. Monsef-Mirzai, M. Ravindran, W.R. McWhinnie, P. Burchill, Rapid microwave pyrolysis of coal. Methodology and examination of the residual and volatile phases, *Fuel*, **74**, 1995, 20-27.

65 S. Bodman, P. Monsef-Mirzai, H. Manak, W.R. McWhinnie, Does microwave heating have a role in functional group reactions of coal?, *Fuel*, **76**, 1997, 1315-1318.

66 World Coal Institute / What is coal? / Coal characteristics / Types of coal http://www.worldcoal.org/pages/content/index.asp?PageID=99

67 S.-F. Zhang, B. Xu, S.A. Moore, A.A. Herod, R. Kandiyoti, Comparison of hydrocracking reactivities of coal extracts from a flowing-solvent reactor, a mini-bomb and a pilot plant, *Fuel*, **75**, 1996, 597–605.

68 S-F Zhang, B. Xu, A.A. Herod, G.M. Kimber, D.R. Dugwell, R. Kandiyoti, Effect of coal rank on hydrocracking reactivities of primary coal extracts prepared in a flowing-solvent reactor. The Argonne premium coal sample set, *Fuel*, **75**, 1996, 1557-1567.

69 V. Begon, A. Megaritis, M.-J. Lazaro, A.A. Herod, D.R. Dugwell, R. Kandiyoti, Changes in sample reactivity and catalyst deactivation during early stages of the hydrocracking of a coal extract, *Fuel*, **77**, 1998, 1261–1272.

70 S.C. Martin, C.E.Snape, Effect of precipitating some of the more intractable material from a hydrogen-donor solvent coal extract solution on its hydroprocessing behaviour, *Energy Fuels*, **12**, 1998, 1228-1234.

71 V. Begon, S.B. Warrington, A. Megaritis, E.L. Charsley, R. Kandiyoti, Composition of carbonaceous deposits and catalyst deactivation in the early stages of the hydrocracking of a coal extract, *Fuel*, **78**, 1999, 681–688.

72 S.M. Kovach, L.J. Castle, J.V. Bennett, J.T. Schrodt, Deactivation of hydrodesulfurisation catalysts under coal liquids - 2. Loss of hydrogenation activity due to adsorption of metallics, *Ind. Eng. Chem. Prod. Res. Dev.*, **17**, 1978, 62-67.

73 D.S. Thakur, M.G. Thomas, Catalyst deactivation during direct coal liquefaction – A review, *Ind. Eng. Chem. Prod. Res. Dev.*, **23**, 1984, 349-360.

74 Y. Yoshimura, K. Hayamiza, T. Sato, H. Shimada, A. Nishijima, The effect of toluene-insoluble fraction of coal on catalytic activities of a NiMo γ-Al_2O_3 catalyst in the hydrotreating of coal liquids, *Fuel. Proc. Technol.*, **16**, 1987, 55-69.

75 F.V. Stohl, H.P. Stephens, A comparative study of catalyst deactivation in integrated 2-stage direct coal liquefaction processes, *Ind. Eng. Chem. Res.*, **26**, 1987, 2466-2473.

76 D.L. Cillo, G.J. Stiegel, R.E. Tischer, N.K. Narain, Catalytic hydrotreatment of coal derived residua, *Fuel Process. Technol.*, **11**, 1985, 273-287.

77 W. Steedman, W. Kemp, M.A. Thomson, D.A. Scott, Comparative reactivities of coal asphaltenes during hydropyrolysis, *Fuel*, **64**, 1985, 1379-1382.

78 W. Steedman, Coal asphaltenes – a review, *Fuel Process. Technol.*, **10**, 1985, 209-238.

79 W. Steedman, W. Kemp, M.A. Thomson, D.A. Scott, Asphaltenes and preasphaltenes in direct coal liquefaction – changes in heteroatom content, *Fuel Process. Technol.*, **15**, 1987, 341-350.

80 C. Song, K. Hanaoka, M. Nomura, Influence of pore structure and chemical properties of supported Mo catalysts on their performance in upgrading heavy coal liquids, *Energy Fuels*, **6**, 1992, 619-628.

81 C.S. Song, T. Nihonmatsu, M. Nomura, Effect of pore structure of $NiMo/Al_2O_3$ catalysts in hydrocracking of coal derived and oil sand derived asphaltenes, *Ind. Eng. Chem. Res.*, **30**, 1991, 1726-1734.

82 E. Furimsky, F.E. Masoth, Deactivation of hydroprocessing catalysts, *Catal. Today*, **52**, 1999, 381-495.

83 A.V. Bridgwater, Production of high grade fuels and chemicals from catalytic pyrolysis of biomass, *Catal. Today*, **29**, 1996, 285-295.

84 J. P. Diebold, S. Czernik, Additives to lower and stabilise the viscosity of pyrolysis oils during storage, *Energy Fuels*, **11**, 1997, 1081-91.

85 F.A. Agblevor, J. Scahill, D.K. Johnson, Pyrolysis char catalysed destabilisation of biocrude oils, AIChE 1997 National meeting Liquid fuels and fuel additives from biomass, paper no. 244a, unpublished.

86 S. Czernik, D.K. Johnson, S. Black, Stability of wood fast pyrolysis oil, *Biomass Bioenergy*, 7 (1-6), 1994, 187-192.

87 A. Oasmaa, S. Czernik, Fuel oil quality of biomass pyrolysis oils- state of the art for the end user, *Energy Fuels*, **13**, 1999, 914-921.

88 S. Yaman, Pyrolysis of biomass to produce fuels and chemical feedstocks, *Energy Convers. Manage.*, **45** (5), 2004, 651-671.

89 R.E. Maggi, D.C. Elliott, Upgrading overview. In Proceedings: Developments in Thermochemical Biomass Conversion, (Bridgwater AV and Boococke GB Eds), Blackie Acad. and Prof., 1997, pp. 575-588.

90 A.V. Bridgwater, Catalysis in thermal biomass conversion, *Appl. Catal. A*, **119**, 1994, 5-47.

91 D.C.Elliott, E.G. Baker, Hydrotreating biomass liquids to produce hydrocarbon fuels. In: Energy from Biomass and Wastes X, Klass DL (Ed), Elsevier Applied Science Publishers and Institute of Gas Technology, 1987, pp. 765-782.

92 E.G. Baker, D.C. Elliott, Catalytic upgrading of biomass pyrolysis oils. In: Research in Thermochemical Biomass Conversion, (Eds Bridgwater AV and Kuester JL), Elsevier Applied Science, 1988, pp. 883-895.

93 W. Baldauf, U. Balfanz, Upgrading of fast pyrolysis liquids at Veba Oel AG. In: Biomass gasification and pyrolysis: state of the art and future prospects, Kaltschmitt M, Bridgwater AV (Eds.), CPL Press, 1997, pp. 392-398.

94 D.C. Elliott, G.G. Neuenschwander, Liquid fuels by low severity hydrotreating of biocrude, In Proceedings: Developments in Thermochemical Biomass Conversion, (Ed. Bridgwater AV and Boococke GB), Blackie Acad. and Prof., 1997, pp. 611-621.

95 D.C. Elliott, Upgrading liquid products: Notes from the workshop at the international conference research in thermochemical biomass conversion. In: Research in Thermochemical Biomass Conversion, (Ed. Bridgwater AV and Kuester JL), Elsevier Applied Science, 1988, pp. 1170-1176.

96 E.J. Soltes, S.C.K. Lin, Hydrotreating of biomass tars for liquid engine fuels. In: Progress in Biomass Conversion, vol.5, Academic press, New York, 1984, p.1.

97 E.J. Soltes, S.C.K. Lin, Y.H.U. Sheu, Catalyst specificities in high pressure hydrotreating of pyrolysis and gasification tars. In: Production, analysis and upgrading of oils from biomass, Vorres KS (Ed.), *Am. Chem. Soc., Div. Fuel Chem. Abstracts*, **32** (2), 1987, 229-239.

98 E. Churin, R. Maggi, Characterisation and upgrading of a bio-oil produced by pyrolysis of biomass. In: Research in Thermochemical Biomass Conversion, (Ed. Bridgwater AV and Kuester JL), Elsevier Applied Science, 1988, pp. 896-909.

99 E. Churin, Upgrading of pyrolysis oils by hydrotreatment. In: Biomass pyrolysis liquids upgrading and utilization, Bridgwater AV, Grassi G (Eds.), Elsevier applied science, London and New York, pp. 103-117, 1991.

100 P. Grange, A. Centeno, R. Maggi, B. Delmon, Hydrotreating of pyrolysis oils: new catalytic systems. In: Thermal biomass processing: Bio-oil production & utilization, Bridgwater AV, Hogan EN (Eds.), CPL Press, 1996, pp.186-197.

101 A. Centeno, E. Laurent, B. Delmon, Influence of the support of CoMo sulfide catalysts and of the addition of potassium and platinum on the catalytic performances for the hydrodeoxygenation of carbonyl, carboxyl, and guaiacol-type molecules, *J.Catal.*, **154**, 1995, 288-298.

102 E. Laurent, B. Delmon, Feasibility of the partial and full hydrorefining of bio-oils produced by rapid thermal pyrolysis studies with model compounds. In: Biomass for Energy and Industry, 7th E.C. Conference, (Ed. Hall DO, Grassi G and Scheer H), Ponte Press, 1994, pp. 177-185.

103 E. Laurent, R. Maggi, B. Delmon, Partial and full hydrorefining of pyrolysis oils: Overview and feasibility assessment. In: Biomass for Energy, Environment, Agriculture and Industry, 8th E.C. Conference, (Ed. Chartier P, Beenackers AACM, Grassi G), Pergamon, 1995, vol.2, pp. 1485-1497.

104 L. Conti, G. Scano, J. Boufala, G. Trebbi, C. Rossi, Upgrading of pyrolysis oils from biomass in a bench-scale continuous plant. In: Biomass for Energy, Environment, Agriculture and Industry, 8th E.C. Conference, (Ed. Chartier P, Beenackers AACM, Grassi G), Pergamon, 1995, vol. 3, pp. 1901-1907.

105 L. Conti, G. Scano, J. Boufala, S. Mascia, Experiments of bio-oil hydrotreating in a continuous bench scale plant. In: Thermal biomass processing: Bio-oil

production & utilization, Bridgwater AV, Hogan EN (Eds.), CPL Press, 1996, pp. 198-205.

106 L. Conti, G. Scano, J. Boufala, S. Mascia, Bio-crude oil hydrotreating in a continuous bench-scale plant. In Proceedings: Developments in Thermochemical Biomass Conversion, (Ed. Bridgwater AV and Boococke GB), Blackie Acad. and Prof., 1997, pp. 622-632.

107 D. Meier, A.V. Bridgwater, C. Di Blassi, W. Prins, Integrated chemicals and fuels recovery from pyrolysis liquids generated by ablative pyrolysis. In: Biomass gasification and pyrolysis: state of the art and future prospects, Kaltschmitt M, Bridgwater AV (Eds.), CPL Press, 1997, pp.516.

108 D. C. Elliott, L.J. Silva, Conceptual process design and cost estimate for a bio-oil hydrotreating plant, report to Aston University from Battelle Pacific Northwest Laboratories PNL, contract no. 18621.

109 M.C. Samolada, W. Baldauf, I.A. Vasalos, Production of a bio-gasoline by upgrading biomass flash pyrolysis liquids via hydrogen processing and catalytic cracking, *Fuel*, **77**, 1998, 1667-1675, 1998.

110 V. Kaloidas, C.A. Koufopanos, N.H. Gangas, N.G. Papayannakos, Scale-up studies for the preparation of pillared layered clays at 1 kg per batch level, *Microporous Mater.*, **5**, 1995, 97-106.

111 http://www.physics.nmt.edu/~raymond/classes/ph13xbook/node66.html

112 IUPAC, Definitions, terminology and symbols in colloid and surface chemistry, *J. Colloid Interface Chem.; Pure Appl. Chem.*, **31**, 1972, 578-638.

113 http://www.staff.ncl.ac.uk/a.j.fletcher/physisorption.htm

114 Quantachrome Instruments, NOVA Manual, High Speed Gas Sorption Analyzer Version 7.11, 2002.

115 The Basics of NMR, a hypertext book on nuclear magnetic resonance spectroscopy. Copyright © 1997 J.P. Hornak. www.cis.rit.edu/htbooks/nmr

116 I. Palinko, I. Kiricsi, Gy. Tasi, K. Varga, Thermal behaviour of montmorillonite pillared with different metal oxides, *J. Thermal Anal.*, **39**, 1993, 197-205.

117 T.J. Pinnavaia, M.S. Tzou, S.D. Landau, Pillared and delaminated clays containing chromium, **US Patent 4,665,045**, 1987.

118 T.J. Pinnavaia, M.S. Tzou, S.D. Landau, New chromia pillared clay catalysts, *J. Am. Chem. Soc.*, **107**, 1985, 4783-4785.

119 E. Booij, J. T. Kloprogge, J. A. R. van Veen, Large pore REE/Al pillared bentonites: Preparation, structural aspects and catalytic properties, *Appl. Clay Sci.* **11**, 1996, 155-162.

120 G. R. Rao, B.G. Mishra, A comparative UV–vis-diffuse reflectance study on the location and interaction of cerium ions in Al- and Zr-pillared montmorillonite clays, *Mater. Chem. Phys.*, **98**, 2005, 110-115.

121 C. Volzone, A.M. Cesio, Changes in OH-Cr-montmorillonite after heating in air and nitrogen atmospheres, *Mater. Chem. Phys.*, **79**, 2003, 98-102.

122 C. Volzone, Pillaring of different smectite members by chromium species (Cr-PILCs), *Micropor. Mesopor. Mat.*, **49**, 2001, 197-202.

123 I. Hannus, I. Palinko, K. Lazar, J.B. Nagy, I. Kiricsi, The chemical state of Sn in Sn montmorillonite; A multinuclear MAS NMR and ^{119}Sn Mössbauer spectroscopic study, *J. Mol. Struct.*, **349**, 1995, 179-182.

124 D. Petridis, T. Bakas, A. Simopoulos, N.H.J. Gangas, Pillaring of montmorillonite by organotin cationec complexes, *Inorg. Chem.*, **28**, 1989, 2439-2443.

125 G. Fetter, P.Salas, L.A. Velazquez, P. Bosch, Ce-Al-Pillared clays: Synthesis, characterization and catalytic performance, *Ind. Eng. Chem. Res.*, **39**, 2000, 1944-1949.

126 J.L. Valverde, P. Canizares, M.R. Sun Kou, C.B. Molina, Enhanced thermal stability of Al-pillared smectites modified with Ce and Al, *Clays Clay Miner.*, **48**, 2000, 424-432.

127 R.C. Ashcroft, Organometallic precursors for pillared clay synthesis, PhD Thesis, Aston University, 1993.

128 S.P. Bond, Interlamellar modification of smectite clays, PhD Thesis, Aston University 1991.

129 C. Mosser, L.J. Michot, F. Villieras, M. Romeo, Migration of cations in copper(II)-exchanged montmorillonite and laponite upon heating, *Clays Clay Miner.*, **45 (6)**, 1997, 789-802.

130 D.M. Kavanagh, Chemical and physical characterization of clay bodies, PhD Thesis, Aston University, 2001.

131 P. Canizares, J.L. Valverde, M.R. Sun Kou, C.B. Molina, Synthesis and characterization of PILCs with single and mixed oxide pillars prepared from two diffrent bentonites. A comparative study, *Micropor. Mesopor. Mat.* **29,** 1999, 267-281.

132 C. Volzone, OH-Cr(III) in dioctahedral and trioctahedral smectites: texture and structure changes, *Mater. Chem. Phys.*, **47**, 1997, 13-16.

133 N. Maes, I. Heylen, P. Cool, E.F. Vansant, The relation between the synthesis of pillared clays and their resulting porosity, *Appl. Clay Sci.*, **12**, 1997, 43-60.

134 H.J. Chae, I.-S. Nam, S.W. Ham, S.B. Hong, Physicochemical characteristics of pillared interlayer clays, *Catal. Today*, **68**, 2001, 31-40.

135 M. Sychev, V.H.J. de Beer, R.A. van Santen, Chromia and chromium sulfide pillared clays differing in pillar density, *Microporous Mater.*, **8**, 1997, 255-265.

136 M.L. Occelli, Delaminated clays and their use in hydrocarbon conversion processes, **U.S. Patent 4,761,391**, 1988.

137 G. Engelhardt, D. Michel (Eds.), High Resolution Solid-State NMR of Silicates and Zeolites, John Wiley and sons, 1987.

138 M. Magi, E. Lippmaa, A. Samoson, G. Engelhardt, A.-R. Grimmer, Solid state high resolution Si-29 chemical shifts in silicates, *J. Phys. Chem.*, **88**, 1984, 1518-1522.

139 D.T.B. Tennakoon, W. Jones, J.M. Thomas, Structural aspects of metal-oxide-pillared sheet silicates. An investigation by magic-angle-spinning nuclear magnetic resonance, fourier-transform infrared spectroscopy and powder X-ray diffractometry, *J. Chem. Soc., Faraday Trans. 1*, 82(10), 1986, 3081.

140 M.L. Occelli, A. Auroux, G.J. Ray, Physicochemical characterization of a Texas montmorillonite pillared with polyoxocations of aluminum. II. NMR and microcalorimetry results, *Micropor. Mesopor. Mat.*, **39**, 2000, 43-56.

141 E. Oldfield, R.A. Kinsey, K.A. Smith, J.A. Nichols and R.J. Kirkpatrick, High resolution NMR of inorganic solids. Influence of magnetic centres on magic angle sample spinning lineshapes in some natural aluminosilicates, *J. Mag. Reson.*, **51**, 1983, 325-329.

142 W.E.E. Stone, The use of NMR in the study of clay minerals, in Developments in Sedimentology, 34, J.J. Fripiat (Ed.), Elsevier, Amsterdam, 1982.

143 I. K. Breakewell, Chemical Modification of Smectite Clays, PhD Thesis, Aston University, 1992.

144 A-P.S. Mandair, P.J. Michael, W.R. McWhinnie, ^{29}Si MASNMR investigations of the thermochemistry of laponite and hectorite, *Polyhedron*, **9**, 1990, 517-525.

145 EPSRC final report, New Catalysts for the Hydrocracking of High RMM Fractions of Coal Derived Liquids and of Heavy Hydrocarbon Liquids, GR/R27464/01 and GR/R27471/01.

146 Marcos Millan, Imperial College, personal communication, 2005.

147 M.E. Boucher, A. Chaala, H. Pakdel, C.Roy, Bio-oils obtained by vacuum pyrolysis of softwood bark as a liquid fuel for gas turbines. Part II: Stability and ageing of bio-oil and its blends with methanol and a pyrolytic aqeous phase, *Biomass Bioenergy*, **19**, 2000, 351-361.

148 B. Scholze, C. Hanser, D. Meier, Characterisation of the water-insoluble fractionfrom fast pyrolysis liquids (pyrolytic lignin) Part II. GPC, carbonyl groups, and 13C-NMR, *J. Anal. Appl. Pyrolysis*, **58-59**, 2001, 387-400.

149 P.Das, T. Sreelatha, A. Ganesh, Bio-oil from pyrolysis of cashew nut shell-characterisation and related properties, *Biomass Bioenergy*, 27, 2004, 265-275.

150 A.E. Pütün, E. Apaydin, E. Pütün, Bio-oil production from pyrolysis and steam pyrolysis of soybean-cake: product yields and composition, *Energy*, **27**, 2002, 703-713.

151 B. Scholze, D Meier, Characterisation of the water-insoluble fraction fro pyrolysis oil (pyrolytic lignin). Part I. Py-GC/MS, FTIR, and functional groups, *J. Anal. Appl. Pyrolysis*, **60**, 2001, 41-54.

152 D. C. Elliott, Water, alkali and char in flash pyrolysis oils, *Biomass Bioenergy*, 7 (1-6), 1994, 179-185.

Appendix 1

X-ray diffraction patterns

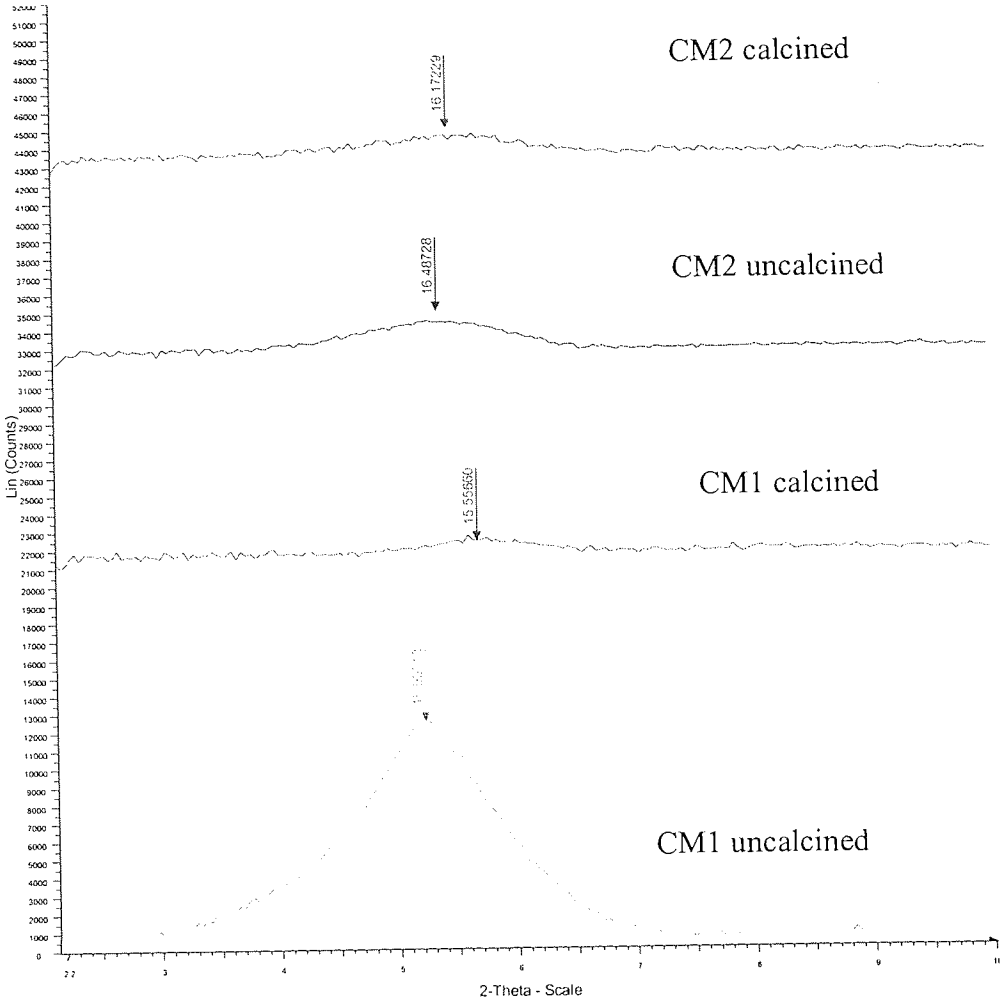

Figure 1.1 XRD patterns for chromia pillared montmorillonites CM1 and CM2

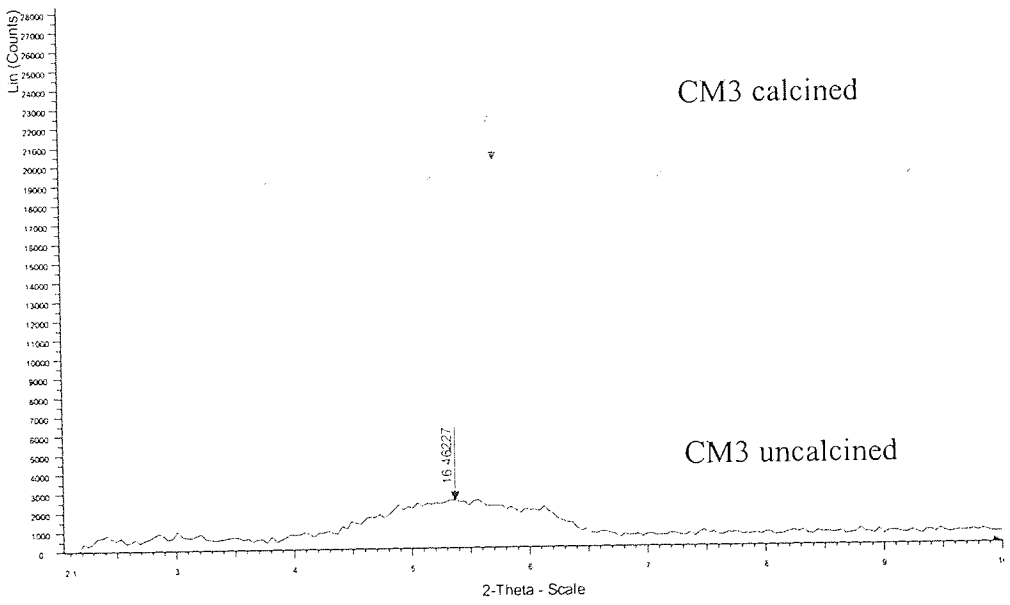

Figure 1.2 XRD patterns for chromia pillared montmorillonite CM3

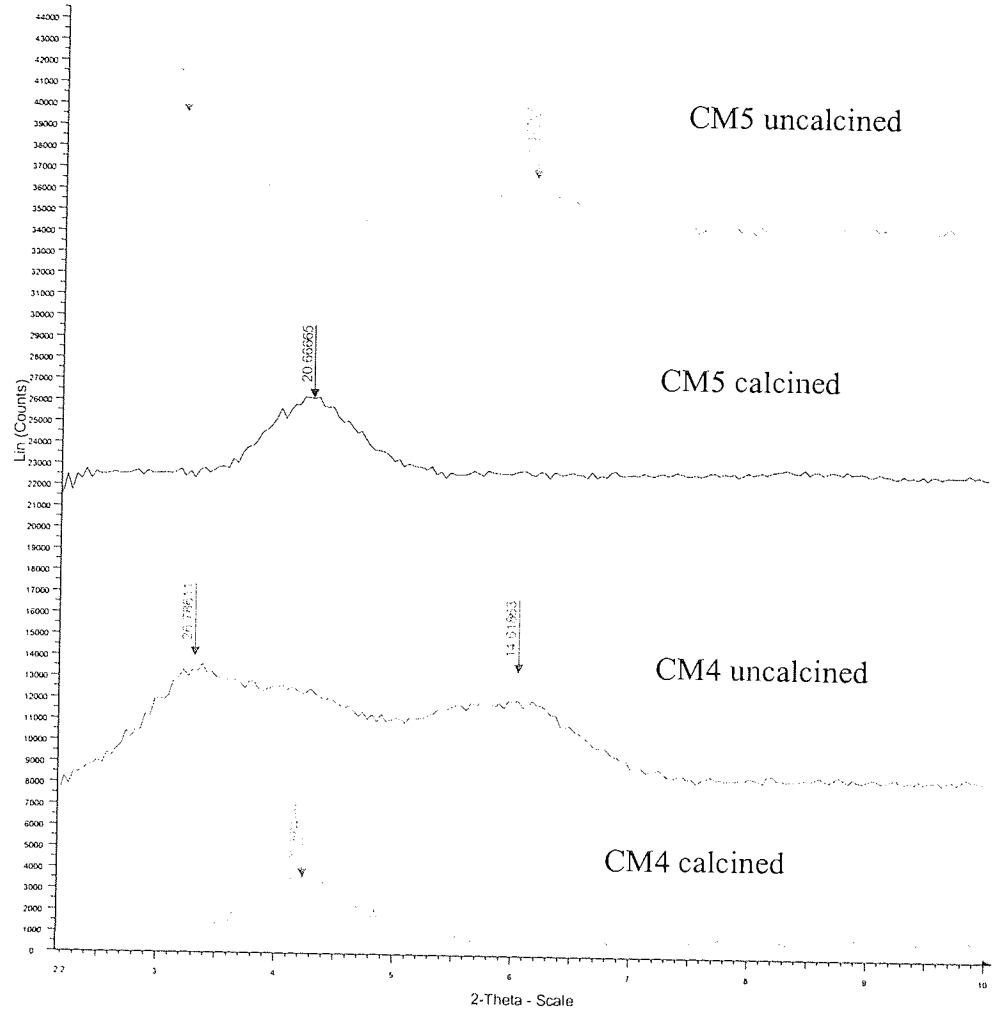

Figure 1.3 XRD patterns for chromia pillared montmorillonites CM4 and CM5

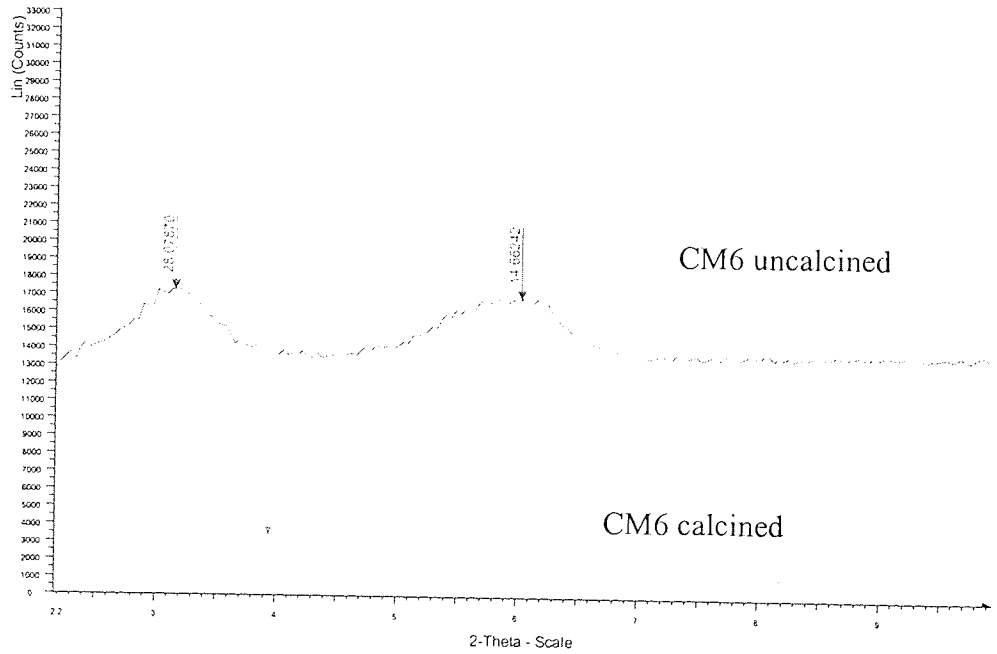

Figure 1.4 XRD patterns for chromia pillared montmorillonite CM6

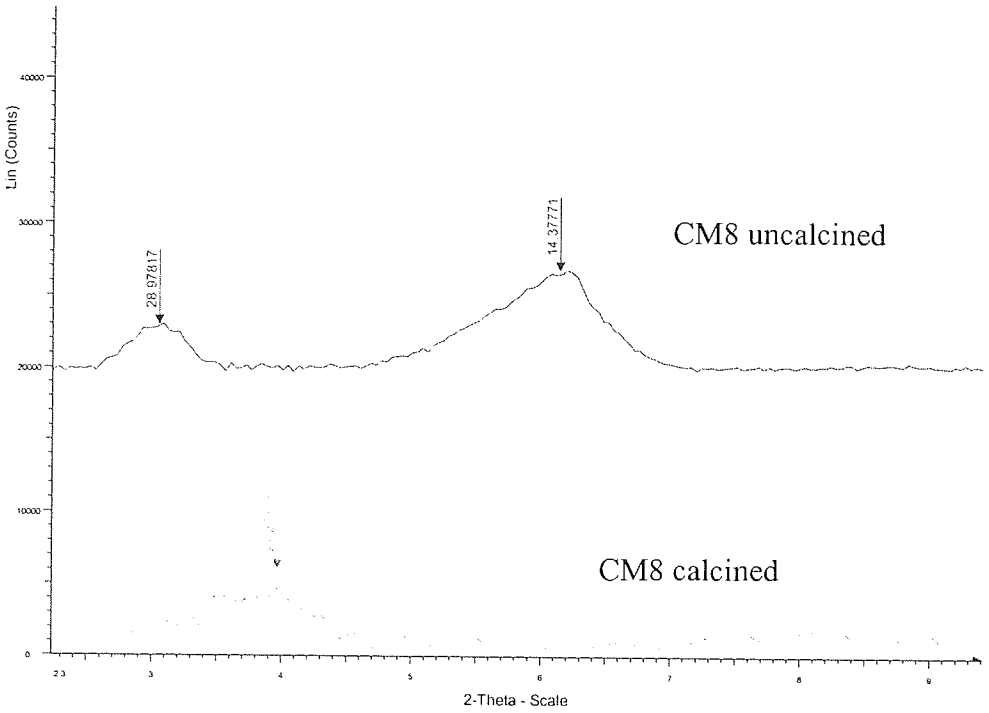

Figure 1.5 XRD patterns for chromia pillared montmorillonite CM8

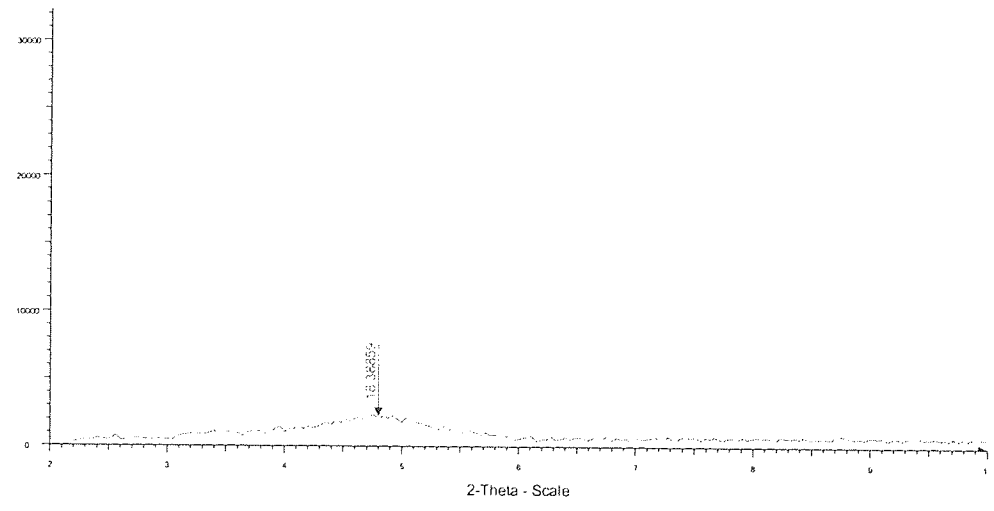

Figure 1.6 XRD pattern for chromia pillared montmorillonite CM13 (uncalcined)

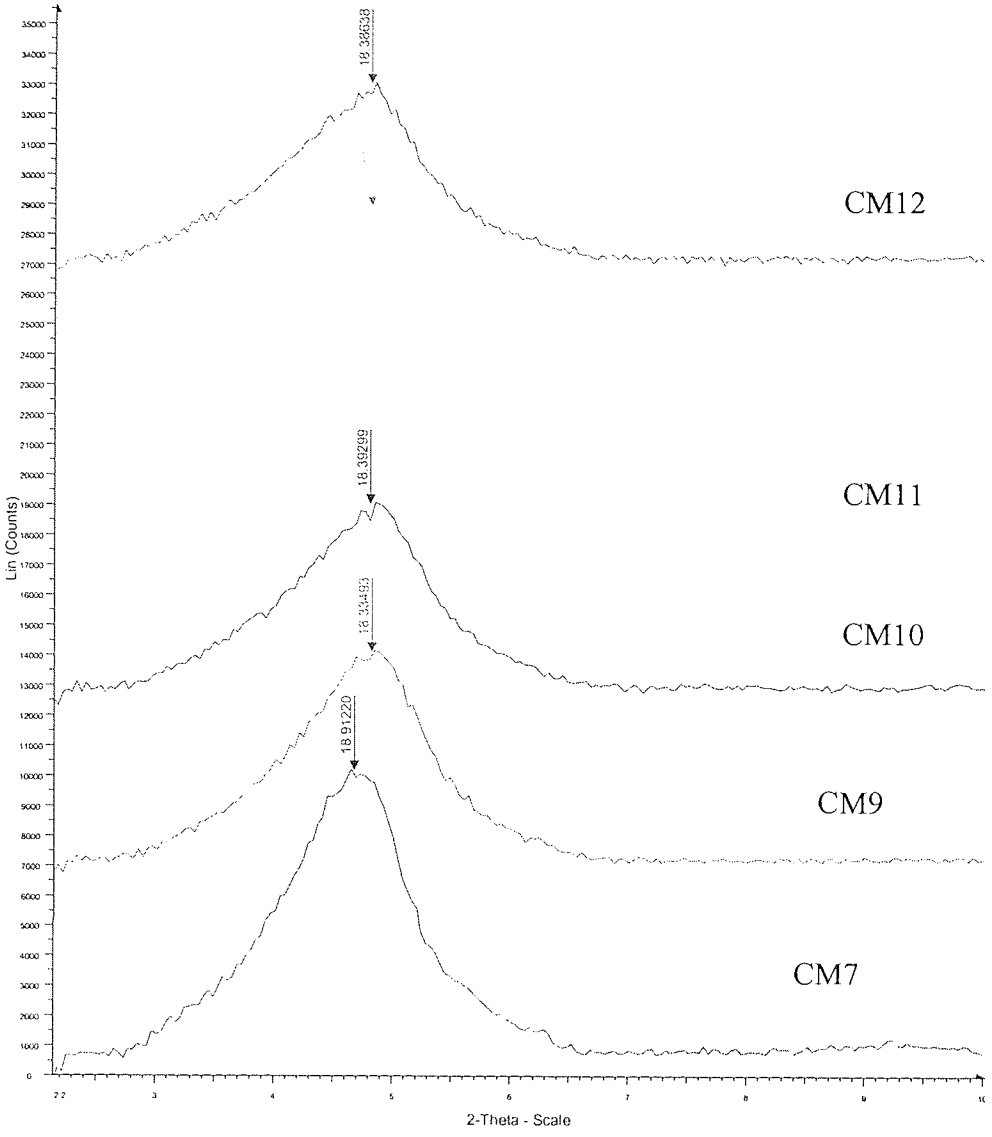

Figure 1.7 XRD patterns for uncalacined chromia pillared montmorillonites prepared via microwave irradiation CM7, CM9, CM10, CM11 and CM12

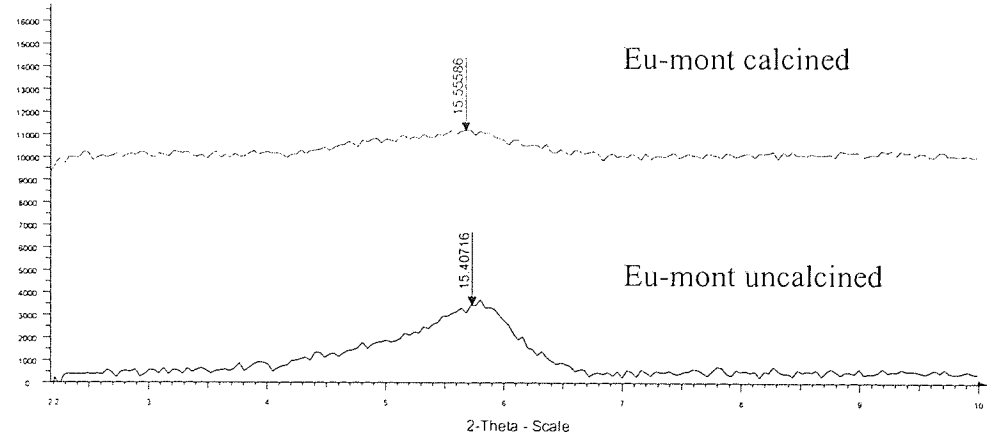

Figure 1.8 XRD patterns for europium pillared montmorillonite

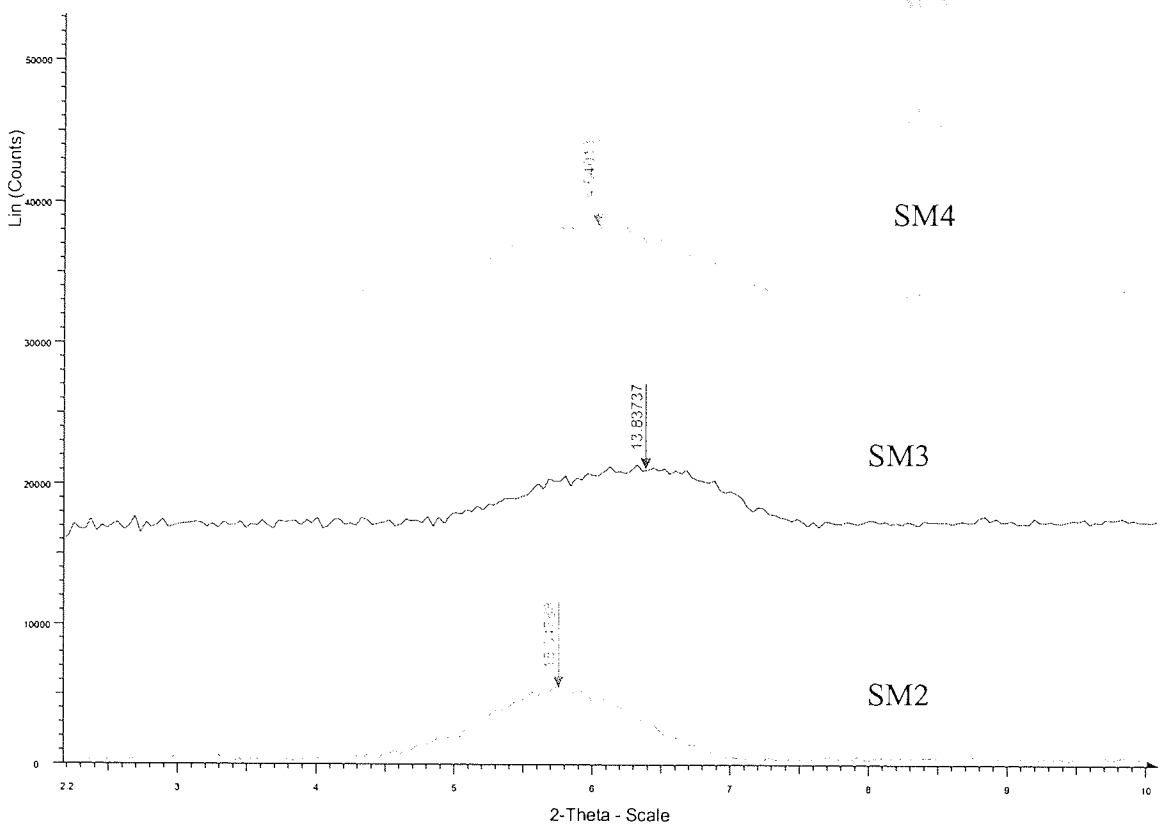

Figure 1.9 XRD patterns for tin oxide pillared montmorillonites (air-dried) SM2, SM3 and SM4

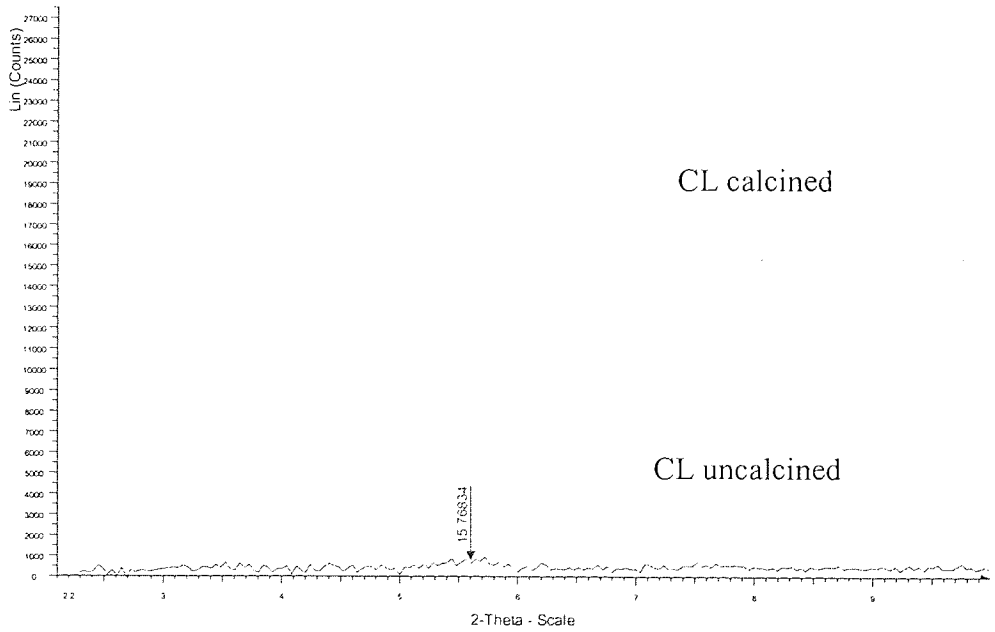

Figure 1.10 XRD patterns for chromia laponite

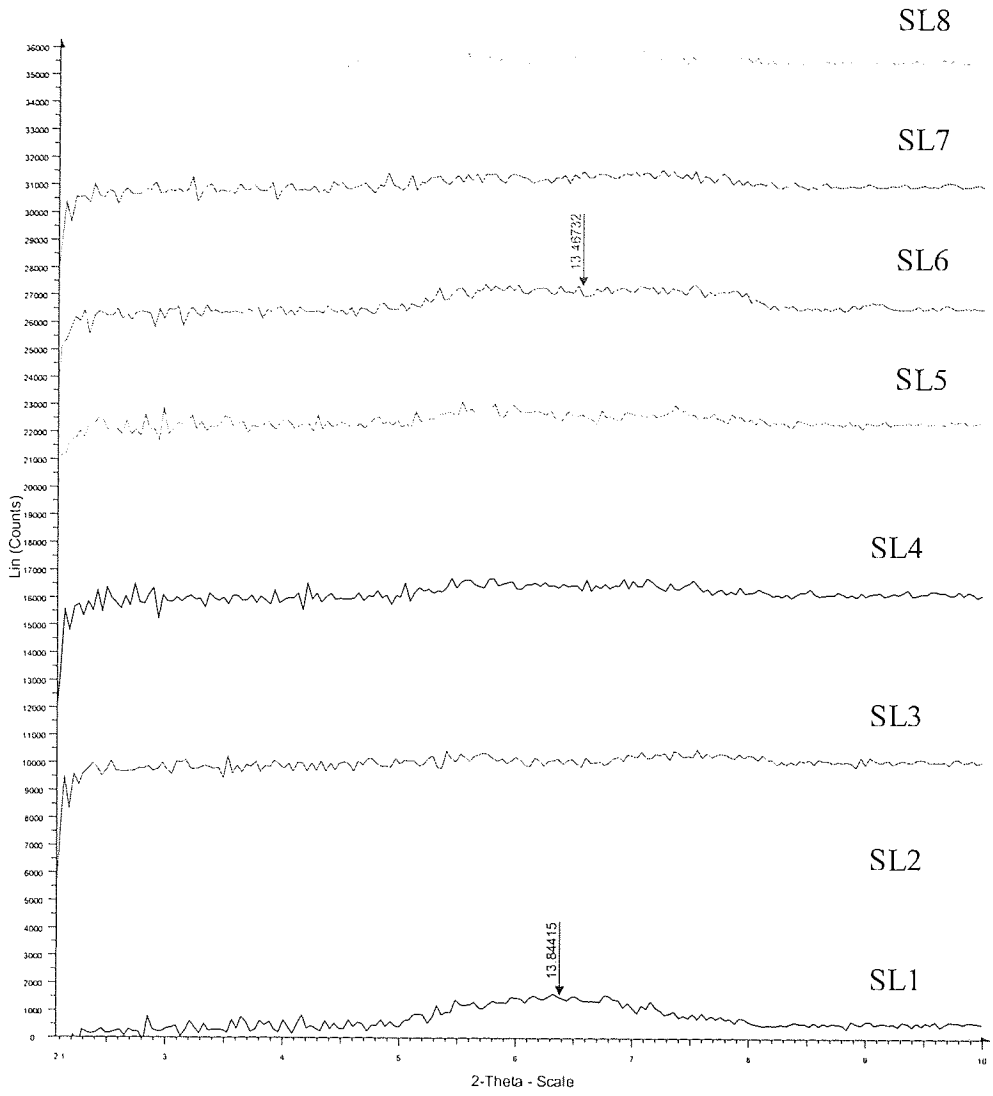

Figure 1.11 XRD patterns for tin laponites SL1 to SL8

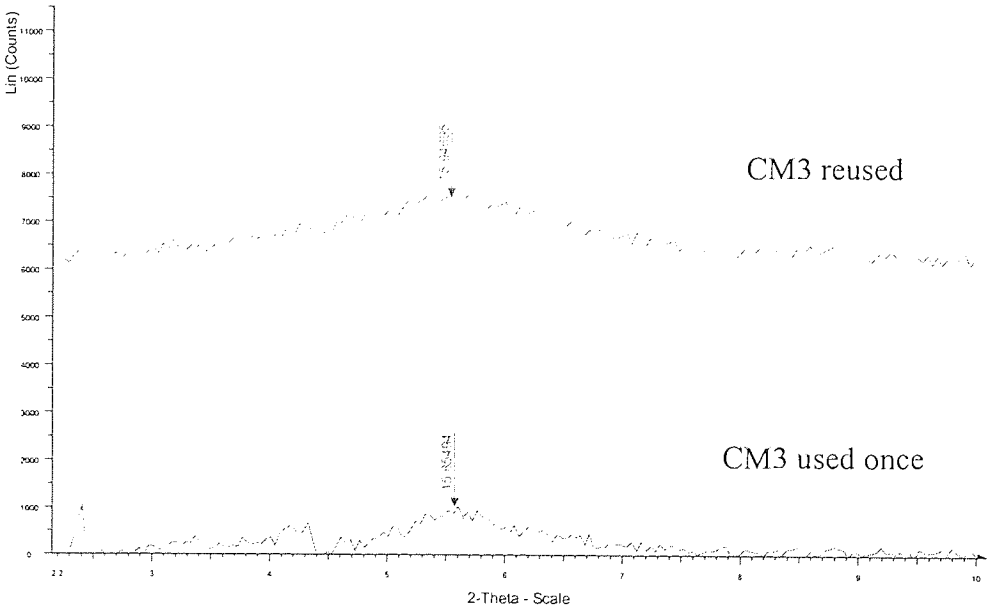

Figure 1.12 XRD patterns for chromia pillared montmorillonite CM3 after use

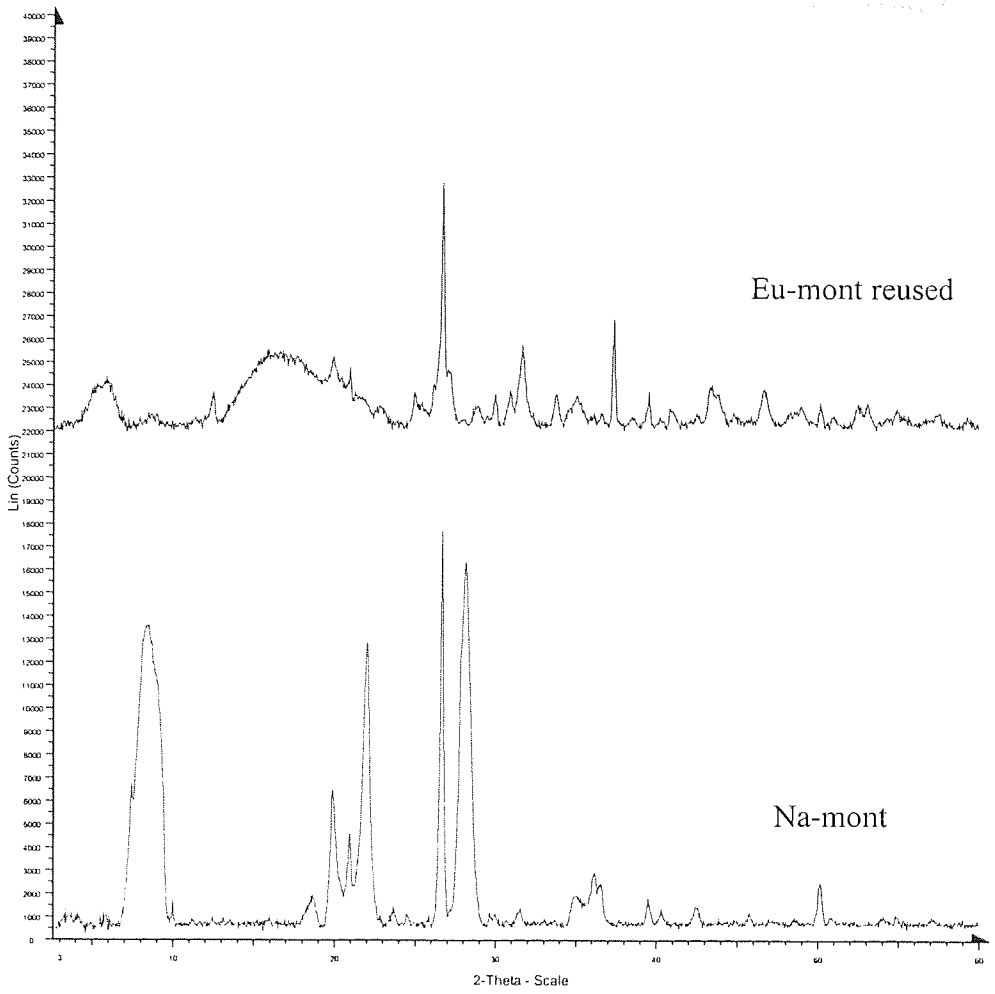

Figure 1.13 Long XRD scans for sodium montmorillonite and reused europium pillared montmorillonite

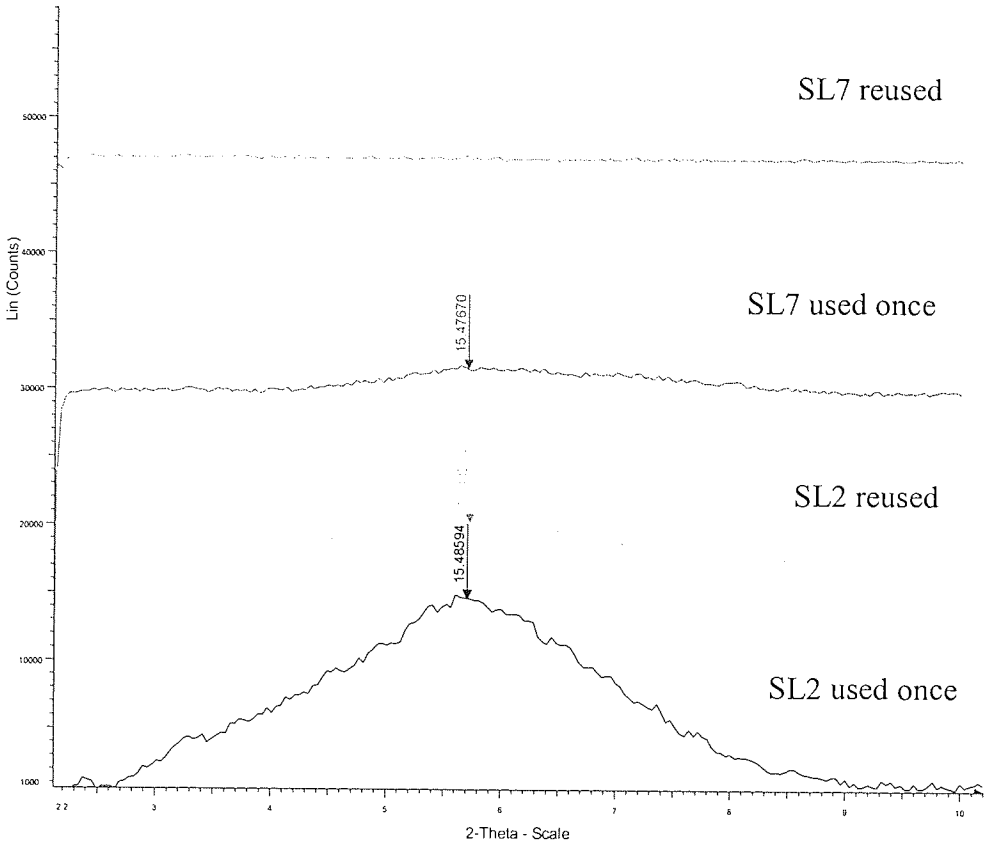

Figure 1.14 XRD patterns for tin laponites SL2 and SL7 after use

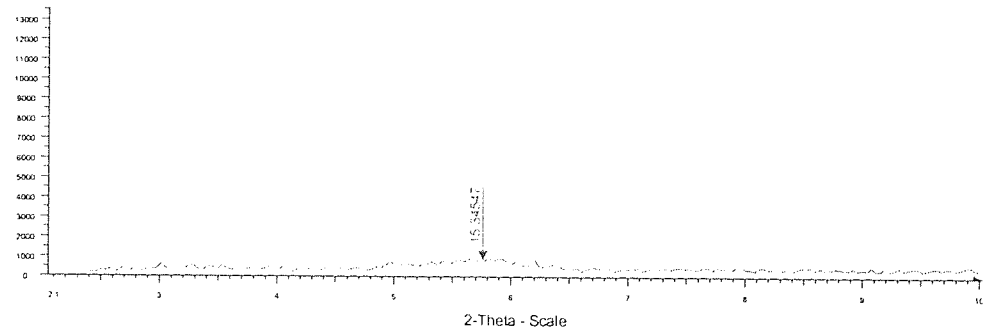

Figure 1.15 Blank XRD scan

Appendix 2

Mass balances of the hydrocracking runs in the microbomb reactor

Table 2.1 Mass balances for the hydrocracking runs with fresh montmorillonite based catalysts

Catalyst	Feed (mg)	Ash free feed (mg)	BP>450 (% of ash free feed)	BP>450 (mg)	Rec. product (mg)	BP>450 (% of rec. product)	BP>450 (mg)	Liquid conv/ion %	Rec. Cat. (mg)	Cat. Wt. Loss by TGA (%)	Cat. Wt. Loss (mg)	Total BP>450 (mg)	Total conv/ion %	Mass balance %
No catalyst	1064.8	1010.5	46.5	469.9	815.4	34	277.2	41.0	146.4*	64	93.7	370.9	21	90
Na-mont	1014	962.3	46.5	447.5	780.4	30.4	237.2	47.0	369.4	28	103.4	340.7	24	92
W.B.	1027.3	974.9	46.5	453.3	773.3	32.6	252.1	44.4	379.7	26	98.7	350.8	23	89
CM2b	1046.2	992.8	46.5	461.7	802.8	33.8	271.3	41.2	356.9	28.1	100.3	371.6	20	91
CM2c	1010.1	958.6	46.5	445.7	791.2	25.6	202.5	54.6	428.6	29.6	126.9	329.4	26	96
CM2d	1072.2	1017.5	46.5	473.1	813.9	32.9	267.8	43.4	412.2	25.6	105.5	373.3	21	90
CM3	1015.7	963.9	46.5	448.2	709.8	22.8	161.8	63.9	453.4	34.5	156.4	318.3	29	90
Cr-lap B14	1090.8	1035.2	46.5	481.4	786.4	31.7	249.3	48.2	401	30.6	122.7	372.0	23	88
Cr-mont B61	1088	1032.5	46.5	480.1	731.2	25.2	184.3	61.6	441.5	38.4	169.5	353.8	26	87
CM6	1096.1	1040.2	46.5	483.7	805.7	30.2	243.3	49.7	405.3	27.2	110.2	353.6	27	88
CM16	1010	958.5	46.5	445.7	722.6	30.9	223.3	49.9	413.7	29.4	121.6	344.9	23	88
Eu-mont	1079.3	1024.3	46.5	476.3	823.9	28.3	233.2	51.0	383.2	22.6	86.6	319.8	33	89
CM3	1025.2	972.9	46.5	452.4	751.6	28.3	212.7	53.0	389.4	26.7	104.0	316.7	30	88
Ce-Cr mont	1013	961.3	46.5	447.0	745.2	29.8	222.1	50.3	405.9	27.7	112.4	334.5	25	89
Ce-mont	1015.4	963.6	46.5	448.1	784.9	30.1	236.3	47.3	343.1	22.5	77.2	313.5	30	89

BP>450: boiling point higher than 450°C, Rec. product: recovered product, Rec. cat. : recovered catalyst, Cat. Wt. Loss: catalyst weight loss, Conv/ion.: conversion, * not catalyst, solids

Liquid conversion % = (Amount of BP>450°C in the feed – Amount of BP>450°C in the product) x 100 / Amount of BP>450°C in the feed

Catalyst weight loss %: determined by thermogravimetric analysis

Total conversion % = [(Amount of BP>450°C in the feed – (Amount of BP>450°C in the product + Cat. Wt. Loss)] x 100 / Amount of BP>450°C in the feed

Table 2.2 Mass balances for the hydrocracking runs with fresh laponite based catalysts and $NiMo/Al_2O_3$

Catalyst	Feed (mg)	Ash free feed (mg)	BP>450 (% of ash free feed)	BP>450 (mg)	Rec. product (mg)	BP>450 (% of rec. product)	BP>450 (mg)	Liquid conv/ion %	Rec. Cat. (mg)	Cat. Wt. Loss (%)	Cat. Wt. Loss (mg)	Total BP>450 (mg)	Total conv/ion %	Mass balance %
Laponite	1009.2	957.7	46.5	445.3	734.1	31.1	228.3	48.7	398.5	20.5	81.7	310.0	30	85
Laponite	1042.3	989.1	46.5	460.0	778.6	26.8	208.7	54.6	412.6	23.6	97.4	306.0	33	89
SL6a	1007.6	956.2	46.5	444.6	752.2	31	233.2	47.6	402.3	20.8	83.7	316.9	29	87
SL7a	993	942.4	46.5	438.2	719.3	27.4	197.1	55.0	378.1	21.4	80.9	278.0	37	85
SL5a	1001.7	950.6	46.5	442.0	773	31	239.6	45.8	385.3	24.2	93.2	332.9	25	91
SL9a	1079.7	1024.6	46.5	476.5	816.4	32	261.2	45.2	414.7	20.3	84.2	345.4	27	88
SL9b	1032.7	980.0	46.5	455.7	708.8	29.1	206.3	54.7	443.1	25.3	112.1	318.4	30	84
SL9c	1057.7	1003.8	46.5	466.7	725.8	30.7	222.8	52.3	431.3	34	146.6	369.5	21	87
SL2a	1029.8	977.3	46.5	454.4	545.7	34.4	187.7	58.7	438.1	42.7	187.1	374.8	18	75
SL3a	1108.7	1052.2	46.5	489.3	842.2	29.3	246.8	49.6	407.5	34.4	140.2	386.9	21	93
SL4a	1049.4	995.9	46.5	463.1	791.1	30.7	242.9	47.6	439.3	34.8	152.9	395.7	15	95
SL2b	1024	971.8	46.5	451.9	723.5	28.9	209.1	53.7	435.4	31.6	137.6	346.7	23	89
SL7b	1020.8	968.7	46.5	450.5	845.8	29.1	246.1	45.4	410.4	26.8	110.0	356.1	21	99
Sn-lap B71	1016.3	964.5	46.5	448.5	761.4	29.7	226.1	49.6	449.2	27.8	124.9	351.0	22	92
Cr-lap	1081.2	1026.1	46.5	477.1	811.2	27.1	219.8	53.9	422.1	29.2	123.3	343.1	28	91
NiMo	1019	967.0	46.5	449.7	759.8	26.7	202.9	54.9	333.3	25.7	85.7	288.5	36	87

Table 2.3 Mass balances for the hydrocracking runs with reused catalyst

Catalyst	Feed (mg)	Ash free feed (mg)	BP>450 (% of ash free feed)	BP>450 (mg)	Rec. product (mg)	BP>450 (% of rec. product)	BP>450 (mg)	Liquid conv/ion %	Rec. Cat. (mg)	Cat. Wt. Loss by TGA (%)	Cat. Wt. Loss (mg)	Total BP>450 (mg)	Total conv/ion %	Mass balance %
CM6	1039	986.0	46.5	458.5	840.1	33.3	279.8	39.0	320.8	8.9	28.6	308.3	33	88
CM3	1085.7	1030.3	46.5	479.1	863.8	29	250.5	47.7	314.9	4.4	13.9	264.4	45	85
SL7a	1027.7	975.3	46.5	453.5	943.1	23.5	221.6	51.1	381.7	36.6	139.7	361.3	20	111
SL2a	1062.5	1008.3	46.5	468.9	893.2	31.5	281.4	40.0	323.4	2.7	8.7	290.1	38	89
Na-mont	1083	1027.8	46.5	477.9	898.4	29.5	265.0	44.5	245.3	9.6	23.5	288.6	40	90
Eu-mont	1024.6	972.3	46.5	452.1	877.1	34.1	299.1	33.8	335.3	12.9	43.3	342.3	24	95
Ce-mont	1095.7	1039.8	46.5	483.5	880	31.4	276.3	42.9	395.8	13.9	55.0	331.3	31	90
Ce-Cr mont	1078	1023.0	46.5	475.7	820	30.8	252.6	46.9	363.2	13.4	48.7	301.2	37	85
WB	1054	1000.2	46.5	465.1	775.3	31.1	241.1	48.2	346.5	13.9	48.2	289.3	38	82
Laponite	1020.6	968.5	46.5	450.4	749.1	28.1	210.5	53.3	347.3	19.4	67.4	277.9	38	84
Cr-lap	1045.5	992.2	46.5	461.4	825.3	30.9	255.0	44.7	257.7	18.5	47.7	302.7	34	88
NiMo	1019.1	967.1	46.5	449.7	758.8	24.4	185.1	58.8	385.3	16.2	62.4	247.6	45	85

Appendix 3

Conversions versus catalysts' structural properties

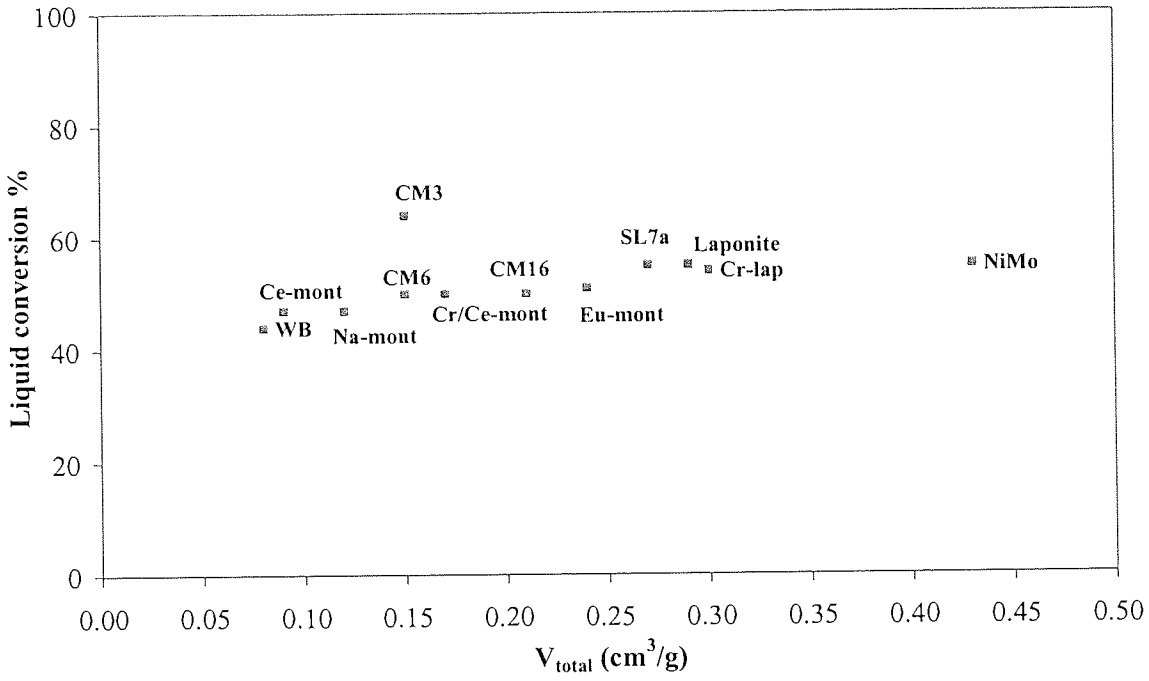

Figure 3.1 Liquid conversion % during 1st use versus catalysts' total pore volume (before use)

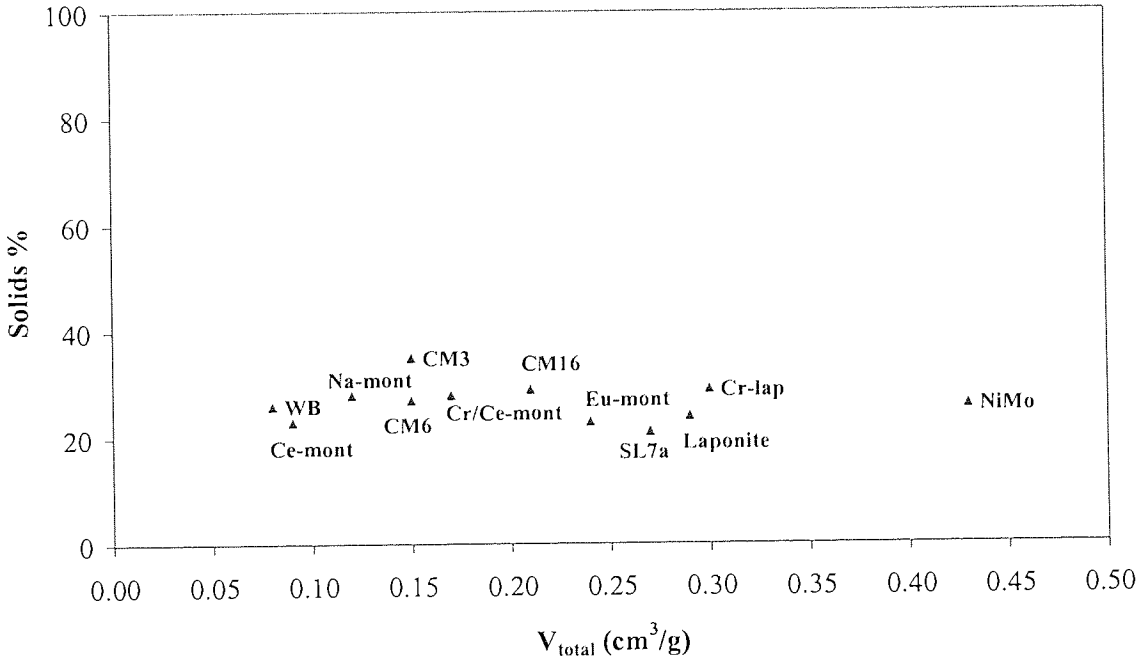

Figure 3.2 Solids % during 1st use versus catalysts' total pore volume (before use)

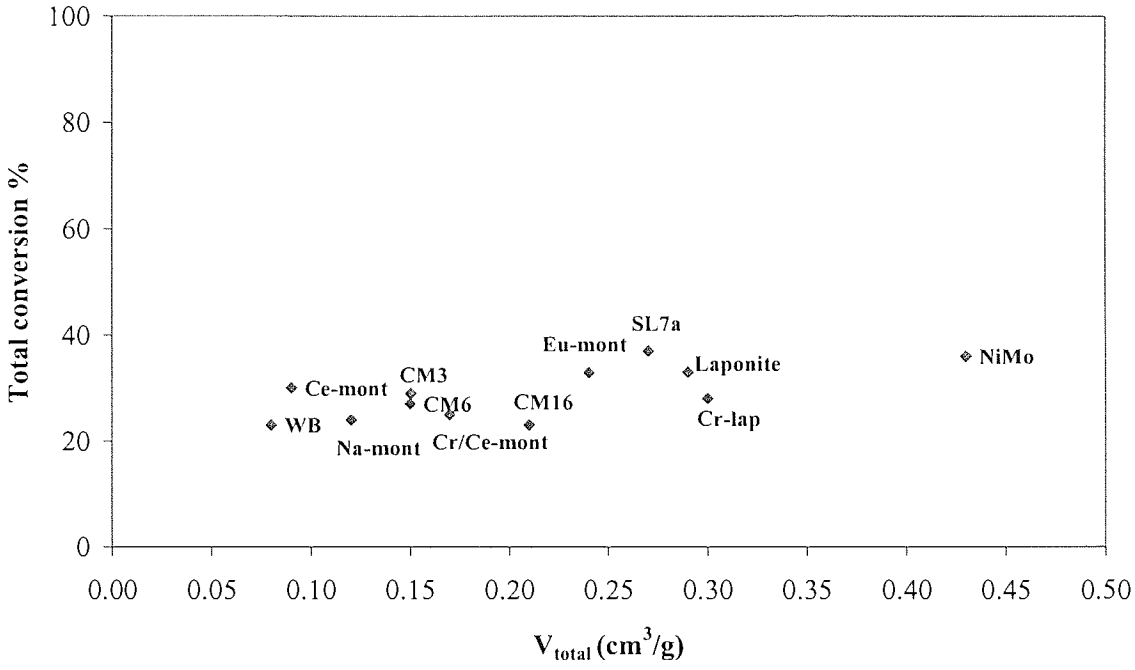

Figure 3.3 Total conversion % during 1st use versus catalysts' total pore volume (before use)

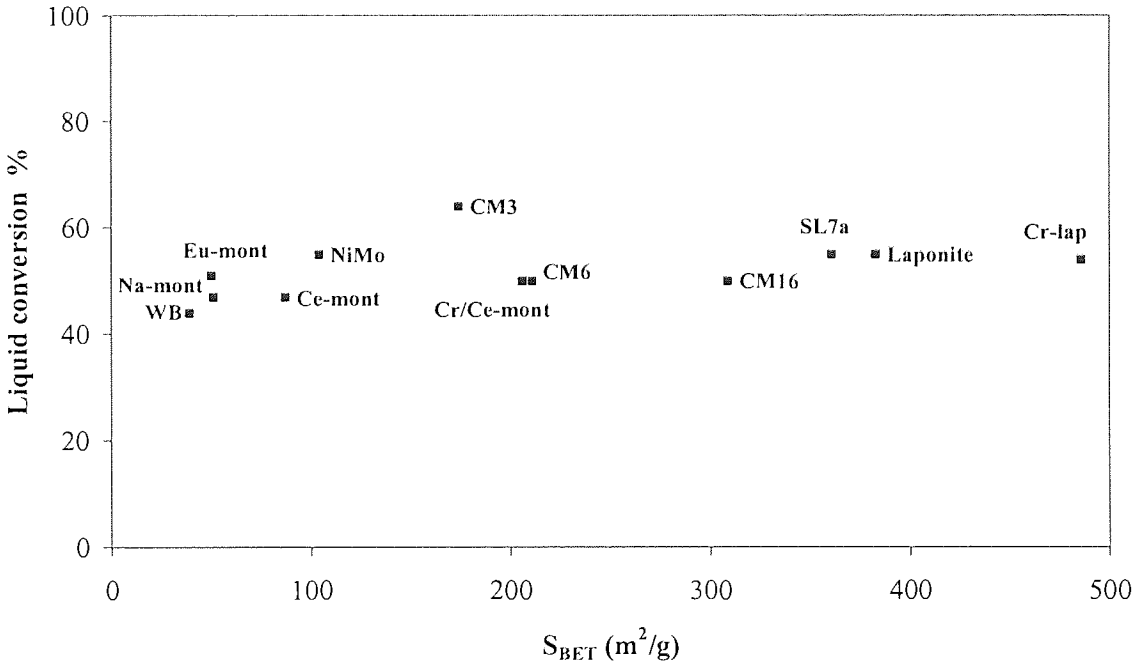

Figure 3.4 Liquid conversion % during 1st use versus catalysts' total (BET) surface area (before use)

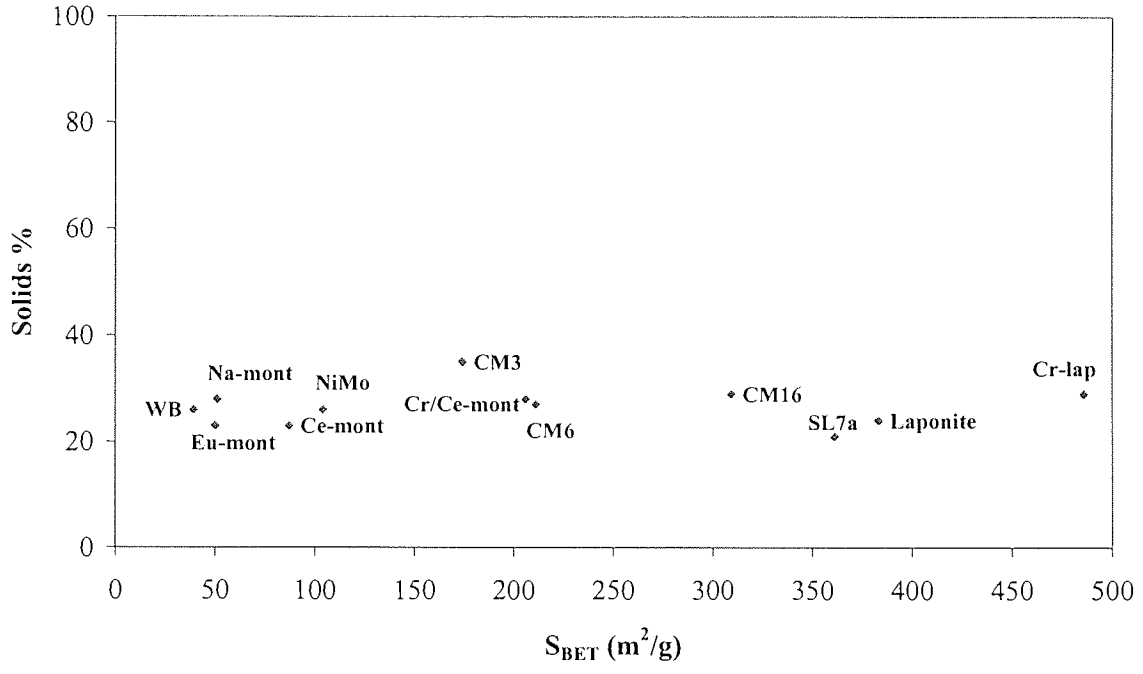

Figure 3.5 Solids % during 1st use versus catalysts' total (BET) surface area (before use)

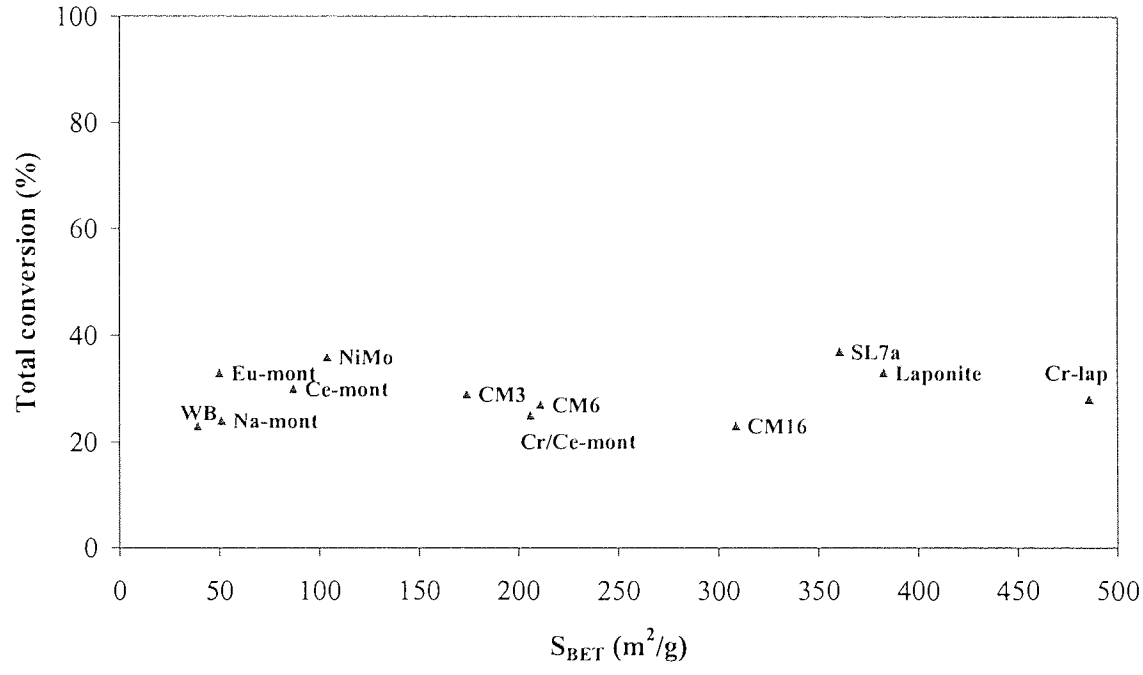

Figure 3.6 Total conversion % during 1st use versus catalysts' total (BET) surface area (before use)

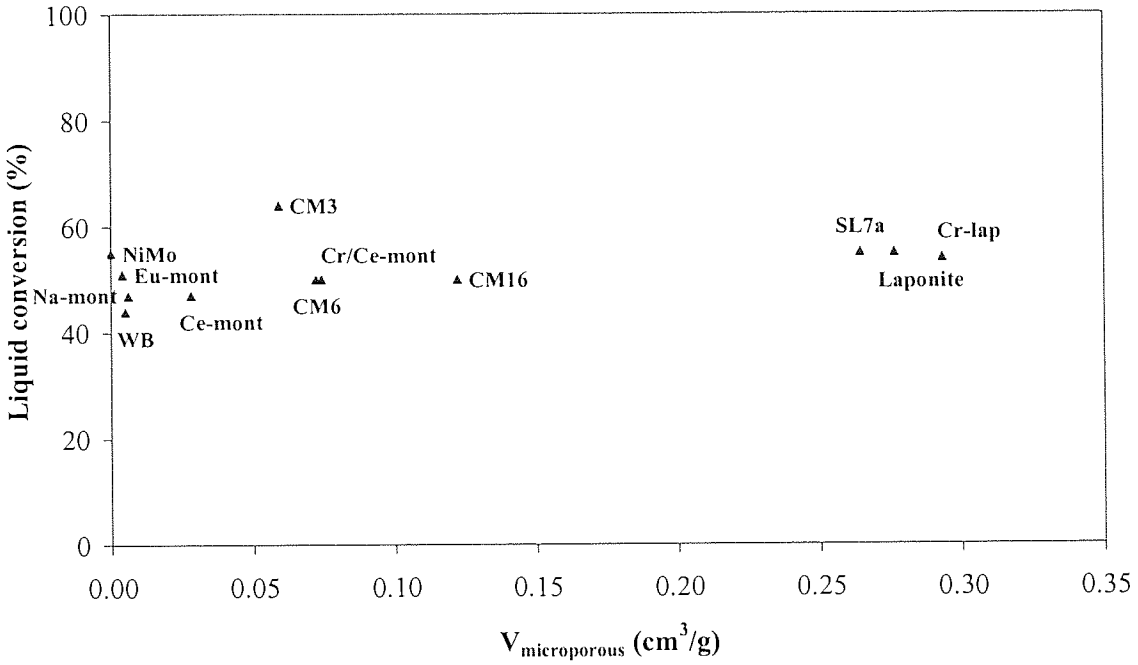

Figure 3.7 Liquid conversion % during 1st use versus catalysts' micropore volume (before use)

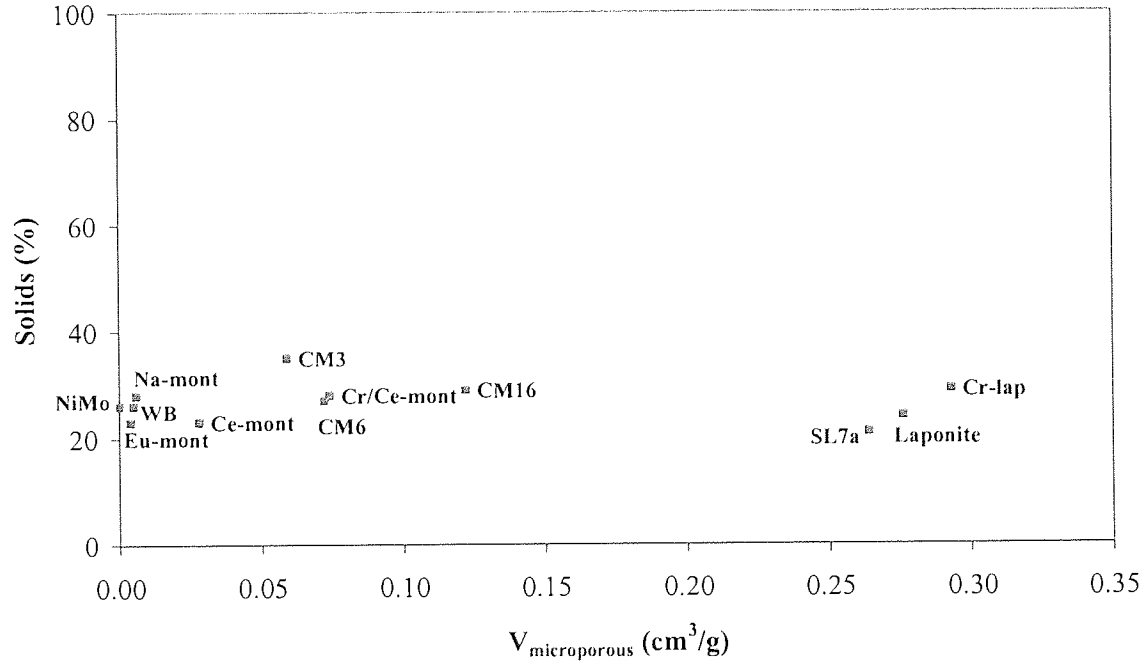

Figure 3.8 Solids % during 1st use versus catalysts' micropore volume (before use)

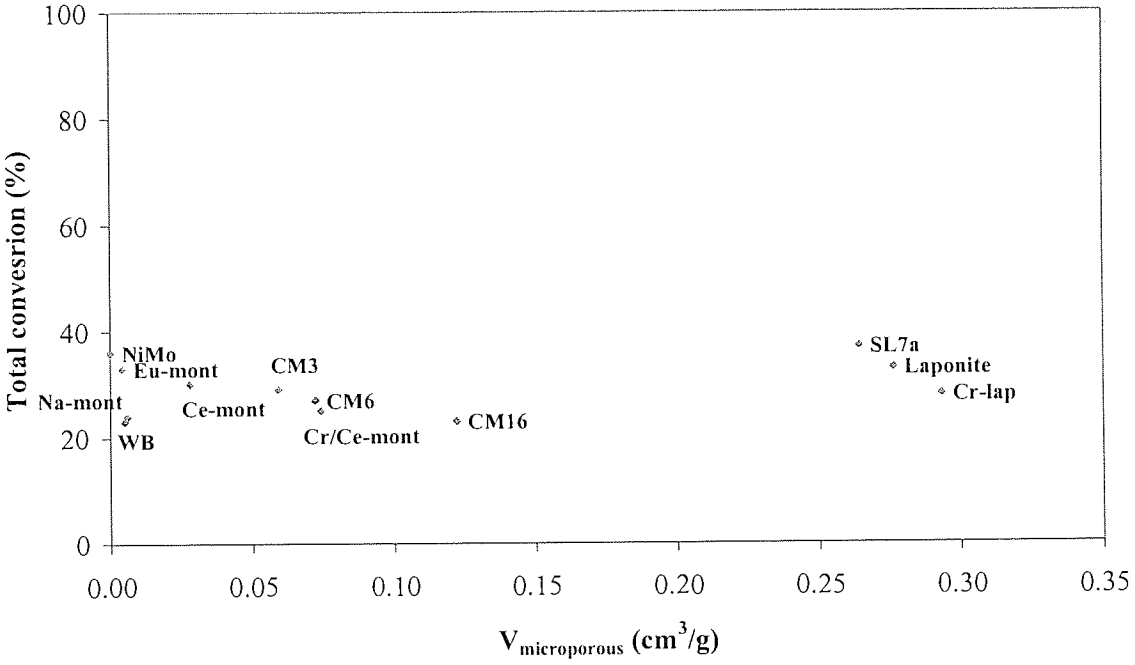

Figure 3.9 Total conversion % during 1st use versus catalysts' micropore volume (before use)

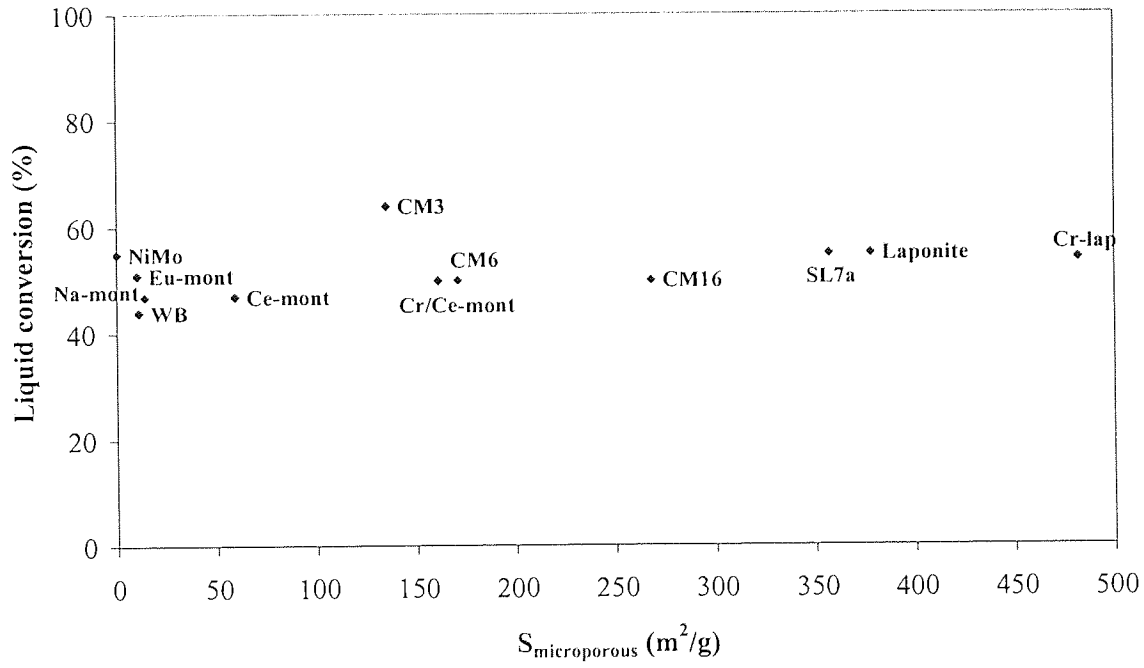

Figure 3.10 Liquid conversion % during 1st use versus catalysts' microporous surface area (before use)

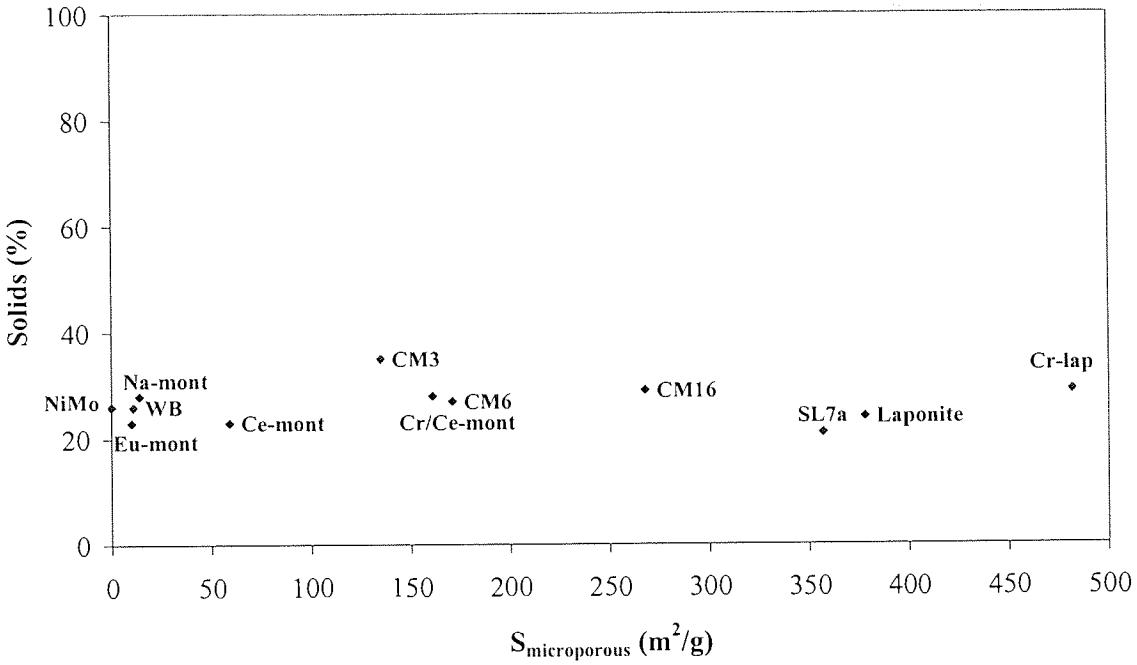

Figure 3.11 Solids % during 1st use versus catalysts' microporous surface area (before use)

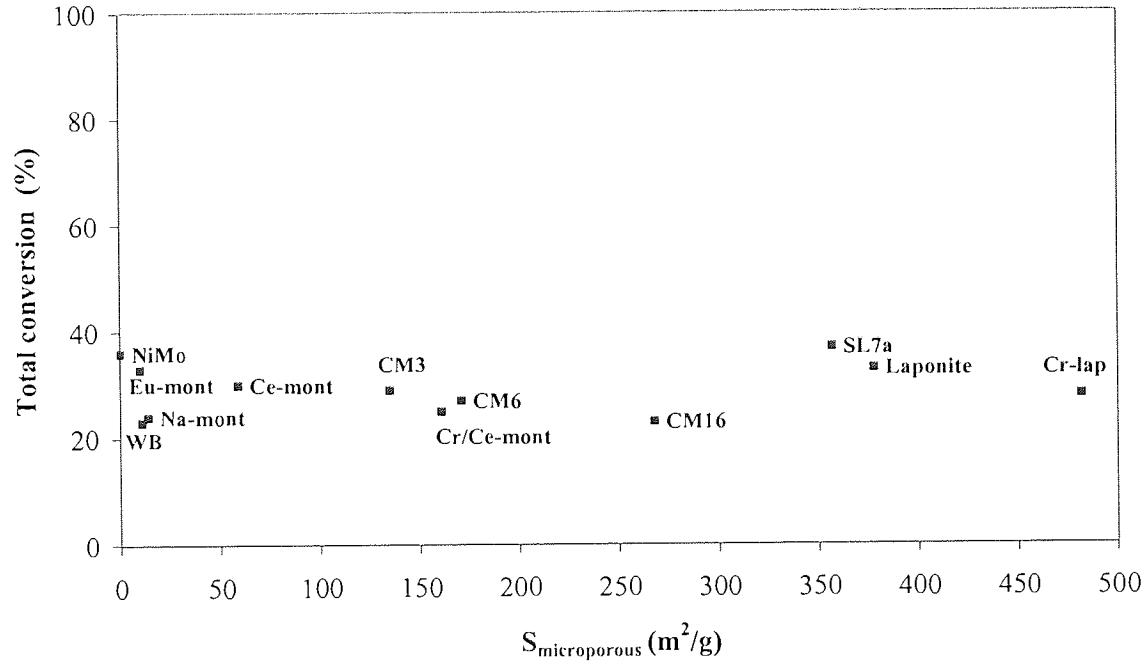

Figure 3.12 Total conversion % during 1st use versus catalysts' microporous surface area (before use)

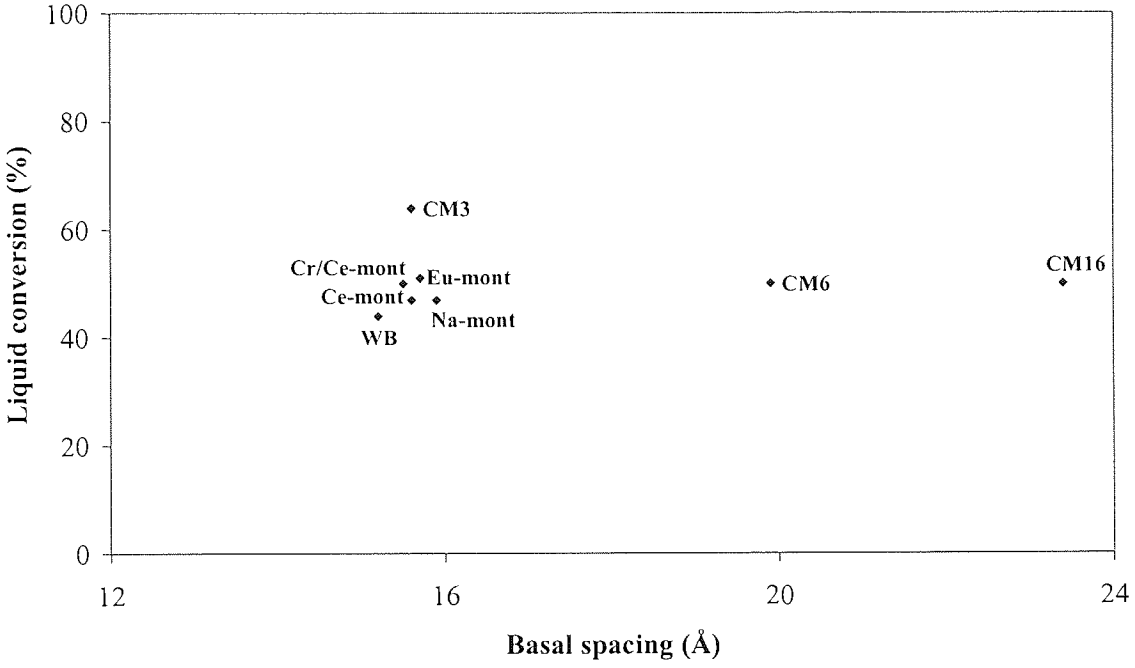

Figure 3.13 Liquid conversion % during 1st use versus catalysts' basal spacing (before use)

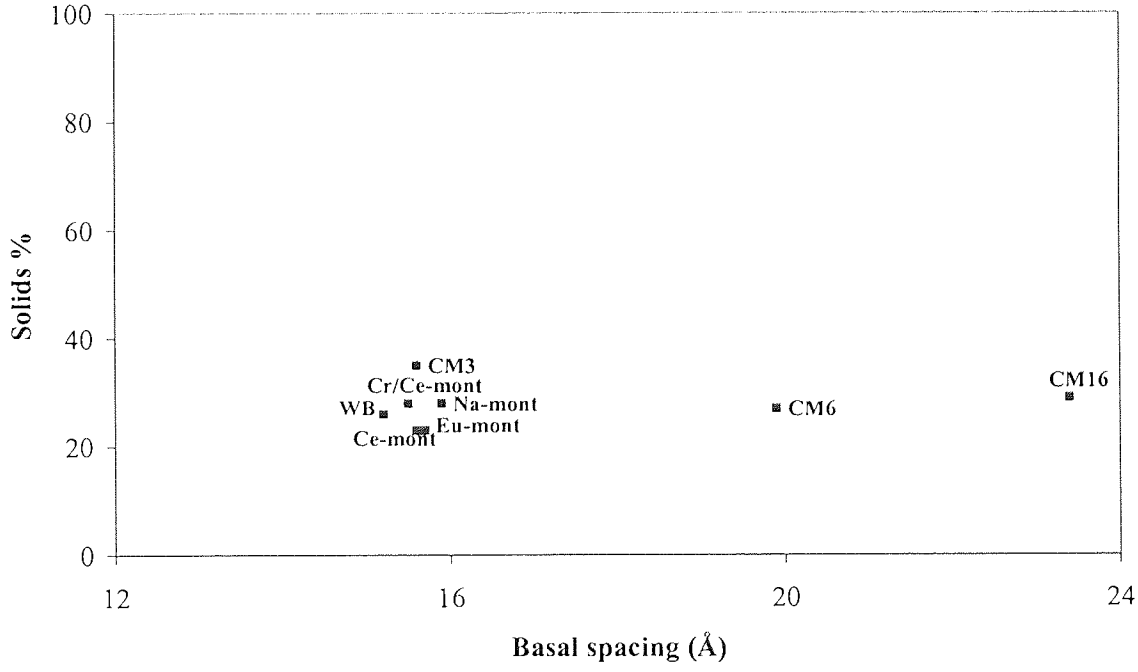

Figure 3.14 Solids % during 1st use versus catalysts' basal spacing (before use)

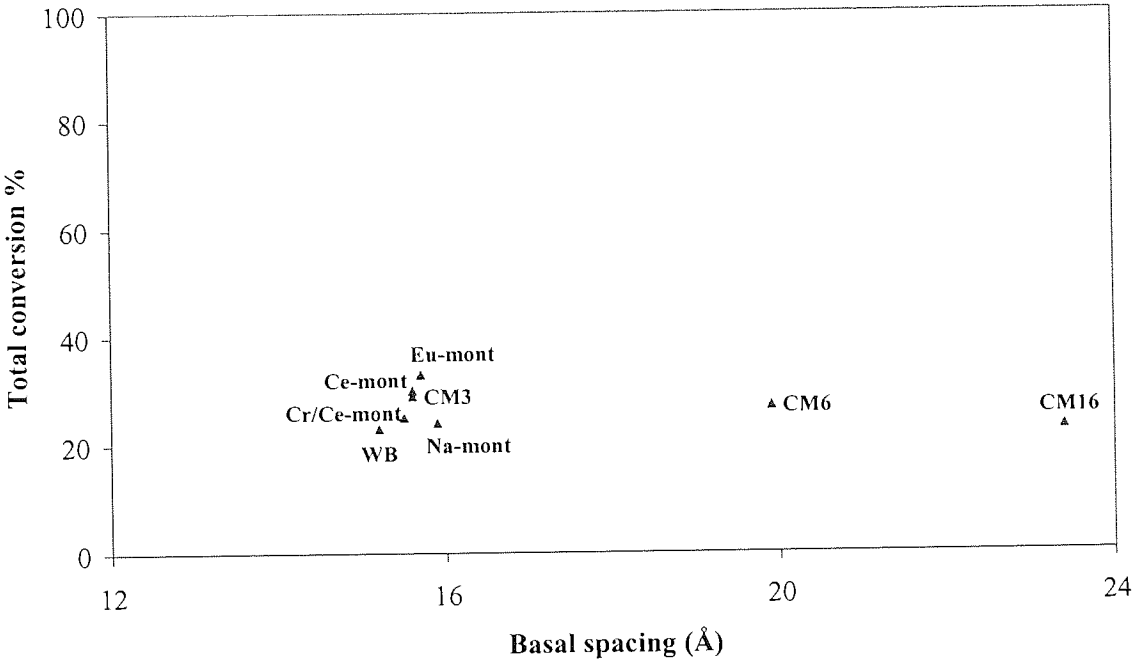

Figure 3.15 Total conversion % during 1st use versus catalysts' basal spacing (before use)

Appendix 4

Cirrus GPC bio-oil injection report

Cirrus GPC Sample Injection Report

Generated by: Cirrus_GPC50 15 September 2005 14:24

Workbook: C:\Cirrus Workbooks\Aston University\Aston University.plw

Sample Details

Sample Name: BTG 1

Acquired: 15/09/2005 14:02:55 By Analyst: Cirrus_GPC50

Batch Name: 15_09_2005

Filename: C:\Cirrus Workbooks\Aston University\15_09_2005-0001.cgrm

Concentration: 0.00 mg/ml K of Sample: 14.1000

Injection Volume: 0.0 ul Alpha of Sample: 0.7000

LIMS ID: Bottle ID:

Workbook Details

Eluent: THF stablised with 250 ppm BHT Flow Rate: 1.00 ml/min

Column Set: Column Set Length: 0 mm

Detector: DRI Temperature:

Analysis Using Method: Data Collection

Comments:

Results File: C:\Cirrus Workbooks\Aston University\15_09_2005-0001.rst

Calibration Used: 27/04/2005 15:50:02

Calibration Type: Narrow Standard Curve Fit Used: 1

Calibration Curve: y = 7.518066 - 0.618159x^1

High Limit MW RT: 5.27 mins Low Limit MW RT: 8.63 mins

High Limit MW: 18299 Low Limit MW: 151

K: 14.1000 FRM Name:

Alpha: 0.7000 Flow Marker RT: 0.00 mins

FRCF: 1.0000

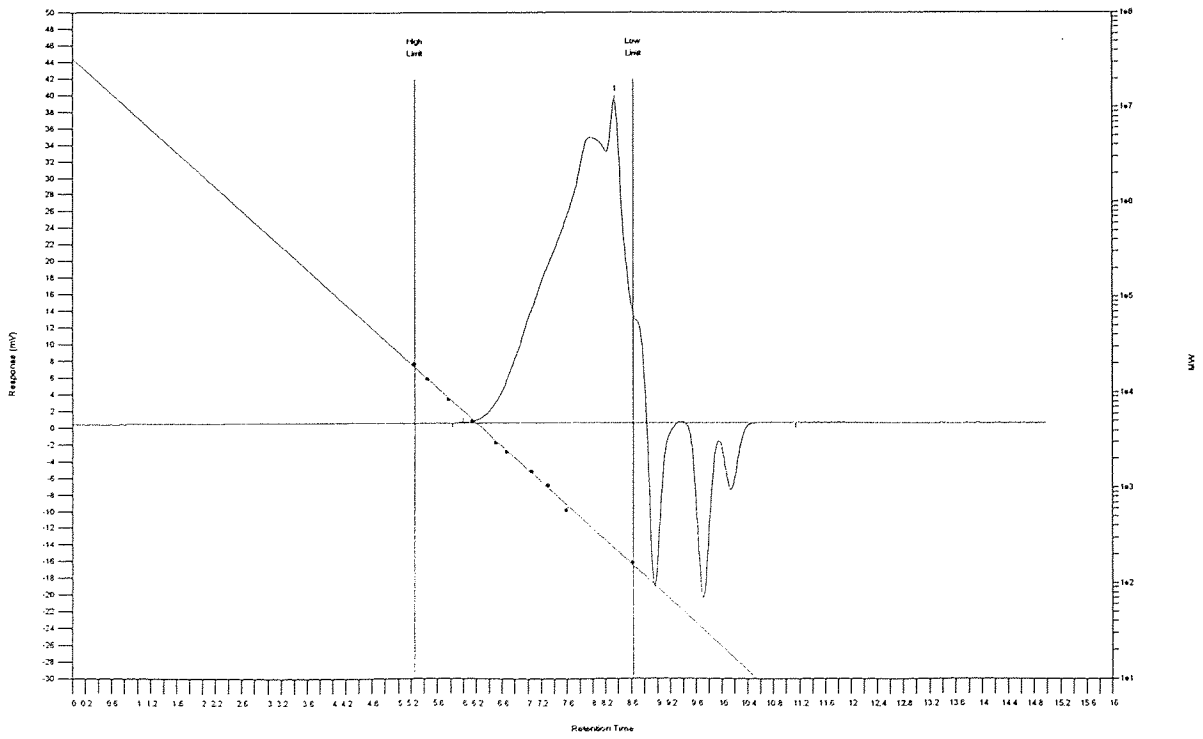

Sample Injection Report

MW Averages

Peak No	Mp	Mn	Mw	Mz	Mz+1	Mv	PD
1	232	366	640	1195	1933	581	1.74863

Processed Peaks

Peak No	Start RT (mins)	Max RT (mins)	End RT (mins)	Pk Height (mV)	% Height	Area (mV.secs)	% Area
1	6.00	8.33	8.83	38.8393	0	2857.12	100

Peak Detection

Peak No	Type	St Detect Code	End Detect Code	Is St Mod	Is Max Mod	Is End Mod
1	0	1	1	No	No	No

Baseline Detection

No	Start RT (mins)	End RT (mins)	Start Height	End Height	Is St Mod	Is End Mod
1	5.83	11.15	0.64	0.59	No	No

Appendix 5

Publication resulted from this thesis